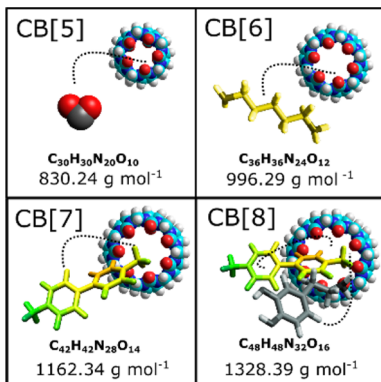


Cucurbituril-Based Molecular Recognition

Steven J. Barrow,^{†,‡} Setu Kasera,^{†,‡} Matthew J. Rowland,^{†,‡} Jesús del Barrio,[†] and Oren A. Scherman^{*,†}

[†]Melville Laboratory for Polymer Synthesis, Department of Chemistry, University of Cambridge, Lensfield Road, Cambridge CB2 1EW, United Kingdom



CONTENTS

1. Introduction	12320
2. Thermodynamics of CB[n]–Guest Binding	12322
3. Specific Binding Properties of CB[5]	12323
4. Specific Binding Properties of CB[6]	12323
5. Specific Binding Properties of CB[7]	12332
6. Specific Binding Properties of CB[8]	12332
7. Encapsulation of Gaseous Species in CB[n]	12363
7.1. CB[5] Gas Sorption	12364
7.2. CB[6] Gas Sorption	12364
7.3. Gas Sorption in Higher CB[n] Homologues	12365
8. Cucurbit[n]urils on Surfaces	12365
8.1. Electrostatic Interactions	12365
8.1.1. Modification and Assembly of Nanoparticles with CB[n]	12366
8.1.2. SERS Sensing	12367
8.1.3. Localization of Ligands	12368
8.2. Guest-Mediated Interactions	12369
8.2.1. Ligand Immobilization	12369
8.2.2. Self-Assembled Architectures	12370
8.2.3. Nanovalves	12370
8.3. Covalent Immobilization	12371
8.3.1. CB[n]-Anchored Silica	12372
8.4. Characterization of CB[n] Host–Guest Binding on Surfaces	12372
8.5. Outlook	12372
9. Supramolecular Polymers	12372
9.1. Small-Molecule-Based Supramolecular Polymers	12373
9.2. CB[8]-Mediated Supramolecular Block Copolymerization	12377
9.2.1. Supramolecular Assembly of Macromolecules	12377
9.2.2. Conclusion and Outlook	12379
10. Molecular Recognition in 3D Supramolecular Networks	12379

10.1. CB[8] Complexes Cross-Link Guest Functional Polymers	12379
10.2. Dynamics of Cross-Linking Influences Material Properties	12381
10.3. Composite Soft Materials Utilizing CB[8] Host–Guest Interactions	12381
10.4. From Monohydroxylated-CB[n] to Functional Materials	12382
10.5. Microcapsule Formation Through CB[8] Ternary Complexation	12383
10.6. CB[n] Cross-Linked Polymer Networks Outlook	12384
11. Catalysis within Cucurbit[n]uril Cavities	12384
11.1. [3 + 2]-Cycloadditions Catalyzed by CB[6]	12384
11.2. CB[n]-Catalyzed Solvolysis Reactions	12385
11.3. CB[n]-Catalyzed Oxidation Reactions	12385
11.4. Photocatalysis	12386
11.5. Metal Cation-Assisted CB[n] Catalysis	12388
11.6. Reaction Inhibition by Cucurbit[n]urils	12388
12. Recognition by CB[n] in Biological Systems	12390
12.1. Amino Acid and Short Peptide Recognition by CB[n]	12390
12.2. Noncovalent Protein Conjugation	12391
12.3. Further Application to Biochemistry	12392
12.4. Profiling Toxicity of Cucurbit[n]uril	12393
12.5. Outlook	12394
13. Summary and Outlook	12394
Associated Content	12394
Special Issue Paper	12394
Author Information	12394
Corresponding Author	12394
Author Contributions	12394
Notes	12394
Biographies	12394
Acknowledgments	12395
References	12396

1. INTRODUCTION

The product of the condensation reaction between glycoluril and formaldehyde was first reported in a thesis by Eberhard Meyer in 1904¹ and then published by Behrend and co-workers in 1905;² however, it was not until 1981 that a product was successfully crystallized from the reaction: a macrocycle consisting of 6 glycoluril units bound together by 12 methylene bridges (see Figure 1).³ The macrocycle was named cucurbituril, given its resemblance to a pumpkin (which belongs to the *cucurbitaceae* family), yet often abbreviated as

Received: June 6, 2015

Published: November 13, 2015

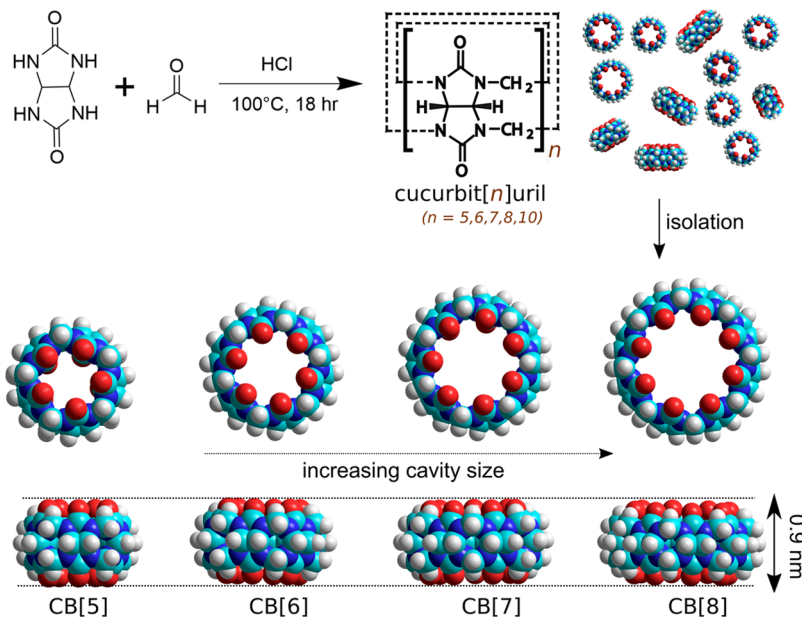


Figure 1. (Top) The reaction between glycoluril and formaldehyde. (Bottom) Space-filling models of CB[5]–CB[8] demonstrating the increasing size yet constant height of the CB[n] macrocycles.

CB[6], highlighting the 6 glycoluril building blocks that constitute the macrocycle.

During the 1980s and 1990s, interest in crystal engineering and noncovalent interactions saw the popularity of cucurbituril increase due to its ability to facilitate noncovalent binding. This is made possible via the formation of complexes with cations through interactions with the carbonyl-lined portals of CB[6], along with its ability to internalize alkyl chains within its hydrophobic cavity. Between 2000 and 2002, Kim⁴ and Day^{5,6} modified the initial reaction conditions of Meyer and Behrend to synthesize a variety of glycoluril-based cucurbituril macrocycles. The new additions to the cucurbituril family were named cucurbit[5]uril, cucurbit[7]uril, cucurbit[8]uril, and cucurbit[10]uril in light of them containing 5, 7, 8, or 10 glycoluril units, respectively. These discoveries enhanced the applicability of cucurbiturils, as the bigger cavity size of the larger CBs enables them to form 1:1 binary complexes (CB[7]) and even 1:1:1 heteroternary complexes (CB[8], see Figure 2) with aromatic compounds. A variety of CB[n] homologues have been discovered since the work of Kim and Day, including

functionalized CB[n],^{7–9} nor-seco-CB[10],¹⁰ inverted CB[n],¹¹ and many others.

CB[5]–CB[8] have found a variety of uses given their ability to form binary and ternary host–guest complexes and therefore impacted a wide variety of scientific research areas. Several previous reviews have specifically highlighted the synthesis, functionalization, and host–guest binding properties of CB[n]^{12–17} and their applications in drug delivery,¹⁸ fluorescence spectroscopy,¹⁹ catalysis,²⁰ and nanotechnology.^{21,22} More recently, the contribution of CB[n] in self-assembly and engineering of nanomaterials has also received attention,²³ where the role of CB[n] as a capping agent to stabilize metallic nanoparticles has been emphasized. The diversity of these reviews are evidence of the far-reaching impact cucurbit[n]urils have had in just the past three decades.

With the vast majority of applications of CB relying on its versatility in forming dynamic complexes with a variety of chemical species, research efforts by the cucurbit[n]uril community continue to be directed toward identifying and characterizing suitable guest molecules. Indeed, designing functional systems containing CB[n] would not be possible without the knowledge of binding strengths and the kinetics of complexation and decomplexation of the host molecule with the guests of interest. While the interactions of the macrocyclic host family have been reported widely, the characterization techniques and conditions under which these are reported have not been comprehensively reviewed. Moreover, the plethora of CB[n] guest species and their binding constants have not been tabulated and made available in one place. The present review highlights the latest developments in the understanding and applications of the molecular recognition properties of CB[n], with particular emphasis on materials design.

In this review, we cover the vast areas of scientific research upon which CB[n]s have impacted, with a focus on the guest recognition properties of CB[n], largely but not wholly concerning of their utilization in solution phase where most applications have arisen. To understand the binding properties of CB[n], a general overview of the thermodynamics of CB[n]

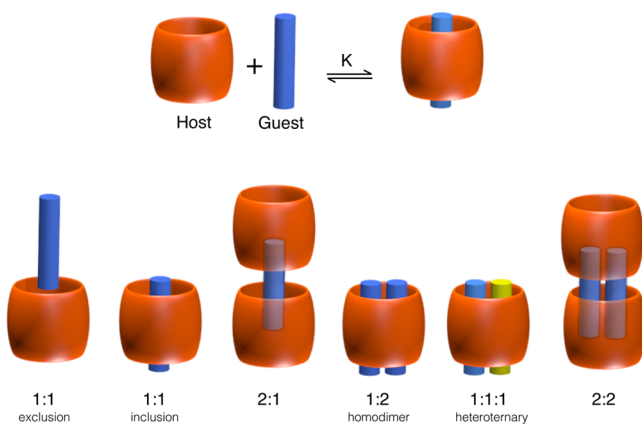


Figure 2. CB[n] inclusion and exclusion complexes.

binding is first discussed, followed by an individual analysis of the specific binding properties of CB[5]–CB[8]. Looking toward the application of CB[n] complexation, the areas of gas encapsulation, CB[n]s on surfaces, CB[n]-mediated supramolecular polymers, molecular recognition in 3D supramolecular networks, CB[n] catalysis and reaction templating, and CB[n] recognition in biological systems will each be discussed in turn.

Additionally, this review provides the reader with a comprehensive guide to the guest molecules that have been studied with CB[5,6,7,8]. The tables cover first guests that have been demonstrated to bind with cucurbiturils and include the binding constants ($\log K$) for each interaction, along with the conditions in which the binding parameters have been reported. For the case of CB[8], tables covering the binding constants for 1:1, 1:2, and 1:1:1 complexes have been included (see Figure 2). The binding constants, as well as the conditions under which the binding constants are measured, have been emphasized with the hope that this will encourage the development of new applications for known guest molecules as well as lead to the realization of new guest species for CB[n] host–guest complexes.

2. THERMODYNAMICS OF CB[n]–GUEST BINDING

Cucurbit[n]urils consist of n glycoluril molecules that are bound in a ring-like arrangement via methylene bridges. This arrangement of the glycoluril subunits is key to understanding the binding and encapsulation properties of CBs, as the number of repeat units defines the portal size and cavity volume and the alignment of the glycoluril units results in a hydrophobic cavity with carbonyl-lined portals. Understanding these aspects of CB[n] macrocycles can enable researchers to design guest species for high-affinity binding, tailored toward specific applications. Each of these aspects will now be considered.

The dipolar nature of the carbonyl-fringed portals of CB[n]s make the portals highly attractive for cation binding through the ion–dipole effect. Figure 3 shows the electrostatic potential for CB[5]–CB[8], which highlights the strength of the negative charge associated with the portals of CB. Indeed, the first reports of CB[n] binding involved metal cations acting as “lids” bound to the portals of CB.²⁴ Alkali metals,^{24,25} alkaline earth metals,^{26–28} transition metals,^{28–30} lanthanides and actinides,^{28,31–33} as well as ammonium and imidazolium ions³⁴ have been shown to bind to CB portals and are often required to enhance the solubility of the less water-soluble CBs. The portals have also been suggested to provide a constrictive steric barrier toward binding, enhancing the persistence of CB[n] complexes.³⁵ The coordination chemistry of CB[n]s has been recently reviewed³⁶ and thus will not be discussed any further here.

While the portals of CB[n]s are highly electronegative, the cavities of the macrocycle are encompassed by the fused rings of the glycoluril subunits, which leave no functional groups or electron pairs accessible to the inner cavity. Thus, the inner cavity of CB[n]s are remarkably hydrophobic and show a preference toward the encapsulation of hydrophobic compounds. Hence, alkylated ammonium and imidazolium ions bind to CB[n]s such that the cation remains at the portal region, while the alkyl chains become encapsulated within the CB cavity given its inherent hydrophobicity.^{37,38} It should not be surprising then to discover that compounds with high binding constants toward CB[n]s tend to be dicationic species where the cations are separated by an organic/hydrophobic

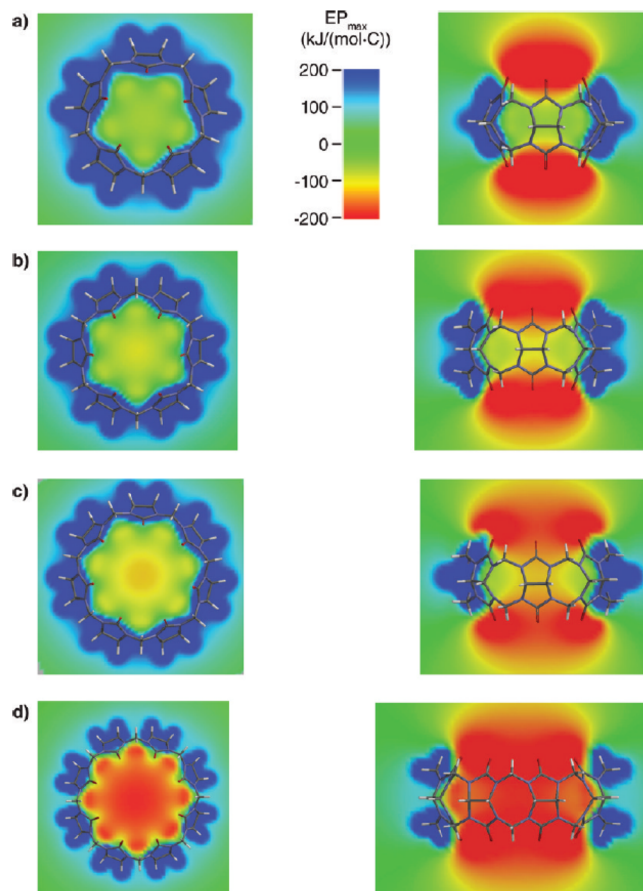


Figure 3. Calculated electrostatic potential (EP) for (a) CB[5], (b) CB[6], (c) CB[7], and (d) CB[8]. Reprinted with permission from ref 42. Copyright 2012 American Chemical Society.

region. Examples of such strong binders for CB[6], CB[7], and CB[8] include cadaverine, methylviologen, and amino-adamantane, respectively, with the size of the hydrophobic region being tailored for the specific volume of each CB cavity.

Another facet to the binding of guest species within CB[n] cavities is how well a guest physically fits within the cavity. A good predictor of CB[n] complex binding comes from the assessment of whether the inner cavity of the host and the shape of the guest display good complementarity. The cavity volumes of CB[5]–CB[8] are shown in Table 1 and range from 82 Å³ for CB[5] to 479 Å³ for CB[8].²⁴ As a result of its small size, CB[5] is mostly suitable for the encapsulation of gases (discussed in section 7), whereas CB[6] can bind alkyl chains, CB[7] can accommodate small aromatic compounds, and CB[8] can simultaneously complex with two molecules,

Table 1. Structural Parameters for Uncomplexed CB[5]–CB[8]

	CB[5] ^a	CB[6] ^a	CB[7] ^a	CB[8] ^a	CB[10] ^b
portal diameter (Å)	2.4	3.9	5.4	6.9	9.5–10.6
cavity diameter (Å)	4.4	5.8	7.3	8.8	11.3–12.4
cavity volume (Å ³)	82	164	279	479	870
outer diameter (Å)	13.1	14.4	16.0	17.5	20.0
height (Å)	9.1	9.1	9.1	9.1	9.1

^aAdapted with permission from ref 4. Copyright 2000 American Chemical Society. ^bReproduced with permission from ref 39. Copyright 2009 The Royal Society of Chemistry.

suggesting that guest size is an important factor when considering CB[n]:guest complexes. This steric aspect of molecular host–guest recognition has been quantified by Mecozzi and co-workers⁴⁰ and termed the packing coefficient. Packing coefficients are defined as the ratio of guest volume to the volume of the host cavity, and this principle has been successfully applied to predict complexation between CB[5] and CB[8] with appropriate guest compounds.⁴¹

The distinct advantage of employing CB[n]s in host–guest molecular recognition is that complexes involving CB[n] can be formed in water with high binding affinity. Typically, aqueous environments cause a drop in host–guest affinity, compared to organic solvents, as water can compete strongly for hydrogen bonds and efficiently solvate charged species. CB[n]s overcome this issue via the presence of high-energy water, which is present in the CB[n] cavity and supplies a driving force for guest complexation.^{42–44} The release of high-energy water and its role in macrocycle complex formation has been comprehensively reviewed (Figure 4).⁴⁵

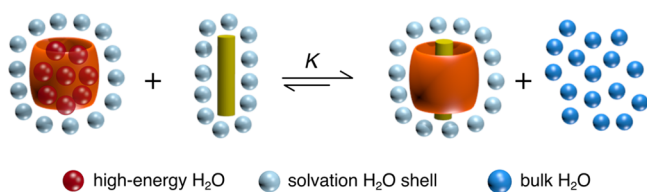


Figure 4. Schematic illustration of the formation of a CB[n] host–guest complex driven by the release of high-energy water. Adapted with permission from Biedermann and co-workers *J. Am. Chem. Soc.* 2012 134 15318–15323.⁴² Copyright 2012 American Chemical Society.

All cavities larger than a critical size contain water molecules, for entropic reasons, even if the breaking of hydrogen bonds is necessary. Such water molecules experience a reduced number of hydrogen bonds compared to bulk water and are thus of high energy. For the case of CB[n]s, the binding of a guest molecule releases the energetically frustrated water molecules, which lowers the energy of the system, providing an enthalpic and entropic gain in favor of complex formation. This hydrophobic effect has been studied using molecular dynamics simulations,⁴³ where it was determined that host–guest affinity is higher for cases where all water molecules are removed from the cavity (related to the packing coefficient) and where the encapsulated water is of high energy. CB[7] was shown to result in the largest energy gain from water expulsion of the whole CB[n] family, as it contains more water molecules than CB[5] and CB[6], and has higher energy water molecules encapsulated than CB[8], as the cavity size of CB[8] allows for encapsulated water to be structurally organized in a manner more closely resembling bulk water.

Ion–dipole binding, host–guest packing coefficients, and hydrophobic effects all need to be taken into account when considering guest molecules for CB[n] complexing with high binding affinity. The tables in this review provide an extensive list of the guest species for CB[5]–CB[8] along with their binding constants ($\log K$). This material should provide the reader with an understanding of the principles behind CB[n] complex formation in addition to a comparative list of CB[n] guests.

3. SPECIFIC BINDING PROPERTIES OF CB[5]

CB[5] is the smallest macrocycle in the cucurbit[n]uril family. With its synthesis and isolation first reported by Kim and co-workers in 2000, it has a portal diameter of 2.4 Å and a cavity volume of 82 Å³ (which is under one-half the volume of CB[6]).⁴ As a result of its small cavity size, CB[5] has found limited use in the encapsulation of guest molecules compared to the larger homologues; however, the carbonyl groups of the glycoluril subunits allow for the binding of cationic species to the portals of CB[5].^{29,34,46} It has been shown that protons can bind to the portals of CB[n]s, and indeed, this is the mechanism by which the more insoluble CBs can be dissolved through the use of aqueous acidic media.³⁴ CB[5] and decamethyl–CB[5] have also been shown to form portal complexes with alkali, alkaline earth, and ammonium cations,⁴⁶ in addition to hexamethylenetetramine, which can act as a lid on the carbonyl portals of CB[5].⁴⁷ CB[5] and decamethyl–CB[5] form very weak complexes with α , β , and γ forms of cyclodextrin, with binding constants ranging between $\log K = 0.74$ and 1.34.⁴⁸ CB[5] also exhibits binding with multicharged cations including Co²⁺, Ni²⁺, Cu²⁺, Pb²⁺, Zn²⁺, Cd²⁺, Cr²⁺, and Fe²⁺.²⁹

CB[5] shares similar portal binding properties with larger members of the cucurbituril family; however, its small internal cavity limits its ability to support host–guest complex formation. Even though CB[5] is not big enough to incorporate large molecules into its cavity, its small size gives rise to its niche: the encapsulation of gaseous molecules. Decamethyl–CB[5] has been demonstrated to encapsulate small gaseous species in both aqueous environments and in solid form. Gases such as N₂, O₂, Ar, N₂O, CO, and CO₂ have been shown to be encapsulated in both powdered and aqueous decamethyl–CB[5], while He, Ne, H₂, Kr, Xe, and CH₄ could only be encapsulated in an aqueous environment, with Kr, Xe, and CH₄ requiring heating of the sample to assist encapsulation.⁴⁹ A full discussion of the gas sorption properties of cucurbit[n]urils is offered in section 7.

4. SPECIFIC BINDING PROPERTIES OF CB[6]

CB[6] is the most abundant homologue, and with a portal diameter of 3.9 Å, it is commonly known to form stable complexes with aliphatic amines. The insolubility of CB[6] in organic solvents and sparing solubility in water has, however, had a limiting impact on its applications in its unmodified form. This is evident in the different solvent conditions in which the binding of CB[6] complexes are often reported. For example, Mock and co-workers first studied the complexation of a variety of alkyl- and aryl-substituted alkylammonium and alkyldiammonium ions in aqueous formic acid.⁵⁰ The results highlighted the size and shape complementarity exhibited by CB[6] contributing to its selective binding properties. It is well established that the stability of these complexes is a result of strong interactions between the positively charged protonated amines and the six electronegative carbonyl moieties at the portals. The hydrophobic nature of the methylene groups favors their positioning inside the cavity of the CB[6] where the solvent water molecules are excluded, adding to further stabilization of the complexes. Therefore, the most stable complex is formed for an optimal length of the aliphatic chain such that the amine groups are positioned in close proximity to the portal groups. As a result, CB[6] shows strongest binding to pentano- and hexano-bridged α,ω -diammonium functionalities.

Table 2. Association Constants Reported for CB[6] Inclusion Complexes with Organic Compounds^a

Entry	CB[6] guest	log K	method	measurement conditions	ref
1		1.95	ITC	0.05 M NaCl	376
2		1.41	ITC	0.05 M CsCl	376
3		3.00	ITC	0.05 M NaCl	376
4		2.11	ITC	0.1M Na acetate buff.; pH 4.7	376
5		2.18	ITC	0.05 M Na citrate buff.; pH 3.1	376
6		2.30 (1:1)	ITC	0.05 M NaCl	376
7		1.18 (1:2)	ITC	0.05 M NaCl	376
8		2.85	ITC	0.05 M NaCl	376
9		2.69	ITC	0.05 M KCl	376
10		2.08	ITC	0.05 M RbCl	376
11		<5	ITC	0.05 M CsCl	376
12		4.08	NMR/UV	1:1 v/v HCOOH	50
13		5.19	ITC	0.05 M NaCl	376
14		3.93	ITC	0.05 M CsCl	376
15		6.34	ITC	0.05 M LiCl	376
16		4.32	ITC	0.1 M Na acetate buffer; pH 4.7	376
17		5.19	ITC	0.05 M Na citrate buffer; pH 4.5	376
18		5.19	ITC	0.05 M Na citrate buffer; pH 3.1	376
19		2.52 (1:1)	ITC	0.05 M NaCl	376
20		0.85 (1:2)	ITC	0.05 M NaCl	376
21		3.09	ITC	0.05 M NaCl	376
22		5.00	NMR/UV	1:1 v/v HCOOH	50
23		6.49	ITC	0.05 M NaCl	376
24		6.74	NMR/UV	1:1 v/v HCOOH	377
25		5.19	NMR/UV	1:1 v/v HCOOH	50
26		7.30	ITC	0.05 M NaCl	376
27		6.57	ITC	50% formic acid	53
28		-	SORI	-	378
29		6.74	ITC	pH 5.8, buffer 25 °C	82
30		4.16	NMR/UV	1:1 v/v HCOOH	50
31		2.61	ITC	0.05 M NaCl	376
32		4.38	NMR/UV	1:1 v/v HCOOH	50
33		6.34	ITC	0.05 M NaCl	376
34		4.55	NMR/UV	1:1 v/v HCOOH	50
35		6.39	NMR/UV	1:1 v/v HCOOH	50
36		8.18	ITC	0.05 M NaCl	376
37		9.98	FL	10 mM NH4OAc	68

Table 2. continued

Entry	CB[6] guest	log K	method	measurement conditions	ref
38		5.57	NMR/UV	1:1 v/v HCOOH	50
39		5.37	NMR/UV	1:1 v/v HCOOH	50
40	$^+\text{H}_3\text{N} \text{---} \text{C}(\text{H}_3)_2 \text{---} \text{CH}_2 \text{---} \text{NH}_3^+$	5.22	ITC	0.05 M NaCl	376
41		1.2	NMR/UV	1:1 v/v HCOOH	50
42		6.44	NMR/UV	1:1 v/v HCOOH	50
43	$^+\text{H}_3\text{N} \text{---} \text{C}(\text{H}_3)_2 \text{---} \text{CH}_2 \text{---} \text{NH}_3^+$	6.91	ITC	50% formic acid	53
44		8.46	ITC	0.05 M NaCl	376
45		5.52	NMR/UV	1:1 v/v HCOOH	50
46		2.23	NMR	D ₂ O with 0.2 M Na ₂ SO ₄ , 25 °C	35
47		2.17	NMR	D ₂ O with 0.2 M Na ₂ SO ₄ , 30 °C	35
48		2.04	NMR	D ₂ O with 0.2 M Na ₂ SO ₄ , 40 °C	35
49		1.94	NMR	D ₂ O with 0.2 M Na ₂ SO ₄ , 50 °C	35
50		1.76	NMR	D ₂ O with 0.2 M Na ₂ SO ₄ , 60 °C	35
51		2.11	NMR	D ₂ O/formic acid (1:1 v/v), 25 °C	35
52		1.95	NMR	D ₂ O/formic acid (1:1 v/v), 33 °C	35
53		1.90	NMR	D ₂ O/formic acid (1:1 v/v), 40 °C	35
54		1.84	NMR	D ₂ O/formic acid (1:1 v/v), 48 °C	35
55		1.61	NMR	D ₂ O/formic acid (1:1 v/v), 60 °C	35
56		1.49	NMR	D ₂ O/formic acid (1:1 v/v), 72 °C	35
57	$^+\text{H}_3\text{N} \text{---} \text{C}(\text{H}_3)_3$	3.76	ITC	0.05 M NaCl	376
58		2.43	ITC	0.05 M NaCl 298.5 K	379
59		4.63	NMR/UV	1:1 v/v HCOOH	50
60	$^+\text{H}_3\text{N} \text{---} \text{C}(\text{H}_3)_2 \text{---} \text{CH}_2 \text{---} \text{NH}_3^+$	7.23	ITC	0.05 M NaCl	376
61		-	SORI	-	378
62		not bound <1.42	NMR/UV	1:1 v/v HCOOH	50
63		2.43	NMR/UV	1:1 v/v HCOOH	50
64	$^+\text{H}_3\text{N} \text{---} \text{C}(\text{H}_3)_2 \text{---} \text{CH}_2 \text{---} \text{N}(\text{H}_3^+) \text{---} \text{C}(\text{H}_3)_2 \text{---} \text{CH}_2 \text{---} \text{NH}_3^+$	8.61	ITC	0.05 M NaCl	376

Table 2. continued

Entry	CB[6] guest	log K	method	measurement conditions	ref
65		3.32	ITC	0.05 M NaCl	376
66		4.92	ITC	50% HCOOH	53
67		6.03	ITC	0.05 M NaCl	376
68		-	SORI	-	378
69		2.51	NMR/UV	1:1 v/v HCOOH	50
70		<1.42	NMR/UV	1:1 v/v HCOOH	50
71		<1.42	NMR/UV	1:1 v/v HCOOH	50
72		9.52	ITC	0.05 M NaCl	376
73		10.73	ITC	0.2 M LiCl	376
74		2.61	ITC	50% HCOOH	53
75		4.22	ITC	0.05 M NaCl	376
76		-	SORI	-	378
77		7.58	-	-	77
78		2.6	ITC	50% formic acid	53

^aAbbreviations: ITC, isothermal titration calorimetry; UV-vis, ultraviolet/visible spectroscopy; NMR, nuclear magnetic resonance spectroscopy; ESI-MS, electrospray ionization-mass spectrometry; SORI, sustained off-resonance irradiation (mass spectroscopy); FL, fluorimetry; EPR, electron paramagnetic resonance; EAS, electronic absorbance spectroscopy.

The binding properties of CB[6] with imidazolium-based guests have also been investigated widely^{37,38,51} and used in the synthesis of monofunctionalized CB[6]⁸ as well as in the isolation of CB[*n*] homologues, Tables 2–4.⁵²

The importance of the surroundings of the complex, however, has a major impact on the strength of the resulting complex as demonstrated by Lee and co-workers.⁵³ In this correlation study of the binding behavior of diammonium guests between the solution phase (50% HCOOH, ITC) and the gas phase (ESI-MS) it is shown that while a correlation exists between the two phases, the stabilities of the complexes are different. They suggest that this contrast is a result of an additional role played by the H bonding with water molecules in the solution phase, while only ion–dipole interactions predominantly exist in the gas phase. In the gas phase, the guest has to undergo a structural distortion in order to maximize ion–dipole interactions with the portal. The distortion is not needed in water because it is compensated in solution through hydrogen bonding with water.

The high binding affinities of CB[6] toward aliphatic amines compared to aromatic groups have led to various rotaxane and pseudorotaxane constructs, where the alkylamines act as an axle and the CB[6] the wheel such as with 1,8-diaminooctane.⁵⁴ A 1:1:1 system with CB[6] and cyclodextrin using a dihexylammonium guest has also been reported.⁵⁵ Threads

containing pyridinium and imidazolium moieties have also been widely reported in constructing pseudorotaxanes and rotaxanes with CB[6]. For example, a [2]pseudorotaxane system was reported using structure A1, where the host is located over the hexamethyl chain of the guest. In a dynamic rotaxane derived from a CB[6] complex with a bispyridinium guest (A2), CB[6] is able to shuttle between the two pyridinium groups.⁵⁶ Self-assembly of pseudorotaxanes constructed with A3-CB[6]⁵⁷ and A4-CB[6]⁵⁸ has been reported to form infinite hydrogen-bonded one-dimensional and two-dimensional networks. Other high-order rotaxane-based structural frameworks have also been reported,⁵⁹ including polypseudorotaxanes.^{60,61} He and co-workers reported the formation of pseudorotaxanes with a series of bis-pyridinium compounds (see A5 in Figure 5), where the binding site of CB[6] could be tailored by increasing length of the chains at the two ends of the guest.⁶²

Several [3]rotaxanes have been reported based on imidazolium-containing structures (A6⁶⁴ and A7⁶⁵). Recently, photoresponsive dithienylethene-based rotaxanes (A8) were constructed with CB[6].⁶⁶ CB[6] has also been used to form water-soluble [5]rotaxane and [5]pseudorotaxane using a meso-tetraphenyl porphyrin (see A9 in Figure 6) with pH-driven switchable properties.⁶³

Table 3. Association Constants Reported for CB[6] Inclusion Complexes with Gases^a

entry	CB[6] guest	log K	method	measurement conditions	ref
79	SF ₆	4.49	¹⁹ F NMR	0.02 M Na ₂ SO ₄	173
80		5.82	¹⁹ F NMR	pure water	176
81	Xe	2.30	¹ H, ¹²⁹ Xe NMR	0.02 M Na ₂ SO ₄	173
82	methane	<3.30	Fl	0.1 mM HCl, pH 3, 298 K	69
83		<1.70	Fl	50 mM NaOAc, pH 5.5, 298 K	69
84	ethane	4.38	Fl	0.1 mM HCl, pH 3, 298 K	69
85		3.41	Fl	50 mM NaOAc, pH 5.5, 298 K	69
86	ethene	3.59	Fl	0.1 mM HCl, pH 3, 298 K	69
87		2.40	Fl	50 mM NaOAc, pH 5.5, 298 K	69
88	acetylene	2.04	Fl	0.1 mM HCl, pH 3, 298 K	69
89		1.67	Fl	50 mM NaOAc, pH 5.5, 298 K	69
90	propane	5.26	Fl	0.1 mM HCl, pH 3, 298 K	69
91		4.00	Fl	50 mM NaOAc, pH 5.5, 298 K	69
92	[D ₃]-propane	5.20	Fl	0.1 mM HCl, pH 3, 298 K	69
93	propene	4.40	Fl	0.1 mM HCl, pH 3, 298 K	69
94		3.15	Fl	50 mM NaOAc, pH 5.5, 298 K	69
95	n-butane	5.45	Fl	0.1 mM HCl, pH 3, 298 K	69
96		3.64	Fl	50 mM NaOAc, pH 5.5, 298 K	69
97	1-butene	4.90	Fl	0.1 mM HCl, pH 3, 298 K	69
98		3.11	Fl	50 mM NaOAc, pH 5.5, 298 K	69
99	cis-butene	5.18	Fl	0.1 mM HCl, pH 3, 298 K	69
100		3.32	Fl	50 mM NaOAc, pH 5.5, 298 K	69
101	trans-butene	4.32	Fl	0.1 mM HCl, pH 3, 298 K	69
102		2.51	Fl	50 mM NaOAc, pH 5.5, 298 K	69
103	isobutane	5.93	Fl	0.1 mM HCl, pH 3, 298 K	69
104		4.36	Fl	50 mM NaOAc, pH 5.5, 298 K	69
105	[D ₁₀]-isobutane	5.96	Fl	0.1 mM HCl, pH 3, 298 K	69
106	isobutene	4.92	Fl	0.1 mM HCl, pH 3, 298 K	69
107		3.28	Fl	50 mM NaOAc, pH 5.5, 298 K	69
108	n-pentane	3.95 ± 3.60	Fl	0.1 mM HCl, pH 3, 298 K	69
109		2.15	Fl	50 mM NaOAc, pH 5.5, 298 K	69
110	isopentane	4.18 ± 3.70	Fl	0.1 mM HCl, pH 3, 298 K	69
111		2.48	Fl	50 mM NaOAc, pH 5.5, 298 K	69
112	neopentane	<3.30	Fl	0.1 mM HCl, pH 3, 298 K	69
113		<1.70	Fl	50 mM NaOAc, pH 5.5, 298 K	69
114	cyclopentane	6.11	Fl	0.1 mM HCl, pH 3, 298 K	69
115		4.40	Fl	50 mM NaOAc, pH 5.5, 298 K	69
116	higher alkanes (n-hexane, isohexane, 2,3-dimethylbutane, cyclohexane, n-heptane)	<3.30	Fl	0.1 mM HCl, pH 3, 298 K	69
117	higher alkanes (n-hexane, isohexane, 2,3-dimethylbutane, cyclohexane, n-heptane)	<1.70	Fl	50 mM NaOAc, pH 5.5, 298 K	69
118	CO ₂				170
119	CH ₄				170
120	CO				170
121	Br ₂		X-ray crystallography		80
122	I ₂	6.15	UV/vis		80

^aAbbreviations: ITC, isothermal titration calorimetry; UV/vis, ultraviolet/visible spectroscopy; NMR, nuclear magnetic resonance spectroscopy; ESI-MS, electrospray ionization-mass spectrometry; SORI, sustained off-resonance irradiation (mass spectroscopy); FL, fluorimetry; EPR, electron paramagnetic resonance; EAS, electronic absorbance spectroscopy.

Table 4. Exclusion Complexes Reported with CB[6]^a

Entry	CB[6] guest	log K	method	measurement conditions	ref
123		2.49	EAS	55% HCOOH, 15 °C	380
124		2.56	EAS	55% HCOOH, 25 °C	380
125		2.68	EAS	55% HCOOH, 45 °C	380
126		7.34	ITC	10 mM NH4OAc, buffer pH 7	68
127		7.15	FL	pH4	70
128		7.15	FL	pH7	70
129		7.63	FL	1 mM HCl	69
130		3.36	FL	50 mM NaOc, pH 5.5 ; pH 4.7	69
131		-	-	0.3 M HCl	67
132		-	-	gas phase, rel. abundance	381
133		-	-	gas phase, rel. abundance	381
134		-	-	gas phase, rel. abundance	381
135		-	-	gas phase, rel. abundance	381
136		-	-	gas phase, rel. abundance	381

Table 4. continued

Entry	CB[6] guest	log K	method	measurement conditions	ref
137		-	-	X-ray cryst.	27
138		-	-	X-ray cryst.	27
139	ubiquitin	-	-	ESI-MS	374

^aAbbreviations: ITC, isothermal titration calorimetry; UV-vis, ultraviolet/visible spectroscopy; NMR, nuclear magnetic resonance spectroscopy; ESI-MS, electrospray ionization-mass spectrometry; SORI, sustained off-resonance irradiation (mass spectroscopy); FL, fluorimetry; EPR, electron paramagnetic resonance; EAS, electronic absorbance spectroscopy.

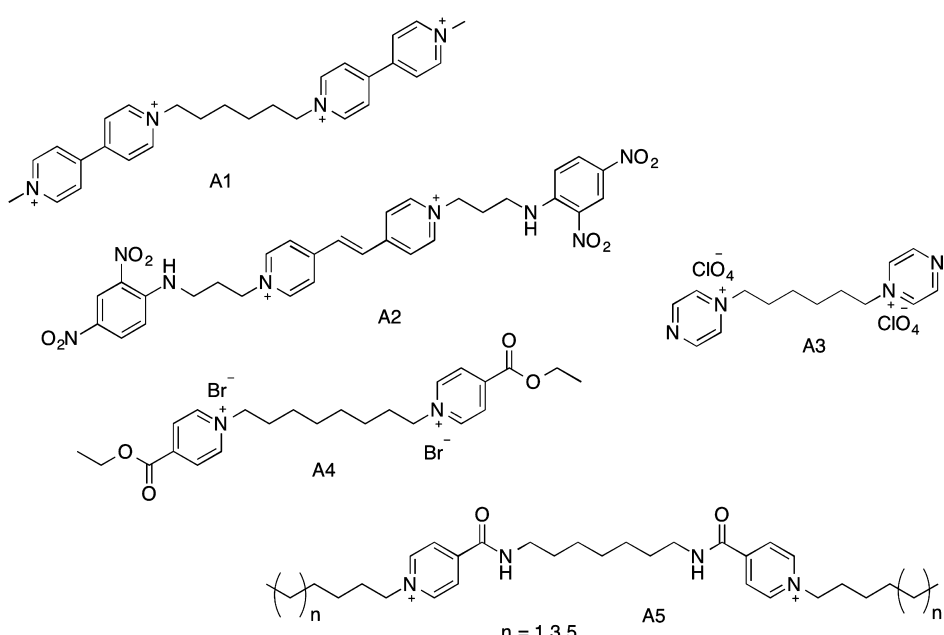


Figure 5. Pyridinium-based structures for the formation of rotaxanes and pseudorotaxanes with CB[6].

These selective recognition properties of CB[6] were first utilized by Kim and co-workers in order to construct a fluorescent molecular switch based on a pseudorotaxane structure.⁶⁷ Various fluorescent sensors have been reported using the indicator-displacement strategy with dye molecules derivatized with diaminoalkyl derivatives (see A10–A13 in Figure 7), whereby the alkyl moiety anchors strongly inside the CB[6] cavity.^{68–70} Recently, the fluorescence emission of pyrene was reported to get enhanced in the presence of CB[6] as a result of external supramolecular interactions between pyrene and CB[6].⁷¹ CB[6] has also been used for the detection of 3,4-methylenedioxymethamphetamine, the active constituent in ecstasy samples, using cyclic voltammetry.⁷²

Catecholamines such as adrenaline⁷³ and isoprenaline⁷⁴ show distinct binding behavior between CB[6]. In particular, a striking transformation of the crystals of the complex from needle-like to prismatic structures can be observed over a period of a few days (Figure 8 a–c).⁷³ This is attributed to the formation of a 1:1 CB[6]·adrenaline complex as a kinetic

product, which slowly evolves to form a 2:1 thermodynamically favored complex (Figure 8 d and 8e). Furthermore, in the same study, binding between dimerized adrenaline and CB[6] in acidic media was also reported (Figure 8f).

Characterization of the binding parameters for CB[6] and its guests is usually challenging in water owing to the poor aqueous solubility of CB[6]. A remarkable number of crystal structures, however, have been reported for CB[6]·guest complexes, which provide important structural insights into the complexed adduct formation. While the binding of CB[6] with aromatic compounds is surprising because of its smaller cavity diameter, it is noteworthy that arylamines with suitable substituents are known to become encapsulated within the CB[6] cavity.⁵⁰ This remarkable observation is particularly clear in the crystallographic structures reported for CB[6]·*p*-xylylenediammonium-ion adducts, whereby an ellipsoidal distortion of the host molecule upon guest encapsulation is clearly observed;^{75,76} however differences may exist between solid and aqueous forms of this complex. Although CB[6] is

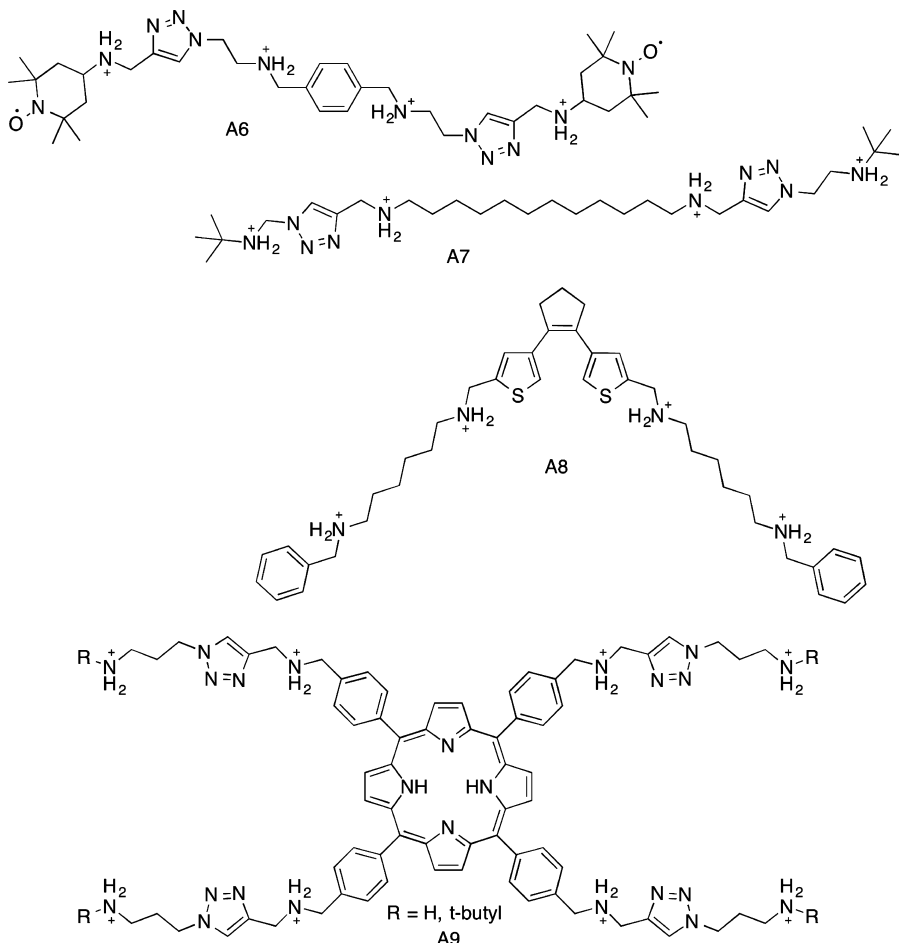


Figure 6. Representative structures for the formation of rotaxanes and pseudorotaxanes with CB[6].⁶³

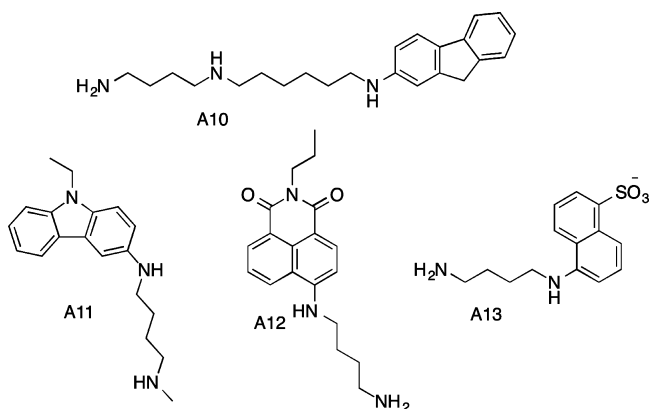


Figure 7. Alkyldiammonium-dye conjugates used for fluorescence sensor designs with CB[6].^{67–70}

typically unable to accommodate six-membered aromatic rings, five-membered aromatic rings such as thiophenes⁵⁰ and furans⁷⁷ are able to bind to CB[6].

CB[6] is widely applied in separation science. For example, in a recent study, monolithic poly(glycidyl methacrylate-*co*-ethylene dimethacrylate) capillary columns were incorporated with CB[6] monorotaxanes for application in polymer monolith microextraction to separate and preconcentrate nitroaromatics. These monoliths were used for trace analysis of nitroaromatic compounds in blood and water with 83–107% recovery.⁷⁸ In another study, a new type of stationary phase was

constructed using CB[6] in combination with a guanidinium-based ionic liquid.⁷⁹

The ability of CB[*n*] to modulate chemical reactions has been known since the first report of the acceleration of 1,3-dipolar cycloaddition reaction under the catalytic influence of CB[6] reported by Mock and co-workers.³ Moreover, using the inclusion of bromine and iodine as was previously reported by Nau and co-workers,⁸⁰ Reddy and co-workers have shown the application of these halogen inclusion complexes such as I₂–CB[6] for catalytic reactions and Br₂–CB[6] to achieve electrophilic bromination of benzene and formation of bromohydrin.⁸¹

Recently, the role of CB[6] in the protection of selenocystamine was demonstrated against redox stimuli (Figure 9). The Se–Se bonds were shown to be stable in the presence of CB[6] when exposed to H₂O₂, a strong oxidizing agent, and tris(2-carboxyethyl)phosphine, a strong reductant. CB[6] is able to modulate the reaction of the selenocystamine by encapsulating the Se–Se bonds inside its cavity. Selenocystamine forms a strong host–guest complex with CB[6] under acidic conditions (pH 5.8) with a log *K* value of 6.7 at 25 °C as measured by ITC. The protection behavior was shown to be applicable over a wide range of pH values (up to 11.8). Furthermore, the reactivity of selenocystamine guest was fully recovered through dissociation with CB[6] upon addition of BaCl₂.⁸² The ability of CB[6] to catalyze and template reactions will be discussed in greater detail in section 11.

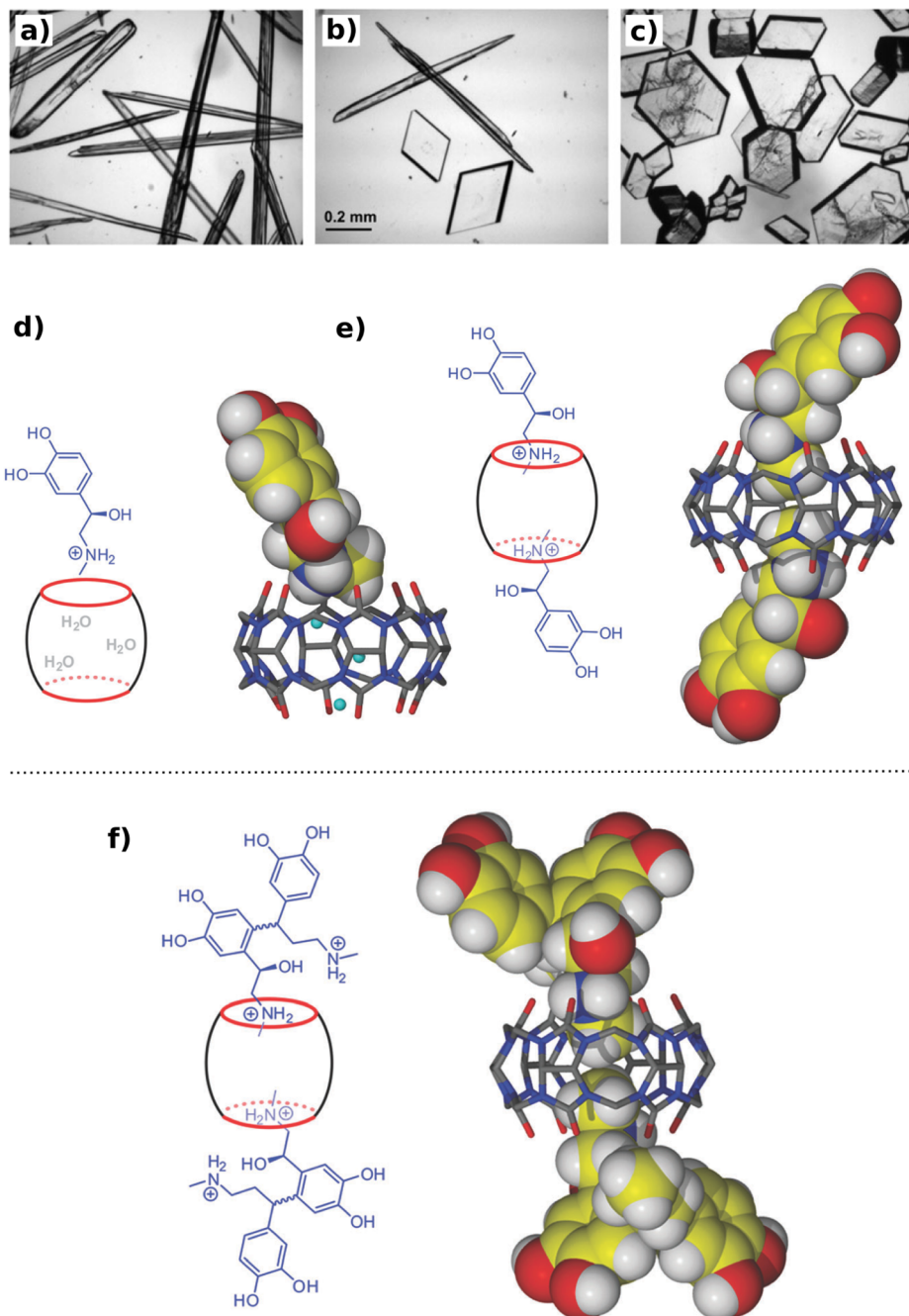


Figure 8. Pictures of crystals of CB[6]-adrenaline complexes after (a) 1 h showing needle-like crystals, (b) 2 days showing both needles and prisms, (c) 1 week showing only prisms. Schematic representation and crystal structures of different complexation modes of CB[6]-adrenaline showing (d) 1:1 kinetic complex, (e) 1:2 thermodynamic complex, and (f) dimerized adrenaline under acidic medium. Figure adapted with permission from ref 73. Copyright 2013. All images reproduced with permission from The Royal Society of Chemistry.

Several CB[6]-ion adducts have been examined recently.^{83–90} Cd(II)-CB[6] complexes have been investigated comprehensively in an electrochemical study through competitive binding with acetic acid, isobutylamine, and 1,5-diaminopentane.⁸⁶ The use of CB[6]-ion complexes is also emerging in materials chemistry, for example, as Sr(II)-CB[6]-based polymers⁸⁷ and hexachloroplatinate(IV) anion-CB[6]-based porous materials have been reported.⁸⁸ Theury and co-workers reported the formation of La⁺ ammoniocarboxylate complexes with CB[6].⁸³ Later, the luminescent properties of CB[6] coordination compounds with La⁺ (Eu, Sm, Tb, and Tm) were also investigated in acidic aqueous media.⁸⁹ In

another study, a new mononuclear dysprosium(III)-cucurbit[6]uril complex was synthesized and characterized structurally and magnetically.⁹⁰ Chen and co-workers also reported the CB[6]-based capture of Cs⁺ cations.⁹¹

The binding of ions such as alkali metals at the portals of the CB[6] have been well known. In a previous study investigating the properties of CB[6] as a sorptive material for (textile) dyes, the presence of cations such as Ca²⁺ or Sr²⁺ enhanced the binding of the dyes to CB[6].⁹² On the contrary, in a study with methyl viologen and CB[6], where methyl viologen is only able to interact with CB[6] externally, even the presence of salt hindered these weak interactions between them.⁹³ Molecular

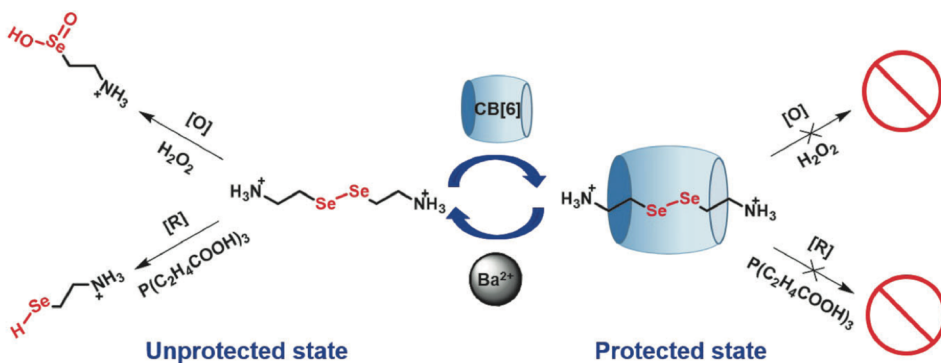


Figure 9. Protection and deprotection of selenocystamine achieved by controlled supramolecular complexation with CB[6]. Reproduced with permission from Ren and co-workers *ChemPhysChem* 2015, 16, 523527. Copyright 2015 John Wiley and Sons, Inc.

dynamic simulations also show evidence of the preferential formation of CB[6]·Na⁺ complexes in the presence of hexamethylene diammonium cations in saline solutions.⁹⁴ Therefore, while the introduction of ions is often necessary in order to enhance the solubility of CB[6] in water, their role as an interferent between CB[6] and binding with other organic guests cannot be ignored.

5. SPECIFIC BINDING PROPERTIES OF CB[7]

CB[7], the third member of the macrocyclic family, is large enough to form inclusion complexes with guest molecules that are typically bulkier than simple aliphatic chains and gas molecules that are usually encapsulated by the smaller homologues, CB[5] and CB[6].¹⁵ On account of its larger cavity size relative to CB[6], a much wider range of guests can be recognized by CB[7] and encapsulated within, often exhibiting highly favorable binding parameters, see Table 5. Specifically, CB[7] has a portal diameter of 5.4 Å and cavity diameter of 7.3 Å, see Table 1.⁹⁵ This affords CB[7] an inner cavity volume of 279 Å³, large enough for the inclusion of simple three-dimensional molecules such as ferrocene and adamantylamine derivatives (see Figure 10 for examples), accompanied by high binding constants ($\log K > 12$). This occurs through excellent cavity-filling effects, expelling all “high-energy” water molecules from the macrocycle core.⁴¹ These particularly impressive binding constants are undoubtedly one reason for the large number of reports in the recent literature, with over 90 individual publications in 2014 alone.

Not only does CB[7] have a cavity size amenable to the encapsulation of sizable guest molecules but also it has a much greater aqueous solubility relative to other members of the CB[n] family, exhibiting a water solubility of 30 mM compared to 0.01 mM for CB[8] (also large enough to encapsulate 3D guest molecules).¹⁵ This greater solubility coupled with the larger cavity volume has resulted in a variety of aqueous specific applications of CB[7], particularly in drug encapsulation as described in a recent review.¹⁸ Drug encapsulation is not the only biomedical area where CB[7] has been utilized; numerous reports from Urbach and others have highlighted binding of CB[7] to peptides, proteins, biomolecules (i.e., neurotransmitters), and dyes, demonstrating applicability to highly accurate biosensing applications at subnanomolar concentrations.^{96–98} CB[7]’s solubility at usual drug therapeutic levels has also leaned the macrocycle toward a wide range of toxicity assessing studies, from *in vitro* studies to mouse and zebrafish models.^{99–102} Although CB[7] is not the perfect representation of biocompatibility for all other members of the CB[n] family,

the good degree of tolerability demonstrated in these studies is promising.

As a result of these highly favorable binding equilibria, CB[7] has found other unique uses, ranging from the assembly of supramolecular energy-transfer motifs, stimuli-responsive underwater adhesives, to catalysis.^{17,103,104} The CB[7] literature has dramatically expanded over the past decade, and potential applications of the macrocycle are continuously emerging. We expect to see vast progress and efforts in the area of controlled functionalization and attachment of CB[7] receptors to a variety of materials, whereby the CB[7] can be isolated within a material still allowing for high-affinity binding.¹⁰⁵

6. SPECIFIC BINDING PROPERTIES OF CB[8]

The cavity volume of CB[8] is 479 Å³, which is similar to γ-CD and 1.7 times larger than that of CB[7], and its binding properties parallel in many ways those of CB[5]–CB[7].¹⁵ CB[8] displays relatively strong binding affinities toward bulky amphiphilic positively charged guests including adamantane and ferrocene derivatives C1–C5 (binding constants were determined by competition with melamine-derived guest C6 for a limiting quantity of CB[8], see Figure 11 and Tables 6 and 7).¹⁰⁶ It can also encapsulate larger macrocyclic guests including cyclen(1,4,7,10-tetra-/aza-/cyclo-/do-/decane) and cyclam(1,4,8,11-tetra-/aza-/cyclo-/tetra-/decane) (C7 and C8 in Figure 11), thus allowing formation of a “macrocycle within macrocycle” complex.¹³ Kim and co-workers were able to metalate the bound tetraaza macrocycles with Cu(II) and Zn(II), thus yielding Russian doll-type metal-ion complexes.^{107,108} This strategy has been further exploited to prepare a large number of inclusion compounds of transition metal complexes including nickel(II).^{109–111} The inclusion of the dimethylated cyclen C9 (Figure 11) has also been reported.¹¹² CB[8] has even shown the ability to bind larger guests such as fullerene, forming complexes with two fullerene guests bound externally to the CB[8] portals, one being bound to each portal.¹¹³ In the presence of CB[8], alkylammonium salts equipped with long aliphatic chains, C10–C15 (Figure 11), bend and are incorporated inside the cavity of the host by adopting a U-shaped conformation.^{114,115} When the same guests are in the presence of the smaller CB[7], only the signals corresponding to the methylene protons near the charged group shift in the ¹H NMR of the complex while the signals of the protons at the terminal end of the guest chain, far away from the charged group, remain unchanged. This suggests that the CB[7] sits nearby the ammonium group with the other end of the guest protruding from the macrocycle cavity. On the

Table 5. Association Constants Reported for CB[7] Inclusion Complexes^a

Entry	CB[7] guest	log K	method	measurement conditions	ref
140		6.00	UV	-	382
141		5.60	UV	-	382
142		6.00	UV	-	382
143		4.47	UV	-	382
144		9.47	ITC	water at 298.15 K	383
145		12.30	ITC	water at 298.15 K	383
146		12.38	ITC	298 K	384
147		12.60	ITC	water at 298.15 K	383
148		12.61	ITC	298 K	384
149		11.47	NMR	Measured by competition with	106
150		11.52	NMR	Conditions: NaO ₂ CCD ₃ (50 mM) buffer, D ₂ O, pH 4.74, room temperature	385
151		13.27	NMR	Iodide counter ion, NaO ₂ CCD ₃ (50 mM) buffer, D ₂ O, pH 4.74, room temperature	385
152		15.47	ITC	-	376
153		15.47	ITC	298 K	384
154		9.50	ITC	298 K	384

Table 5. continued

Entry	CB[7] guest	log K	method	measurement conditions	ref
155		12.11	NMR	competitive guest: 1-aminoadamantane	386
156		4.39	NMR		106
157		4.39	UV	50 mM NaOAc buffer, pH 4.74	387
158		4.63	NMR		106
159		4.80	NMR		106
160		4.90	NMR		106
161		5.55	NMR		106
162		6.31	NMR		106
163		6.32	UV	50 mM NaOAc buffer, pH 4.74	387
164		6.92	NMR		106

Table 5. continued

Entry	CB[7] guest	log K	method	measurement conditions	ref
165		7.12	NMR	Cl ⁻ counter ions. Measured by competition with 	106
166		5.35	UV	0.03 M Tris Buffer, 298 K	388
167		5.22	UV	0.01 M NaCl, 0.03 M Tris Buffer, 298 K	388
168		5.01	UV	0.05 M NaCl, 0.03 M Tris Buffer, 298 K	388
169		4.83	UV	0.1 M NaCl, 0.03 M Tris Buffer, 298 K	388
170		4.39	UV	0.2 M NaCl, 0.03 M Tris Buffer, 298 K	388
171		5.12	UV	0.01 M CaCl, 0.03 M Tris Buffer, 298 K	388
172		4.65	UV	0.05 M CaCl, 0.03 M Tris Buffer, 298 K	388
173		4.21	UV	0.1 M CaCl, 0.03 M Tris Buffer, 298 K	388
174		3.75	UV	0.2 M CaCl, 0.03 M Tris Buffer, 298 K	388
175		5.01	UV	0.2 M NaCl, 298 K	166
176		7.11	UV	Cl ⁻ counter-ion, 50 mM NaOAc buffer, pH 4.74	387
177		5.08	NMR	Cl ⁻ counter-ions, 0.1 M phosphate buffer (pH 7)	389
178		6.82	ITC	Br ⁻ counter-ions, 10 mM sodium phosphate buffer (pH 7)	161
179		7.25	NMR	Measured by competition with 	106
180		7.26	NMR	Measured by competition with 	106
181		7.35	NMR	Measured by competition with 	106
182		7.36	UV	50 mM NaOAc buffer, pH 4.74	387
183		7.58	NMR	Measured by competition with 	106
184		5.46	FL	298 K, phosphate buffer (pH=7.0) and 0.1 M NaCl	390
185		7.71	NMR	Measured by competition with 	106

Table 5. continued

Entry	CB[7] guest	log K	method	measurement conditions	ref
186		7.95	NMR	Measured by competition with	106
187		7.95	UV	50 mM NaOAc buffer, pH 4.74	387
188		8.31	NMR	Measured by competition with	106
189		8.51	NMR	Measured by competition with	106
190		8.95	NMR	Measured by competition with	106
191		9.26	NMR	Measured by competition with	106
192		9.25	UV	50 mM NaOAc buffer, pH 4.74	387
193		12.23	NMR	Measured by competition with	106
194		12.62	NMR	Measured by competition with	106
195		11.63	UV	50 mM NaOAc buffer, pH 4.74	387
196		12.29	NMR	Measured by competition with	106
197		4.88	ITC	298 K	391
198		5.48	ITC	298 K	391
199		6.35	ITC	298 K	391

Table 5. continued

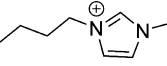
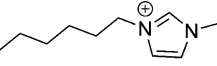
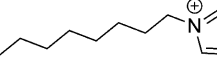
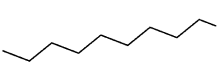
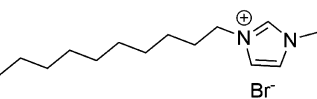
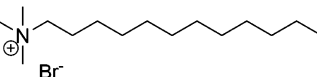
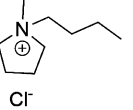
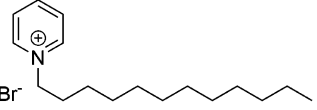
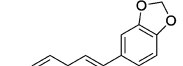
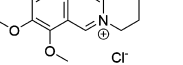
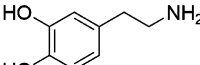
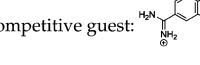
Entry	CB[7] guest	log K	method	measurement conditions	ref
200		6.84	ITC	Br ⁻ counter ion, 298 K	391
201		6.82	ITC	Cl ⁻ counter ion, 298 K	392
202		6.88	ITC	BF ₄ ⁻ counter ion, 298 K	392
203		6.88	ITC	PF ₆ ⁻ counter ion, 298 K	392
204		7.31	ITC	Br ⁻ counter ion, 298 K	391
205		6.92	ITC	Br ⁻ counter ion, 298 K	392
206		7.30	ITC	Cl ⁻ counter ion, 298 K	392
207		7.04	ITC	Br ⁻ counter ion, 298 K	391
208		6.15	ITC	Cl ⁻ counter ion, 298 K	392
209		6.95	ITC	Cl ⁻ counter ion, 298 K	392
210		6.74	ITC	298 K	391
211	Br ⁻	6.72	ITC	298 K	392
212		6.46	ITC	298 K	391
213		6.16	ITC	298 K	391
214	Br ⁻	5.93	ITC	298 K	392
215		6.46	ITC	298 K	392
216		6.08	ITC	298 K	391
217	Br ⁻	5.77	ITC	298 K	392
218		7.55	ITC	298 K	392
219		5.90	ITC	298 K	392
220		6.20	FL	-	393
221		5.29	FL	0.05 M NaCl	393
222	Cl ⁻	5.50	FL	0.05 M NaI	393
223		5.51	FL	Phosphate buffer 0.05 M Na ⁺	393
224		5.00	FL	competitive guest:  + HCl, 296 K	392
225		5.66	ITC	water	98

Table 5. continued

Entry	CB[7] guest	log K	method	measurement conditions	ref
226		4.24	ITC	water	98
227		4.83	ITC	water	98
228		7.04	FL, UV, NMR	Mean value obtained by three independent methods	392
229		6.49	FL	-	394
230		4.52	UV	citrate buffer solution (0.10 M, pH 6.0) at 298 K	395
231		5.08	FL	-	396
232		4.95	UV	0.2 M NaCl, 298 K	396
233		19.65, 4.91 per step (4 binding sites)	FL	-	397
234		2.53	NMR	0.1 M phosphate buffer (pH 7)	389
235		3.84	UV	citrate buffer solution (0.10 M, pH 6.0) at 298 K	395
236		3.84	UV	citrate buffer solution (0.10 M, pH 6.0) at 298 K	395

Table 5. continued

Entry	CB[7] guest	log K	method	measurement conditions	ref
237		3.70	UV	citrate buffer solution (0.10 M, pH 6.0) at 298 K	395
238		12.62	NMR	NaO ₂ CCD ₃ (50 mM) buffer, D ₂ O, pH 4.74, room temperature	385
239		14.32	ITC	298 K	384
240		11.11	NMR	NaO ₂ CCD ₃ (50 mM) buffer, D ₂ O, pH 4.74, room temperature, competitive guest:	385
241		11.14	NMR	NaO ₂ CCD ₃ (50 mM) buffer, D ₂ O, pH 4.74, room temperature, competitive guest:	385
242		15.27	NMR	NaO ₂ CCD ₃ (50 mM) buffer, D ₂ O, pH 4.74, room temperature, competitive guest:	385
243		15.32	NMR	NaO ₂ CCD ₃ (50 mM) buffer, D ₂ O, pH 4.74, room temperature, competitive guest:	385
244		13.38	NMR	NaO ₂ CCD ₃ (50 mM) buffer, D ₂ O, pH 4.74, room temperature, competitive guest:	385
245		15.70	ITC	-	384
246		9.94	NMR	NaO ₂ CCD ₃ (50 mM) buffer, D ₂ O, pH 4.74, room temperature, competitive guest:	385
247		9.78	ITC	298 K	384

Table 5. continued

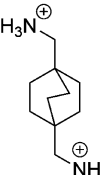
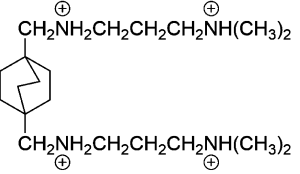
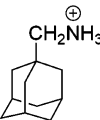
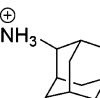
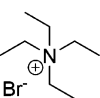
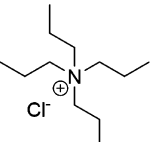
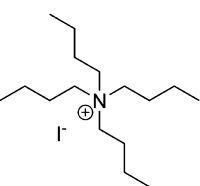
Entry	CB[7] guest	log K	method	measurement conditions	ref
248		14.30	ITC	298 K	384
249		15.08	ITC	298 K	384
250		10.36	ITC	298 K	384
251		14.88	ITC	298 K	384
252		14.00	ITC	298 K	384
253		5.08	NMR	From a competitive binding experiment using 1,2-phenylenediamine	398
254		6.00	NMR	From a competitive binding experiment using 1,4-phenylenediamine	398
255		3.95	NMR	From a competitive binding experiment using 1,2-phenylenediamine	398
256		3.44	NMR	From NMR chemical shift titration.	398

Table 5. continued

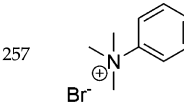
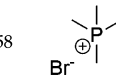
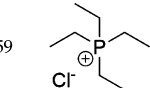
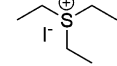
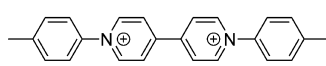
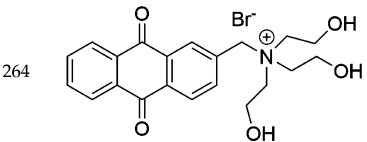
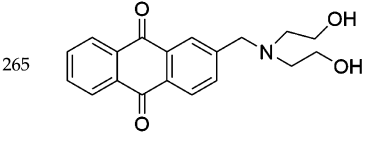
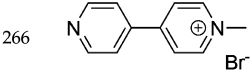
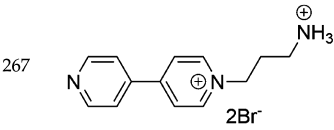
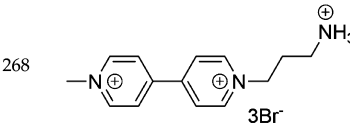
Entry	CB[7] guest	log K	method	measurement conditions	ref
257		8.39	NMR	From a competitive binding experiment with 3-trimethylsilylpropionic acid	398
258		6.34	NMR	From a competitive binding experiment using 1,4-phenylenediamine	398
259		5.11	NMR	From a competitive binding experiment using 1,4-phenylenediamine	398
260		4.53	NMR	From a competitive binding experiment using 1,2-phenylenediamine	398
261		6.71	NMR	From a competitive binding experiment using 1,4-phenylenediamine	398
262	 2Cl ⁻	4.08	NMR/UV	1:1 DTV:CB[7]	399
263		4.00	NMR/UV	1:2 DTV:CB[7]	399
264		3.11	NMR	298 K, 0.01 M DCI	400
265		3.44	NMR	298 K, 0.01 M DCI	400
266		6.08	ITC	10 mM sodium phosphate, pH 7.0, 300 K	161
267		6.63	ITC	10 mM sodium phosphate, pH 7.0, 300 K	161
268		7.14	ITC	10 mM sodium phosphate, pH 7.0, 300 K	161

Table 5. continued

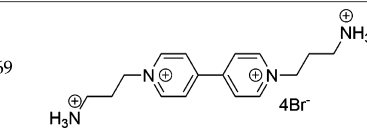
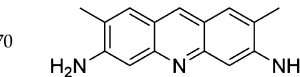
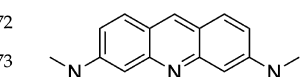
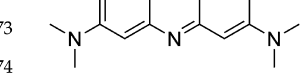
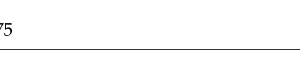
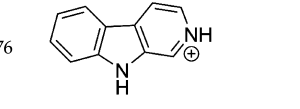
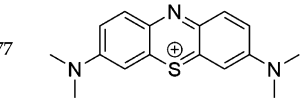
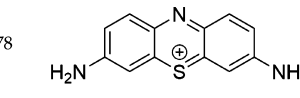
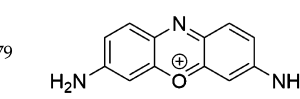
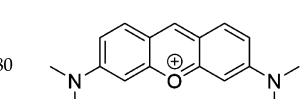
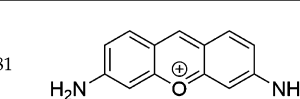
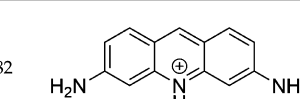
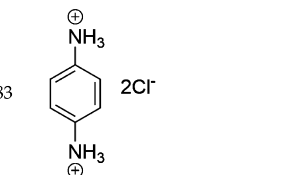
Entry	CB[7] guest	log K	method	measurement conditions	ref
269		7.08	ITC	10 mM sodium phosphate, pH 7.0, 300 K	161
270		4.09	FL	1:1 Acridine yellow:CB[7]	401
271		4.23	FL	300 K	402
272		4.10	FL	313 K	402
273		3.92	FL	323 K	402
274		3.75	FL	333 K	402
275		6.08	FL	-	403
276		4.95	UV	pH 5	404
277		7.10	FL		403
278		7.13	FL		403
279		7.08	FL		403
280		6.66	FL		403
281		7.16	FL		403
282		7.23	FL		403
283		4.30	NMR		405

Table 5. continued

Entry	CB[7] guest	log K	method	measurement conditions	ref
284		4.30	NMR	Competitive guest:	405
285		5.52	NMR	Competitive guest:	405
286		5.55	NMR	Competitive guest:	405
287		5.76	NMR	Competitive guest:	405
288		5.81	NMR	Competitive guest:	405
289		6.17	NMR	Competitive guest:	405
290		6.25	NMR	Competitive guest:	405
291		6.25	NMR	Competitive guest:	405
292		7.04	NMR	Competitive guest:	405
293		7.23	NMR	Competitive guest:	405

Table 5. continued

Entry	CB[7] guest	log K	method	measurement conditions	ref
294		7.38	NMR	Competitive guest: 	405
295		8.11	NMR	Competitive guest: 	405
296		8.25	NMR	Competitive guest: 	405
297		8.49	NMR	Competitive guest: 	405
298		8.66	NMR	Competitive guest: 	405
299		8.66	NMR	Competitive guest: 	405
300		9.71	NMR	Competitive guest: 	405
301		10.32	NMR	Competitive guest: 	405
302		6.30	ITC	-	406
303		<2.47	FL	Lower limit, no detectable binding (<3%) was observed.	176
304		4.11	FL		176

Table 5. continued

Entry	CB[7] guest	log K	method	measurement conditions	ref
305		2.92	FL		176
306		1	FL		176
307		6.17	FL		176
308		3.55	FL		176
309		8.04	FL		176
310		5.00	FL		176
311		2.85	FL		176
312		7.08	FL		176
313		4.38	FL		176
314		3.92	FL		176
315		1.69	FL		176

Table 5. continued

Entry	CB[7] guest	log K	method	measurement conditions	ref
316		5.16	NMR		
317		>6	ITC	pH 2	407
318		>5	ITC	pH 4	407
319		>5	ITC	pH 7	407
320		5.93	UV	-	408
321		6.24	ITC	298 K	376
322		>5.00	ITC	pH 2	407
323		>4.00	ITC	pH 4	407
324		>2.00	ITC	pH 7	407
325		2.90	ITC	10 mM NH4OAc, pH 6, 303 K	409
326		2.93	FL	10 mM NH4OAc, pH 6, 298 K	409
327		>5.00	ITC	pH 2	407
328		>2.00	ITC	pH 4	407
329		2.52	ITC	10 mM NH4OAc, pH 6, 303 K	409
330		2.49	FL	10 mM NH4OAc, pH 6, 298 K	409
331		>3.00	ITC	pH 2	407
332		>2.00	ITC	pH 4	407
333		1.90	UV	-	408
334		2.60	FL	10 mM NH4OAc, pH 6, 298 K	409
335		2	UV	-	408
336		2.43	UV	-	408
337		2.64	UV	-	408
338		2.17	UV	-	408
339		1.55	UV	-	408
340		>5.00	ITC	pH 2	407
341		>4.00	ITC	pH 4	407
342		>4.00	ITC	pH 7	407
343		5.36	UV	-	408
344		4.34	ITC	10 mM NH4OAc, pH 6, 303 K	409
345		4.38	FL	10 mM NH4OAc, pH 6, 298 K	409

Table 5. continued

Entry	CB[7] guest	log K	method	measurement conditions	ref
346		>3.00	ITC	pH 2	407
347		>3.00	ITC	pH 4	407
348		>3.00	ITC	pH 7	407
349		5.57	UV	-	408
350		3.27	ITC	10 mM NH ₄ OAc, pH 6, 303 K	409
351		3.20	FL	10 mM NH ₄ OAc, pH 6, 298 K	409
352		4.54	NMR	pD 4.75, competitive guest: 1,2-phenylenediamine	410
353		5.64	NMR	pD 1.0, competitive guest: (trimethylsilyl)propionic acid	410
354		4.17	NMR	pD 4.75, competitive guest: 1,2-phenylenediamine	410
355		6.04	NMR	pD 1.0, competitive guest: (trimethylsilyl)propionic acid	410
356		4.89	NMR	pD 4.75, competitive guest: 1,2-phenylenediamine	410
357		4.74	NMR	pD 1.0, competitive guest: (trimethylsilyl)propionic acid	410
358		5.25	NMR	pD 4.75, competitive guest: 1,2-phenylenediamine	410
359		7.04	NMR	pD 1.0, competitive guest: (trimethylsilyl)propionic acid	410
360		4.41	NMR	pD 4.75, competitive guest: 1,2-phenylenediamine	410
361		4.32	NMR	pD 1.0, competitive guest: (trimethylsilyl)propionic acid	410
362	(CH ₃) ₃ N(CH ₂) ₂ OH ⁺	5.81	NMR	competitive guest: 1,4-phenylenediamine	411
363	(CH ₃) ₃ N(CH ₂) ₂ O ₂ CCH ₃ ⁺	5.84	NMR	competitive guest: 1,4-phenylenediamine	411
364	(CH ₃) ₃ NCH ₂ CH(CH ₃)O ₂ CCH ₃ ⁺	6.69	NMR	competitive guest: TMSP	411
365	(CH ₃) ₃ N(CH ₂) ₂ O ₂ C(CH ₂) ₂ CH ₃ ⁺	7.23	NMR	competitive guest: 1,4-phenylenediamine	411
366	(CH ₃) ₃ N(CH ₂) ₁₁ CH ₃	4.76	NMR	-	411
367	(CH ₃) ₃ N ⁺ CH ₂ CH(OH)CH ₂ CO ₂ ⁻	2.57	NMR	pD 7.0	411
368	(CH ₃) ₃ NCH ₂ CH(OH)CH ₂ CO ₂ H ⁺	4.90	NMR	D ₂ O	411
369	(CH ₃) ₃ N ⁺ (CH ₂) ₂ OP(O)(OH)O ⁻	3.08	NMR	D ₂ O	411
370	(PhCH ₂)(CH ₃) ₂ N(CH ₂) ₂ OH ⁺	8.61	NMR	competitive guest: TMSP	411
371	(CH ₃ CH ₂) ₃ N(CH ₂) ₂ OH ⁺	6.25	NMR	competitive guest: TMSP	411
372	(CH ₃ CH ₂) ₃ N(CH ₂) ₄ CH ₃ ⁺	5.92	NMR	competitive guest: NEt ₄ ⁺	411
373	Quin(CH ₂) ₂ OH ⁺	9.11	NMR	competitive guest: p-xylylenediamine	411

Table 5. continued

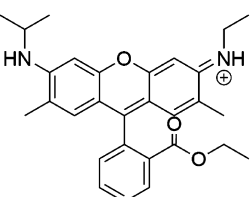
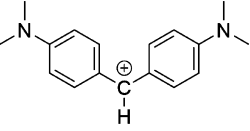
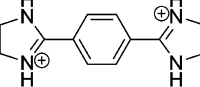
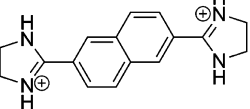
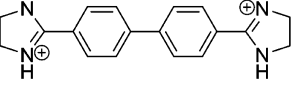
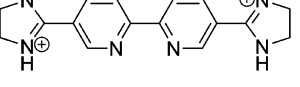
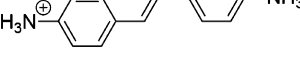
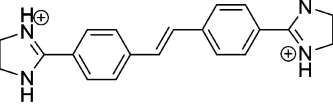
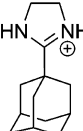
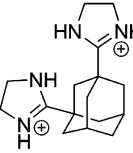
Entry	CB[7] guest	log K	method	measurement conditions	ref
374	(CH ₃) ₃ P(CH ₂) ₄ CH ₃ ⁺	7.14	NMR	competitive guest: 1,4-phenylenediamine	411
375	(CH ₃) ₃ P(CH ₂) ₂ OH ⁺	6.83	NMR	competitive guest: NEt ₄ ⁺	411
376	(CH ₃) ₃ P(CH ₂) ₂ O ₂ CCH ₃ ⁺	5.95	NMR	competitive guest: 1,4-phenylenediamine	411
377	(CH ₃ CH ₂) ₃ P(CH ₂) ₄ CH ₃ ⁺	6.20	NMR	competitive guest: NEt ₄ ⁺	411
378	(CH ₃ CH ₂) ₃ P(CH ₂) ₂ OH ⁺	5.11	NMR	competitive guest: NEt ₄ ⁺	411
379	(CH ₃ CH ₂) ₃ P(CH ₂) ₂ O ₂ CCH ₃ ⁺	5.93	NMR	competitive guest: 1,4-phenylenediamine	411
380	(CH ₃ CH ₂) ₃ P(CH ₂) ₂ O ₂ CCH ₃ ⁺	5.93	NMR	competitive guest: 1,4-phenylenediamine	411
381		4.69	UV	-	207
382		4.30	UV	pH 7	412
383		9.71	NMR	competitive guest: sodium (trimethylsilyl)propionate-2,2,3,3-d ₄	3- 413
384		10.78	NMR	competitive guest: (trimethylammonio) methyl-ferrocene iodide	413
385		8.23	NMR	competitive guest: sodium (trimethylsilyl)propionate-2,2,3,3-d ₄	3- 413
386		7.95	NMR	competitive guest: sodium (trimethylsilyl)propionate-2,2,3,3-d ₄	3- 413
387		5.52	UV	trans-form	414
388		5.08	V-Vis titration	cis-form	414
389		8.74	NMR	competitive guest: sodium (trimethylsilyl)propionate-2,2,3,3-d ₄	3- 413

Table 5. continued

Entry	CB[7] guest	log K	method	measurement conditions	ref
390		8.14	NMR	competitive guest: sodium (trimethylsilyl)propionate-2,2,3,3-d4	3- 413
391		4.00	NMR	competitive guest: sodium (trimethylsilyl)propionate-2,2,3,3-d4	3- 413

^aAbbreviations: ITC, isothermal titration calorimetry; UV-vis, ultraviolet/visible spectroscopy; NMR, nuclear magnetic resonance spectroscopy; ESI-MS, electrospray ionization-mass spectrometry; SORI, sustained off-resonance irradiation (mass spectroscopy); FL, fluorimetry; EPR, electron paramagnetic resonance; EAS, electronic absorbance spectroscopy.

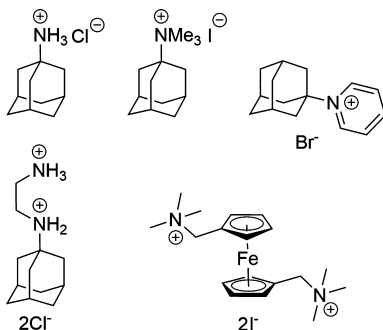


Figure 10. Examples of first guests with high binding constants for CB[7].

contrary, all methylene proton signals are shifted when in the presence of CB[8], suggesting that the larger width of the CB[8] cavity allows the aliphatic chain to form a U-shape so that the entire guest can be encapsulated. The U-shaped conformation of the guest inside the cavity of CB[8] was supported by X-ray crystal structures and ROESY NMR. The authors suggested that van der Waals contact between the hydrophobic chain and the cavity can be the main cause of the significantly large enthalpic gain overcompensating the entropic penalty associated with the conformational restriction of the U-shaped aliphatic chain. It has been nevertheless suggested that dispersion interactions inside the CB[n] cavity do not present a significant enthalpic driving force for guest inclusion.³⁵ Other doubly charged alkylammonium salts including 1,4-butylidene and 1,10-decyldenedipyridinium (C16 and C17 in Figure 11) and 1,12-dodecane diammonium (C18 in Figure 11), in the presence of 1 equiv of CB[8], also exhibit the previously described U-shaped folding of C10–C15.^{116,117} In the case of C18, both charged groups bind to the same CB[8] portal with one water molecule bridging the two ammonium groups.

The encapsulation of nitroxide derivatives inside CB[8] has recently been described on several occasions by Kaifer, Lucarini, Tordo, Ouari, Turro, Ramamurthy, and others.^{118–127} Lucarini and co-workers reported in 2009 the encapsulation of an amino-TEMPO nitroxide derivative, C19, inside CB[8] and observed changes in the nitrogen hyperfine splitting by electron paramagnetism resonance (EPR), which were attributed to the formation of a host–guest complex.¹¹⁸ Furthermore, cooling of an aqueous solution of CB[8]·C19

from room temperature to 5 °C led to the formation of a macroscopic fibrous network, which exhibited the characteristic EPR spectrum of a polyyradical (solid fibers). The authors suggested the formation of the supramolecular ternary radical CB[8]₃·C19₃ to explain the EPR spectrum of the fibers dissolved in a NaCl (1 mM) aqueous solution at room temperature. The existence of a supramolecular ternary radical was demonstrated by Tordo, Ouari, and co-workers, who used nitroxide C20 as a probe to investigate the binding properties of CB[8].¹¹⁹ These authors established the concentration-dependent aggregation behavior of CB[7]·C20 and CB[8]·C20 and the formation of a CB[8]₃·C20₃ trinitroxide supraradical both in solution and in the solid state. Similar conclusions were obtained by Turro, Ramamurthy, and co-workers after investigating the interactions between CB[8] and nitroxides C21–C23.¹²⁰ Kaifer and co-workers investigated the interaction between CB[n] and a series of cobaltocenium and ferrocene derivatives incorporating nitroxide units into their structures (see C24–C28 in Figure 11).^{121–123} Nitroxide derivative C24 exhibits a bimodal binding interaction with CB[7] and CB[8]. While CB[7] prefers to bind to the cobaltocenium group, CB[8] interacts with the nitroxide group, forming a highly stable host–guest complex (see Table 6). On the other hand, C25 contains two nitroxide radicals, thus allowing the quantitative formation of a ternary CB[8]₂·C25 host–guest complex at micromolar concentrations. The binding of CB[8] imparts rigidity to the final supramolecular structure and effectively hinders any spin exchange coupling, which results in a simple three-line EPR spectrum of the complex. The ternary complex was even characterized by solid state by X-ray diffraction. Tordo and co-workers recently reported the reversible modulation of the spin exchange interaction in tetranitroxide C29 controlled by the allosteric complexation of CB[8].¹²⁴ Addition of CB[8] to an aqueous solution of C29 transforms the nine-line spectrum of the tetranitroxide into a three-line spectrum characteristic of a mononitroxide. The noncovalent interaction between CB[8] and C29 involves a highly cooperative asymmetric complexation ($\log K_1 = 3.60 \text{ M}$; $\log K_2 = 5.30$; $\alpha = 201$) whereby two CB[8] molecules bind tightly to a single C29 guest, leading to a rigid complex with remote nitroxide moieties. The authors attribute the high allosteric interaction energy ($\Delta\Delta G_{\text{allo}} \cdot \text{C29} \approx 13 \text{ kJ}\cdot\text{mol}^{-1}$) to a combination of different factors including the preorganized skeleton of the multivalent guest which is multiply

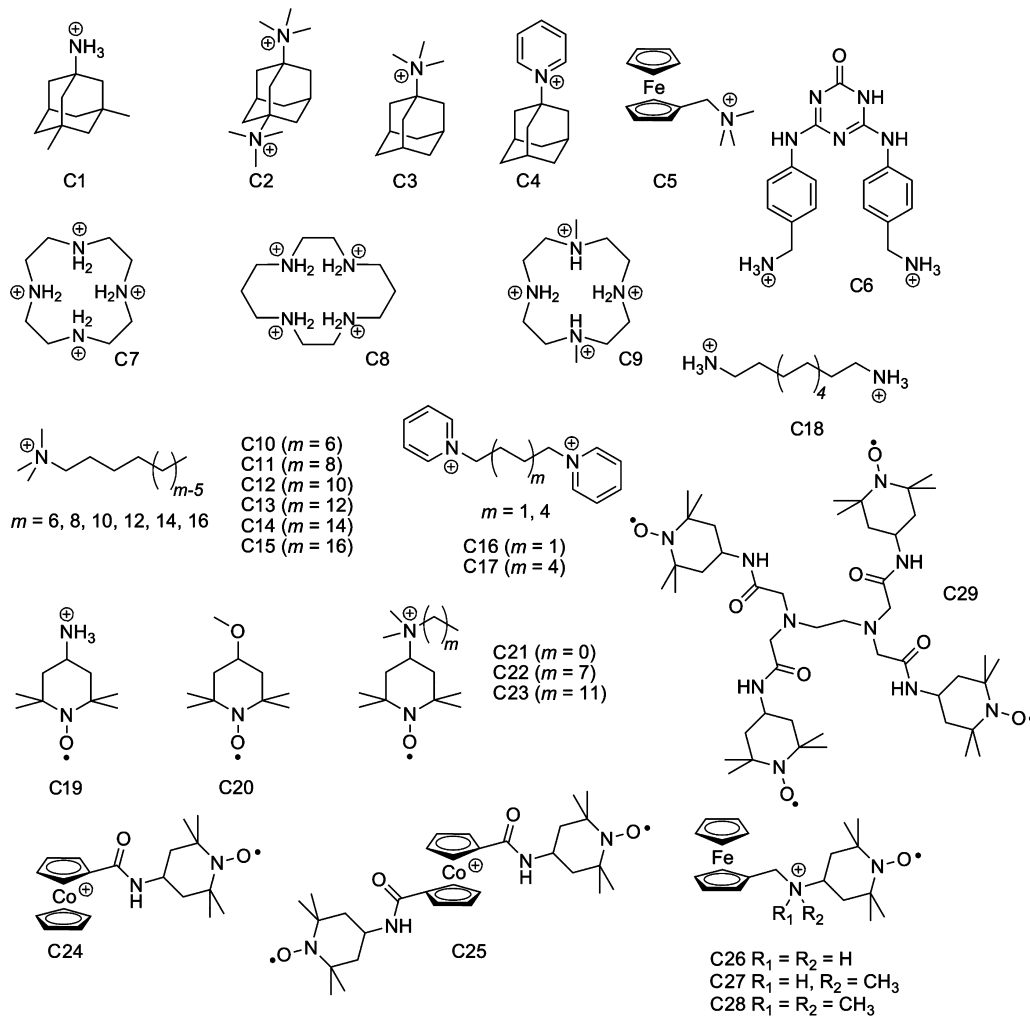


Figure 11. Selected guests for CB[8].

H-bond donating, a potential CB[8]-induced shift of the pK_a of the internal amines, and the intrinsic conformational properties of **C29**. The binding of the first CB[8] molecule in this instance induces a large conformational change in the guest, which favors the binding of the second CB[8] molecule.

Although the smaller homologues of the CB[n] family can bind only one guest inside the cavity, CB[8] is unique in its ability to bind two guests, as has been shown by Kim and others.^{128–132} This rather unique binding property has been exploited in a wide variety of applications including novel supramolecular polymeric materials,^{133–135} catalysis,^{20,136–138} and sensing.^{98,139–141} CB[8] promotes (hetero)dimerization of two π systems in aqueous solution, and Kim and co-workers have shown that CB[8]-C30 can bind to a variety of other aromatic guests including 2,6-dihydroxynaphthalene, 1,4-dihydroxybenzene, tyrosine, dopamine and thymine, phenylalanine, tryptophan, tryptophan derivatives, and tryptophan-containing peptides.^{128,129,142} On the basis of this concept, a CB[8] heteroternary complexation strategy to the reversible PEGylation of bovine serum albumin and protein–protein dimer formation was developed by Scherman and co-workers.¹⁴³ Brunsved and co-workers also exploited this concept in protein–protein binding and protein-to-surface attachment by using methylviologen and naphthalene-functionalized fluorescent proteins and CB[8].^{144,145}

Scherman and co-workers studied in detail the equilibria of a series of ternary complexes based on CB[8]-C30 and a wide variety of aromatic second guest molecules by ITC and ESI-MS (see Table 8 and Figure 12). The binding constants were found to be between $\log K = 2.00$ and 6.00. An excellent agreement between solution-based titrations (ITC) and gas-phase studies was found when free energies of solvation are taken into consideration.¹⁴⁶ Kaifer and co-workers reported the formation of CB[8] ternary complexes between 2,7-dimethyldiazapyrenium, as first guest, and catechol and dopamine as second guests.¹⁴⁷ In an analogous fashion, 2,7-dimethyldiazaphenanthrenium can also form ternary complexes in the presence of CB[8] with tryptophan and serotonin.¹³² Scherman and co-workers also identified a group of doubly charged molecules as potential alternatives that increase the repertoire of first guests for CB[8]. These include tetramethylbenzobis(imidazolium),¹⁴⁸ aryl-bisimidazolium salts,¹⁴⁹ aryl viologen derivatives,⁴² and water-soluble perylene bis(diimides).¹⁵⁰ The binding of dicationic dyes such as 2,7-dimethyldiazapyrenium, as first guest to CB[8], has been cleverly used by Biedermann, Nau, and co-workers to construct a chirality sensor and peptide-sequence recognition system at micromolar analyte concentrations.^{45,151}

Alternatively to the previously mentioned heteroternary complexes, a number of guests have been shown to undergo double encapsulation into CB[8] including naphthyl deriva-

Table 6. Association Constants Reported for CB[8] First Guests^a

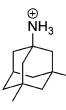
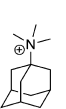
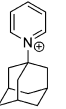
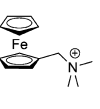
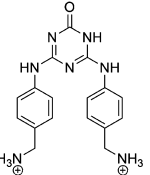
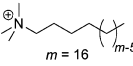
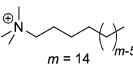
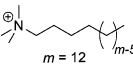
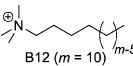
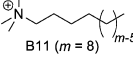
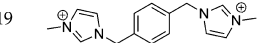
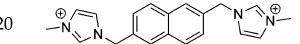
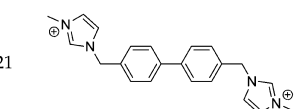
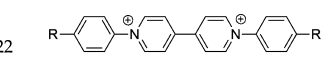
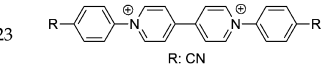
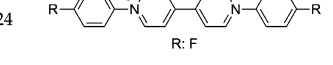
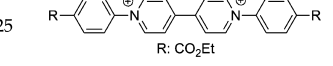
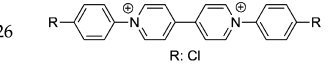
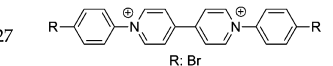
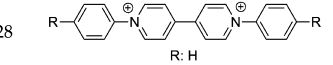
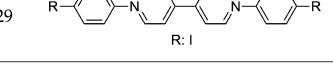
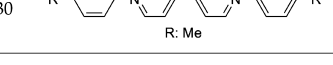
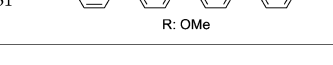
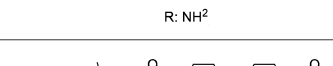
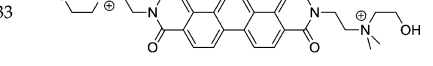
Entry	guest	log K	method	conditions	ref
392		11.63	NMR	Measured by competition with melamine-derived guest for limiting quantity of CB[8] at 298 K. 50 mM NaO ₂ CCD ₃ -buffered D ₂ O (pD 4.74)	¹⁰⁶
393		11.04	NMR	Measured by competition with melamine-derived guest for limiting quantity of CB[8] at 298 K. 50 mM NaO ₂ CCD ₃ -buffered D ₂ O (pD 4.74)	¹⁰⁶
394		10.98	NMR	Measured by competition with melamine-derived guest for limiting quantity of CB[8] at 298 K. 50 mM NaO ₂ CCD ₃ -buffered D ₂ O (pD 4.74)	¹⁰⁶
395		9.30	NMR	Measured by competition with melamine-derived guest for limiting quantity of CB[8] at 298 K. 50 mM NaO ₂ CCD ₃ -buffered D ₂ O (pD 4.74)	¹⁰⁶
396		9.49	NMR	Measured by competition with melamine-derived guest for limiting quantity of CB[8] at 298 K. 50 mM NaO ₂ CCD ₃ -buffered D ₂ O (pD 4.74)	¹⁰⁶ re- ported by kaifer
397		10.77	NMR	Measured by competition with amantadine hydrochloride for limiting quantity of CB[8] at 298 K. 50 mM NaO ₂ CCD ₃ -buffered D ₂ O (pD 4.74)	¹⁰⁶
398		6.00	ITC	50 mM NaO ₂ CCH ₃ -buffered H ₂ O	¹¹⁵
399		6.17	ITC	50 mM NaO ₂ CCH ₃ -buffered H ₂ O	¹¹⁵
400		6.44	ITC	50 mM NaO ₂ CCH ₃ -buffered H ₂ O	¹¹⁴
401		6.68	ITC	50 mM NaO ₂ CCH ₃ -buffered H ₂ O	¹¹⁵
402		6.00	ITC	50 mM NaO ₂ CCH ₃ -buffered H ₂ O	¹¹⁵

Table 6. continued

Entry	guest	log K	method	conditions	ref
403		5.58	ITC	50 mM NaO ₂ CCH ₃ -buffered H ₂ O	115
404		5.58	UV	-	116
405		5.17	UV	-	116
406		6.04	ITC	50 mM NaO ₂ CCH ₃ -buffered H ₂ O	117
407		3.11	ITC	50 mM NaO ₂ CCH ₃ -buffered H ₂ O	119
408		8.32	UV Competitive binding experiment with amantadine	0.1 M NaCl	121
409		$K_1=3.60$	EPR titration	H ₂ O	124
410		$K_2=5.30$	EPR titration	H ₂ O	124
411		$K_3=2.20$	EPR titration	H ₂ O	124
412		5.04	Potentiometric titration	H ₂ O	142
413		4.68	Fluorescence titration	-	389
414		8.80	NMR	Measured by competition between CB[7], CB[8], and 2,7-dimethyldiazapyrenium diiodide. 50 mM NaO ₂ CCD ₃ -buffered D ₂ O	106
415		5.95	-	147	
416		5.92	-	147	
417		5.00	UV/FL	0.1 M sodium phosphate, pH 7.0	132
418		5.75	ITC	10 mM sodium phosphate, pH 7.0	148

Table 6. continued

Entry	guest	log K	method	conditions	ref
419		6.28	ITC	10 mM sodium phosphate, pH 7.0	149
420		6.55	ITC	10 mM sodium phosphate, pH 7.0	149
421		5.30	ITC	10 mM sodium phosphate, pH 7.0	149
422	 R: NO ₂	5.47	ITC	10 mM sodium phosphate, pH 7.0	42
423	 R: CN	5.83	ITC	10 mM sodium phosphate, pH 7.0	42
424	 R: F	5.46	ITC	10 mM sodium phosphate, pH 7.0	42
425	 R: CO ₂ Et	5.97	ITC	10 mM sodium phosphate, pH 7.0	42
426	 R: Cl	3.96	ITC	10 mM sodium phosphate, pH 7.0	42
427	 R: Br	5.25	ITC	10 mM sodium phosphate, pH 7.0	42
428	 R: H	4.36	ITC	10 mM sodium phosphate, pH 7.0	42
429	 R: I	5.32	ITC	10 mM sodium phosphate, pH 7.0	42
430	 R: Me	<3.00	ITC	10 mM sodium phosphate, pH 7.0	42
431	 R: OMe	3.11	ITC	10 mM sodium phosphate, pH 7.0	42
432	 R: NH ²	3.46	ITC	10 mM sodium phosphate, pH 7.0	42
433		5.30	ITC	H ₂ O	150

^aAbbreviations: ITC, isothermal titration calorimetry; UV-vis, ultraviolet/visible spectroscopy; NMR, nuclear magnetic resonance spectroscopy; ESI-MS, electrospray ionization-mass spectrometry; SORI, sustained off-resonance irradiation (mass spectroscopy); FL, fluorimetry; EPR, electron paramagnetic resonance; EAS, electronic absorbance spectroscopy.

Table 7. Association Constants Reported for Homodimers with CB[8]^a

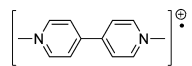
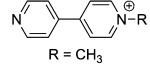
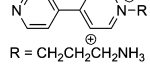
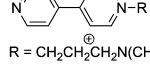
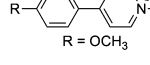
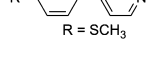
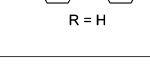
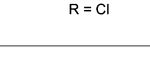
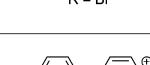
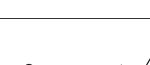
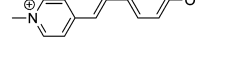
Entry	guest	log K	method	conditions	ref
434		7.30	Spectroelectrochemical experiments	Solvent: H ₂ O	142
435	H_3N^+ -Phe-Gly-Gly-COO ⁻	11.17	-	Sodium phosphate, 10 mM, pH 7.0	165
436	H_3N^+ -Trp-Gly-Gly-COO ⁻	9.55	-	Sodium phosphate, 10 mM, pH 7.0	165
437	H_3N^+ -Ala-Glu-Phe-Arg-His-CONH ₂	10.56	-	Sodium phosphate, 10 mM, pH 7.4	164
438	H_3N^+ -Leu-Val-Phe-Ile-Ala-CONH ₂	9.88	-	Sodium phosphate, 10 mM, pH 7.4	164
439	H_3N^+ -Val-Ile-Phe-Ala-Glu-CONH ₂	13.20	-	Sodium phosphate, 10 mM, pH 7.4	164
440		10.23	-	Sodium phosphate, 10 mM, pH 7.0	161
441		11.08	-	Sodium phosphate, 10 mM, pH 7.0	161
442		10.95	-	Sodium phosphate, 10 mM, pH 7.0	161
443		12.53	ITC	Tris-buffer solution, 10 mM, pH 7.0	160
444		12.54	ITC	Tris-buffer solution, 10 mM, pH 7.0	160
445		13.64	ITC	Tris-buffer solution, 10 mM, pH 7.0	160
446		13.47	ITC	Tris-buffer solution, 10 mM, pH 7.0	160
447		14.11	ITC	Tris-buffer solution, 10 mM, pH 7.0	160
448		12.34	ITC	Tris-buffer solution, 10 mM, pH 7.0	160
449		4.58	ITC	Formic acid-water (2:3)	343
450		8.00 (minimum value estimated)	UV	H ₂ O	159

Table 8. Association Constants Reported for Heteroternary Complexes with CB[8]^a

Entry	first guest	second guest	log K	method	conditions	ref
465			4.63	ITC	10 mM sodium phosphate, pH 7.0	¹³⁰
466			3.72	ITC	10 mM sodium phosphate, pH 7.0	¹³⁰
467			3.34	ITC	10 mM sodium phosphate, pH 7.0	¹³⁰
468			4.80	ITC	10 mM sodium phosphate, pH 7.0	¹³⁰
469			4.73	ITC	10 mM sodium phosphate, pH 7.0	¹³⁰
470			3.49	ITC	10 mM sodium phosphate, pH 7.0	¹³⁰
471			3.36	ITC	10 mM sodium phosphate, pH 7.0	¹³⁰
472	H ₃ N ⁺ -Trp-Gly-Gly-COO ⁻		5.11	ITC	10 mM sodium phosphate, pH 7.0	¹³⁰
473	H ₃ N ⁺ -Gly-Trp-Gly-COO ⁻		4.32	ITC	10 mM sodium phosphate, pH 7.0	¹³⁰
474	H ₃ N ⁺ -Gly-Gly-Trp-COO ⁻		3.49	ITC	10 mM sodium phosphate, pH 7.0	¹³⁰
475	H ₃ N ⁺ -Gly-Gly-Trp-Gly-Gly-COO ⁻		4.40	ITC	10 mM sodium phosphate, pH 7.0	¹³⁰
476			5.83	ITC	10 mM sodium phosphate, pH 7.0	¹⁴⁶
477			5.79	ITC	10 mM sodium phosphate, pH 7.0	¹⁴⁶
478			5.77	ITC	10 mM sodium phosphate, pH 7.0	¹⁴⁶

Table 8. continued

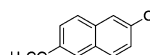
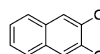
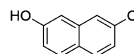
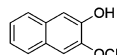
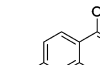
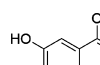
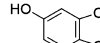
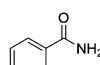
Entry	first guest	second guest	log K	method	conditions	ref
479			5.70	ITC	10 mM sodium phosphate, pH 7.0	146
480			5.60	ITC	10 mM sodium phosphate, pH 7.0	146
481			5.51	ITC	10 mM sodium phosphate, pH 7.0	146
482			5.20	ITC	10 mM sodium phosphate, pH 7.0	146
483			5.20	ITC	10 mM sodium phosphate, pH 7.0	146
484			5.11	ITC	10 mM sodium phosphate, pH 7.0	146
485			4.90	ITC	10 mM sodium phosphate, pH 7.0	146
486			4.88	ITC	10 mM sodium phosphate, pH 7.0	146
487			4.78	ITC	10 mM sodium phosphate, pH 7.0	146
488			4.73	ITC	10 mM sodium phosphate, pH 7.0	146
489			4.34	ITC	10 mM sodium phosphate, pH 7.0	146
490			4.32	ITC	10 mM sodium phosphate, pH 7.0	146
491			4.11	ITC	10 mM sodium phosphate, pH 7.0	146
492			4.11	ITC	Solvent: 10 mM sodium phosphate, pH 7.0	146

Table 8. continued

Entry	first guest	second guest	log K	method	conditions	ref
493			4.11	ITC	10 mM sodium phosphate, pH 7.0	¹⁴⁶
494			4.04	ITC	10 mM sodium phosphate, pH 7.0	¹⁴⁶
495			4.00	ITC	10 mM sodium phosphate, pH 7.0	¹⁴⁶
496			3.96	ITC	10 mM sodium phosphate, pH 7.0	¹⁴⁶
497			3.83	ITC	10 mM sodium phosphate, pH 7.0	¹⁴⁶
498			3.81	ITC	10 mM sodium phosphate, pH 7.0	¹⁴⁶
499			3.81	ITC	10 mM sodium phosphate, pH 7.0	¹⁴⁶
500			3.72	ITC	10 mM sodium phosphate, pH 7.0	¹⁴⁶
501			3.72	ITC	10 mM sodium phosphate, pH 7.0	¹⁴⁶
502			3.70	ITC	10 mM sodium phosphate, pH 7.0	¹⁴⁶
503			3.63	ITC	10 mM sodium phosphate, pH 7.0	¹⁴⁶
504			3.62	ITC	10 mM sodium phosphate, pH 7.0	¹⁴⁶
505			3.51	ITC	10 mM sodium phosphate, pH 7.0	¹⁴⁶

Table 8. continued

Entry	first guest	second guest	log K	method	conditions	ref
506			3.28	ITC	10 mM sodium phosphate, pH 7.0	146
507			2.57	ITC	10 mM sodium phosphate, pH 7.0	146
508			4.16	ITC	-	221
509			5.62	FL	-	132
510			5.15	FL	-	132
511			6.04	FL	-	132
512			5.15	ITC	10 mM sodium phosphate, pH 7.0	148
513			4.86	ITC	10 mM sodium phosphate, pH 7.0	148
514			4.86	ITC	10 mM sodium phosphate, pH 7.0	148
515			4.18	ITC	10 mM sodium phosphate, pH 7.0	148
516			3.61	ITC	10 mM sodium phosphate, pH 7.0	148
517			5.26	ITC	10 mM sodium phosphate, pH 7.0	148
518			4.53	ITC	10 mM sodium phosphate, pH 7.0	148
519			3.62	ITC	10 mM sodium phosphate, pH 7.0	148

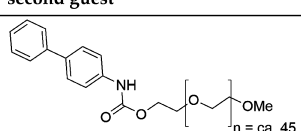
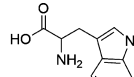
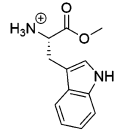
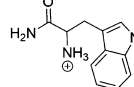
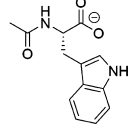
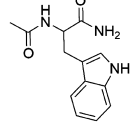
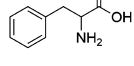
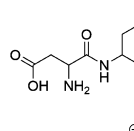
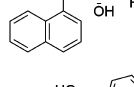
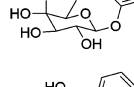
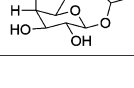
Table 8. continued

Entry	first guest	second guest	log K	method	conditions	ref
520		H ₃ N ⁺ -Trp-Gly-Gly-COO ⁻	5.08	ITC	10 mM sodium phosphate, pH 7.0	148
521		H ₃ N ⁺ -Gly-Trp-Gly-COO ⁻	4.23	ITC	10 mM sodium phosphate, pH 7.0	148
522		H ₃ N ⁺ -Gly-Gly-Trp-COO ⁻	3.61	ITC	10 mM sodium phosphate, pH 7.0	148
523			3.30	ITC	10 mM sodium phosphate, pH 7.0	149
524			3.00	ITC	10 mM sodium phosphate, pH 7.0	149
525		-C≡N	<3.00	ITC	10 mM sodium phosphate, pH 7.0	149
526			<3.78	ITC	10 mM sodium phosphate, pH 7.0	149
527			4.04	ITC	10 mM sodium phosphate, pH 7.0	149
528			4.49	ITC	10 mM sodium phosphate, pH 7.0	149
529			3.08	ITC	10 mM sodium phosphate, pH 7.0	149
530			3.59	ITC	10 mM sodium phosphate, pH 7.0	149
531			3.60	ITC	10 mM sodium phosphate, pH 7.0	149
532			4.11	ITC	10 mM sodium phosphate, pH 7.0	149
533			3.96	ITC	10 mM sodium phosphate, pH 7.0	149
534			4.32	ITC	10 mM sodium phosphate, pH 7.0	149
535			3.72	ITC	10 mM sodium phosphate, pH 7.0	149
536			3.865	ITC	10 mM sodium phosphate, pH 7.0	149
537			4.04	ITC	10 mM sodium phosphate, pH 7.0	149
538			5.48	ITC	H ₂ O	42

Table 8. continued

Entry	first guest	second guest	log K	method	conditions	ref
539			5.83	ITC	10 mM sodium phosphate, pH 7.0	42
540			5.46	ITC	H ₂ O	42
541			5.97	ITC	H ₂ O	42
542			4.97	ITC	H ₂ O	42
543			5.26	ITC	H ₂ O	42
544			4.36	ITC	H ₂ O	42
545			5.32	ITC	H ₂ O	42
546			<3.00	ITC	H ₂ O	42
547			3.11	ITC	H ₂ O	42
548			3.46	ITC	H ₂ O	42
549			5.70	ITC	H ₂ O	150
550			5.70	ITC	H ₂ O	150
551			5.70	ITC	H ₂ O	150
552			4.60	ITC	H ₂ O	150
553			4.60	ITC	H ₂ O	150

Table 8. continued

Entry	first guest	second guest	log K	method	conditions	ref
554			4.48	ITC	H ₂ O	150
555			5.20	ITC	H ₂ O	416
556			5.70	ITC	H ₂ O	416
557			5.66	ITC	H ₂ O	416
558			4.70	ITC	H ₂ O	416
559			5.04	ITC	H ₂ O	416
560		H ₃ N ⁺ -Trp-Pro-COO ⁻	4.70	ITC	H ₂ O	416
561		H ₃ N ⁺ -Glu-Pro-COO ⁻	4.40	ITC	H ₂ O	416
562			3.60	ITC	H ₂ O	416
563		H ₃ N ⁺ -Phe-Gly-COO ⁻	4.40	ITC	H ₂ O	416
564		H ₃ N ⁺ -Phe-Ala-COO ⁻	4.08	ITC	H ₂ O	416
565		H ₃ N ⁺ -Phe-Val-COO ⁻	4.04	ITC	H ₂ O	416
566		H ₃ N ⁺ -Val-Phe-COO ⁻	3.70	ITC	H ₂ O	416
567		H ₃ N ⁺ -Asp-Phe-COO ⁻	2.90	ITC	H ₂ O	416
568			2.90	ITC	H ₂ O	416
569			3.48	ITC	H ₂ O	416
570			5.04	ITC	H ₂ O	416
571			4.70	ITC	H ₂ O	416

^aAbbreviations: ITC, isothermal titration calorimetry; UV-vis, ultraviolet/visible spectroscopy; NMR, nuclear magnetic resonance spectroscopy; ESI-MS, electrospray ionization-mass spectrometry; SORI, sustained off-resonance irradiation (mass spectroscopy); FL, fluorimetry; EPR, electron paramagnetic resonance; EAS, electronic absorbance spectroscopy.

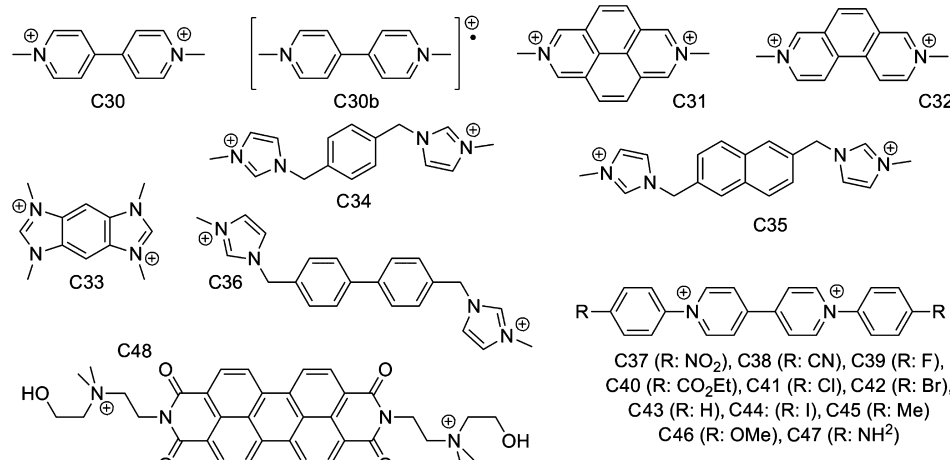


Figure 12. Selected guests for CB[8] that can act as a first guest for heteroternary complex formation.

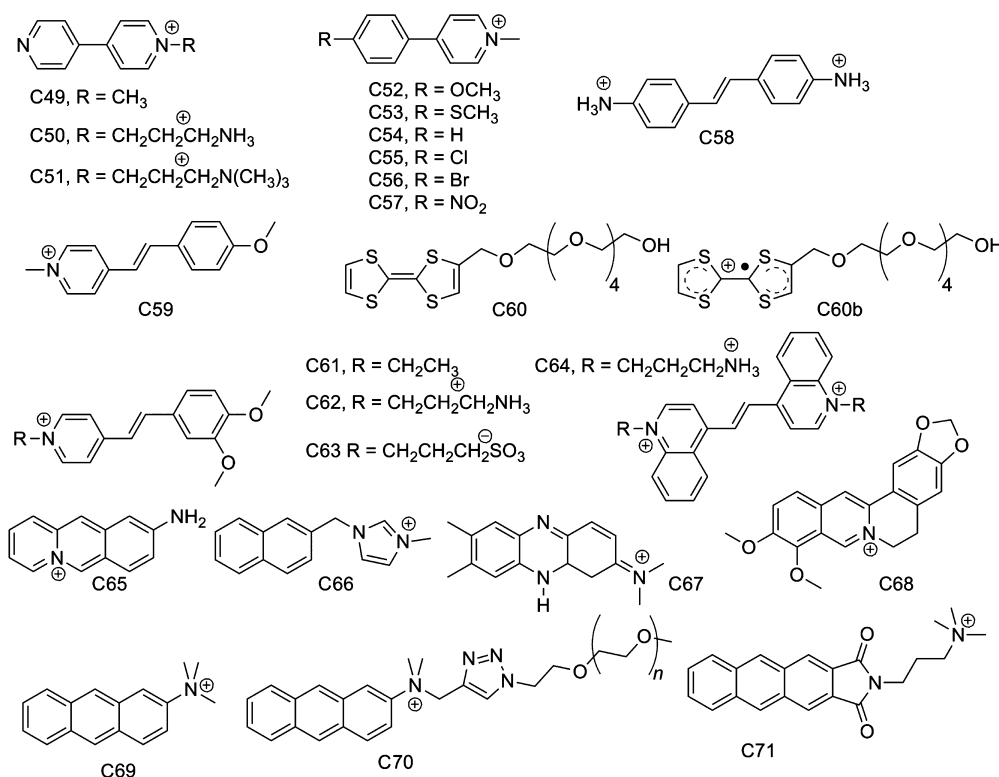


Figure 13. Selected guests for CB[8] that can undergo homodimerization.

tives,⁴ coumarin,¹⁵² *N*-phenylpiperazine,¹⁵³ 9-aminoacridinium,¹⁵⁴ neutral red,¹⁵⁵ 1-[2-methylnaphthalyl]-3-methylimidazolium,¹⁵⁶ berberine,¹⁵⁷ *p*-dimethylaminobenzonitrile,¹⁵⁸ phenylpyridinium derivatives,^{159,160} bipyridinium salts,¹⁶¹ anthracene derivatives,^{162,163} and some specific peptide sequences containing tryptophan or phenylalanine residues.^{164,165}

Some selected radical cations can also dimerize inside CB[8] in an analogous fashion to homodimer complexes. Kim and co-workers described that a high-affinity CB[8] homoternary complex can be produced when methyl viologen is reduced to its radical cation species.¹⁴² Kaifer and co-workers have shown that CB[8] can be used to exert redox control over the dimerization of dendrons. For instance, dendrons containing a dicationic viologen group at their focal point can form stable 1:1 inclusion complexes with CB[8].¹⁶⁶ Upon one-electron

reduction, the radical cation group of the dendron–viologen species forms a dimer inside the CB[8] cavity, in analogy to simple viologen. This idea has been further exploited to control the structure of dimeric dendritic assemblies from viologen– and dialkoxybenzene–dendrons.¹³¹ Another interesting example of a redox CB[8]-mediated switch consists of an equimolar mixture of methylviologen, TTF derivative C60, and CB[8]. This ternary mixture results in the formation of a heteroternary complex CB[8]·MV²⁺·C60 potentially stabilized by electron-rich–electron-poor π–π stacking interactions.¹⁶⁷ Upon treatment with Na₂S₂O₈, viologen is reduced to MV^{•+}, which results in complex disproportionation, yielding CB[8]·(MV^{•+})₂. Exposure to O₂ returns the system to the parent heteroternary complex state. On the contrary, treatment of CB[8]·MV²⁺·C60 with Fe(ClO₄) oxidizes C60 to C60b^{•+}, thus resulting in a

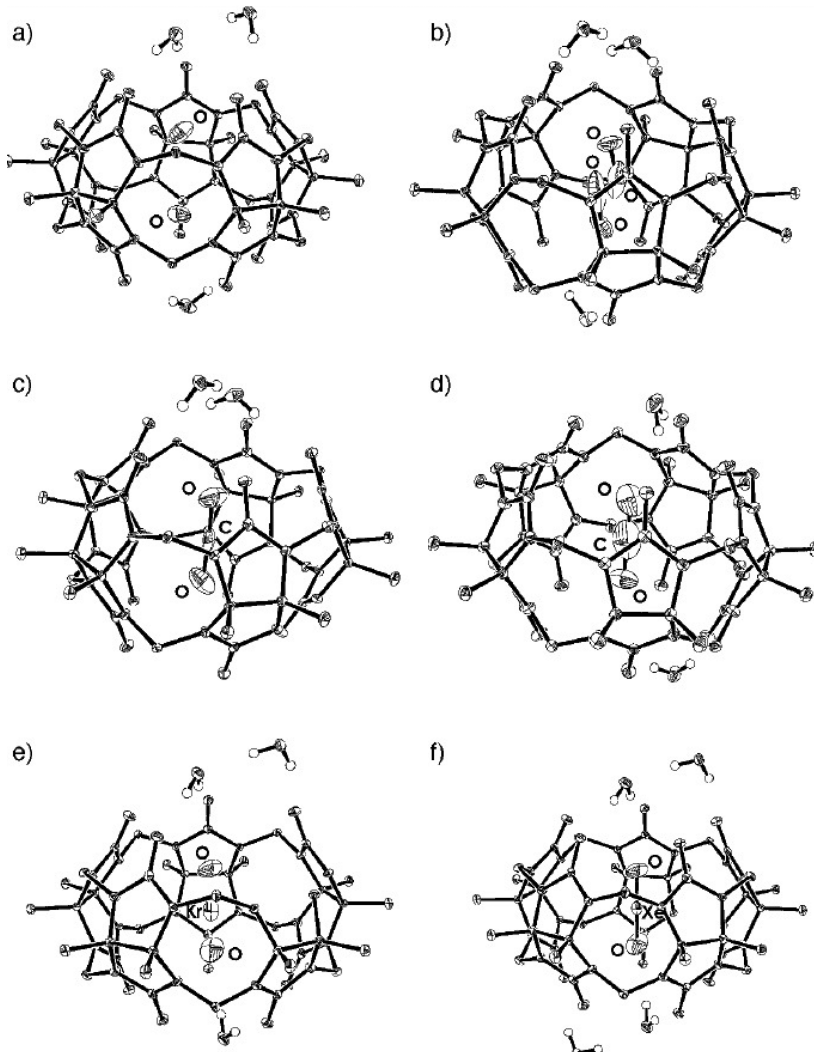


Figure 14. X-ray crystal structures of decamethylcucurbit[5]uril–gas complexes: (a) He complex, (b) O₂ complex, (c) CO₂ complex, (d) CH₄ complex, (e) Kr complex, (f) Xe complex. Reproduced with permission from ref 171. Copyright 2002 John Wiley and Sons, Inc.

disproportionation to yield CB[8]·(C60b^{•+})₂, as evidenced by UV/vis spectroscopy. This last transformation can be reverted upon addition of ascorbic acid. The ternary complex CB[8]·MV²⁺·C60 can therefore be defined as a reversible molecular switch that exists in three different states in a stimulus-dependent manner.

7. ENCAPSULATION OF GASEOUS SPECIES IN CB[n]

Cucurbiturils have shown great promise in applications that include polymer and nanoparticle constructs because of their ability to sequester specific molecules within their unique inner cavities. This, in addition to cucurbiturils' high chemical and thermal stability, has driven researchers to utilize cucurbiturils in the area of gas encapsulation and storage. Sorption of gases such as CO₂, CO, and CH₄ could lead to effective greenhouse gas capture technologies, in addition to being incorporated into nanoparticle structures for advanced sensing and photochemical applications.

In the area of gas sorption research, metal organic frameworks (MOFs) have garnered interest. Along with porous coordination polymers (PCPs), MOFs have very high surface areas and have demonstrated selectivity and capacity for adsorbing gases like CO₂, making them competitive candidates

for gas encapsulation.¹⁶⁸ The issues that MOFs and PCPs face is that they can be sensitive to water, which minimizes their utility in cleaning flue gases. Cucurbiturils, on the other hand, are stable in the presence of water and are easily made from cheap organic molecules, paving the way toward stable and effective alternatives in gas sorption. They have demonstrated gas uptake capacities comparable to some MOFs and PCPs.^{169,170}

On account of the small nature of gaseous molecules, gas absorption tends to be favored by the smaller cucurbiturils. This is because the smaller inner cavities of CB[5] and CB[6] favor encapsulation of small guests as compared to the larger internal cavities of CB[7] and CB[8]. Furthermore, the solubilities of CB[5] and CB[6] have allowed their application in sorption of gases in different ways, with the water-soluble CB[5] finding use in aqueous-phase gas sorption and the less soluble CB[6] being favored for use in powdered form geared toward the cleaning of flue gases. However, CB[6] is not limited in its use in aqueous phase gas sorption by its low aqueous solubility because its solubility can be enhanced in water through the use of alkali metal ions and water-soluble guest molecules. Also, it is readily soluble in strongly acidic solutions.^{25,69}

7.1. CB[5] Gas Sorption

A permethylated form of CB[5] (decamethylcucurbit[5]uril) has been shown by Miyahara and co-workers to encapsulate a variety of gases in both solid form and aqueous media.¹⁷¹ It was found that gases of intermediate size could be encapsulated within the cavity of solid decamethylcucurbit[5]uril, such as N₂, O₂, Ar, N₂O, CO, and CO₂, and readily released upon heating, with N₂O and CO₂ being the most readily absorbed of the gases (crystal structures shown in Figure 14). Smaller gases (He, Ne, and H₂) move too freely in and out of the portals to be absorbed, and larger gases (Kr, Xe, and CH₄) could also not be encapsulated. In the aqueous phase, however, all of the aforementioned gases could be absorbed, with the larger gases requiring heating to 80 °C to be incorporated. This suggests that the solvent molecules play a role in encouraging the encapsulation of the larger gases, as it is unlikely that the portal size of the CB[5] would increase significantly upon heating as a result of the rigidity of the macrocycle.¹⁷¹

7.2. CB[6] Gas Sorption

Solid CB[6] has been shown to have an affinity for CO₂ encapsulation, with a sorption capacity that is comparable to that of MOFs, including HKUST-1 and [Pd(2-pymo)₂]_n.¹⁷⁰ In 2010, Kim and co-workers studied the CO₂ sorption properties of solid CB[6], precipitated from HCl with a honeycomb-like crystal structure. Gas absorption isotherms for CO₂, CH₄, and CO showed a high capacity for CO₂ storage and selectivity for CO₂ over both CO and CH₄, with 45 cm³ g⁻¹ absorbed at 298 K (1 bar). This could be increased to 97 cm³ g⁻¹ at 196 K (1 bar). X-ray analysis of CB[6] after CO₂ sorption demonstrated that CO₂ was bound not only to the inner cavity of the cucurbiturils but also externally to the CB molecules via hydrogen-bonding and dipole–quadrupole interactions with the carbonyl portals (Figure 15a). This demonstrated that the selectivity of solid CB[6] toward CO₂ could be useful in removing CO₂ from flue gases.

Continuing on from the work of Kim and co-workers, Tian and co-workers successfully synthesized three alternate crystalline forms of CB[6], termed forms I, II, and III, via the mixing of ethanol into a solution of CB[6] in 6 M HCl.¹⁷² Form I crystals were shown to be in the monoclinic point group, with the CB[6] molecules stacking into a double bilayer structure (Figure 15b). Form III crystals were shown to be rhombohedral in nature, with the molecules stacking in a bilayer structure (Figure 15c), while form II crystals were unable to be characterized by X-ray crystallography owing to difficulties in growing suitable crystals for diffraction. Despite this, form II exhibited the best thermal stability, with forms I and III losing crystallinity upon heating, as well as the highest surface area, with BET isotherms yielding values of 276 m² g⁻¹. The high surface area and thermal stability of form II gives the material promise in gas storage applications, with 76 cm³ g⁻¹ of CO₂ uptake at 298 K (1 bar). Although more focused on catalytic applications, Reddy and co-workers demonstrated that solid CB[6] has a propensity to absorb I₂ and Br₂ vapor, leading to distinctly colored CB[6]–halogen powders.⁸¹ The catalytic properties of these materials shall be discussed in section 11.

While pure CB[6] is generally not suitable for gas encapsulation in aqueous environments because of its inherently low solubility, it can be made soluble through the use of metal ions, aliphatic or aromatic ammonium ions, or neutral saline aqueous solutions. In such environments, CB[6]

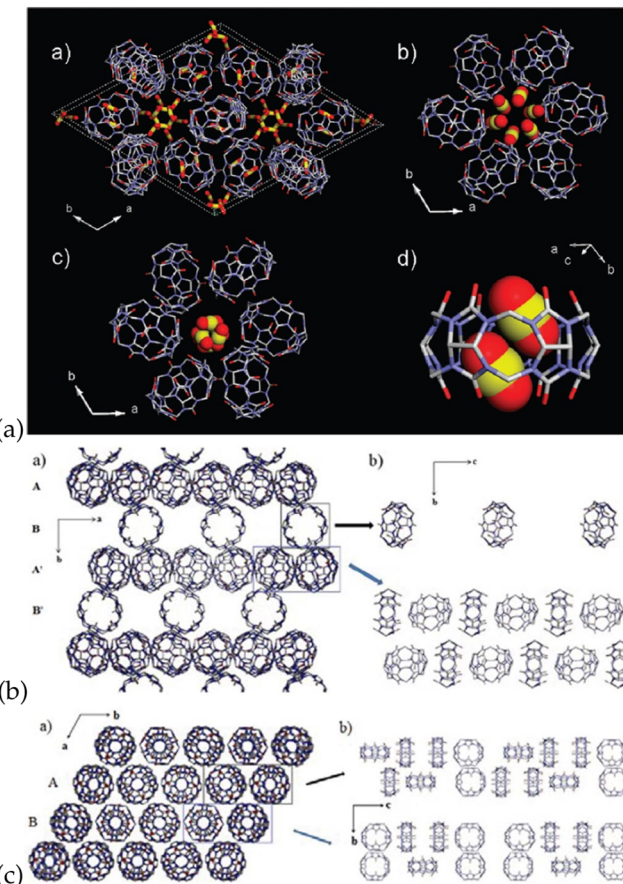


Figure 15. (a) X-ray crystal structures of CB[6]–CO₂ binding at different sorption sites. (b) Crystal structure of CB[6] arranged in the form I lattice. (c) Crystal structure of CB[5] arranged in the form III lattice. (a) Reprinted with permission from ref 170. Copyright 2010 American Chemical Society. (b and c) Reprinted with permission from ref 172. Copyright 2013 The Royal Society of Chemistry.

has been demonstrated to encapsulate Xe,^{173,174} SF₆,^{175,176} as well as gaseous alkanes and alkenes.⁶⁹

El Haouaj and co-workers demonstrated the encapsulation of Xe by CB[6] in a 0.2 M solution of Na₂SO₄, with binding constants ranging from 2.1×10^2 M⁻¹ (although 3.4×10^2 M⁻¹ has been reported for an alkylated CB[6] with higher water solubility¹⁷⁷). The reversible binding was confirmed through ¹H and ¹²⁹Xe NMR, and it was shown that pH played little role in the sorption of the noble gas. SF₆ has also been shown to be encapsulated in aqueous CB[6], however binding constants vary.^{175,176} The first report of SF₆ binding, confirmed via ¹⁹F NMR, yielded a binding of 3.1×10^4 M⁻¹ in 0.2 M Na₂SO₄; however, binding in pure water yields a binding constant of 6.6×10^5 M⁻¹.¹⁷⁶ The higher binding constant in pure water could be attributed to the absence of cations in the solution, which would potentially block the carbonyl portals of the CB[6] and perturb gas encapsulation.

The difficulty of determining binding constants for gases in aqueous CB[6] systems arises from the low solubility of CB[6] in water. To overcome this, Florea and co-workers adopted a dye displacement titration method for measuring the binding constants of hydrocarbon gases (see Figure 16 for schematic).⁶⁹ A compound with a putrescine moiety for binding to CB[6] tethered to a 1-naphthylamine-5-sulfonic acid chromophore was used as the displacement dye owing to the enhancement in

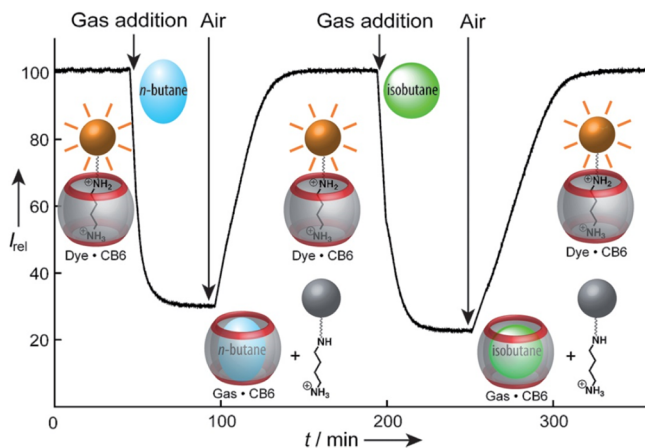


Figure 16. Fluorescent dye displacement method for gas sensing in aqueous solutions of CB[6]. Reproduced with permission from ref 69. Copyright 2011 John Wiley and Sons, Inc.

its fluorescence upon binding to CB[6] and its ability to dramatically increase the solubility of CB[6] in water. The fluorescence of the dye was monitored as gases were introduced into the aqueous system, and binding constants were calculated from the final fluorescence intensity, assuming 1:1 stoichiometric binding. Binding constants ranged from $<2\text{ M}^{-1}$ for methane and neopentane up to $1300 \pm 300\text{ M}^{-1}$ for cyclopentane (binding constants from the cited work can be found in Table 3).

7.3. Gas Sorption in Higher CB[n] Homologues

To date there has only been one report on gas sorption in CB[7], which has shown a high sorption capacity for various gases, including CO₂, SO₂, and H₂S.¹⁶⁹ Of the three gases, SO₂ showed the highest capacity for being absorbed, with uptake as high as $105\text{ cm}^3\text{ g}^{-1}$, followed by H₂S ($62.5\text{ cm}^3\text{ g}^{-1}$) and CO₂ ($50\text{ cm}^3\text{ g}^{-1}$). Although CH₄ and N₂ were tested, low uptakes of $5.5\text{--}6\text{ cm}^3\text{ g}^{-1}$ were observed. Reports of gas absorption in CB[8] and CB[10] have not yet appeared.

8. CUCURBIT[n]URILS ON SURFACES

The influence of the overall electrostatic potential map of CB[n] on its molecular encapsulation properties is evident. The high electron density at its carbonyl portals, however, governs the external interactions of CB[n] with materials such as cations and metallic surfaces (Figure 17a). The latter property is increasingly drawing attention for applications ranging from nanoparticle synthesis, assembly, catalysis, and plasmon-assisted molecular sensing. In addition, CB[n] can also be localized at interfaces through interactions with immobilized guests on surfaces (Figure 17b) as well as by covalently linking

functionalized homologues of CB[n] directly to a surface (Figure 17c). Although electrostatic interactions of CB[n] are mainly limited to metallic substrates, the other two types of binding strategies are applicable to other substrates such as silica and quantum dots. These interactions have been applied successfully to design novel sensors and reversible architectures. Progress in these fields will be discussed in this section.

8.1. Electrostatic Interactions

The direct supramolecular interaction of CB[n] with gold was first successfully characterized by An and co-workers in 2008,¹⁷⁸ where the interaction between gold nanoparticle colloids and CB[n] was established using TEM and UV/vis characterization. CB[n] acted as a “glue” between adjacent nanoparticles, resulting in the formation of coagulates (Figure 18a and

a CB[n]-induced gold nanoparticle cluster formation

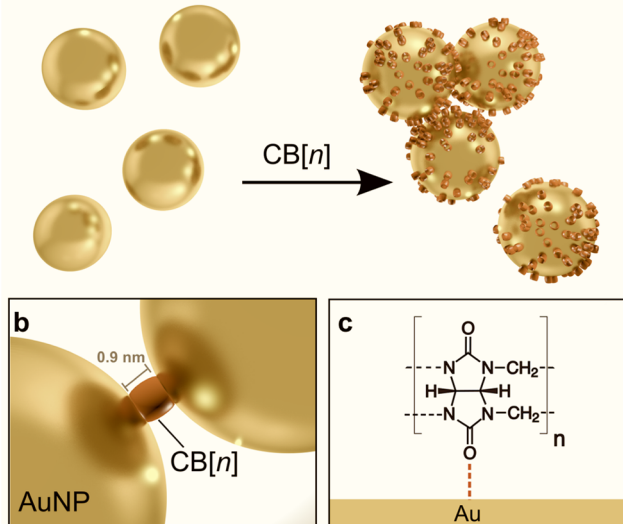


Figure 18. (a) CB[n] acts as a “glue” in between gold nanoparticles forming nanoparticle coagulates, (b) nanoparticles are held apart by CB[n] molecules at a precise distance of 0.9 nm, and (c) CB[n]’s bind to metallic surfaces through its carbonyl portals and are oriented perpendicular with respect to the gold surface.

18b). In a further step, the formation of CB[7] self-assembled monolayers was achieved simply by dipping a planar gold substrate into a saturated aqueous solution of CB[7]. The CB[7] molecules physisorb on the gold surface. Surface characterization techniques, including Fourier transform IR reflection absorption spectroscopy and XPS, indicated that the interactions between CB[7] and gold occurred through the electronegative carbonyl portals of CB[7], where the CB[7] portals were oriented in a perpendicular fashion with respect to

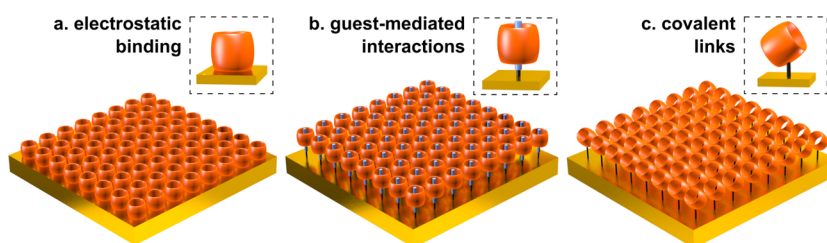


Figure 17. Strategies used for immobilizing CB[n] on various substrates: (a) carbonyl portal-mediated binding electrostatic interactions, (b) threading of CB[n] through guests tethered on the surface, and (c) direct linking using functionalized homologues of CB[n].

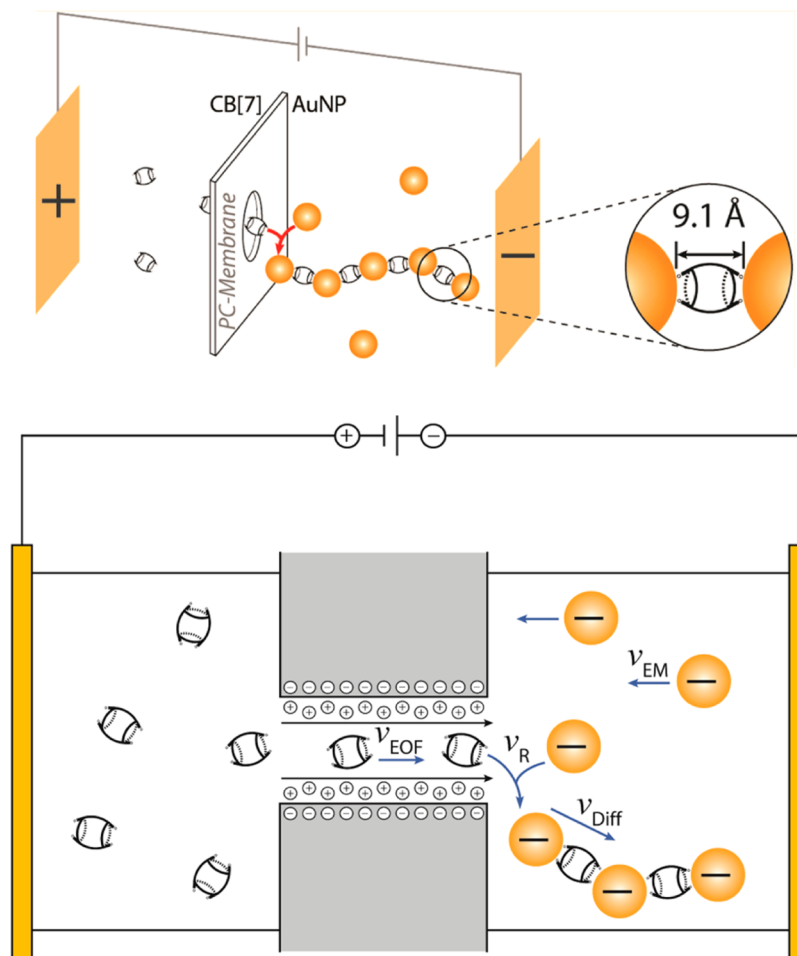


Figure 19. (a) Formation of one-dimensional chains of gold nanoparticles using an electrophoresis cell, where a nanoporous polycarbonate membrane separates two compartments containing gold nanoparticles and CB[7]. (b) Nanoparticle chains are formed through synergistic electroosmotic flow of CB[7] and electrophoretic motion of the gold nanoparticles. Reprinted with permission from ref 198. Copyright 2013 American Chemical Society.

the gold surface (Figure 18c). In the same study, the surface packing of CB[7] was estimated to be >48% using an indirect electrochemical method; nevertheless, the true density of CB[n] molecules on flat metallic surfaces remains unascertained.

8.1.1. Modification and Assembly of Nanoparticles with CB[n]. Despite the limited fundamental knowledge about CB[n] interactions with metallic surfaces, particularly in colloidal systems, CB[n] has been shown to be useful in the synthesis of nanoparticles, mainly as a “capping agent” or “stabilizing ligand”. The first synthesis of CB[n]-assisted nanoparticles was reported by Geckeler and co-workers, where CuO nanoparticles (diameter \approx 5 nm) were formed using precursor-encapsulated CB[7].¹⁷⁹ The same group later reported a one-pot synthesis of silver¹⁸⁰ and gold nanoparticles¹⁸¹ by the reaction of aqueous CB[7] solutions containing the respective precursor salts and NaOH at room temperature. In both cases, CB[7] acted as a stabilizing ligand and generated well-dispersed nanoparticles. Since no additional reducing agents were used, the role of CB[7] as a reducing agent, in addition to stabilizing ligand, in nanoparticle synthesis was also established. However, it should be noted that the oxidized organic species resulting from salt reduction remains unidentified. The same applies to the reaction mechanism.

In the same year, Scherman and co-workers reported the formation of dynamic aggregates of gold nanoparticles using CB[5].¹⁸² In this case, the nanoparticles were prepared in the presence of a reducing agent as well as CB[5], where concurrent with other reports^{180,181} CB[5] was once again shown to act as a capping agent. The sizes of these aggregates could be controlled by varying the ratio between CB[5] and the gold precursor and was based on the interactions of one or both carbonyl portals of the CB[5] molecules. The symmetric structure of the CB[n] is of particular importance to allow the CB[5] molecules to bridge two nanoparticles. The aggregation process was monitored by measuring the changes in the surface plasmon resonance of the colloidal solution. Typically, monodisperse gold nanoparticles absorb in the green region of the visible spectrum and appear as red solutions. Upon aggregation, the absorbance signal undergoes a red shift and the solutions appear purple or blue instead. The kinetic evolution of these plasmonic modes was reported later in greater detail.¹⁸³

This was followed by another study, where CB[5], CB[7], as well as the less water-soluble homologues, CB[6] and CB[8], were also investigated as capping agents using metastable gold nanoparticles.¹⁸⁴ Importantly, the interparticle spacing between neighboring nanoparticles was confirmed by TEM to be approximately 1 nm, which is consistent with the height of

CB[n] molecules. This further indicates the portal–metal interactions between CB[n] and gold. The longer stability (~ 3 months) of the resulting nanoparticles was further attributed to the presence of sodium atoms bound to the carbonyl portals of the CB[5] ligands. Once again, the aggregates exhibited reversible control as before.

More recently, CB[7]-stabilized gold nanoparticles were synthesized in order to demonstrate the increase in catalytic efficiency of nanoparticles free from organic ligands and metal cations.¹⁸⁵ The stabilization of silver nanoparticles with CB[n] homologues has also been further investigated,¹⁸⁶ whereby computational studies supported the assumption that the stabilizing effect of CB[7] is a result of lateral interactions between the oxygen atoms at the CB[7] carbonylated rim and the metal surface.

It is noteworthy, however, that the role of CB[n]-capped gold nanoparticles is not restricted to stabilization of nanoparticles. Plasmonic coupling between aggregated nanoparticles affects their optical response and leads to strongly enhanced electric fields in the gaps between them.^{187,188} The magnitude of those fields increases near-exponentially as the distance between the particles is reduced and is limited only by electron tunneling for gaps below ~ 0.5 nm.^{189–193} Owing to the symmetrical geometry of CB[n], the presence of CB[n] in between nanoparticles ensures that they are held precisely 0.9 nm apart from each other (Figure 18b).¹⁸³ This provides both extremely high and reproducible local field enhancements in the gap junctions^{194,195} while maintaining an accessible gap for small molecules.^{139,141} Since such precision at these scales is not easily achievable, physicists have to predominantly rely on theoretical simulations in order to understand the optics at such nanoscale regimes. Therefore, CB[n] provides a support handle to experimentally investigate the plasmon modes and near-field properties of nanoparticle clusters with well-defined separations.¹⁹⁶

The precise gap distances between adjacent nanoparticles produced by CB[n] has further useful implications. For example, these CB[n]–gold nanoparticle hybrids have been utilized to create near-identical, continuous strings of nanoparticles joined by a conducting gold thread.¹⁹⁷ In this study, precise control over the formation of the nanomaterial was achieved on a large scale by irradiating the CB[n]-mediated nanoparticle assemblies with a suitable femtosecond pulsed laser. As a result of high field intensities in the gap junctions between the nanoparticles, the surface atoms are drawn into the gap through optical forces and nonthermal melting and form solid metal threads between the particles. The extreme enhanced fields in the crevices of the resulting threads open up prospects for applications of these metamaterials in photovoltaics and sensing probe construction.

In consideration of the interesting plasmonic and electronic properties afforded by CB[n]-mediated gold nanoparticle assemblies, sophisticated strategies have been developed in order to control the morphologies of these clusters. One such strategy allows the well-defined growth of one-dimensional chains of gold nanospheres, spaced by CB[n] molecules.¹⁹⁸ This is achieved in a chamber consisting of gold nanoparticles and CB[n] solution separated by a nanoporous polycarbonate membrane. The one-dimensional chains are then formed at the membrane interface by the electrophoretic flow of the nanoparticles under an applied voltage and the electroosmotic flow of the CB[n] (Figure 19).

End-to-end gold nanorod alignments can also be formed through CB[n] linkers.¹⁹⁹ Centrifugation of CTAB-coated gold nanorod solutions preferentially destabilizes the CTAB bilayer at the curved {111} end facets of the nanorods. Therefore, upon subsequent addition, CB[5] is only able to interact with the nanorod ends, consequently forming nanorod chain-like topologies. The surface plasmon resonance bands of gold nanorods can be tuned over a wider range than those of nonanisotropic analogues, making them interesting candidates for plasmonic applications.

8.1.2. SERS Sensing. An important property of CB[n] interactions with metallic surfaces is its ability to retain its molecular recognition properties. In other words, CB[n] can facilitate guest molecules from the bulk solution to approach the metal–liquid interface by acting as a “receptor” on the surface. Surface-dependent phenomena, such as catalysis and surface-enhanced spectroscopic (SERS) techniques, generally require molecules to be localized near the surfaces and often rely on the innate affinity of the molecules toward these surfaces. Since not all molecules of interest interact with surfaces spontaneously, covalent functionalization strategies are often used to immobilize them on surfaces. However, such strategies usually reduce the direct interactions of the molecules with the surface, thereby interfering with the efficiency of the surface processes. Therefore, it is evident that the ability of CB[n] to confine molecules of interest near the surface has dramatic significance in surface-dependent mechanisms.

The molecular recognition properties of CB[n] can be harnessed for sensing with SERS.^{98,139–141,183,200} In brief, Raman spectroscopy is a vibrational technique, which probes the inelastic scattering of photons with molecules and is able to provide a unique fingerprint for each analyte. While this method is comparable to infrared spectroscopy, the lack of interference from water molecules (in the fingerprint region) makes this method desirable for probing chemical structures, particularly in aqueous environments. However, the inherent weakness of Raman signals requires the use of enhancement mechanisms, such as the use of plasmonic surfaces, to improve sensitivity. One particularly popular approach is surface-enhanced Raman spectroscopy, and the reader is referred to the literature on this topic for further details.^{201–204}

Although Raman spectroscopy was used as an analytical method to characterize encapsulation of a polymer in multiple CB[n] units,²⁰⁵ the first report of a detailed study of the Raman and SERS signature of CB[n] appeared in the literature in 2010.²⁰⁶ Clearly identifiable peaks for CB[n] are observed in the fingerprint region ($400\text{--}2000\text{ cm}^{-1}$) of the Raman spectra (Figure 20). Two characteristic intense signals at approximately 450 and 830 cm^{-1} are attributed to complex ring breathing modes of the CB[n] molecules. Interestingly, these signals show slight red and blue shifts, respectively, with an increase in the ring sizes of the different CB[n] homologues. The same signals and a similar trend in peak shifts is observed in the corresponding SERS spectra. A SERS enhancement factor of $10^7\text{--}10^9$ is achieved with CB[n]:gold nanoparticle aggregates.^{183,200}

SERS-based sensing of a dye molecule, Rhodamine 6G (Rh6G), with the aforementioned CB[7]:gold nanoparticle constructs was first demonstrated by Scherman and co-workers in 2011.¹⁸³ CB[7] binds to Rh6G in a 1:1 stoichiometric ratio ($K_a > 5 \times 10^4\text{ M}^{-1}$).²⁰⁷ Besides acting as an aggregating agent to glue together adjacent gold nanoparticles, CB[n] positions the guest molecules precisely at the point of closest approach

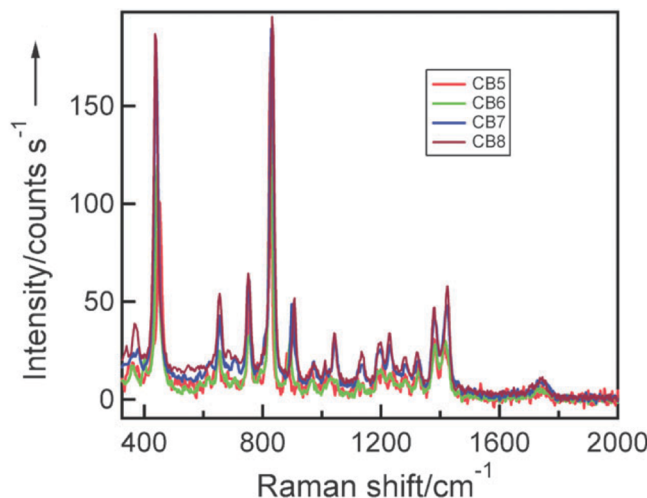


Figure 20. Raman spectra of $\text{CB}[n]$ showing characteristic signals between 400 and 2000 cm^{-1} . Reproduced with permission from ref 206. Copyright 2010 The Royal Society of Chemistry.

between nanoparticles, which is where the highest field enhancement occurs, also known as a “hot spot”. By bringing the analyte into the hot spot, tremendous enhancement of the Raman signal can be seen, even for molecules with a low Raman cross-section. Thus the role of $\text{CB}[n]$ is particularly significant. For example, another SERS study used neutral ferrocene with $\text{CB}[7]$ (Figure 21).²⁰⁰ In addition, ferrocene does not have an affinity for gold surfaces but can be localized in the hot spot using $\text{CB}[7]$. In this case, a three-step approach was used to prepare the SERS substrates, in which gold nanoparticles were first assembled on amino-functionalized glass. Ferrocene-encapsulated $\text{CB}[7]$ was subsequently physisorbed on the substrate, followed by another layer of Au nanoparticles. As a result, gold nanoparticle clusters, predominantly dimers and trimers, were obtained on the glass surface with ferrocene-encapsulated $\text{CB}[7]$ in the hot-spot regions.

The utility of this SERS-based sensor has been extended to studying $\text{CB}[n]$ host–guest chemistry. Computational studies had shown that $\text{CB}[n]$, particularly $\text{CB}[7]$, is expected to undergo a subtle structural distortion on encapsulation of a guest.²⁰⁸ These structural changes can be seen in the SERS spectra of $\text{CB}[n]$ complexes as slightly shifted peaks.¹³⁹ These structural changes are not as apparent in the solid-state Raman spectra of the complexes. These changes, however, are more pronounced in the Raman signals of the guest molecules.²⁰⁹

Not only did these results present experimental evidence to support the outcomes of the theoretical predictions, the shifted and unshifted signals also provided a tool to be able to distinguish the amounts of complexed and uncomplexed $\text{CB}[n]$ s. Therefore, the system could be used for characterizing $\text{CB}[n]$ host–guest binding parameters as well as absolute quantification of guest analytes, such as polycyclic aromatic hydrocarbons.¹³⁹ Roldán and co-workers reported the use of this strategy through the incorporation of silver nanoparticles for the detection of pH-dependent changes in the complexation behavior of diquat with $\text{CB}[8]$.¹⁴⁰ The system has also been used to monitor the real-time photodimerization of diaminostilbene inside the $\text{CB}[n]$ cavity in situ.¹⁴¹

One of the advantages of the SERS technique is its ability to resolve analytes in a mixture, which is particularly advantageous for structurally similar molecules. $\text{CB}[n]$ complements this property of SERS by acting as a receptor for several molecular analogues. A recent report used this property to test the multiplexing abilities of $\text{CB}[n]$ in sensing structurally similar metabolites in urine.⁹⁸

8.1.3. Localization of Ligands. $\text{CB}[n]$ adsorbed to gold surfaces have also been used as a platform for immobilizing biomolecules.²¹⁰ In this case, methyl ferrocene was functionalized with a glycol spacer and a cysteine end group for ligation with a yellow fluorescent protein thioester (YFP) (Figure 22). The protein could then be immobilized on SAMs of $\text{CB}[7]$ on gold surfaces through the strong interactions with the ferrocene moiety. The proteins from the surfaces could be displaced by using a competitive guest, such as (ferrocenylmethyl)-trimethylammonium iodide ($K = 10^{11} \text{ M}^{-1}$). This strategy gave access to a strong, reversible, and uniform protein immobilization on surfaces. Similarly, SNAP-fusion cyan fluorescent protein functionalized with ferrocene was immobilized on SAMs of $\text{CB}[7]$, generating fluorescent patterns on the surfaces.²¹¹ This method was then developed further to immobilize cells on $\text{CB}[7]$ -coated surfaces using cyclic RGD peptide–ferrocene conjugates.²¹² The RGD peptide allows enhanced cell adhesion and wound healing. The studies showed that the cells remained viable on the surfaces when linked via RGD. In addition, a wound assay also showed successful cell recovery within 8 h.

$\text{CB}[7]$ has also been used to physisorb unsubstituted methylviologens onto the surface of TiO_2 semiconductor nanoparticle films. The redox-active properties of the viologen guests were further used to prepare electrochromic windows that exhibited reversible color switching under applied potential.²¹³

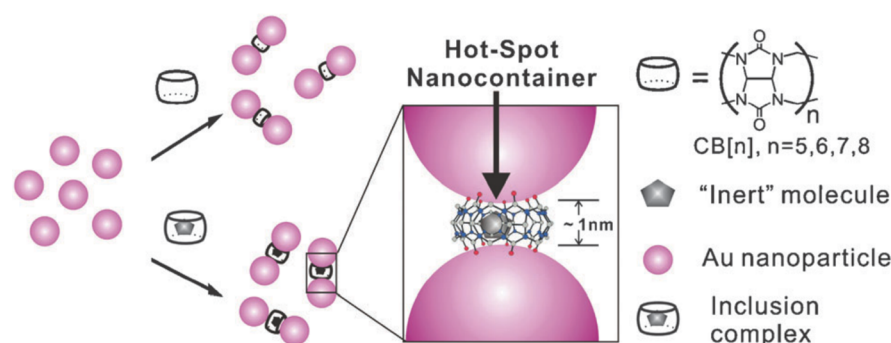


Figure 21. Formation of uniform hot spots and localization of analytes in them for efficient surface-enhanced Raman spectroscopy through aggregation of gold nanoparticles with $\text{CB}[n]$. Reproduced with permission from ref 200. Copyright 2011 The Royal Society of Chemistry.

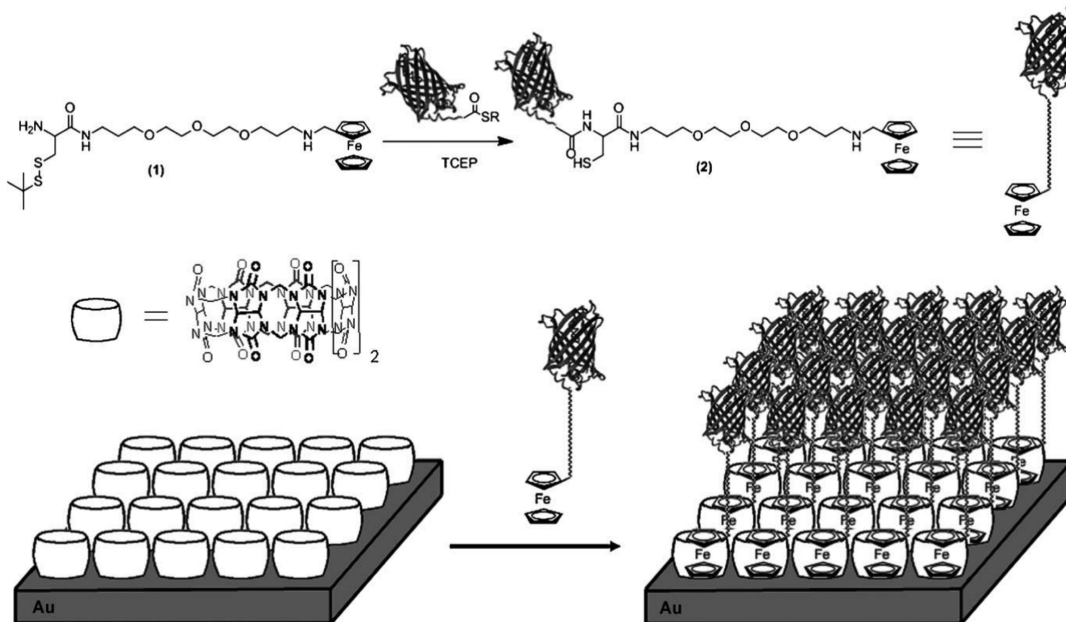


Figure 22. Immobilization of ferrocene-ligated yellow fluorescent protein on gold surfaces through interaction of ferrocene guests with the $\text{CB}[7]$ monolayer. Reproduced with permission from ref 210. Copyright 2010 John Wiley and Sons, Inc.

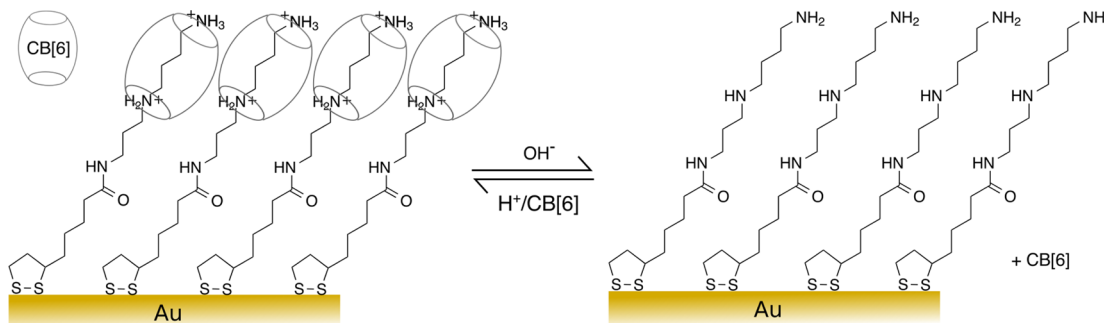


Figure 23. Self-assembled monolayer of pseudorotaxane on gold surfaces and dethreading and rethreading of molecular bead $\text{CB}[6]$. Adapted with permission from ref 214. Copyright 2003 John Wiley and Sons, Inc.

8.2. Guest-Mediated Interactions

Direct supramolecular interactions of surfaces with $\text{CB}[n]$ has undoubtedly opened up avenues for various promising applications, but controlling these spontaneous interactions remains challenging. One strategy, which is widely being reported to gain precise control over the behavior of $\text{CB}[n]$ near surfaces, is to covalently functionalize the surfaces with molecular structures containing guest moieties. The guest-mediated interaction of $\text{CB}[n]$ with the surfaces also provides additional handles for stimuli-responsive and reversible architectures and is particularly attractive for designing colloidal systems.

The earliest example of such a system was illustrated through the construction of a pseudorotaxane self-assembled monolayer on a planar gold surface using $\text{CB}[6]$. The molecular thread was anchored on a gold surface through a 1,2-dithiolane functionality, whereas its diaminobutane unit allowed binding to $\text{CB}[6]$ (Figure 23). The threading of $\text{CB}[6]$ could then be controlled by changing the pH of the system. Furthermore, the pseudorotaxane acted as a gate to control the access of an electroactive species, $[\text{Fe}(\text{CN})_6]^{3-}$, to the gold surface.²¹⁴ Similarly, gold nanorods decorated with a hydrophilic $\text{CB}[7]$ -based pseudorotaxane have also been prepared.²¹⁵

In another example, this method was used to disrupt aggregation of dye molecules on surfaces where high-density Rhodamine B-functionalized glass slides showed a higher degree of heterogeneity and fluorescence quenching. The addition of $\text{CB}[7]$ reduced the heterogeneity and increased the emission significantly to match that of monomeric Rhodamine B species.²¹⁶ More recently, glassy carbon electrodes were modified with $\text{CB}[7]$ in order to construct a glucose sensor using glucose oxidase as a catalyst.²¹⁷ In this case, however, a graphene oxide layer on the electrode was used to enhance the stability of the $\text{CB}[7]$ on the surface. Ferrocenemonocarboxylic acid, the electron-transfer mediator, can then be captured through molecular recognition by $\text{CB}[7]$. The applicability of this sensor was demonstrated in human serum samples.

8.2.1. Ligand Immobilization. On the basis of the finding that $\text{CB}[8]$ is able to induce aggregation in proteins in aqueous solutions, a layer-by-layer construction of homo- and heteroprotein stacks on surfaces has been reported (Figure 24).²¹⁸ In this study, a quartz glass substrate was first modified with amino groups using 3-aminopropyltriethoxysilane. The formation of multiple layers of hemoglobin was then achieved by alternately immersing the substrate in solutions of $\text{CB}[8]$ and protein. The $\text{CB}[8]$ acted as a “glue” within the proteins

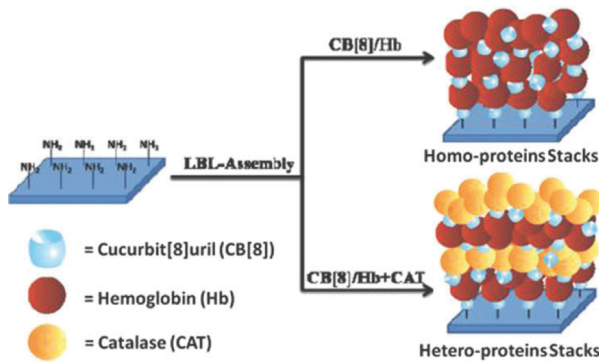


Figure 24. Layer-by-layer construction of protein stacks on surfaces using CB[8] “glue” molecules. Reproduced with permission from ref 218. Copyright 2012 Royal Society of Chemistry.

stacks. The lack of need to pretreat or modify the proteins was particularly highlighted in this work by verification of this strategy with several unmodified proteins such as catalase, glutathione-S-transferase agents, and insulin. Recently, Rotello and co-workers were able to regulate the interactions between green fluorescent protein and monolayer-coated gold nanoparticles using CB[7].²¹⁹ The threading of CB[7] on the surfaces of the nanoparticles led to an increased affinity for the proteins. The authors consider this to be an outcome of the increased cationic charge on the nanoparticle surface based on the slightly positive charge on the outer surface of the equatorial region of CB[7]. However, potential repulsion from the negatively charged carbonyl portals was not accounted for in this proposed mechanism.

Scherman and co-workers reported the utility of viologen-functionalized gold substrates using CB[8] as a supramolecular “handcuff” for patterning surfaces with polymeric colloids. Both 1D and 2D patterns were attained.²²⁰ The same group also described a system in which orthogonal switching was achieved controllably and reversibly by using redox- and photoresponsive guest molecules and CB[8].²²¹ In this system, a SAM of thiol-containing azobenzene derivatives was immobilized on a gold substrate by microcontact printing. Methyl viologen conjugated with fluorescein dye could be assembled on the surface from solution via CB[8] “handcuffs” to afford spontaneously formed 2D fluorescent patterns. UV irradiation of the surface converted the azobenzenes to their cis configuration, which in turn dissociated the second guest from the CB[8] to turn off the fluorescence. This process could be reversed by irradiation with visible light to convert the azobenzene moieties back to their

trans state. Redox-controlled reversibility of the ternary complex formation provided orthogonal control over the system. In a more recent study, a facile method was reported for the preparation of rotaxanes on gold based on CB[8] threaded onto a viologen axle, Figure 25.²²² These surface-bound rotaxanes yielded an interlocked structure, which prevented the dissociation of the binary complex MV^{2+} ·CB[8]. The stability of the functional surface was thus maintained for binding with electron-rich second guests for CB[8] such as small molecules like dopamine and prefunctionalized colloidal particles.

8.2.2. Self-Assembled Architectures. The ternary complex formation ability of CB[8] has been used to form and control end-to-end assemblies of gold nanorods.²²³ This was accomplished by first preparing viologen end-functionalized gold nanorods. Then telechelic linker molecules carrying second guest moieties were added to these gold nanorods in the presence of CB[8] to form aligned chains. The rigidity of the resulting chains could be controlled by changing the length of the linker molecules. Another example of reproducible SERS with colloids was demonstrated using gold nanoparticles precoated with cystamine using CB[6] as linkers to generate gold nanoparticle dimers.²²⁴

A colorimetric assay for protein detection was reported based on CB[8]-induced formation of bulky aggregates of functionalized gold nanoparticles.²²⁵ This was achieved by modifying the gold nanoparticles with peptides containing N-terminal aromatic residues, which can be accommodated inside the CB[8] cavity. CB[8] is only able to bind to the peptide in the absence of the target protein, inducing a visible color change in the gold nanoparticle solution. The feasibility of this system has been shown in spiked serum samples with a detection limit of 0.2 nM.

CB[8] has also been used to link methyl viologen-functionalized polymeric nanoparticles onto silica cores decorated with 4-hydroxyazobenzene moieties to yield hybrid “raspberry” colloidal structures in water (Figure 26).²²⁶ The presence of azobenzene groups allows reversible assembly and disassembly of the constructs with photoirradiation.

8.2.3. Nanovalves. Pioneered by Stoddart and co-workers, CB[n]-based pseudorotaxane systems on mesoporous silica have made substantial contributions in the field of gated nanotechnology.^{227–230} The release of molecular cargo from mesoporous silica nanoparticles (MNPs) is achieved by blocking and unblocking the silica pores by using CB[n] as a gating moiety. Early reports were based on pH-dependent actuation of the MNPs.²³¹ Increasing levels of sophistication

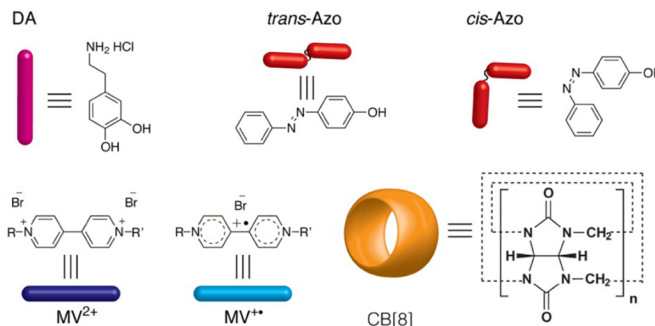
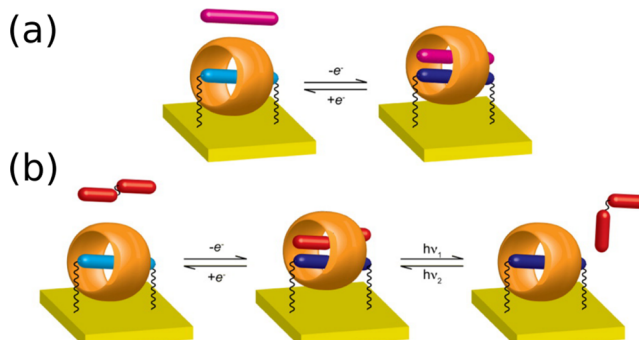


Figure 25. (a) Redox-controlled ternary complexation of $(MV^{2+}\cdot DA)\cdot CB[8]$ on the Au surface. (b) Redox-controlled and photoresponsive ternary complex formation of $(MV^{2+}\cdot Azo)\cdot CB[8]$ on the Au surface. Adapted with permission from ref 222. Copyright 2014 American Chemical Society.

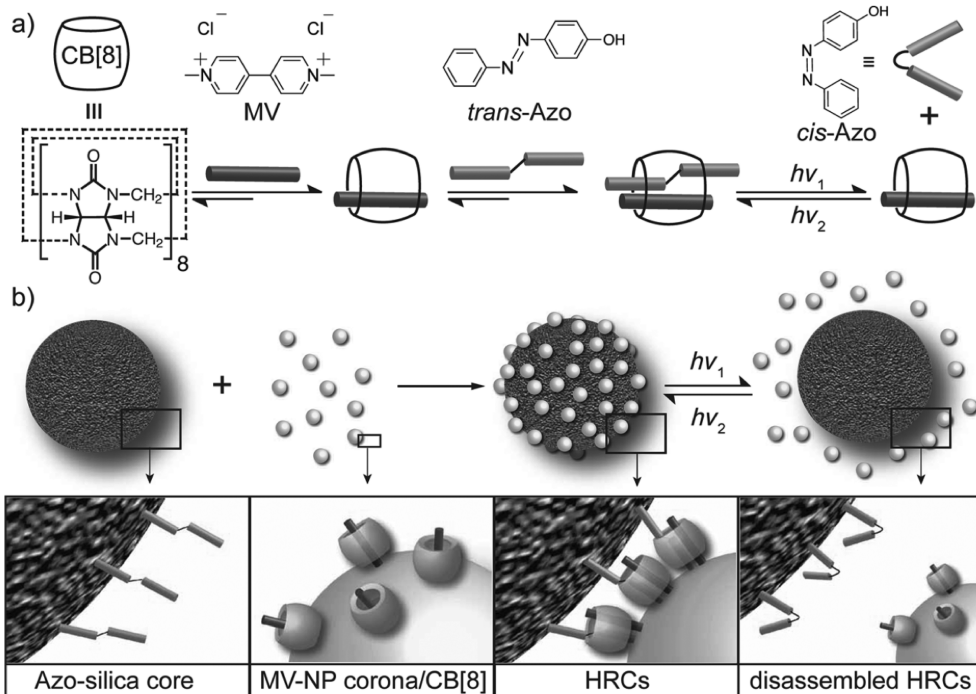


Figure 26. Formation and reversible assembly of hybrid raspberry colloids through $\text{CB}[8]$ ternary complexes. Reproduced with permission from ref 226. Copyright 2014 John Wiley and Sons, Inc.

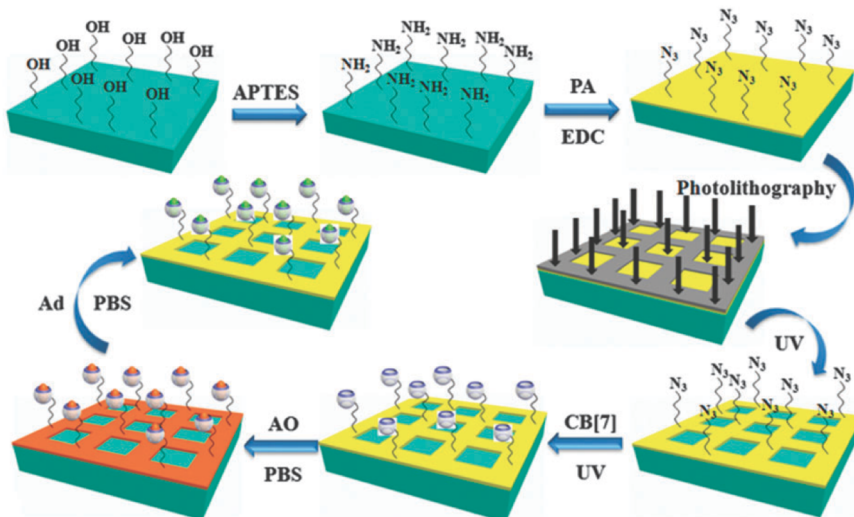


Figure 27. Immobilization of $\text{CB}[7]$ on a silica substrate through photochemical reaction with azides. APTES, 3-aminopropyltriethoxy-silane; PA, 4-azidobenzoic acid; EDC, 1-(3-(dimethylamino)propyl)-3-ethylcarbodiimide hydrochloride; AO, Acridine Orange; Ad, 1-adamantanecarboxylic acid. Reproduced with permission from ref 248. Copyright 2013 Royal Society of Chemistry.

were steadily introduced to these systems by addition of features such as tuning of the pH at which the MNPs responded,²³² dual-stimuli constructs capable of exhibiting logic,²³³ and magnetic activation.²³⁴ Later, $\text{CB}[7]$ -based gating behavior^{235,236} and alternative approaches to activate the nanovalves were also published. These include competitive binding,²³⁵ enzyme-triggered systems,²³⁶ reductive chemistry (cleavage of disulfide bonds),²³⁷ and light response.²³⁸

8.3. Covalent Immobilization

Reversibility in the binding of $\text{CB}[n]$ to surfaces may not always be desirable in order to achieve better stability and recovery of functionality of the surfaces. Evidently, among the various strategies that have been explored to link $\text{CB}[n]$ and surfaces,

the ability to functionalize $\text{CB}[n]$ has been pivotal in addressing these requirements.

Covalently anchored $\text{CB}[7]$ on gold surfaces was first reported for the production of a glucose sensor.²³⁹ The system was constructed by attachment of allyloxy- $\text{CB}[7]$ on vinyl-terminated alkanethiolate SAMs using olefin cross-metathesis. Ferrocenylated glucose oxidase (GOx) was subsequently immobilized on the surface by means of strong Fc- $\text{CB}[7]$ host-guest interactions. Glucose concentrations could then be monitored electrochemically using this system. The modification of quantum dots with functionalized $\text{CB}[6]$ using thiol linker groups has been reported to significantly improve their stability.²⁴⁰

In another example, the utility of functionalized CB[n] on surfaces was elegantly demonstrated by Kim and co-workers in the development of synthetic adhesives, which are functional even under water.¹⁰⁴ Their velcro-type system is based on a “hook-and-loop” approach where a silicon surface functionalized with CB[7] was used to loop around the guest “hooks” immobilized on a second silicon surface. In order to immobilize the CB[7], alkene-functionalized monoallyloxy-CB[7] was attached to thiol-decorated Si surfaces in a thiol–ene reaction. The guests 1,1'-bis(trimethylammoniomethyl)ferrocene (BFc) and aminomethylferrocene (Fc) were chosen on account of their particularly high binding affinities for CB[7] in water at 10^{12} and 10^{15} M^{-1} , respectively. Tunability of adhesiveness was achieved through varying the densities of “hooks” and “loops” on the surfaces to control the number of multivalent interactions between the two silicon surfaces. A reasonable level of reversibility was also shown with this adhesive through both chemical and mechanical means. It is noteworthy that water molecules often act as a contaminating agent in conventional synthetic adhesives for use under water. On the contrary, this particular CB[n]-based approach relies on the expulsion of water molecules in the formation of the CB[7]–guest complexes to fabricate the desired synthetic adhesives.

8.3.1. CB[n]-Anchored Silica. The use of CB[n]-anchored silica has been widely reported in separation science. The production of CB[n]-based stationary phase materials and their use in chromatography was disclosed in patents by Kim and co-workers.²⁴¹ The separation of several organic compounds, including alkaloids, alkanes, aromatic hydrocarbons, alcohols, esters, ketones, and amines, using silica gel grafted with perhydroxy-CB[6] has been described in the literature.^{242,243} However, this method suffers from the presence of excess potassium sulfate, which hinders immobilization. In order to address this drawback, another method to fabricate functionalized silica using perallyloxy-CB[6] has also been developed.²⁴⁴ Additionally, silica–CB[n] hybrids prepared using a sol–gel approach also yields stationary phases for efficient chromatographic separations.^{245–247}

As an alternative to using covalently modified CB[n], another method to functionalize CB[7] on surfaces has been reported using a photochemical reaction with azido groups (Figure 27).²⁴⁸ In this strategy, silica substrates were first modified with 3-amino-propyl-triethoxy-silane to introduce amino groups on the surface. The primary amine was then reacted with 4-azidobenzoic acid in the presence of 1-(3-(dimethylamino))-propyl)-3-ethylcarbodiimide hydrochloride at basic pH. The azido groups were then exposed to CB[7] and reacted under UV irradiation for 10 min to form covalent linkages. While the mechanism of the functionalization could not be elucidated, the authors propose the formation of the highly reactive singlet nitrenes from the azido groups upon UV irradiation. This is followed by their subsequent insertion into the equatorial C–H bonds of CB[7].

Lastly, functionalization of electrodes for enhanced analytical performance has been demonstrated using CB[n]. One such study particularly exploits the molecular recognition properties of CB[8] to enhance the selectivity and sensitivity of the electrochemical determination of tryptophan.²⁴⁹ In brief, the glassy carbon electrode was modified by exposing it to a suspension of Nafion and CB[8]. The nature of interaction with CB[8] in the construction of this system, however, has not been studied and remains unclear. Investigations with common interferents such as acetylcholine (ACh), ascorbic acid (Asc),

and different amino acids, namely, D-phenylalanine (Phe), L-tyrosine (L-Tyr) or L-cysteine (L-Cys), arginine (Arg), and lysine (Lys), showed that Phe, Arg, and Lys exhibited a decrease in the electrochemical signal when present at a minimum of 5-fold concentrations to that of Trp, while L-Tyr could be determined simultaneously with the concentration of Trp. The system was also shown to work in human serum, but there remains room for improvement in the reproducibility for real-life applications.

8.4. Characterization of CB[n] Host–Guest Binding on Surfaces

In the systems involving CB[n] and surfaces, the binding properties of the CB[n] is usually studied in solution and it is assumed that CB[n] retains its molecular recognition behavior on surfaces. However, with the availability of sophisticated tools such as force spectroscopy, these interactions can now be quantified down to the single-molecule level even on surfaces. For example, atomic force microscopy (AFM) has been used to measure the rupture force between individual host–guest complexes of CB[6] covalently tethered on gold substrates and a spermine-functionalized AFM tip.²⁵⁰ A rupture force value of 120 pN was obtained for this system. In another study, the interactions between self-assembled monolayers of CB[7] and neutral adamantyl guests have been resolved at the single-molecule level using dynamic force spectroscopy.²⁵¹ It is noted from such studies that the close proximity of a surface does not appear to significantly alter CB[n] molecular recognition properties. Furthermore, the spontaneous adsorption of CB[6] and CB[7] on gold has been compared by AFM.²⁵²

8.5. Outlook

Direct interactions between CB[n] and gold continues to show progress in self-assembly of colloidal nanoparticles and sensing applications, particularly in SERS-based applications. The tunability of these systems is one of their major advantages, where the probe can be adapted to the sample. Nonetheless, there remains a need to further explore and elucidate the interactions of CB[n] with gold on planar surfaces, which may be possible with advances in techniques like AFM and STM. It should also be noted that nanoparticles that have been synthesized using CB[n] as the capping ligand are limited in their size to below ~10 nm in diameter. While nanoparticles with small diameters might be exceptionally suited for catalysis, larger nanoparticles are much more applicable in plasmonics.

As it is evident from the wide variety of systems being reported, formation of covalent links between CB[n] and the surfaces is moving fast toward interesting applications. However, these strategies still often require time-consuming prefunctionalized CB[n]. Therefore, the use of host–guest interactions to immobilize CB[6] and CB[8] on surfaces continues to be a promising strategy where irreversibility is desirable.

9. SUPRAMOLECULAR POLYMERS

CB[n] supramolecular polymers can be divided into two areas: (a) small-molecule-based supramolecular polymers and (b) CB-mediated bridging of polymer chains and other macromolecular structures. There are a number of excellent reviews in the area of CB[n] supramolecular polymers and the more general host–guest driven polymerization.^{253–258} In this section, we focus on summarizing the current status of research and development toward CB[n]-supramolecular polymers and highlight some relevant examples in the field, largely dominated

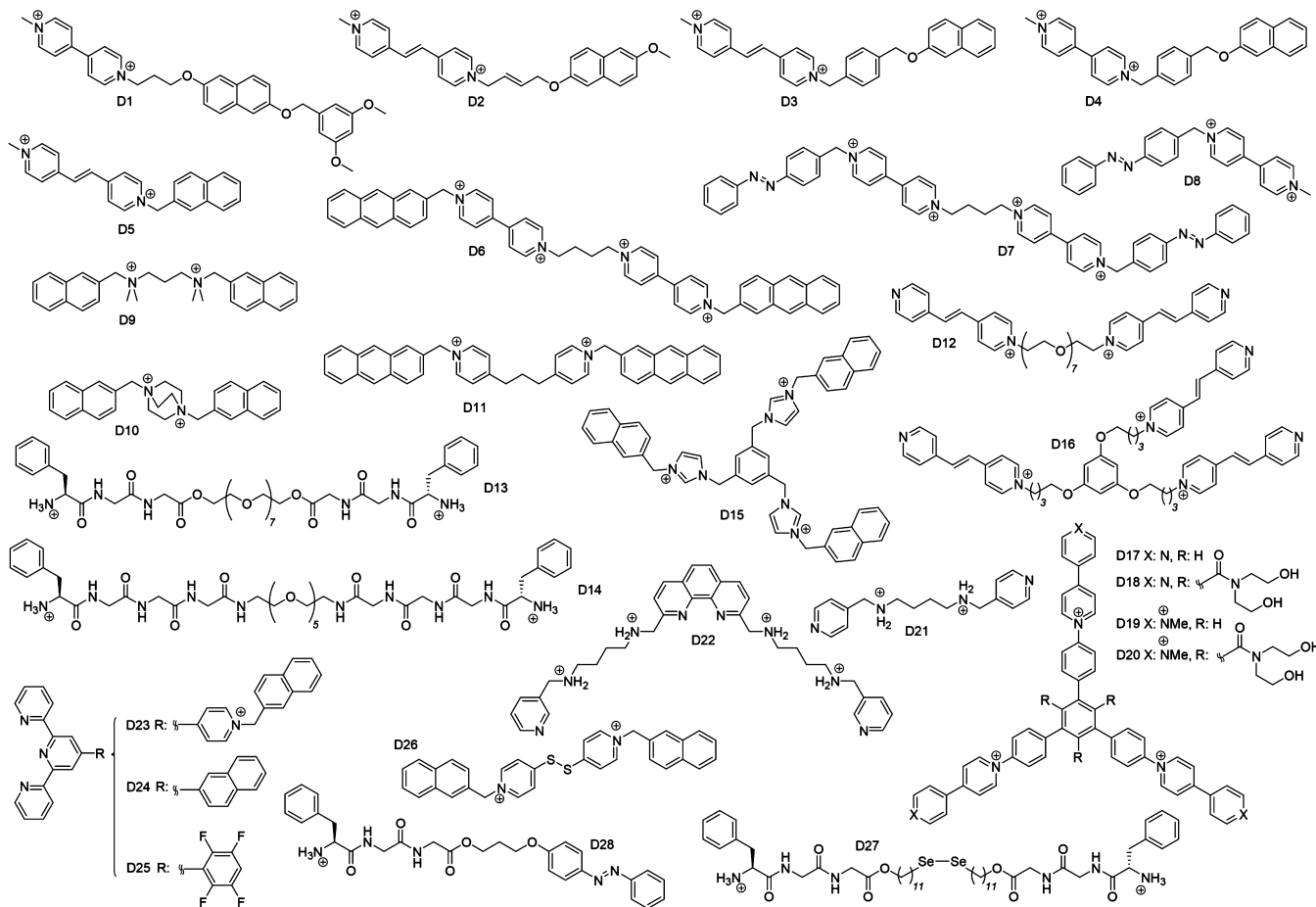


Figure 28. Structures of monomers.

by CB[8] complexes, which has attracted increasing interest in recent years.

9.1. Small-Molecule-Based Supramolecular Polymers

The construction of CB[n] noncovalent polymers based on low molecular weight monomers is analogous to a polycondensation reaction^{259–261} and involves the binding of small-molecule guest molecules through CB[n] host–guest interactions where CB[n] acts mainly as a “molecular handcuff” holding together the repeating units of the supramolecular polymer. There exist several design parameters that must be considered in order to produce systems that take full advantage of the properties of CB[n] and generate dynamic polymeric constructs with controlled molecular weight and structure.

The degree of association of supramolecular moieties is strongly affected by both their concentration in solution and their equilibrium constant and is approximately proportional to $(K_{\text{eq}} \cdot C)^{1/2}$.²⁶² Therefore, both the concentration and the binding strength between the repeating units have to be high in order to achieve a high degree of polymerization. The solubility of CB[n] and their complexes varies largely across this family of host molecules—CB[5] and CB[7] are much more water soluble than CB[6] and CB[8]¹⁵—and depends on a number of parameters including solvent, temperature, ionic strength, and guest. The majority of investigations on CB[n] supramolecular polymers involve CB[8] complexes, which typically exhibit a limited solubility in water. The advantages afforded by the high binding constants of CB[n] complexes,

however, supersede the potential drawbacks from low water solubility.

Another key consideration associated with such dynamic systems is the formation of macrocycles and the presence of ring–chain or ring–ring equilibria, which will impact the size of the polymeric aggregates that can be obtained.^{263–265} As with all equilibrium polymerization, a percentage of the chains will be cyclized and the distribution of rings vs linear chains will depend on a number of factors including monomer shape, length, flexibility, strength of the binding motif, concentration, and temperature.

The third consideration is related to the binding mode between repeating units. There is a myriad of “complementary” or “self-complementary” binding motifs that have been utilized for the preparation of supramolecular polymers.²⁶² Complementary motifs can be either two-component or three-component, whereby a third moiety is required for association. Some metal–ligand systems including 2,6-di(2-pyridyl)pyridine and 1,10-phenanthroline constitute a three-component binding whereby two moieties of the same type are complexed by a single metal ion. Indeed, metal–ligand interactions have been widely exploited and afforded a facile synthesis of linear and branched supramolecular polymers.²⁶⁶ CB[8] is a relatively large member of the CB[n] family and can bind two organic guests simultaneously. Kim and co-workers have shown that a stable ternary charge-transfer complex between MV, as a first guest, and 2,6-dihydroxynaphthalene, as a second guest, readily forms inside the cavity of CB[8].¹²⁸ Furthermore, the ternary complex is known to form in a stepwise manner with two

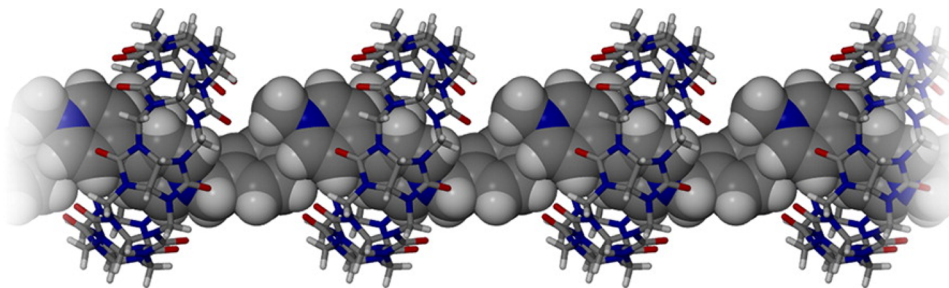


Figure 29. Side view of the X-ray crystal structure of $\text{CB}[8]_n \cdot \text{D}8_n$. C, gray; N, blue; O, red; H, white. Reprinted with permission from ref 276. Copyright 2013 American Chemical Society.

subsequent equilibria. This three-component binding motif is rather unique and reflects molecular recognition of complementary moieties in the presence of a macrocyclic host molecule. In addition, $\text{CB}[8]$ can also accommodate two molecules of the same kind including coumarin,¹⁵² anthracenyl,¹³⁶ and naphthyl¹⁵⁶ derivatives. $\text{CB}[10]$ and *nor-seco-CB[10]*, similarly to $\text{CB}[8]$, can bind two organic guests simultaneously inside their cavities, and their application in the area of aqueous supramolecular polymerization, although with limited success, has also been explored.^{267,268} Nevertheless, it is without a doubt that progress in creating novel $\text{CB}[n]$ -mediated polymers has been so far strongly tied to the discovery of new $\text{CB}[8]$ complexes and novel guest design. A facile route to small-molecule $\text{CB}[8]$ guest polymerization involves the covalent attachment of a first guest to a second guest moiety. Alternatively, a monomer equipped with two moieties that can be dimerized inside $\text{CB}[8]$ can also yield linear polymeric structures. A third option is based on an equimolar mixture of two complementary divalent monomers—first and second guest dimers. We next summarize recent research efforts in the area of $\text{CB}[8]$ supramolecular polymers.

Kim and co-workers were the first to investigate the host–guest complex formation between $\text{CB}[8]$ and a guest molecule having both a first and a second guest moiety connected by an organic linker. Several types of supramolecular assemblies were obtained by this process depending on the length and flexibility of the linker between the binding moieties. It was reported that the long and flexible trimethylene linker of **D1** favors 1:1 complexation with $\text{CB}[8]$ (Figure 28).²⁶⁹ A similar result was obtained for the apparently more rigid but-2-enyloxy linker of **D2** (Figure 28). The introduction of an even more rigid *p*-xylylene linker **D3** in Figure 28 effectively prevented 1:1 complexation inside $\text{CB}[8]$ but failed in promoting chain extension as only a 2:2 complex was produced.²⁷⁰ When $\text{CB}[8]$ and monomer **D4** were mixed in equimolar amounts (2 mM, aqueous solution) a mixture of a 2:2 complex and oligomeric species (3:2 ratio) was produced.²⁷¹ The hydrodynamic volume of the oligomeric, likely cyclic, species was estimated by diffusion-ordered NMR spectroscopy, and a degree of polymerization of ca. 4 was proposed. Linear supramolecular polymers were successfully grown from a gold surface functionalized with dipyridylmylethylene units. A surface-anchored poly(pseudorotaxane) was grown by soaking the functional gold surface in an aqueous solution of $\text{CB}[8]$ and monomer **D4** (1 mM, water). After a 1 day incubation period, the poly(pseudorotaxane) reached a degree of polymerization of 4. The surface-anchored poly(pseudorotaxane) was characterized by surface plasmon resonance and atomic force microscopy images. Monomer **D5** contains a naphthalene and a dipyridylmylethylene unit connected by a methylene bridge.

Although the short linker prevents intramolecular complexation, the structural design again promotes cyclization rather than linear polymer formation. An equimolar mixture of $\text{CB}[8]$ and **D5** resulted in a stable cyclic pentamer comprising five $\text{CB}[8]$ molecules and five guest molecules.²⁷²

In order to circumvent cyclization, Zhang and co-workers designed a monomer containing up to four $\text{CB}[8]$ binding sites in a single monomeric structure. The structure of such a monomer contains two central viologen moieties and two terminal anthracene groups, providing what was called a “double handcuff” to hold repeating units together (**D6** in Figure 28).²⁷³ The short methylene linker between the anthracene and the viologen moieties avoids intramolecular complexation, while the pair of central viologens effectively prevents the formation of 2:2 complexes—the positively charged viologens will sit too close to each other in a cyclic 2:2 complex. When $\text{CB}[8]$ was mixed with **D6** in a 1:1 ratio the appearance of a charge-transfer band evidenced heteroternary complex formation. The 1:1 stoichiometry of the complex was corroborated by Job’s plot analysis. AFM-based single-molecule force spectroscopy analysis showed the formation of extended polymer chains. The force curves of the supramolecular polymer were similar to traditional macromolecules, and a Kuhn and chain length of ca. 2.2 and 60.0 nm, respectively, were determined [comparatively, the Kuhn length for DNA in water²⁷⁴ and poly(*tert*-butyl methacrylate)²⁷⁵ in toluene are approximately 100 and 2 nm, respectively]. Dynamic light scattering experiments provided further evidence of polymer formation, with the Rh of the chains determined to be on the order of 30 nm.

Inspired by the previous monomer design proposed, Scherman and co-workers investigated an analogous guest structure equipped with azobenzene instead of anthracene moieties (**D7** in Figure 28). The formation of supramolecular polymers was characterized both in solution and in the solid state through a combination of dynamic and static light scattering and synchrotron SAXS and SANS, see Figure 29.²⁷⁶ Interestingly, the shorter monomer **D8** can also form relatively long linear structures in solution, which coexist with the more stable 2:2 complex. These polymers can be readily depolymerized by UV light irradiation as the *E*-azobenzene moieties isomerize into the *Z*-isomer that fully occupies the $\text{CB}[8]$ cavity with a high binding constant. The formation of a 1:1 complex between $\text{CB}[8]$ and *Z*-azobenzene was investigated in solution by ITC and NMR. Additionally, single crystals of the polymeric structure were obtained and analyzed by X-ray crystallography. This light-controlled formation of $\text{CB}[8]$ complexes is substantially different to other light-actuated host–guest systems and may find applications in biological and materials sciences.

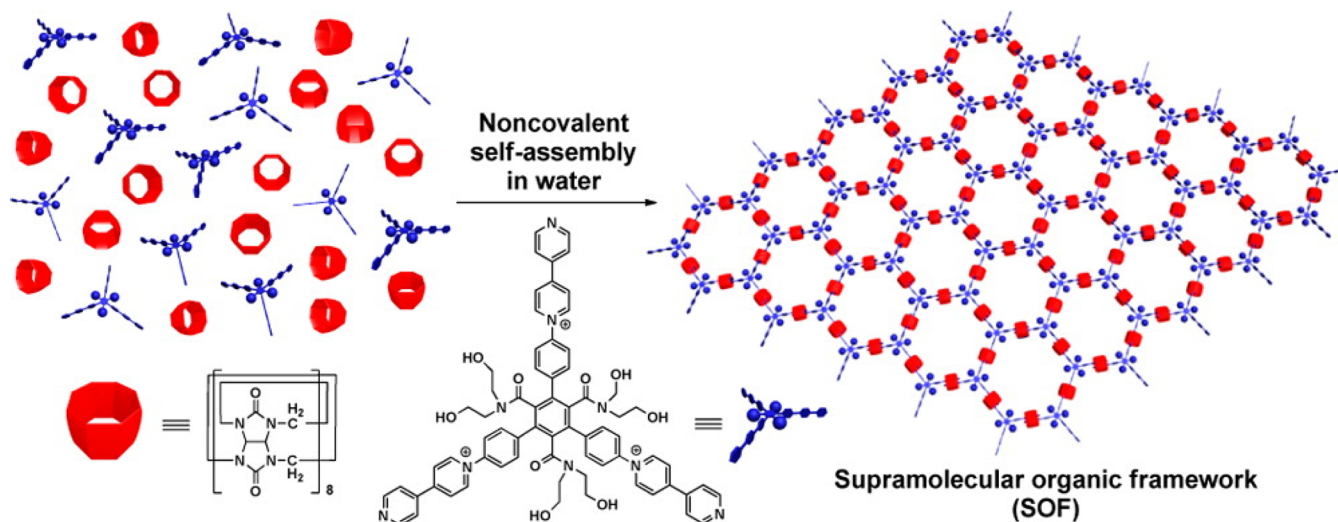


Figure 30. Schematic representation of the self-assembly of monomer D20 and CB[8]. Reproduced with permission from ref 286. Copyright 2014 The Royal Society of Chemistry.

Zhang and co-workers investigated the formation of supramolecular polymers based on a wide variety of homotopic divalent monomers containing self-complementary CB[8] binding moieties including naphthalene, anthracene, phenylalanine, and quaternized azastilbene groups (see D9–D13 in Figure 28).^{277–280} These moieties readily dimerized inside the cavity of CB[8], thus promoting polymerization. Monomers D9 and D10 contain two naphthalene moieties in close proximity to positively charged quaternary amines.²⁷⁸ The flat aromatic groups can form host–guest enhanced π – π complexes in the presence of CB[8], and the positive charges ensure the water solubility of the final polymer and further stabilization through ion–dipole interactions with the ureidyl carbonyl portals. While D9 only formed cyclic oligomeric species in the presence of CB[8], D10 resulted in long, linear polymeric structures. This was attributed to the rigid, shape-persistent 1,4-diazabicyclo[2.2.2]octane-1,4-diium linker, which can effectively inhibit cyclization. The degrees of polymerization estimated by DOSY NMR spectroscopy were on the order of 64 for the polymer based on D10 and 7 for the oligomeric species derived from D9 (1 mM, water), thus highlighting the crucial role of the monomer spacer. The same group nevertheless showed that other monomers D12 and D13 (Figure 28) with much longer and flexible linkers than D10 can also polymerize. One interesting example is provided by the comparison of monomers D13 and D14. Zhang and co-workers investigated the supramolecular polymerization of D13 in the presence of CB[8] based on MALDI-TOF mass spectrometry and AFM-based single-molecule force spectroscopy. Both techniques evidenced the formation of polymers with a degree of polymerization on the order of 20–60. Dankers and co-workers recently investigated the binding properties of D14 through a combination of ITC, DOSY NMR spectroscopy, and QTOF and MALDI-TOF mass spectrometry and found no evidence of polymer formation.²⁸¹ Data suggests that ring–chain equilibrium is in fact fully directed to ring formation (1:1 complex). The formation of this complex can be described by an overall binding constant $K_{\text{ring}} = 9.0 \times 10^6 \text{ M}^{-1}$ and an effective concentration of 750 μM . The well-defined ring structure of the cyclic dimer D14·CB[8], with a high equilibrium constant, provided a very efficient inhibition

mechanism for CB[8] protein dimerization processes as it can readily displace phenylalanine-containing peptide sequences from different proteins.²⁸² MALDI-TOF analysis of CB[8] polymers from both D13 and D14 revealed peaks at high molecular weight, which were attributed to supramolecular polymer formation by Zhang and co-workers, whereas Dankers and co-workers ascribed them to CB[8] aggregates artifacts.

The concept of CB[8] homoternary complexation has also been expanded toward the preparation of hyperbranched polymer structures, networks, and 2D polymer networks from monomers equipped with at least 3 binding sites (D15, D16, and D18 in Figure 28).^{283–287} It is noteworthy that, again, the flexibility of the monomer will determine the final structure of the polymers; monomers with flexible linkers (D15 and D16) will result in hyperbranched polymers, whereas 2D networks are produced from the more rigid monomer D18.

Another interesting concept consists of exploiting CB[8]-enhanced radical dimerization as a driving force in supramolecular polymerization. Kim and co-workers reported in 2002 that methyl viologen binds to CB[8] in 1:1 stoichiometry with a binding constant on the order of 10^5 M^{-1} .¹⁴² When methyl viologen is reduced to the radical cation, a 1:2 complex is formed exclusively. The apparent binding constant for the dimerization process is on the order of 10^7 M^{-1} . This homoternary complex is extraordinarily stable on account of extensive ion–dipole interactions between the ureidyl carbonyl portals of CB[8] and MV^{+} . In addition, the host provides the dimer with a hydrophobic cavity of the right size to host the couple of radical cations. Thus, the presence of CB[8] affords a convenient, simple, and reversible mechanism to drive self-assembly of a variety of organic moieties. Kaifer and co-workers reported in 2004 that the complexation-enhanced dimerization of viologen radical cations can be utilized to self-assemble Newkome-type dendrons equipped with a MV moiety at their focal point.²⁸⁸ Zhan-Ting Li, Yi Liu, and co-workers recently described the formation of 2D supramolecular organic frameworks from shape-persistent viologen-containing trimers (monomers D19 and D20).²⁸⁶ The viologen moieties of the trimers can be easily reduced in the presence of sodium dithionite, thus inducing self-association in water. The reduced trimer D19 stacks strongly in a face-to-face fashion, forming

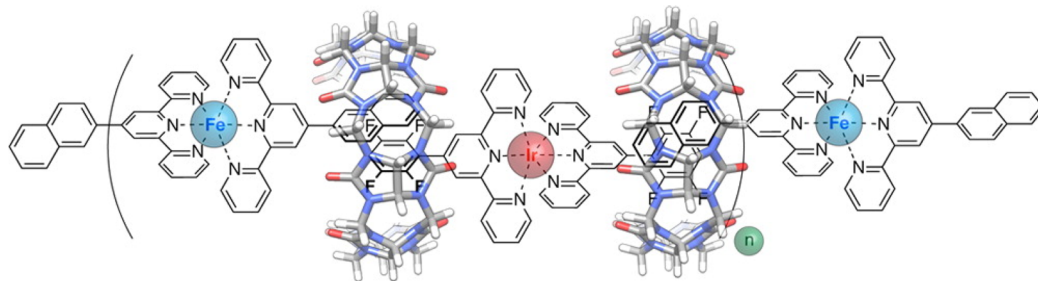


Figure 31. Schematic representation of the alternating polymer resulting from an equimolar mixture of $([\text{Fe}\cdot\text{D}24]^{2+}\cdot\text{CB}[8])_n$ and $([\text{Ir}\cdot\text{D}25]^{3+}\cdot\text{CB}[8])_n$. Reprinted with permission from ref 302. Copyright 2014 American Chemical Society.

discrete 2 + 3 complexes with CB[8]. However, the presence of the bulky bis(2-hydroxyethyl) carbamoyl groups of D20 avoids face-to-face stacking, thus leading, after reduction, to the formation of a single-layer 2D supramolecular organic framework, which is stabilized by the strong complexation of CB[8]. The new supramolecular networks were characterized by UV/vis absorption, EPR, DLS, as well as solution and solid-phase small-angle X-ray diffraction experiments. The single-layer feature of the network was confirmed by AFM imaging as the average thickness of the supramolecular framework was consistent with the diameter of CB[8]. Analogous monomeric trimers derived from 4,4-bipyridin-1-ium (monomers D17 and D18) also self-assemble in the presence of CB[8] in a similar fashion to the previously described reduced trimers, Figure 30.²⁸⁷

In 2004, Kim and co-workers described the first stable π dimer of a tetrathiafulvalene radical cation encapsulated inside the cavity of CB[8].²⁸⁹ This was demonstrated through a combination of NMR, UV/vis, and EPR spectroscopies. TTF binds to CB[8] and is simultaneously oxidized to the radical cation species forming a stable three-component complex as a red precipitate. Although no quantitative binding study was performed, this work demonstrated the effectiveness of CB[8] in stabilizing unstable species through molecular encapsulation. TTF radical dimerization has been shown to be extremely useful in exerting redox control over a wide variety of polymeric structures and mechanically interlocked constructs. However, supramolecular polymer formation driven by encapsulation of the TTF radical cation inside the cavity of CB[8] has not been realized yet.

Supramolecular polymers constructed by orthogonal self-assembly based on host–guest, including CB[n]s, and other dynamic covalent/noncovalent interactions are attracting increasing attention.^{295,296} Kim and co-workers pioneered the area CB[n] orthogonal self-assembly by designing a wide variety of metal–organic CB[n] polyrotaxanes.²⁹⁷ One of these structures consists of a pseudorotaxane—prepared by a simple mixture of D21 and CB[6]—that yields a linear polymer in the presence of Cu²⁺ through pyridine–metal-ion coordination.²⁹⁸ A polycatenated 2D polyrotaxane net is formed, however, if Ag⁺ is used instead of Cu²⁺.²⁹⁹ The same strategy combined with a more complex ligand D22 produces double-chained and zigzag-shaped 1D polyrotaxanes in the presence of Cd²⁺ and Co²⁺.³⁰⁰ The repeating units of these metal–organic structures are held together by metal–ligand, not host–guest, interactions; however, the CB[n] complex plays a crucial role as it imparts rigidity to the organic linker. More recently, Zhang and co-workers investigated the preparation of CB[8] supramolecular polymers through a combination of host–guest and terpyridine–Fe²⁺ interactions.³⁰¹ Monomer D23 is a heteroditopic

molecule consisting of a naphthalene and terpyridine moiety which can be dimerized in the presence of Fe²⁺, forming a monomer with two terminal naphthalene moieties, [Fe·D23]²⁺. This new metal-containing monomer can undergo polymerization when mixed with an equimolar amount of CB[8] in a similar fashion to monomer D10. It was claimed that the cationic metallic center enhances the water solubility of the complex while serving as a rigid spacer between the CB[8] binding sites. Masson and co-workers further explored this concept and demonstrated that Coulombic interactions between metal centers and CB[n] can actually be mediated by an organic ligand and showed that, even in the second coordination sphere, CB[n] form strong CH···O hydrogen bonds with the ligand surrounding the metallic core.³⁰² This recognition process is driven by a combination of favorable enthalpies (up to 20.2 kcal·mol⁻¹) and very unfavorable entropic contributions (as low as -10.2 kcal·mol⁻¹). The recognition properties of the metal–ligand complexes were extended to CB[8], and dynamic supramolecular oligomers were prepared by mixing equimolar amounts of ligand D24 and CB[8] in the presence of Fe²⁺ and Ir³⁺. The approximate degrees of polymerization of the oligomers, based on DOSY NMR spectroscopy, were 11 and 54 for the Fe²⁺ and Ir³⁺ polymers (1 mM, water). CB[8] can also encapsulate 2,3,5,6-tetrafluorophenyl units, and supramolecular oligomers were also produced when mixing [Fe·D25]²⁺ and [Ir·D25]³⁺ with CB[8] in equimolar amounts (Figure 28). Degrees of polymerization of 27 and 15 were estimated for the Fe²⁺ and Ir³⁺ polymers, respectively. Also, social self-sorting was observed for an equimolar mixture of $([\text{Fe}\cdot\text{D}24]^{2+}\cdot\text{CB}[8])_n$ and $([\text{Ir}\cdot\text{D}25]^{3+}\cdot\text{CB}[8])_n$, thus generating well-defined oligomers with alternating Fe²⁺ and Ir³⁺ cationic centers, Figure 31. The preference for naphthalene–tetrafluorophenyl pairing was attributed to favorable quadrupole–quadrupole interactions in a similar fashion to those present in benzene–perfluorobenzene pairs.^{303,304} In addition to metal–organic interactions, other types of dynamic covalent chemistries have been combined with CB[8] host–guest interactions to produce linear supramolecular polymers. These include thiol–disulfide, diselenides, and cyclodextrin host–guest interactions (monomers D26–D28 in Figure 28).^{305–307} D28, as an example, comprises an azobenzene moiety covalently attached to a phenylalanine residue. The monomer can dimerize in the presence of CB[8] to form a 2:1 D28₂·CB[8] complex, which can undergo subsequent polymerization when mixed with an equimolar amount of a β -cyclodextrin dimer.³⁰⁷

The concept of CB[8]-mediated phenylalanine dimerization was also exploited by Liu and co-workers in the design and synthesis of protein polymers.³⁰⁸ In this case, a homodimer glutathione S-transferase was selected as the building block for

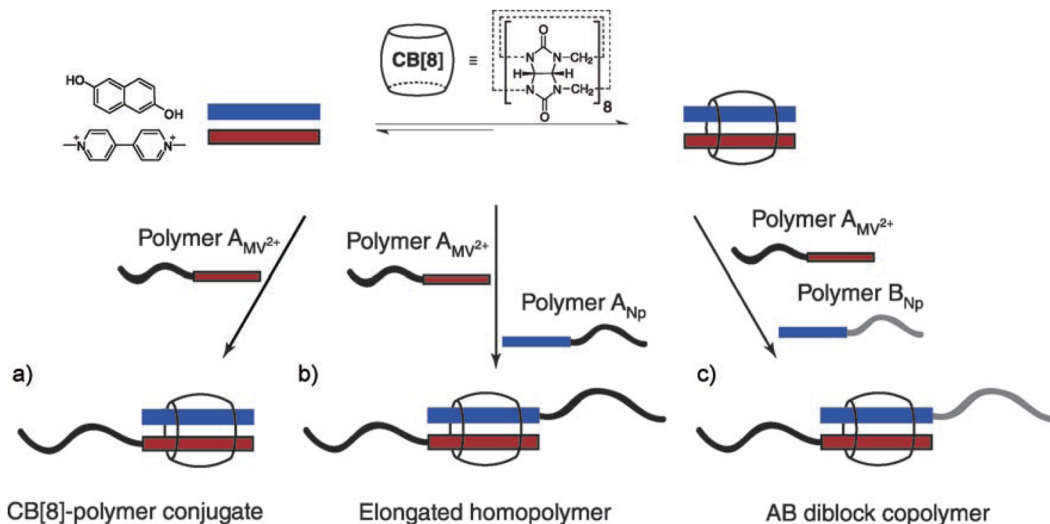


Figure 32. Host-stabilized charge-transfer complexes allow for the formation of a variety of macromolecular materials from CB[8]-polymer conjugates, elongated or chain-extended linear homopolymers and AB diblock copolymers. Reproduced with permission from ref 310. Copyright 2008 John Wiley and Sons, Inc.

genetic fusion with phenylalanine-glycine-glycine oligopeptides at each side of its N-termini. The homodimer protein polymerizes via homoternary complex formation between two phenylalanine residues and CB[8] as demonstrated by the increase of the molecular weight of the aggregate. The protein-based polymer had a wire-shaped structure with an average length of 128 nm (degree of polymerization around 25) and a height of about 4.8 nm. This protein assembly was highly stable and could even undergo separation by gel permeation chromatography and further functionalization with glutathione peroxidase.

Finally, Zhang and co-workers recently reported a novel polymerization methodology controlled by CB[8] and CB[7] self-sorting.³⁰⁹ The supramolecular polymerization of a tetracationic monomer composed of *p*-phenylene and naphthalene moieties was promoted by the selective recognition of the central *p*-phenylene ring by CB[7] followed by a CB[8] naphthalene double encapsulation. A degree of polymerization of ca. 28 was obtained by asymmetric flow field flow fractionation (that conveniently bypasses the use of GPC stationary phases) coupled to multiangle light scattering.

9.2. CB[8]-Mediated Supramolecular Block Copolymerization

Not only is supramolecular polymerization possible by CB[8] complexation of small molecules, higher molecular weight molecules such as polymers can also be complexed at their termini or via side chains to other polymers, small molecules, biomolecules, etc. As the following section will demonstrate, this process can lead to large and facile increases in molecular weight, not only affording chain-extended polymers. However, by relying on the specific heteroternary 1:1:1 CB[8]-stabilized charge-transfer complex, self-sorted amphiphilic supramolecular block copolymers can be produced allowing formation of micelles and vesicles that can be assembled, disassembled, and reassembled using various stimuli-responsive triggers.

9.2.1. Supramolecular Assembly of Macromolecules.

Kaifer and co-workers first demonstrated macromolecular assembly with CB[8] by centrally and noncovalently complexing two distinct dendrimers, one functionalized with MV (electron acceptor) and a second with *p*-dialkoxybenzene

(electron donor).¹³¹ In this study, dendrimers were selectively assembled on account of the guest covalently attached, and the efficiency of this process was shown to be dependent on the size of the corresponding dendritic units. Electrochemical one-electron reduction of viologen resulted in homodimerization of dendrimer units on account of 2:1 complexation of the MV radical cations to CB[8], and therefore, redox switching between discrete molecular weight dynamic dendrimer dimers was possible.

A facile methodology of block copolymerization by supramolecular complexation is that of the dimerization of MV-terminated polymers to Np-terminated polymers by CB[8] addition, Figure 32.³¹⁰ This leads to the formation of linear dynamic elongated homopolymers and AB-diblock copolymers, as demonstrated by Scherman and co-workers. Dynamic amphiphilic polymers of PEG and *cis*-1,4-poly(isoprene) or octadecane were prepared, and these were also able to form larger vesicular structures in a highly versatile manner.

Ji and co-workers reported similar aqueous structures of a linear hyperbranched polyphosphate with a terminal MV unit that complexed to CB[8] and poly(D,L-lactide) with terminal indole units.³¹¹ This formed an amphiphilic block copolymer structure that would assemble into a biocompatible micellar structure. Disassembly of these micelles was possible by reduction of the MV units with sodium dithionite, breaking the heteroternary complex.

Actual polymeric chain extension by CB[8] complexation at polymer termini was investigated by Jiang and co-workers, Figure 33a.³¹² Low molecular weight poly(*N,N*-dimethylacrylamide) and poly(*N*-isopropylacrylamide) with naphthyl moieties at both termini were synthesized via reversible addition–fragmentation chain transfer (RAFT). These polymers were then combined in solution with a viologen dimer and CB[8] to form host-stabilized charge-transfer complexes and higher molecular weight supramolecular polymers from the lower molecular weight building blocks. The existence of these higher molecular weight supramolecular polymers was observed using viscometry techniques. The resultant supramolecular pNIPAm also expressed interesting LCST behavior, which was strongly dependent on concentration (higher concentrations

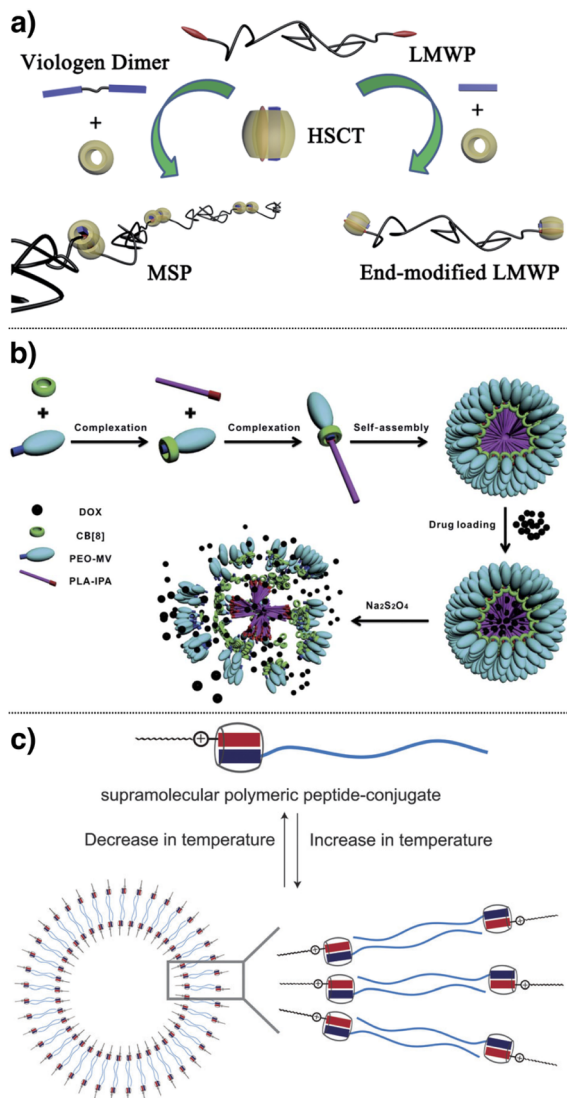


Figure 33. Higher order structures afforded through CB[8] host-guest chemistry. (a) Chain-extended polymers by CB[8] complexation of terminally functionalized polymers to viologen dimers. Adapted with permissions from ref 312. Copyright 2014 The Royal Society of Chemistry. (b) Supramolecular assembly of amphiphilic block copolymers leads to micelle formation which has utility in drug delivery. Adapted with permission from ref 316. Copyright 2014 The Royal Society of Chemistry. (c) Aqueous self-sorting of supramolecular polymers allows for vesicle formation. Adapted with permission from ref 318. Copyright 2014 The Royal Society of Chemistry.

are associated with lower LCSTs), unlike covalent pNIPAm, which exhibits very limited concentration dependence on its critical temperature.

Not only is supramolecular complexation possible at the polymer terminus, indeed Scherman and co-workers also demonstrated the reversible and stimuli-responsive loading of side chains onto hydrophilic polymer chains by utilizing CB[8] ternary complexation motifs.³¹³ A copolymer of oligoethylene glycol acrylate and a naphthol-bound monomer was synthesized via RAFT polymerization. MV derivatives were then reversibly complexed to the naphthol residues. In particular, MV-bound hydrophobic residues such as C18 chains could be “pulled” into aqueous solution using this complexation method.

Upon addition of sodium dithionite, the MV moieties were reduced from dicationic species to radical cations, breaking the 1:1:1 heteroternary complexes. This process was in turn reversible by bubbling air through the solution, oxidizing the MV and regenerating the charge-transfer complexes. This work holds design features amenable to controlled or triggered release delivery devices. Monosaccharides and multivalent ligand–lectins have similarly been noncovalently attached to such copolymers to add biorecognition modalities.³¹⁴ A supramolecular glycopolymer was produced, which could bind lectins and then be released from the copolymer backbone using redox methods. Such polymer designs could be further used to probe cellular activity and biomarkers. Development of this area has led to the development of drug delivery applications with both Scherman and Ji reporting the delivery of doxorubicin, a commonly used chemotherapeutic, from supramolecular micellar structures. In both cases, CB[8] heteroternary complexation was employed to form supramolecular amphiphilic block copolymers, which would in turn form micelles through hydrophobic interactions, Figure 33b.^{315,316} Scherman and co-workers constructed triply stimuli-responsive micelles from temperature- and chemo-responsive CB[8], pH-responsive naphthalene-terminated poly(dimethylaminoethyl methacrylate) (PDMAEMA-Np), and temperature-responsive MV-terminated poly(*N*-isopropylacrylamide) (PNIPAAm-MV). Mixing these components in aqueous solution in an equimolar ratio resulted in micelle formation in which doxorubicin was encapsulated. Changes in pH and temperature or addition of the competitive guest, adamantylamine, resulted in disassembly of the micelles and release of doxorubicin, which was shown to have a direct effect on cell viability. Moreover, exposed cell lines exhibited good tolerance of the doxorubicin-loaded micelles, only exhibiting detrimental effects upon triggered release. Ji and co-workers reported a similar assembly of micelles utilizing a different heteroternary supramolecular motif. In this example, the hydrophobic block consisted of an indole-terminated poly(lactic acid) whereby indole is an electron-rich moiety utilized in the charge-transfer handcuff motif. The hydrophilic block consisted of MV-terminated PEO. Furthermore, both poly(ethylene oxide) and poly(lactic acid) have been FDA approved for medical use, and the latter also has an excellent biodegradability profile. Again, doxorubicin encapsulation was possible within the hydrophobic core of the micelle, and release could be triggered by addition of sodium dithionite, reducing the MV and causing disassembly.

Indeed, supramolecular assembly of higher order structures is not limited to micelles, and the aqueous construction of double-layer vesicles was also reported by Scherman and co-workers in 2012.³¹⁷ Assembly of a pyrene-GGGKKK peptide with a MV-lipid through host–guest ternary complexation with CB[8] afforded 200 nm spherical double-layered vesicles, observed by DLS and TEM. Furthermore, these vesicles were readily absorbed by cells, and fluorescence imaging of the cells could be achieved by uptake of either 1,6-dihydroxynaphthalene or adamantylamine to break the ternary complex, releasing the fluorescent pyrene–peptide. Supramolecular polymeric analogues of these vesicles (Figure 33b) are pertinent for use as delivery devices of large biomolecules, in particular, basic fibroblast growth factor (bFGF).³¹⁸ These vesicles protected bFGF against several freeze–thaw cycles and were effective delivery devices to cells, therefore showing good promise as an injectable therapy. Das and co-workers expanded work in this

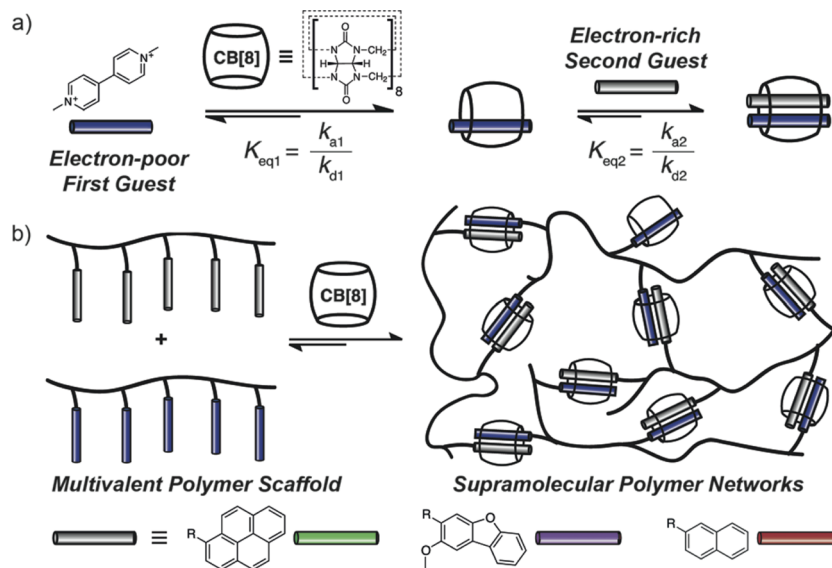


Figure 34. Combination of multivalent polymers bearing first guest (MV) and second guest (either Pyr, DBF, or Np) with CB[8] in water leads to supramolecular network formation and viscoelastic materials. Figure reproduced with permission from ref 328. Copyright 2014 John Wiley and Sons, Inc.

area to form mixed micelles of viologen amphiphiles and tetralkylammonium salts in water. These micelles could then be transformed into vesicles through host–guest complexation with CB[8].³¹⁹ Furthermore, the rearrangement of these mixed micelles into vesicles was mechanistically studied, appearing to progress through a stable mixed-micelle stage; upon addition of CB[8], a dynamic mixture of nonspherical mixed micelles is formed, and then on addition of naphthalene-derived guests, the micelles structurally promoted into self-sorted vesicles.³²⁰

9.2.2. Conclusion and Outlook. Supramolecular block copolymerization is an exciting area with ongoing development of facile routes toward producing multiply responsive materials. From mechanistic studies of formation to advancement into bioapplicable delivery of growth factors, this area is undergoing new and extensive investigation. Supramolecular block copolymer materials are now poised for use in real-life applications, and we hope to see *in vivo* progression in the near future.

10. MOLECULAR RECOGNITION IN 3D SUPRAMOLECULAR NETWORKS

Hydrogels are becoming an important class of material on account of their high water content, tunable properties, and biocompatibility. In the example of polymeric hydrogels, water is encapsulated within a chemically or physically cross-linked macroscopic network by capillary forces and their stiffness and elasticity defined by polymer loading and cross-link density. Hydrogels formed via molecular recognition of CB[n] for specific chemical motifs pendant from polymer chains have become increasingly widely studied since 2010. The fabrication of such soft materials has been reviewed specifically in recent years, perhaps however prematurely, as the field of CB[n] cross-linked hydrogels is still developing.^{133–135} In the following examples, exploiting the host–guest complexes of CB[6], CB[7], and CB[8] to form physical polymer–polymer cross-links will be discussed and how the dynamics and control over such cross-linking has been investigated and utilized.

10.1. CB[8] Complexes Cross-Link Guest Functional Polymers

Scherman and co-workers extensively explored the formation of CB[8]-stabilized charge-transfer complexes between electron-poor and electron-rich species that are covalently bound to polymers. The random attachment of first and second guests, methyl viologen (MV) and naphthoxy (Np), respectively, to a variety of independent synthetic polymers was first achieved through the copolymerization of guest-bound monomers with either neutral, cationic, or anionic monomers in a ratio of 1:10.³²¹ Upon addition of CB[8] to a mixture of MV–polymer and Np–polymer (5 wt %) in water, viscoelastic materials were formed that expressed a responsiveness to stress and shear on account of the formation of multiple noncovalent ternary complexes between polymers, Figure 34. Moreover, this work also demonstrates a wide tolerance of charge on the formation of hydrogels through the CB[8] recognition motif through the utility of a variety of anionic and cationic polymers, as well as the appearance of viscoelastically tunable supramolecular networks through controlled CB[8] concentration.

Scherman and co-workers continued their exploration of these materials, focusing on the ability to form a predominantly elastic material with minimal polymer content (0.5 wt %).³²² To achieve this a high molecular weight polysaccharide, hydroxyethyl cellulose (HEC, MW = 1.3 MDa) was functionalized with Np moieties to a degree of 5 mol %. The resulting material was then combined in solution with CB[8] and a high molecular weight commodity polymer poly(vinyl alcohol) (PVA, M_n = 1.5 MDa) functionalized with MV. It was found that a range of soft material properties could be achieved and were accessible simply by modifying polymer loading. Impressively, a broad spectrum of storage moduli spanning 2 orders of magnitude ($10 > G' > 1000$) could be readily attained. Moreover, these materials were also shown to have excellent shear-thinning properties (resulting from the very low polymer loadings and noncovalent cross-linking) and also exhibited rapid self-healing behavior. The authors exemplified this by performing step-shear rheology experiments and demonstrated the viscosity of the material returned within

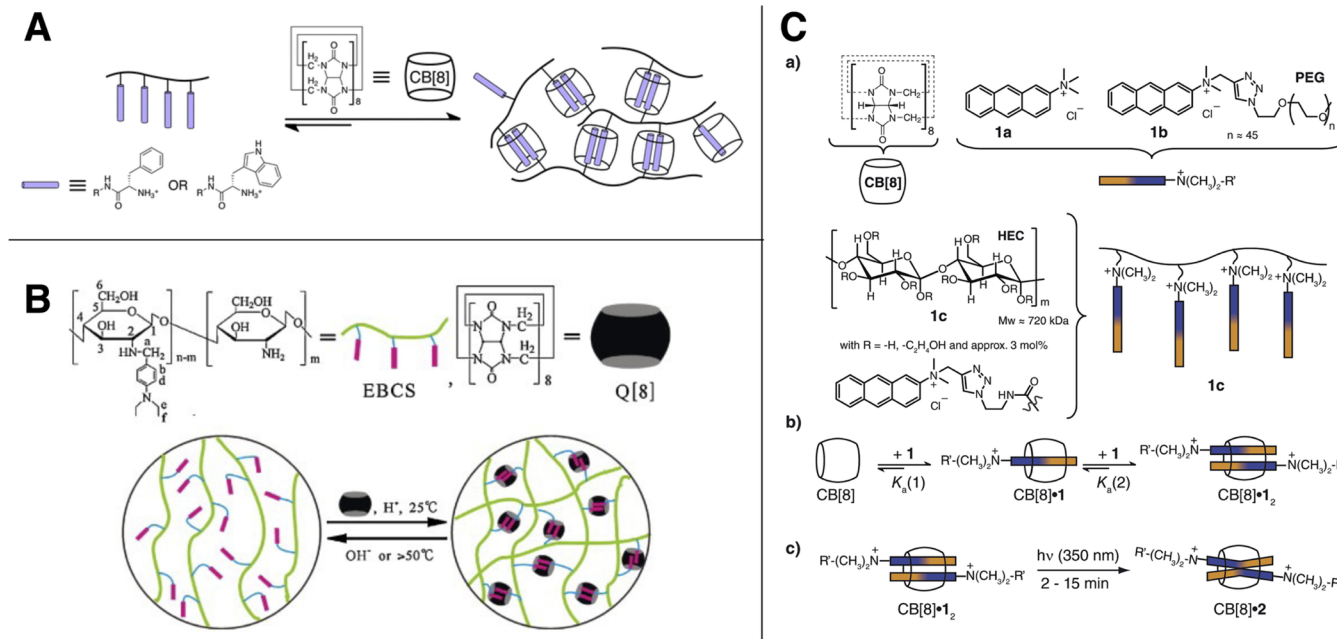


Figure 35. Combination of multivalent polymers bearing residues that can bind in a 2:1 fashion with CB[8] (i.e., (A) phenylalanine, tryptophan, (B) N-4-diethylaminobenzene, (C) anthracene) in water leads to supramolecular network formation. (A) Adapted with permission from ref 325. Copyright 2013 The Royal Society of Chemistry. (B) Adapted with permission from ref 327. Copyright 2013 Elsevier. (C) Adapted with permission from ref 162. Copyright 2014 The Royal Society of Chemistry.

seconds upon release of the high shear rates and that the process was also recyclable. Rapid recognition of Np-HEC by CB[8]_nMV-PVA complexes upon relaxation of the material facilitates healing, whereby the dissociated complexes are quickly reassociated under mechanical stimuli rather than the actual breaking and making of any covalent bonds, and so the properties are always 100% restored.

Furthermore, the release of small (lysozyme) and large (BSA) proteins from the HEC hydrogels has also been demonstrated.³²³ In this example, polymer concentration was altered in order to modulate the mesh size of the supramolecular network. By raising the polymer content, the mesh size was decreased and the proteins could be released at slower rates. Specifically, in the case of a 1.5 wt % HEC gel, BSA release was sustained for 160 days, showing excellent utility for these materials as biomedical delivery devices.

Modification of the system to use the polysaccharide chitin afforded hydrogel materials that were antimicrobial; however, they have found utility as a consolidant for archeological wood conservation, specifically on the Mary Rose, a 16th Century warship.³²⁴ By adding extra CB[8] binding moieties onto the chitin backbone, such as naphthalene and dopamine derivatives, a system was produced that could not only gelate and express all previous properties of such supramolecular hydrogels but also complex Fe³⁺ ions that persist in the water-logged artifacts. This system is therefore pulled into the porous wooden artifacts, strengthening them and “locking” the iron in place, preventing its transport and therefore further degradation as well as providing biocidal protection.

Focusing on further improving CB[8] hydrogel utility in the biomedical field, harnessing 2:1 binding of amino acids to CB[8] was also investigated as a route to hydrogel formation.³²⁵ Scherman and co-workers demonstrated hydrogel formation with synthetic cationic styrenic polymers bearing either phenylalanine or tryptophan derivatives, Figure 35a. It

was shown that phenylalanine 2:1 complexation to CB[8] afforded much stronger hydrogels than the tryptophan-derived polymers and that the material properties could be tuned by controlling CB[8] content and therefore cross-link density. This system is inherently simpler than the previous hydrogels as the network is only comprised of two components, a multivalent amino acid bearing polymer and CB[8], opposed to two different polymers (one bearing the first guest and the other the second guest) and CB[8]. However, the authors found that rigid polymers were required to form hydrogels as this prevented intrachain complexation of CB[8], as previously observed when polymers containing both first and second guest formed soft nanoparticles on addition of CB[8].³²⁶ In the future, the authors look to apply these amino acid recognition motifs to larger and more biomedically relevant polymers to improve water content and biocompatibility further.

A second example of 2:1 guest to CB[8] binding facilitating hydrogel formation was reported by Lin and co-workers in 2013, Figure 35b.³²⁷ Here, N-(4-dimethylaminobenzyl)chitosan (EBCS) was shown to form hydrogels of a variety of strengths upon addition of CB[8] under various pH conditions, allowing for control of release rates of the model drug cargo 5-fluorouracil. In this case, hydrogelation likely occurs through recognition and affinity of the protonated aminobenzyl groups by the ureido–carbonyl portals of CB[8]. Due to protonation of the aminobenzyl groups being a necessity, weak hydrogels were formed at pH 6.8 and strengthened at lower pH levels. Therefore, the facility to use this material in biomedical applications is quite restricted; however, pH control over specific recognition of aminobenzyl-derived moieties has been clearly demonstrated.

A further photoresponsive hydrogel construct from the Scherman group was reported in 2014. In this study, CB[8]-catalyzed photodimerization of anthracene in water was exploited in hydrogel formation, Figure 35c.⁴⁵ In this system,

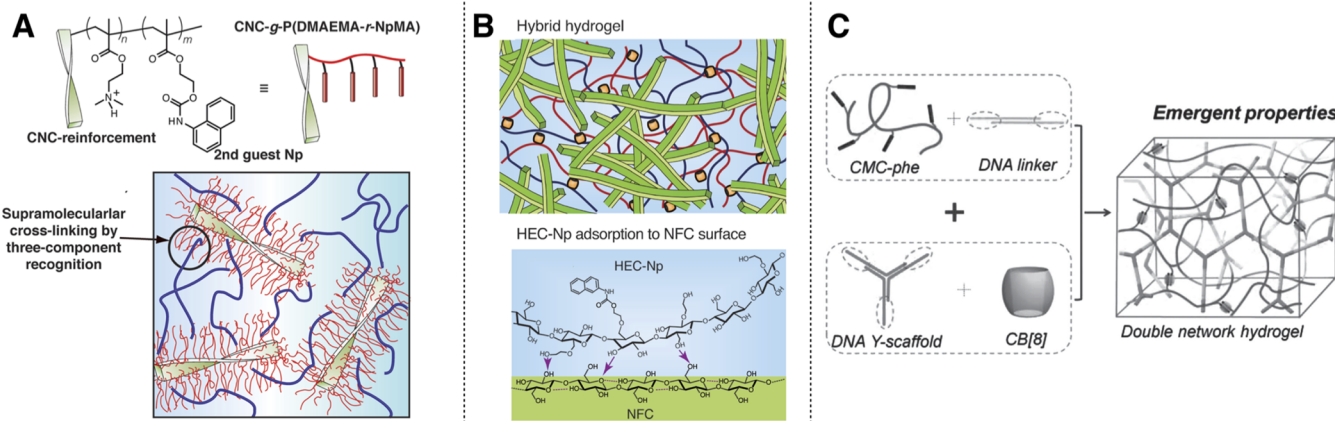


Figure 36. Examples of composite materials. (A) CNC dispersions physically cross-linked to MV-polymers via CB[8]. Reproduced in part with permissions from ref 330. Copyright 2014 John Wiley and Sons, Inc. (B) Colloidal NFCs with length scales crossed by supramolecular hydrogel adsorption to offset stress. Reproduced in part with permissions from ref 331. Copyright 2015 John Wiley and Sons, Inc. (C) Purely supramolecular double-networked hydrogel comprised of a DNA network and a cellulose/CB[8] network. Reproduced in part with permissions from Li and co-workers *Adv. Mater.* 2015, 10.1002/adma.201501102. Copyright 2015 John Wiley and Sons, Inc.

the anthracene-derived moieties form 2:1 inclusion complexes with CB[8] and were conjugated to an HEC backbone via a copper-accelerated cycloaddition to azide-derived HEC. The 2:1 anthracene:CB[8] complexation alone afforded elastic soft materials. Upon photoirradiation at 350 nm for 15 min the material experienced a hardening effect and the moduli roughly tripled in magnitude, accounted for by the covalent dimerization of the two anthracene moieties within the CB[8], resulting in the HEC network becoming covalently cross-linked. The presence of CB[8] within the system was shown to rapidly catalyze the formation of the anthracene dimers as irradiation of the same material in the absence of CB[8] did not yield materials of the same strength. Unfortunately, the dimerization of anthracene in this system was not shown to be reversible, so the hydrogelation via this photochemical CB[8]-catalyzed cross-linking process is a seemingly permanent conversion.

10.2. Dynamics of Cross-Linking Influences Material Properties

The nature of microscopic thermodynamic properties of physical cross-links within a supramolecular network can have a large impact on the material. Recognition of different small-molecule motifs by CB[8] in hydrogel formation thus has a great effect on the resulting hydrogel. In 2014, Scherman and co-workers explored the nature of the CB[8] ternary complex cross-linking motif and how the dynamic complexation of such motifs contributes toward defining hydrogel viscoelastic behavior.³²⁸ Investigation of different second guests beyond Np that have slightly different energetic binding properties to CB[8]_nMV was undertaken, Figure 34. The other second guests studied alongside Np were dibenzylfuran (DBF) and pyrene (Pyr), which have very similar overall equilibrium constants in the formation of the heteroternary complexes with CB[8]_nMV (1.5, 1.4, and 1.3×10^4 M⁻¹, respectively), determined by stopped-flow fluorescence experiments. Despite these seemingly similar equilibrium constants, the activation energies of dissociation (E_{ad}) of the second guest were found to be vastly different (Np 30 kJ mol⁻¹, DBF 54 kJ mol⁻¹, Pyr 89 kJ mol⁻¹). Physically cross-linked materials were prepared from multivalent poly(dimethylacrylamide) bearing one of the second guests, polystyrene-MV and CB[8]. Remarkably, all

materials were found to have virtually identical X-ray scattering profiles; however, frequency-dependent oscillatory rheology showed that the Pyr gels were the “most elastic” and the Np gels the least. This was attributed to the dissociative rates of the second guest. The authors showed that when scaling the rheology data with the value of E_{ad} for each second guest, the measured frequency-dependent rheology profiles overlaid almost exactly. Therefore, the strength and viscoelastic property of the hydrogels is not only dependent on conventional polymer physics and polymer interactions but also dependent on the dynamics of cross-linking, in particular, the choice of second guest used in the CB[8] ternary complex cross-linking motif, and specifically dependent on the E_{ad} of the second guest. In simpler terms, higher dissociative barriers of the second guest affords longer cross-link lifetimes and therefore stronger materials.

In a subsequent study, Scherman and co-workers investigated how the dynamics of physical cross-linking in these systems affect release of rhodamine from the supramolecular network.³²⁹ Higher release constants were observed for materials bearing second guests with lower E_{ad} values. This was accounted for through faster cross-link dynamics, allowing faster diffusive rates of solvent and cargo in and out of the gel network. Faster cross-link dynamics also led to faster erosion rates of the hydrogels as water is able to diffuse into the hydrogel easier, facilitating erosion through swelling mechanisms. By studying these phenomena, erosive and diffusive mechanistic contributions to rhodamine release could be understood, and material lifetimes are now potentially predictable. This study demonstrates that cross-link dynamics play a subtle yet important role in release of cargo from hydrogels and that the ability to robustly fine tune release and erosive rates is possible.

10.3. Composite Soft Materials Utilizing CB[8] Host–Guest Interactions

Collaboration between the Scherman and Ikkala groups resulted in the development of soft domain–hard domain composite hydrogels whereby homogeneous dispersions of cellulose nanocrystals (hard domains, CNCs) were cross-linked with soft polymeric domains via host–guest interactions between MV, Np, and CB[8], Figure 36a.³³⁰ This was achieved

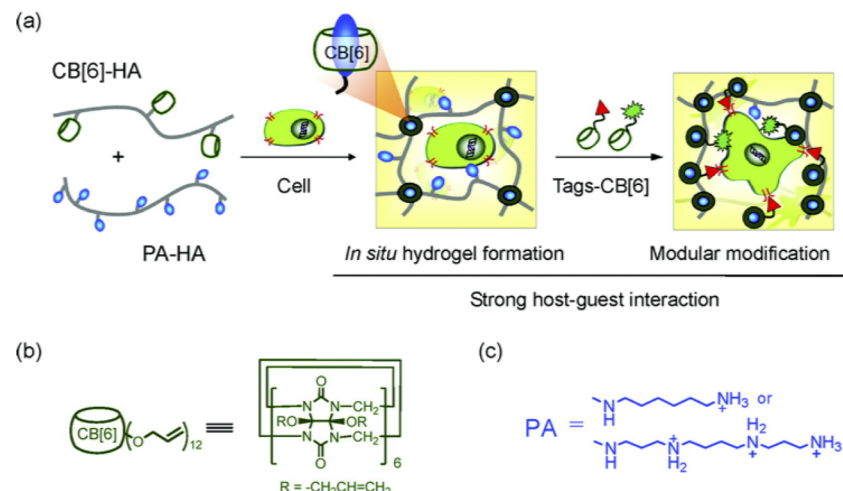


Figure 37. Attachment of CB[6] directly to hyaluronic acid and combination with PA–HA affords a good cell culture scaffold with further opportunity to complex cell-signaling moieties to the hydrogel network for tissue-engineering applications. Reprinted with permission from ref 333. Copyright 2012 American Chemical Society.

by using CNCs decorated with surface ATRP initiator moieties to graft methacrylate polymers bearing multiple Np units. Mixing the functionalized CNCs with PVA–MV polymers and CB[8] produced supramolecular materials that were 85% water, extremely well structured as exemplified by frequency-dependent rheology, highly elastic ($G' \gg G''$), and rapidly self-healing (healing time < 6 s). These are combined and desirable properties of both hard and soft materials which would usually be seen to be conflicting or unable to operate together in the same material. Moreover, materials that were cut in half and kept separate for 4 months were pushed back together and their viscoelastic property completely restored after just a few seconds. This property is remarkable in that the material was not passivated even after months and did not require any activation, something that had not been previously demonstrated in other supramolecular systems.

A follow-up study between the two groups led to the development of a composite hydrogel of nanofibrillar cellulose (NFC) and HEC, again supramolecularly cross-linked with CB[8] host–guest interactions.³³¹ More specifically, a supramolecular HEC network, cross-linked by heteroternary complexation to CB[8], was adsorbed onto NFC colloidal domains as a sacrificial yet self-healing network, connecting stiffer NFC domains that would usually form stiff hydrogels alone through crystalline fibril–fibril entanglements, Figure 36b. These crystalline domains however have little ability to dissipate stress and as the materials are stiff allow for very little yielding. By adsorbing a supramolecular network to bridge the length scales between NFC colloidal domains, a soft material was produced whereby the yield strain could be offset dependent on the supramolecular content of such formulations, and materials were also self-healing.

Scherman, Liu, and co-workers later reported a purely supramolecular double-network hydrogel comprised of one DNA-hybridized system and one CB[8] host–guest system, Figure 36c.³³² This work is particularly interesting because of the multiple levels of stimuli responsiveness arising from the two present networks including temperature, chemical, mechanical, and enzymatic responses. By mixing carboxymethyl cellulose-phe (CMC-phe), CB[8], and DNA motifs, interpenetrating networks were afforded that did not appear to have any interaction as imaged by confocal microscopy; however, the

brittleness of the DNA gel was offset by the presence of the interpenetrating CMC-phe/CB[8] dynamic system, which can rapidly reorganize and heal on distortion. Ultimately, a system was recognized that exhibited a higher than predicted mechanical strength of the combined gels and also the self-healing and rapid reorganization of CB[8] gels. The material was also shown to be responsive to excess free phenylalanine, which could compete for the CB[8] cavities, as well as having full biodegradability profiles on account of enzyme addition such as nuclease and cellulase. This material offers an interesting opportunity to consider new 3D cell culture scaffolds as well as injectable delivery devices for triggered release of DNA motifs in novel therapies.

10.4. From Monohydroxylated-CB[n] to Functional Materials

Kim and co-workers reported preparation of CB[6]-grafted hyaluronic acid (HA) via reaction of thiol-modified HA (HA-SH) with $(\text{allyloxy})_{12}\text{CB}[6]$.³³³ Hydrogels were formed when HA functionalized with diaminohexane (DAH) was mixed with HA–CB[6] as a result of the specific inclusion complexation of the DAH to the CB[6] cavity. These hydrogels could be returned to their sol state upon addition of spermine to the material, which displaces the DAH moieties from the CB[6] cavities based on having a 100-fold higher binding constant, destroying the interchain cross-links, suggesting gelation is promoted by CB[6]–DAH complexation. At 2 wt % polymer loading, these hydrogels exhibited exceptionally high storage moduli (~ 2 kPa) and also reasonable biocompatibility. Any remaining HA–DAH moieties were able to be capped with further CB[6] derivatives that were tagged with biorelevant molecules such as adhesion peptides and fluorescent markers demonstrating utility in 3D cell culture and tissue engineering.

These hydrogels were later implicated in controlling chondrogenesis of human mesenchymal stem cells (HMSCs).³³⁴ Here, spatial control of the HMSCs was achieved by modulating cross-link density of the hydrogel by controlling the amount of functionalization of HA with monoallyloxy–CB[6] and differentiation of the cells controlled by release profiles of transforming growth factors and dexamethasone-bound CB[6] (Dexa-CB[6]). Dexa-CB[6] was shown to have slower release rates from the gels in comparison to free

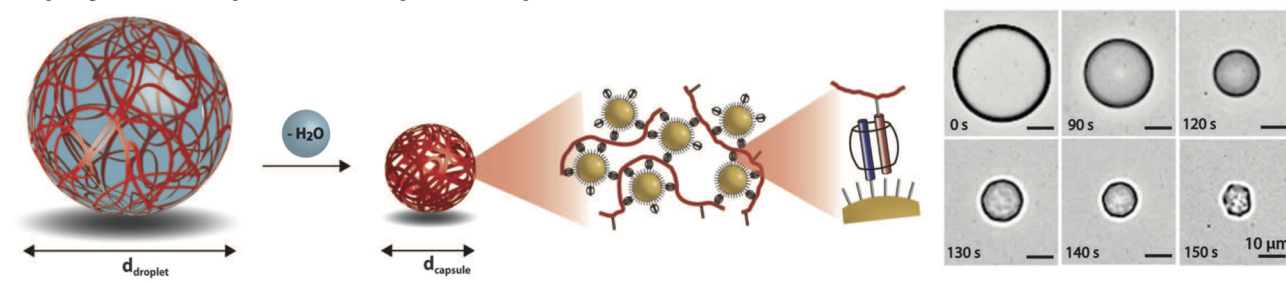
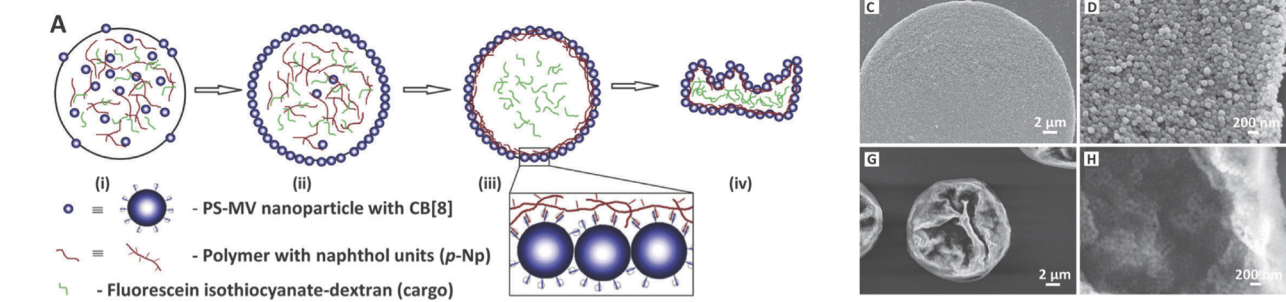
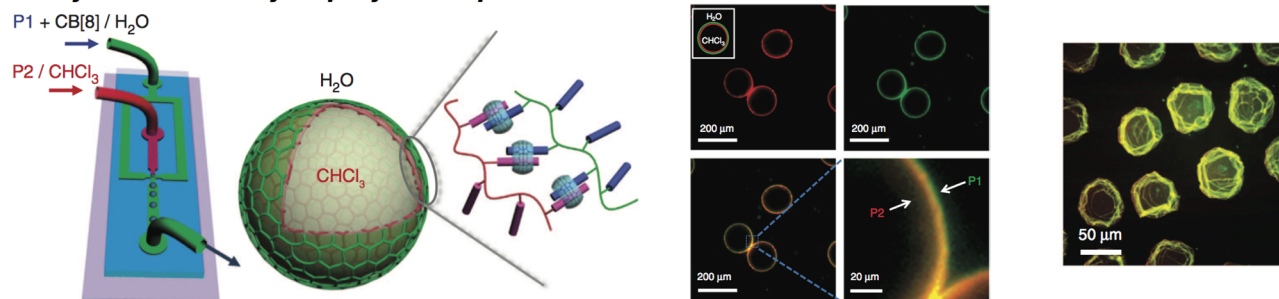
A: polymer/nanoparticle composite capsules**B: colloidosomes****C: layered assembly of polymer capsules**

Figure 38. Microfluidic methods for supramolecular capsule formation. (A) CB[8] host–guest interactions between gold nanoparticles and multivalent guest polymers provide entanglements strong enough to build microcapsule walls. Reproduced with permission from ref 336. Copyright 2012 AAAS. (B) Colloids cross-linked with CB[8] into polymeric microcapsule walls controlling intercolloid distance alters release rates of encapsulated cargos. Reproduced with permission from ref 337. Copyright 2014 The Royal Society of Chemistry. (C) Layered assembly of polymer-only microcapsules by dissolving multivalent guest polymers in both aqueous and nonaqueous phases of the microfluidic device whereby CB[8] facilitates complexation at the oil–water interface. Reproduced with permission from ref 338. Copyright 2014 NPG.

dexamethasone (in the order of days compared to hours) on its complexation to free DAH residues conjugated to the polymer network.

Similarly to Kim’s work, promise of useful materials with multiple anchored CB[7] molecules has also recently been reported by Tan and co-workers.¹⁰⁵ In this work, the synthesis of a 4-vinylbenzyloxy–CB[7] monomer is reported followed by the copolymerization with *N*-isopropylacrylamide (NiPAAm). The authors found that they could copolymerize 0.86 mol % of 4-vinylbenzyloxy–CB[7] into NiPAAm using redox-initiated polymerization in water with $M_n = 2.10 \times 10^5$ Da and PDI of 1.69 while retaining thermoresponsive properties. Although no specific materials were produced from this copolymer, a wide variety of guest molecules were still able to bind to a proportion of the CB[7] residues, even in their anchored form, and thus, these materials could become useful in the construction of higher order supramolecular materials or in surface attachment applications.

10.5. Microcapsule Formation Through CB[8] Ternary Complexation

CB[8] recognition motifs have also found utility in the formation of synthetic microcapsules whereby complete control of the composition of the shell and also the content is paramount. Work by Scherman and co-workers saw development of multistimuli-responsive polymer–gold nanoparticle composite materials held together by CB[8] heteroternary complexes.³³⁵ The later developed, through collaboration between Scherman, Abell, and co-workers, into composite gold nanoparticle–polymer microcapsules produced by microfluidic methods, Figure 38a.³³⁶ Similarly to the formation of supramolecular polymers and hydrogels, heteroternary complexation was achieved by encapsulation of an electron-deficient first guest followed by complexation of an electron-rich second guest. To control structure formation, separate aqueous solutions of MV-functional gold nanoparticles, Np–copolymer, and CB[8] were simultaneously injected into a microfluidic device with a fluorous-oil carrier phase perpendicular to the aqueous flow. As the oil and water phases meet, shear forces at the interface initiate formation of monodisperse droplets

whereby the Np–copolymer and MV–nanoparticles were cross-linked at the oil–water interface by CB[8] (having been drawn to the interface to stabilize the water/oil surface energy), forming spherical capsules upon dehydration; subsequent rehydration was carried out with minimal rupturing of the 3D structures. The size of the microcapsules could also be controlled by moderating the difference in flow rate between the oil carrier phase and the aqueous phases. These capsules were resistant to high temperatures and low pressures, and no capsules were formed on replacing CB[8] with CB[7] as only binary complexes can be formed, and therefore, no cross-linking is achieved. Sustained encapsulation of FITC-labeled dextran (500 kDa) was also demonstrated, the integrity of the capsule shell was not compromised, and the cargo was distributed evenly throughout. Release of the cargo could even be triggered by reduction of the MV moieties with sodium dithionite, which breaks the CB[8] complexation, causing dissolution of the capsule walls. Extra utility of the capsules arose from the presence of gold nanoparticles in the shell, and this allowed for the analysis and/or detection of materials encapsulated within by surface-enhanced Raman spectroscopy (SERS) as well as mapping of the microcapsule surface.

In a follow-up communication, Abell and co-workers demonstrated the fabrication of colloidosomes via analogous microfluidic methods, Figure 38b.³³⁷ Passive diffusive release of cargo from colloidosomes is highly dependent on pore sizes, which is determined by the spacing between colloids. Therefore, the ability to control distances between colloids in microcapsule walls as well as anchoring the colloids in place is extremely desirable. Similarly to the production of the aforementioned gold nanoparticle–polymer composite capsules, polystyrene colloids were functionalized with MV and then mixed with CB[8] and a copolymer bearing Np moieties, forming capsules, which were stable upon dehydration. Encapsulation and passive release of various molecular weight FITC–dextran was explored, and the authors demonstrated that 150 kDa FITC–Dextran could be encapsulated for a prolonged time period as a result of the small gap distance between colloids. Release could also be triggered by addition of a competitive guest (adamantyl amine, ADA) by disassembly of the cross-links and therefore the capsule. The authors hypothesize that the release rates could be altered by controlling the intercolloid distance, and this could be achieved by changing polymer concentrations, cross-link density, or parameters of the microfluidic device.

The latest example of microcapsule formation facilitated by the efficient recognition of molecular moieties by CB[8] under microfluidic conditions was shown by Scherman and co-workers in 2014.³³⁸ Assembly of multiple polymer layers and cross-linking with CB[8] was achieved at a water/chloroform interface, allowing for microcapsule formation. In this system there is no requirement for nanoparticles to undergo direct assembly at the interface as guest-bearing copolymers were applied to both the aqueous (MV–polymer) and the oil (Np–polymer) phases to template capsule formation along the oil/water interface, and layered assembly was demonstrated by confocal microscopy of rhodamine- and fluorescein-labeled components, Figure 38c.

Adding extra functionality to the microcapsules, the hydrophobic polymer could be replaced with a branched dendritic polymer bearing azobenzene moieties. Incorporation of the branched dendritic polymer system allowed small molecules to be encapsulated within the microcapsules and the skin

formation facilitated through 1:1:1 complexation of CB[8], MV, and azobenzene. Disassembly could be triggered by UV irradiation, switching the azobenzene configuration from *E* to *Z*, thereby breaking the heteroternary complexes, facilitating cargo release. These systems have demonstrated robust assembly techniques and excellent tuning capabilities and therefore have many potential applications in future delivery devices.

10.6. CB[n] Cross-Linked Polymer Networks Outlook

CB[n], specifically CB[8], have shown excellent utility in the development and formation of novel materials. Robust and efficient recognition motifs allow for rapid assembly of macroscopic polymer networks of which the dynamics of such ternary complexes have been shown to have an impact on material properties. In the example of supramolecular hydrogels, the mere fact that polymer concentration can be retained and yet a series of different material properties can be accessed by simply modulating CB[8] concentration, and therefore, cross-link density allows for a wide applicability of these hydrogels to future technologies, e.g., 3D cell culture. This is of particular importance in biomedical applications whereby fast-healing materials are required as injectables; CB[8] cross-linked hydrogels would be highly impactful on modern medicines. Manipulation of polymeric materials by microfluidic devices has led to novel microcapsule structures with excellent control over assembly processes and potentially excellent utility in future molecular manipulation and delivery systems.

However, the science of covalently attaching CB[8] to polymers has yet to be reported but is envisaged to lead to the development of extremely responsive multicomponent materials with fantastic tuning properties. Therefore, in the future we hope and expect to see many efforts in reproducible and scalable methods to monofunctionalize CB[8] with reactive groups and covalently attach such a molecule to polymer architectures.

11. CATALYSIS WITHIN CUCURBIT[n]URIL CAVITIES

The ability of CB[n]s to encapsulate various guest molecules has led to them being used to catalyze and template various chemical reactions. The first report detailed the catalysis of [3 + 2] cycloadditions³³⁹ in the presence of CB[6], which paved the way for the development of click-chemistry reactions. Since then, CB[n]s have been used to catalyze solvolysis reactions,³⁴⁰ oxidation reactions,³⁴¹ and metal-ion-assisted reactions.³⁴² Furthermore, CB[n]s have been utilized in photocatalysis and templating photochemical reactions³⁴³ and, in contrast, have been employed in reaction inhibition through the protection of reactive functional species by encapsulation.³⁴⁴ The following section will focus on key research outcomes in the area of catalysis and reaction modulation through interactions with CB[n] macrocycles.

11.1. [3 + 2]-Cycloadditions Catalyzed by CB[6]

The first instance of CB catalysis was reported by Mock and co-workers in the late 1980s, whereby a [3 + 2] cycloaddition of an alkyne (E1) and an azide (E2) was shown to occur within the cavity of CB[6] molecules.³³⁹ In an aqueous formic acid solution at 40°C, the cycloaddition occurs slowly with the formation of substituted triazoles; however, the addition of catalytic amounts of CB[6] led to a 6×10^5 increase in reaction rate with triazole (E3) being the only isomer formed as a result of the orientation of E1 and E2 within the 1:1:1 complex formed with CB[6]³³⁹ (see Figure 39). The catalytic rate

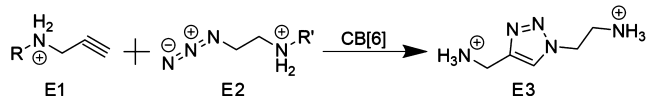


Figure 39. Schematic of an azide–alkyne click reaction mediated by CB[6].³³⁹

increase of the reaction was attributed to an overcoming of entropic constraints through optimal orientation, in addition to strain-induced compression of the reactants within the CB[6] cavity. This pioneering work inspired the development of azide–alkyne cycloadditions toward “click chemistry” reactions, with rotaxanes, polyrotaxanes, and pseudorotaxanes being successfully synthesized from CB[6] catalyzed [3 + 2] cycloadditions.^{345–349}

11.2. CB[n]-Catalyzed Solvolysis Reactions

In 2009, Nau and co-workers reported the catalysis of amides, carbamates, and oximes by CB[6] and CB[7] through an acid hydrolysis reaction.³⁴⁰ In the presence of CB[6] or CB[7], the rate of hydrolysis of an amide with a cadaverine moiety (**E4**) rose by a factor of 5 ($k_{\text{cat}}/k_{\text{uncat}}$) at pD 0.9, while at pD 1.4 the reaction rate increased by a factor of 11.6. For carbamate (**E5**), the reaction rate increased by a factor of approximately 30 in the presence of CB[6]. For oxime (**E6**) in the presence of CB[7], the reaction rate increased by factors of between 50 and 285 dependent on the pD value, which was varied between 4 and 5.8. The catalytic effect of CBs was proposed to be through the coloumbic stabilization of the protonated nitrogen intermediate that occurs during the hydrolysis, in addition to increasing their apparent pK_a values.

Garcia-Rio and co-workers investigated the hydrolysis of substituted benzoyl chlorides (**E7**) in the presence of either CB[7] or methylated- β -cyclodextrin, with each macrocycle

displaying contrasting effects on the reaction.³⁵⁰ For the case of benzoyl chlorides substituted with electron-donating groups, CB[7] showed a catalytic effect toward the formation of benzoic acid (**E8**), whereas methylated- β -cyclodextrin inhibited the reaction. Conversely, electron-withdrawing substituted benzoyl chlorides were inhibited by CB[7] and catalyzed by methylated- β -cyclodextrin. The opposing effects are explained through differences in the cavities and portals of these two macrocycles. For electron-donating substituted benzoyl chlorides, CB[7] catalyzes the reaction through stabilization of the acylium cation intermediate by its carbonyl-lined portals, lowering the energy barrier for the reaction. For the electron-withdrawing substituted benzoyl chlorides, methylated- β -cyclodextrin shows a catalytic effect as a result of the hydroxyl groups of the portals participating in the reaction. This work demonstrated the role that macrocycle portals can play influencing reaction rates.

11.3. CB[n]-Catalyzed Oxidation Reactions

In 2009, Zhu and co-workers demonstrated the ability of CB[8] to catalyze the oxidation of veratryl alcohol to veratraldehyde by *o*-iodoxybenzoic acid³⁴¹ and then extended the approach to the oxidation of aryl, allyl, and alkyl alcohol compounds.³⁵¹ The catalysis was found to be highly dependent on temperature and moderately dependent on pH, with neutrality favored over more extreme pH levels. Although the role of CB[8] in the catalysis was not clear, an increase in the oxidative conversion of 16.3% was observed at 95 °C in the presence of CB[8].

Reddy and co-workers investigated the catalysis of a series of reactions involving halogen inclusion complexes with CB[6].⁸¹ Fine CB[6] powders were exposed to either I₂ or Br₂ vapor to form I₂–CB[6]·4H₂O and Br₂–CB[6]·10H₂O, respectively. Reactions were then performed in the presence of the halogen complex or its complex with CB[6], with resulting yields being

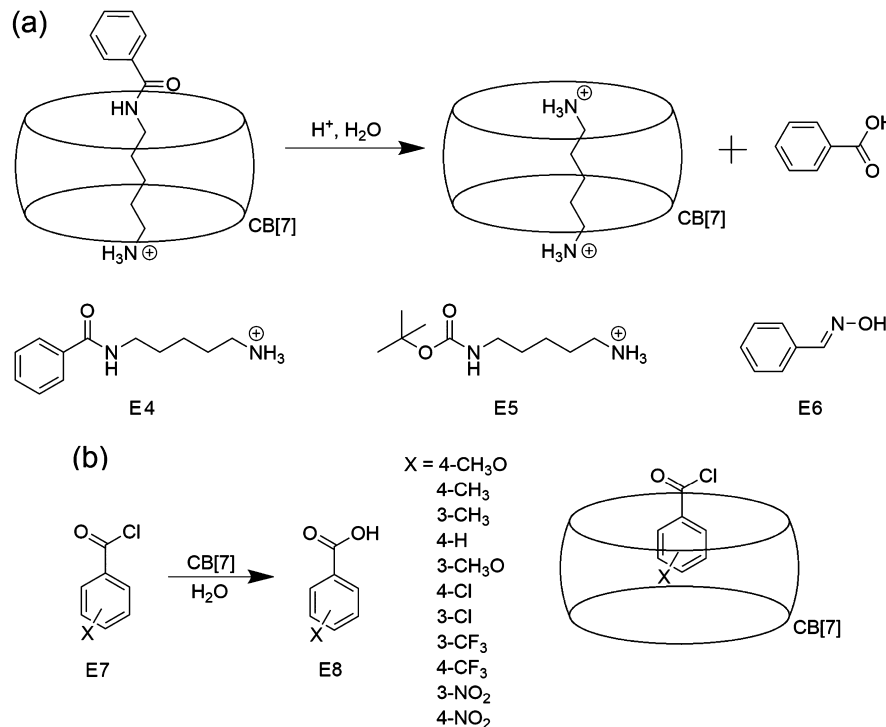


Figure 40. (a) Acid hydrolysis of an amide (**E4**), a carbamate (**E5**), and an oxime (**E6**) catalyzed by CB[7].³⁴⁰ (b) CB[n]-mediated hydrolysis of benzoyl chlorides to benzoic acid.³⁵⁰

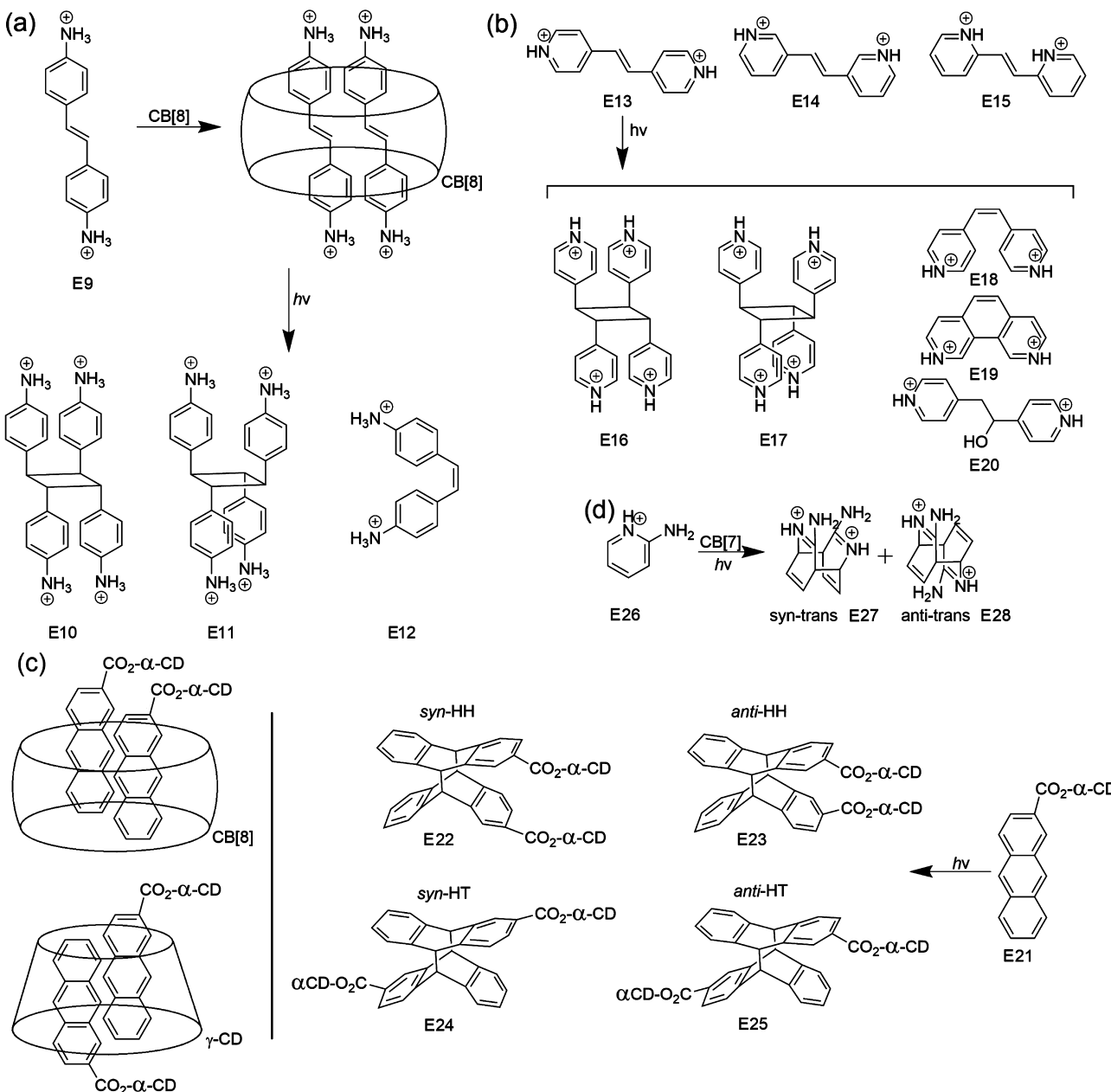


Figure 41. (a) Photodimerization of (*E*)-diaminostilbene in the presence of CB[8].³⁴³ (b) Photoreactivity of *trans*-1,2-bis(*n*-pyridyl)-ethylenes and stilbazoles in the presence of CB[8].^{352,353} (c) Photodimerization of cyclodextrin-functionalized anthracene in the presence of CB[8] and γ -cyclodextrin.¹³⁶ (d) Photodimerization of aminopyridine derivates encapsulated in CB[7].¹³¹

compared. The greatest increase in yield was seen for that of the iodine-catalyzed Prins cyclization, where the yield was 7% higher than that reported in the literature. The remaining reactions tested all showed yields comparable to what had been demonstrated in the literature for the uncomplexed halogens. Nevertheless, this represents a novel use of CB[6] complexes in halogen-catalyzed reactions.

11.4. Photocatalysis

The efficiency of photochemical reactions can suffer when performed in solvated environments and where specific molecular orientations and alignments of reactants are required. In order to proceed effectively, such barriers need to be overcome. Molecules that have been excited with photons can relax either radiatively or nonradiatively (via solvent collisions etc.), which can drastically reduce reaction efficiency. In

addition, the lack of control over molecule orientation can lead to many products arising from a single photochemical reaction or indeed a reaction may not proceed at all if a particular molecular orientation of the reactants is not met. The use of CB[*n*] macrocycles in photochemical reactions may help to overcome these obstacles. CB[*n*]*s* create a reaction environment that can be solvent free, preventing nonradiative relaxation. Also, CB[*n*]*s* allow for precise orientation of guest molecules, allowing for specific stereoselectivity of the reaction product. Lastly, CB[*n*]*s* are transparent in the near UV and visible regions of the electromagnetic spectrum, promoting photochemical processes within the CB[*n*] internal cavity.

Kim and co-workers demonstrated the first use of CB in the catalysis of a photochemical reaction involving (*E*)-diaminostilbene (E9).³⁴³ The 2:1 complexes of stilbene:CB[8] were

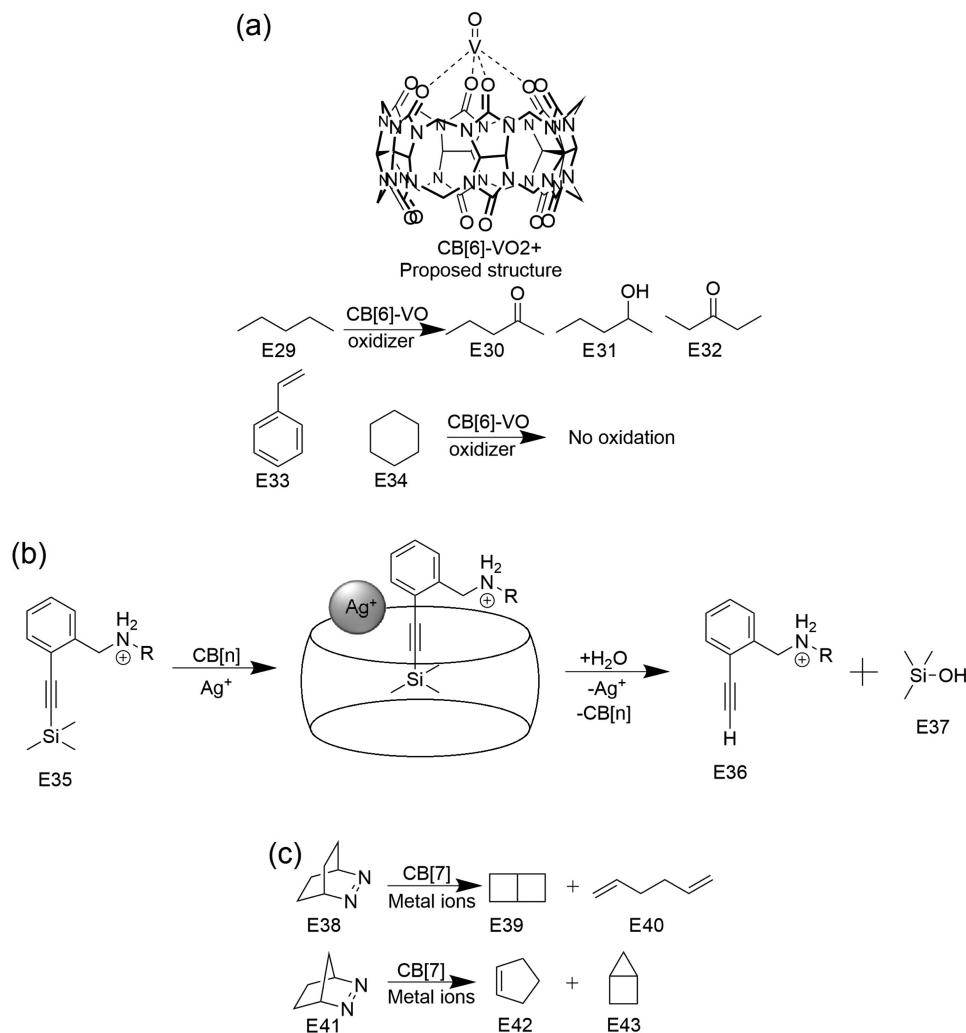


Figure 42. (a) Size-selective oxidation of alkanes within a oxovanadium(IV)– $\text{CB}[6]$ complex. Adapted from ref 358. (b) Desilylation of trimethoxysilane compounds, catalyzed by silver ions in the presence of cucurbiturils.³⁴² (c) Photoreactivity of azoalkanes through $\text{CB}[7]$ –metal-ion interactions in a two-phase system.³⁵⁹

shown to form in an aqueous environment as confirmed by ^1H NMR. The ternary complex then underwent a cycloaddition after UV irradiation (300 nm, 0.5 h) to form a [2 + 2] syn adduct (**E10**) within the $\text{CB}[8]$ cavity with high selectivity over the anti adduct (**E11**). The same experiment performed in the absence of $\text{CB}[8]$ yielded the (*Z*)-isomer (**E12**) as the major product, a product that was not evident at all when $\text{CB}[8]$ was present. It was also demonstrated that the addition of base (NaOH) to the postphotoreaction complex saw the ejection of the cyclized compound from the $\text{CB}[8]$ cavity, regenerating the cucurbituril catalyst as a result. This work highlighted the use of $\text{CB}[8]$ as a template nanoreactor that can influence regio- and stereoselectivity in photochemical reactions.

Continuing on from the work of Kim and co-workers, Ramamurthy and co-workers explored the use of $\text{CB}[8]$ in controlling the photoreactivity of a range of olefin molecules (some of which include **E13**, **E14**, and **E15**).^{352,353} The olefins were irradiated with UV light for 1 h both in the presence and in the absence of $\text{CB}[6]$ and $\text{CB}[8]$. In the presence of $\text{CB}[7]$, compounds **E13**, **E14**, and **E15** formed their own structural variations on the (*Z*)-isomer (**E18**) and the bridged (*Z*)-isomer (**E19**) with compound **E5** also yielding the hydrolysis compound (**E20**). With $\text{CB}[8]$ present, photodimerization

was favored, with the product distribution favoring the syn adduct (**E16**), with minor amounts of the anti adduct (**E17**) and the bridged and nonbridged (*Z*)-isomers also present. This reaction scheme was then extended to the formation of symmetric and asymmetric cyclized dimers by localizing asymmetric olefins within the $\text{CB}[8]$ cavity.³⁵³

In an effort to expand the versatility of $\text{CB}[8]$ in enhanced photoreactions, Pemberton and co-workers reported the photodimerization of neutral and cationic coumarin species.^{20,354} Irradiation of an aqueous solution of a coumarin and $\text{CB}[8]$ in a 2:1 complex led to the formation of the head-to-tail adduct as the major product, a result that was independent of the functional group substitution of the coumarin derivatives used. The type of head-to-tail adduct (whether syn or anti) could be controlled by varying the substituents on the coumarin moiety, with polar substituents favoring the anti adduct and nonpolar substituents favoring the syn adduct.

Kim and Inoue and co-workers moved away from [2 + 2] cycloadditions to concentrate on [4 + 4] cycloadditions in the presence of both $\text{CB}[8]$ and γ -cyclodextrin (CD).¹³⁶ Both anthracene and anthracene tethered to α -CD via an ester linkage (**E21**) were investigated as photoactive compounds to

demonstrate that the stereoselectivity of the [4 + 4] cycloaddition can be manipulated via conditions outside the host cavity. Photoexcitation in the absence of CB[8] or γ -CD led to a mixture of *syn*-head-to-head (HH, (E22)), *anti*-HH (E23), *syn*-head-to-tail (HT, (E24)), and *anti*-HT (E25) isomers forming in roughly the same ratios (with the HT isomers being favored) for both anthracene and anthracene- α -CD. The presence of CB[8] or γ -CD during photodimerization of anthracene led to a minor shift toward the formation of HT isomers. Photodimerization of anthracene- α -CD in the presence of γ -CD showed a larger shift toward the HT isomers, with a ratio as high as 98:2 HT:HH at -20°C and 210 MPa. The introduction of CB[8] into the anthracene- α -CD system gave rise to a HT:HH ratio of 2:98; an extreme inversion compared to that of the γ -CD system, showing that the α -CD attached to the anthracene, which is too large to be incorporated into the cavities of either γ -CD or CB[8], can drastically effect the stereochemistry of the products formed by photocycloaddition. More recently, the photodimerization of anthracene in CB[8] has been utilized by Biedermann and co-workers in the ligation and cross-linking of polymer networks.¹⁶²

While CB[8] has also been applied to the stereocontrol of photochemical reactions involving styryl dyes,¹³⁸ cinnamic acids,³⁵⁵ 2-naphthalenecarbonitrile, and naphthoate compounds toward the formation of cubane-like photodimers^{137,356} as well as the photohydrolysis of benzoimidazole,³⁵⁷ CB[7] has been shown to accommodate smaller yet similarly designed guests for photodimerization. Macartney and co-workers investigated the [4 + 4] photodimerization of 2-aminopyridine (E26) when encapsulated in CB[7] in a 1:2 host–guest complex.¹³¹ In the absence of CB[7], a mixture of the *syn*-trans (E27) and *anti*-trans (E28) photodimers formed in a 1:4 ratio. In the presence of 50 mol % CB[7], the *anti*-trans dimer was formed exclusively. It was also found that CB[7] stabilized the dimer at room temperature, preventing it from reverting back to the monomeric 2-aminopyridine.

11.5. Metal Cation-Assisted CB[n] Catalysis

Given their negatively charged carbonyl fringed portals, cucurbiturils are highly efficient at binding to metal cations, a property that makes them useful at promoting catalysis reactions that utilize ionic metal species. Despite cation binding to CB[n]s being a well-established area of research,³⁶ the idea of using such complexes for catalysis is relatively new and hence fairly unexplored. Demets and co-workers investigated the catalytic properties of an oxovanadium(IV)–CB[6] complex toward the oxidation of various organic compounds.³⁵⁸ It was demonstrated that pentane (E29), a linear alkane, could be oxidized to compounds E30, E31, and E32; however, larger organic molecules such as styrene (E33) and cyclohexane (E34) could not. This was explained through the nature of the VO_2^+ binding, whereby the vanadium atom bound to the carbonyl portal of the CB[6], with the oxygen atom pointing away from the CB[6] cavity, in a distorted square-pyramidal configuration. This meant that only small molecules that can enter the CB[6] cavity could be oxidized as the oxygen atom in the VO_2^+ species blocked direct access to the vanadium atom from the other side of the complex. In this way, Demets and co-workers demonstrated a size-selective heterogeneous catalyst based on CB[6] through metal-ion interactions.

Masson and Lu reported a multistep catalytic cycle for the desilylation of trimethylsilylalkynyl-containing compounds via a

heteroternary complex formed with Ag^+ ions and CB[7].³⁴² The desilylation of E35 in the presence of CB[7] and Ag^+ , which led to the formation of an alkyl–silver organometallic complex, was monitored through the ^1H NMR response of the trimethylsilanol byproduct E37 complexed with the CB[7] cavity. The mechanism proposed for the reaction begins with E35 forming a complex with CB[7] whereby the trimethylsilyl group binds to the CB[7] cavity. A silver cation then forms a π complex with the triple bond of E35 and the carbonyl portal of the CB[7]. Molecule E35 then undergoes a nucleophilic substitution with water, cleaving the trimethylsilyl group, yielding the trimethylsilanol byproduct (E37) and a alkynyl–silver complex, which is subsequently hydrolyzed to form the desilylated alkyne (E36) and the regenerated silver cation.

Nau and co-workers extended the concept of metal–CB[n] catalysis by utilizing such complexes to effect product formation from photoreactions involving azoalkanes in a two-phase system.³⁵⁹ First, the formation of complexes between CB[7] and metal ions, including Fe^{3+} , Co^{2+} , Cu^{2+} , Zn^{2+} , Ag^+ , and Ti^+ , was confirmed by noting hypsochromic shifts and fluorescence intensity changes in optical titrations. The complexes were then tested for their activity toward the photoreactivity of 2,3-diazabicyclo[2.2.2]oct-2-ene (E38) and diazabicyclo[2.2.1]hept-2-ene (E41) in a two solvent system, consisting of water and pentane. Analysis of the organic reaction mixture from a reaction of E38 by gas chromatography showed a product ratio of 65:35 for E39/E40 in both the presence and the absence of CB[7] and a ratio of 70:30 with just metal ions present. This ratio shifted to 87:13 in the presence of CB[7] and metal ions (Ti^+ , Fe^{3+} , Co^{2+} , Ni^{2+} , Cu^{2+} , and Ag^+). The preferential formation of the diene (E40) was theorized to have arisen from a triplet excited state caused by heavy-atom-doped intersystem crossing. The photoreaction of E41 resulted in a 100% preferential conversion to housane (E43), over the secondary product cyclopentene (E42), in the presence and absence of CB[7], metal ions, and most metal–CB[7] complexes. A distinct change in reactivity occurred in the presence of the CB[7]– Ag^+ complex, where a product ratio of 59:41 for E43/E42 was observed. It was postulated that a photoinduced electron transfer was likely due to the new mechanism that led to the formation of cyclopentene, a mechanism that must be supported by the CB[7]– Ag^+ complex, as no cyclopentene formed in the presence of Ag^+ alone, even at concentrations as high as 1 M. This work demonstrated the potential of CB[n]–cation complexes in promoting otherwise unobtainable reaction products via photochemistry.

11.6. Reaction Inhibition by Cucurbit[n]urils

Cucurbiturils show a strong capacity to encapsulate guests within their hydrophobic cavities. While we have seen that this can lead to the catalysis of reactions through efficient orientation of guests and carbonyl portal interactions, in addition to effecting reaction products through templating, the encapsulation of guests can also lead to the inhibition of reactions. In this way, CB[n]s can act in much the same manner as a protecting group in organic synthesis, shielding specific molecules and functional moieties from chemical attack.

The redox chemistry of thiol groups and disulfide bridges has been manipulated through CB[6] binding.³⁴⁴ Kaifer and co-workers first highlighted that compounds such as cysteamine (E44) and cystamine (E45) and derivatives based on these compounds can be encapsulated within CB[6] in an orientation such that the sulfur-containing groups remain inside the

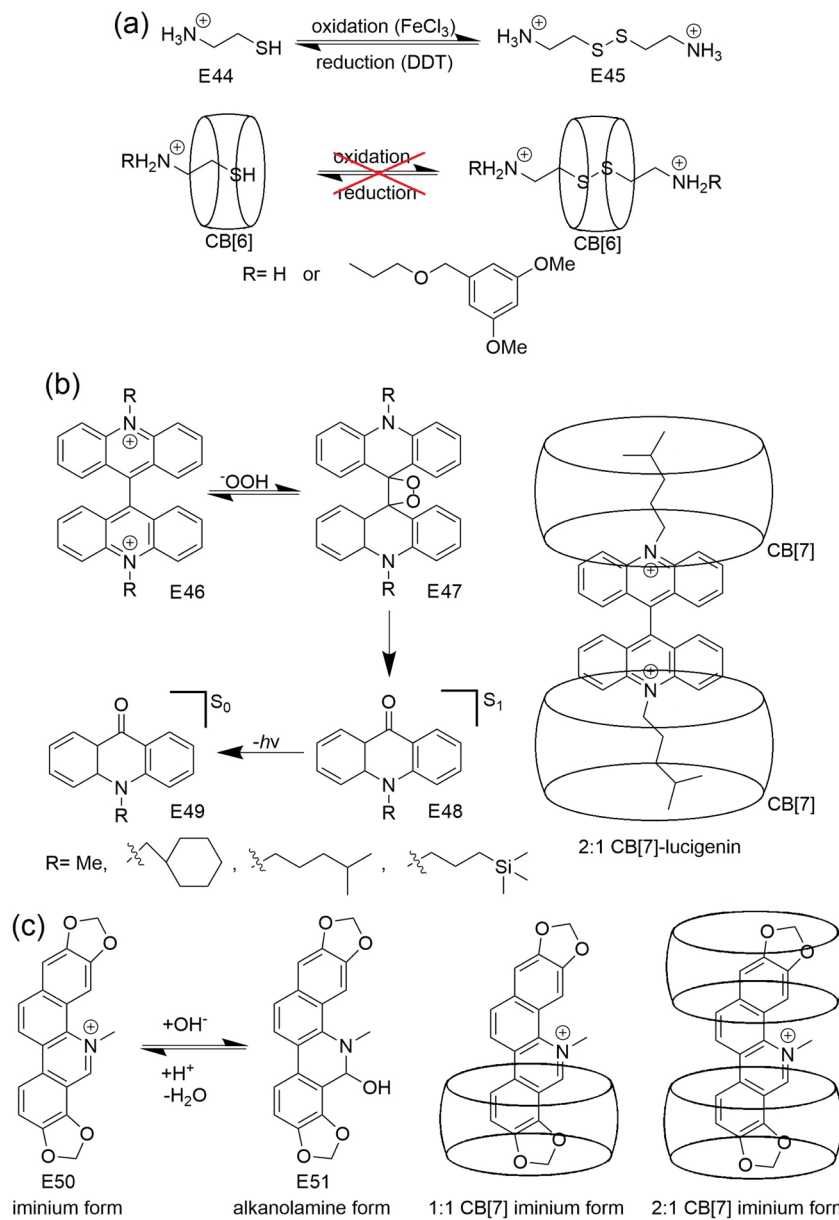


Figure 43. (a) Inhibition of redox reactions involving thiols and disulfides through protection within CB[6] cavities.³⁴⁴ (b) Chemiluminescent reaction of lucigenin, modulated by CB[7].³⁶⁰ (c) Inhibition of the photo-oxidation and nucleophilic attack of sanguinarine by CB[7] encapsulation.³⁶¹

hydrophobic cavity. They then investigated the oxidation and reduction of these compounds in the presence and absence of CB[6]. When reacted with an excess of dithiothreitol (DTT), cystamine was shown to be reduced to the thiolated form, cysteamine, with the reaction coming to completion after approximately 1 h. In the presence of CB[6], no formation of cysteamine was observed after 50 h of reaction time. Similar results were obtained for the oxidation of cysteamine, with no formation of cystamine in the presence of CB[6], while in its absence, FeCl₃ was able to oxidize cystamine to cysteamine to completion after approximately 6–7 h. This reduction in reactivity was also seen when different oxidants were used, including dissolved oxygen and chloropicrin. This work highlighted the impressive ability of CBs to not only protect a species from chemical attack but also kinetically hinder both forward and reverse reactions as a result of host–guest complex formation.

Masson and co-workers demonstrated the use of CB[7] in modulating the chemiluminescence of Lucigenin (E46).³⁶⁰ Lucigenin undergoes chemiluminescent degradation upon the addition of sodium peroxide, which leads to the formation of dioxetane (E47). Dioxetane then undergoes homolytic cleavage to produce singlet excited acridone (E48), which relaxes to the ground state (E49) via photon emission. CB[7] was shown to modulate this reaction by binding to various R group substituents of Lucigenin that are present on either side of the biacridine unit. The binding decreased dioxetane formation and dimmed the chemiluminescent reaction. Chemiluminescence could be restored through the addition of a competitive CB[7] guest. In this way, CB[7] can be utilized in regulating the rate of chemiluminescent reactions.

Cong and co-workers reported the use of CB[6] and CB[7] in the prevention of acylation of the antituberculosis drug, isoniazid.³⁶² For all acylating agents tested, stoichiometric

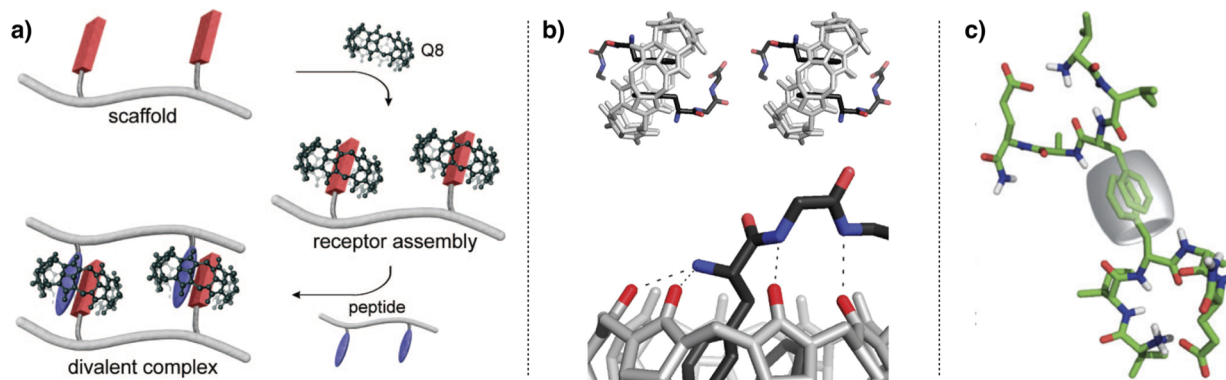


Figure 44. (a) Self-assembled multivalent receptors of “MV-peptide” and CB[8] complex aromatic residues in complementary peptides. Reproduced in part with permission from ref 365. Copyright 2009 American Chemical Society. (b) Crystal structure of two FGG peptides complexed to CB[8]. Hydrogen-bonding interactions between peptide backbone and CB[8] carbonyl portals exemplified by dashed lines. Reproduced in part with permission from ref 165. Copyright 2006 American Chemical Society. (c) 2:1 complexation of pentapeptides to CB[8] via midchain Phe residues. Reproduced in part from ref 165. Copyright 2013 The Royal Society of Chemistry.

additions of either CB[6] or CB[7] rendered isoniazid completely unreactive to acylation, with the initial rate of acylation decreasing between 10 and 100 fold in the presence of 0.8:1 CB to isoniazid. The mechanism for the protection was concluded to arise because of an increase in the pK_a value of the isoniazid, as a result of the amino protons binding to the carbonyl portals of CB. This work demonstrates the potential for CB[n]s to be used as drug carriers for isoniazid, increasing its bioavailability in the presence of acetylators.

CB[7] has also been shown to stabilize biologically active molecules from various chemical degradation pathways. Biczok and co-workers utilized inclusion complexes with CB[7] and sanguinarine, a natural biologically active benzophenanthridine alkaloid, to stave off photo-oxidation and nucleophilic attack.³⁶¹ The iminium form (E50) of sanguinarine formed both 1:1 and 2:1 host–guest complexes with CB[7], with binding constants of 10^6 and 10^3 M^{-1} , respectively. The iminium form of sanguinarine is susceptible to nucleophilic attack by hydroxide ions at the 6 position, leading to the uncharged alkanolamine form (E51), a reaction that was prevented when complexed with CB[7]. The hydroxylated form of sanguinarine can also form a complex with CB[7], with a binding constant of $2.45 \times 10^2\text{ M}^{-1}$. The alkanolamine form can undergo an irreversible photo-oxidation reaction to produce 6-oxy sanguinarine. This reaction was hindered by the presence of CB[7], likely through preventing oxygen from reaching the sanguinarine while encapsulated within the CB cavity.

In addition to modulating the rate of chemical reactions, CB[7] has been exploited to regulate the activity of enzymes. Ghosh and co-workers designed bifunctional inhibitor molecules with affinities for both CB[7] and either bovine carbonic anhydrase (BCA) or acetylcholinesterase (AChE).³⁶³ The addition of inhibitor molecules in stoichiometric ratios to BCA saw a decrease in its catalytic activity as a result of the blocking of its active site. The addition of CB[7] to the *enzyme-inhibitor* complex saw the formation of *enzyme-inhibitor-CB[7]* complexes that underwent prompt dissociation, releasing *inhibitor-CB[7]* and reforming the active enzyme. The inhibition could then be cycled by adding a competitive guest for CB[7], releasing the inhibitor molecule. While BCA was shown to follow the inhibition cycle mentioned, AChE did not give the formation of stable complexes with both inhibition molecules and CB[7] simultaneously. This meant that CB[7]

was unable to actively dissociate the inhibitor molecule from AChE. By using tailored inhibitor molecules with affinities for both enzymes and CB[7] macrocycles, cucurbiturils could play an important role in allowing for dynamic manipulation over the activity of enzymes.

12. RECOGNITION BY CB[n] IN BIOLOGICAL SYSTEMS

Molecular recognition and detection of biomolecules in aqueous solution, particularly peptides and proteins, is an important target within biomedical sectors, especially those focused on sensing and separation. Research from the Brunsdorf, Buschmann, Kim, Li, Nau, Scherman, and Urbach groups has brought the art of amino acid complexation and recognition by CB[n] receptors forward to protein–protein conjugation and solution-phase structure elucidation. This area has seen a large expansion in the number of publications on the binding of amino acids, peptides, and proteins in the past 10 years, and a wealth of knowledge of binding constants and conformations has been developed through utilization of a variety of spectroscopic and modeling techniques.

12.1. Amino Acid and Short Peptide Recognition by CB[n]

An early example of short polypeptide recognition by CB[n] was reported by Buschmann and co-workers in 2005.³⁶⁴ This research determined binding constants for a small library of di- or tripeptides through ion–dipole interactions between the protonated N-terminus of the peptides and the portals of CB[6]. The authors found that there was no significant dependence on peptide size to CB[6] binding, inferring that only an exclusion complex is formed (unlike alkylamino cations), likely resulting from the polarity of the peptide bonds. Nevertheless, the portal interaction is entropically favorable as two molecules of water are released from CB[6] upon peptide complexation.

Concurrently, Urbach and co-workers essentially pioneered the art of amino acid sensing when they reported the ability of CB[8]-MV to recognize and complex with tripeptides of glycine and a single tryptophan residue (WGG, GWG, GGW) forming charge-transfer complexes. This was monitored by UV absorption spectroscopy, fluorescence, and NMR spectroscopies as well as ITC.¹³⁰ The authors found WGG had the overall highest K_a of the three peptides ($1.3 \times 10^5\text{ M}^{-1}$, 6-fold higher than GWG and 40-fold higher than GGW) to CB[8]-MV and that electrostatic interactions of the C-terminus played

a large part in the binding affinity on account of repulsion between the carbonyl portals of CB[8] and the carboxylate of the peptides. Binding of the tryptophan residue to the CB[8] cavity was accompanied by charge-transfer complexation with MV and consequent fluorescence quenching of the indole group as well as broadening of signals in ^1H NMR. This work was later extended into recognition of multivalent peptides by self-assembled receptors.³⁶⁵ Here peptide scaffolds were functionalized with multiple MV units (1–3) that each recruit one CB[8] host. This self-assembled receptor was then able to bind in a 1:1 fashion with identical peptides bearing complementary tryptophan residues in place of the MV of the receptors, Figure 44a.

Urbach and co-workers also observed 2:1 binding of aromatic amino acids to CB[8].¹⁶⁵ Consistent with the previous study, tripeptides consisting of 2 glycine residues and a single tryptophan or phenylalanine were investigated, and it was again found that the distance of the aromatic residue from the C-terminus had a large effect on binding affinity. Sequential binding modeling of ITC data demonstrated, in the case of WGG, the second binding constant is a magnitude lower than the first; however, this could not be determined for FGG due to cooperativity in binding. WGG was found to bind to CB[8] in a 2:1 fashion in a noncooperative manner unlike FGG, whereby ITC data suggests positive cooperativity. The authors also managed to isolate a crystal structure of FGG bound in a 2:1 fashion to CB[8], with the aromatic residues encapsulated in a stacking geometry within the cavity, Figure 44b. Hydrogen-bonding interactions between the peptide N-H's and the CB[8] carbonyl portals were also apparent. Other aromatic amino acid residues were investigated (tyrosine, histidine); however, binding to CB[8] was not observed for these derivatives.

The study of 2:1 binding of middle-chain phenylalanine residues in pentapeptides to CB[8] has also been investigated by Scherman and co-workers.¹⁶⁴ This is the first example of strong 2:1 binding in a longer peptide chain where the Phe residue is not located at the N-terminus. The pentapeptides selected were based on the aggregation-promoting region of wild-type human amyloid β ($A\beta$), a peptide that has been linked to the development of Alzheimer's disease. The $A\beta$ fragments explored were AEFRH, LVFIA, and VIFAE, of which the latter two were overlapping regions of the $A\beta$ sequence but with one of the F residues exchanged for I (isoleucine). In wild-type $A\beta$ this region actually contains two neighboring Phe units, and the authors chose to replace one of these residues in each sequence with isoleucine to ease synthesis and analysis of results when combined with CB[8]. The 2:1 binding modes were confirmed by fluorescence and NMR spectroscopies and ITC analyses, and despite differing charges, hydrophobicity, and steric hindrance, all sequences formed strong homoternary complexes on the order of 10^9 – 10^{13} M^{-2} , Figure 44c. This study demonstrates CB[8] is able to access potentially hindered Phe residues in non-N-terminal sites of peptides and may also hold advantages to the future of understanding $A\beta$ fibrillation mechanisms in Alzheimer's disease.

The 1:1 binding of phenylalanine derivatives to CB[7] has also been investigated by Urbach and co-workers. Remarkably, one derivative, 4-aminomethyl-phenylalanine, was reported to have a K_d of 0.95 nM (500 times stronger affinity than phenylalanine).³⁶⁶ However, biomolecule detection often has to be performed at much lower concentrations. Other chemical modifications of phenylalanine were investigated such as *tert*-

butyl and hydroxyl groups at the 4-phenyl position, but none of these modifications provided such a stark increase in binding affinity as the amino-methyl group. A later report by Urbach and co-workers detailed nanomolar detection of peptides harnessing CB[8] complexes of tetramethylbenzobisimidazolium (MBBI).⁹⁷ MBBI-CB[8] was shown to have an intriguing response to tripeptides Tyr-Leu-Ala and Tyr-Ala-Leu within nanomicromolar detection limits. In the former case, a fluorescence enhancement was observed upon combination, elucidating displacement of MBBI from CB[8], and this result was confirmed by NMR studies. In the latter example, fluorescence was seemingly quenched by the formation of a 1:1:1 charge-transfer inclusion complex of CB[8], Tyr-Ala-Leu, and MBBI. Therefore, MBBI-CB[8] is able to act as both a nanomolar “fluorescence-off” receptor for Tyr-Ala-Leu and a “fluorescence on” receptor of Tyr-Leu-Ala, simultaneously. This is the first example of highly specific recognition of N-terminal Tyr tripeptides by CB[8], whereby in certain cases the peptide chain can fold and be mostly included within the CB[8] cavity (as modeled) at the expense of dissociation of MBBI. The authors suggest that given the minimal structure of this Tyr-Leu-Ala peptide, it could easily be engineered into recombinant proteins as an affinity tag.

Urbach and co-workers also demonstrated inhibition of a nonspecific exopeptidase porcine amino peptidase N (APN) with CB[7] via binding of phenylalanine units present within the peptide.³⁶⁷ N-Exopeptidases degrade peptides by sequential cleavage of amino acids from the N-terminus. With CB[7] bound to a Phe residue within a peptide sequence (Thr-Gly-Ala-Phe-Met), cleavage of the amide bond was completely inhibited upon reaching the CB7-Phe complex, and therefore, Phe-Met was stable to APN degradation. The authors elude to the applicability of this system in the protection of longer peptides from APNs, which could prolong peptide lifetimes *in vitro* and *in vivo*.

Collaboration between the Urbach and the Nau groups led to the development of a tandem assay whereby discrimination of CB[7] affinity for fluorescent dyes and peptides allowed for determination of protease substrate selectivity and inhibitor activities.³⁶⁸ In this study, mixtures of acridine orange (fluorescent dye), CB[7], peptides (with Phe residues), and proteases were formulated. Initially acridine orange is encapsulated by CB[7] on account of a stronger binding constant than the midchain Phe residue of the peptide and fluoresces. Upon cleavage of the peptide by proteases, the Phe unit was revealed in the new N-terminus position, the acridine orange was displaced from the CB[7] by the peptide, and fluorescence of the dye was quenched. This system was utilized to quantify the activity of several proteases but also was able to determine the activity of protease inhibitors. This method proved to be a robust way to determine both enzyme and inhibitor activity at nanomolar levels in a label-free manner. However, it is limited to peptides that yield products with N-terminal aromatic amino acids upon enzymatic degradation.

This area has seen excellent progression over the past decade from recognition of amino acids by CB[8]-MV toward the development of sensitive detection assays and dimerization of larger peptides by CB[8].

12.2. Noncovalent Protein Conjugation

In more recent literature, the groups of Scherman, Brunsved, and various others have developed methods to conjugate macromolecules to larger proteins via CB[8] recognition. An

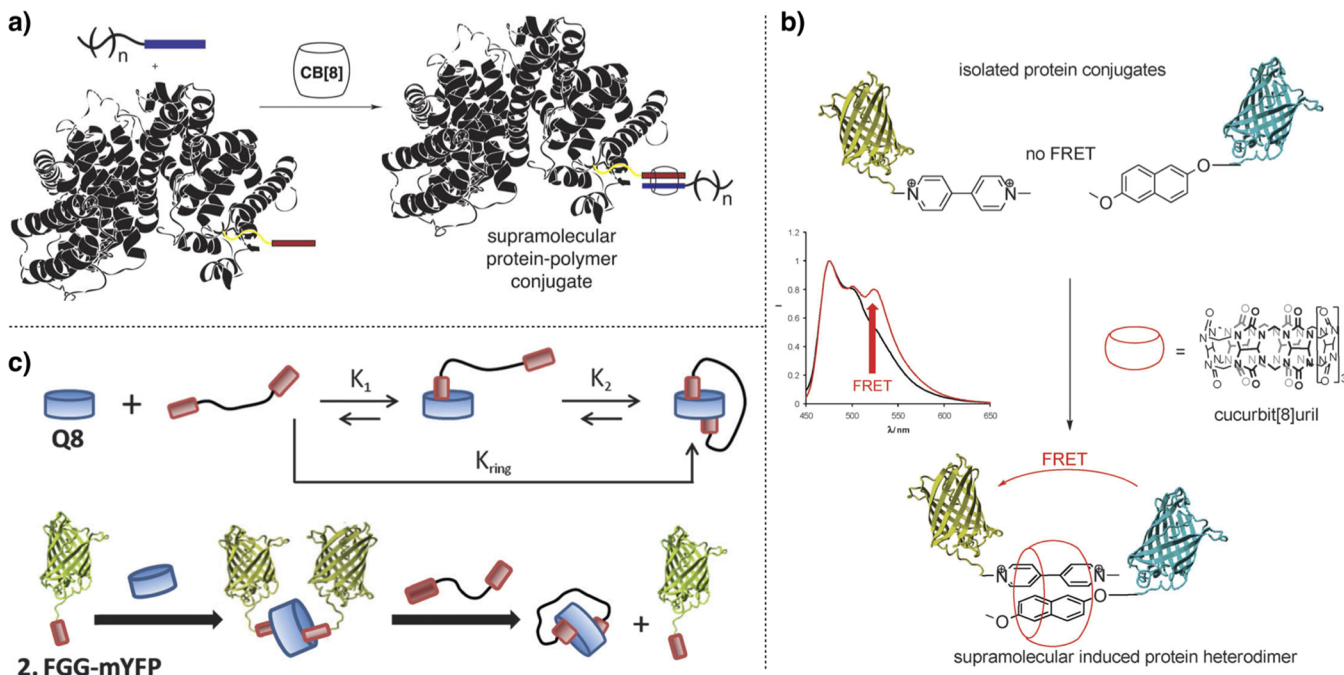


Figure 45. (a) Reversible BSA PEGylation through heteroternary complex formation with CB[8]. Reproduced with permission from ref 143. Copyright 2011 The Royal Society of Chemistry. (b) Dimerization of protein FRET pairs with CB[8]. Reproduced with permission from ref 144. Copyright 2011 The Royal Society of Chemistry. (c) Controlling protein dimerization by utilizing FGG-PEG-GGF polymer. Reproduced with permission from ref 281. Copyright 2015 The Royal Society of Chemistry.

early example of noncovalent conjugation was of PEG to BSA through CB[8] ternary complex formation, as reported by Scherman and co-workers in 2011, Figure 45a.¹⁴³ PEGylated proteins have distinct physicochemical properties (resistance to biodegradation, etc.), and therefore, bioconjugation of polymers in a site-specific and dynamic manner is applicable to many biological sectors, especially therapeutic protein delivery. In this example, a BSA fraction was functionalized with a single naphthoxy moiety at its only free thiol cysteine residue. Combining this in solution with PEG-MV and CB[8] led to ternary complex formation, and a PEG–BSA bioconjugate was observed by DOSY NMR, DLS, UV/vis, and fluorescence spectroscopies and ITC. This work, as described in the authors conclusions, demonstrated controlled supramolecular formation of PEG–protein bioconjugates, which is a proof of concept for further translation or potentially protein–protein supramolecular conjugation.

Protein–protein heterodimerization of MV- and Np-bearing proteins with CB[8] was reported by Brunsved and co-workers several months later.¹⁴⁴ This study demonstrated the selective dimerization of two different proteins, one bearing MV to a second protein bearing Np, following on from previous work by Brunsved, which was limited to dimerization of identical proteins through 2:1 complexation of FGG–protein sequences with CB[8], Figure 45b.²⁸² In both cases protein FRET pairs could be dimerized, and therefore, the assembly process was studied by fluorescence spectroscopy. A follow-up SAXS study eluded to the compact nature of packing of such dimers when complexed in solution.³⁶⁹ Collaboration between the Brunsved and the Dankers groups saw the production of (FGGG)_npenta(ethylene glycol), which could form ring structures on the binding of its 2 FGGG units to CB[8] and modulate protein dimerization with more control than simple competitive FGG molecules, Figure 45c.²⁸¹ CB[8]-mediated homotetrameriza-

tion of fluorescent proteins was later reported by Brunsved and co-workers.³⁷⁰ This was achieved by combining the 2:1 complexation motif of FGG (encoded at the N-terminus of many proteins) to CB[8] with intrinsic affinities between proteins, essentially producing supramolecular dimers of dimers.

Brunsveld and co-workers later reported a further study on the dimerization of inactive enzyme monomers with CB[8] to form an active enzyme supramolecular dimer.³⁷¹ Here Caspase-9, which is only active in its dimeric form, was complexed together via recognition of FGG moieties by CB[8]. Perhaps most importantly, the activity of the enzyme was not compromised by the supramolecular elements that induce dimerization, and a great deal of molecular control over the system was achieved, i.e., CB[8] concentration controlled the degree of dimerization and therefore activity of the Caspase solution.

In summary, significant progress has been made in the understanding of protein conjugation facilitated by CB[8] recognition motifs, and this insight is starting to be translated toward modulation in protein activity showing great promise for the future applicability of this field.

12.3. Further Application to Biochemistry

Urbach and co-workers reported a 1:1 binding stoichiometry between CB[7] and insulin at the N-terminal phenylalanine of the insulin B chain.⁹⁶ This is a particularly interesting result as there are three Phe residues in the insulin sequence; however, replacement experiments of these other residues confirmed that it is solely the N-terminal Phe that binds to CB[7]. This is starkly different to other methods of recognizing proteins as no modifications to the peptide sequence in terms of histidine tagging have been performed. Recognition has simply been achieved through mixing the native protein with CB[7], and large binding constants upward of 10^6 M^{-1} were reported.

Kim and co-workers showed that CB[7] binding to Phe residues of insulin and amyloid β prevented aggregation of such proteins.³⁷² This is very important for both insulin storage and understanding development of Alzheimer's disease through amyloid aggregation. These studies show that by masking the hydrophobic residues of A β or insulin with CB[7] or at least increasing steric hindrance around these regions via complex formation significant inhibition of the aggregation process can be achieved. Through a variety of biological assays and binding studies the authors demonstrate that CB[7]–Phe complexation is much faster than protein–protein dimerization, and the Phe-specific binding of CB[7] successfully modulates intermolecular interactions, preventing fibrillation processes, and is therefore a pathway for new potential treatments for amyloid linked diseases.

A 2011 report by Kim and co-workers demonstrated the gas-phase host guest chemistry of CB[6] and Lys-containing peptides.³⁷³ Through collisional activation, CB[6] was found to efficiently complex to Lys residues of model peptides in the gas phase, often resulting in common fragmentation products. This was used to elucidate protein structure, specifically in the case of ubiquitin, by employing tandem mass spectrometry techniques on CB[6]–protein complexes formed in aqueous conditions to determine solution-phase conformations. A follow-up study investigated the conformational changes of ubiquitin proteins upon CB[6] complexation in the gas phase at a variety of different charge states of which specific Lys residues complexed with CB[6] were able to be determined. CB[6] complexes inhibited salt bridge formations and therefore triggered conformation changes. This could be reversed and the protein refolded upon CB[6] detachment.³⁷⁴ In the future this research will hopefully be translated to other protein structures and improve mass spectrometry techniques for determining protein structure as well as determining protein sequences that in turn determine higher order conformations.

Inhibition of DNA restriction enzymes by CB[6] and CB[7] was reported by Pischel and collaborators.³⁷⁵ In this example binding of CB[6] and CB[7] to DNA restriction enzymes is hypothesized to be the cause of inhibition of DNA hydrolysis; however, the authors were unable to determine exactly which residues of the restriction enzyme were bound by the CBs. It was shown that DNA hydrolysis could be reactivated by simple addition of spermine, which competes for the macrocycle cavity, likely releasing the restriction enzymes and allowing continuation of DNA hydrolysis.

12.4. Profiling Toxicity of Cucurbit[n]uril

The year 2010 saw two reports showing CB[n]-type containers exhibiting good biocompatibility profiles. Isaacs, Briken, and co-workers examined the viability of HepG2 (liver derived) and RAW264.7 (macrophage) cells after 24 h exposure to CB[5] and CB[7].¹⁰⁰ Both cell lines showed good tolerance to CB[5] and CB[7] up to 1 mM with cell viabilities exceeding 90%. Moreover, the internalization of CBs with encapsulated FITC by macrophages was proven to be very efficient, and treatment of mycobacteria with CB[7]-bound drug molecules did not see any significant decrease in efficacy of the therapeutic compound. Furthermore, acyclic analogues of CB[n] were also studied, and the cells also expressed high tolerance for such compounds beyond usual therapeutic levels.

Day, Nau, and co-workers also explored the in vitro activity of CB[7] and CB[8], specifically against CHO-K1 cells (ovarian cell line from hamsters).⁹⁹ An IC₅₀ value of 0.53 \pm

0.02 mM was determined, which roughly corresponds to 620 mg kg⁻¹ of cell material. The authors also tested CB[8] toxicity and found that the macrocycle expressed no significant toxicity within its solubility limits. Further to these results, live cell imaging of cells exposed to nonlethal CB[7] concentrations demonstrated that there were no detrimental or adverse effect on the cellular integrity.

Progressing toward in vivo studies on mice, intravenous injections determined a maximum tolerable dose of CB[7] to be 250 mg kg⁻¹ with the mice initially losing some superficial weight but recovering within 5–8 days. For oral administration, a 600 mg kg⁻¹ one-off dose of 1:1 CB[7]:CB[8] mixture did not give rise to any significant toxicity.

The Wheate group studied the ex vivo toxicology of CB[6] and CB[7] under more specific circumstances, analyzing the neuro-, myo-, and cardiotoxic activity of the compounds.¹⁰¹ To study neurotoxicity, a mouse sciatic nerve (removed from between the knee and spinal cord) was exposed to 1 mM solutions of CB[6] or CB[7] and the conductivity of the nerve monitored for 2 h; no significant neurotoxicity was observed. Furthermore, cisplatin·CB[7] did not show a decrease in neurotoxicity as compared to free cisplatin. Myotoxicity was also studied by extracting biventer cervicis nerve muscles from chicks, and their contraction response to chemical or electrical stimuli was monitored before and after exposure to 0.3 mM CB[6] and CB[7] solutions. CB[6] caused only a very small change in the strength of muscle contraction, so it can be considered relatively safe. However, CB[7] had a much greater effect on muscle contraction, and the authors hypothesize that this is due to CB[7] binding to postsynaptic nicotinic receptors, interfering with the depolarization ability of the muscle membrane. β -Cyclodextrin exposure also resulted in small decreases in muscle contraction, was not myotoxic in vivo, and may possibly also be the case for CB[6] and CB[7]. Cardiotoxicity was examined using a similar method but with rat heart atria. Both CB[6] and CB[7] showed significant ex vivo cardiotoxicity, exemplified by changes in contraction forces. However, the authors of this study conclude that these experiments represent very high exposure levels to the macrocycles with direct contact with the tissues and so may not be accurate predictions of activity in human clinical models.

To better understand specific organ toxicity in vivo, Wang and collaborators employed zebrafish models to further study the contribution of CB[7] exposure to neuro-, myo-, and cardiotoxicity as well as hepatotoxicity, developmental toxicity, locomotion, and behavioral toxicity.¹⁰² Mortality studies determined an LD₅₀ (lethal dose) to be at 750 μ M when zebrafish were incubated with CB[7] for 2 days. No morphological abnormalities were observed on developing zebrafish exposed to even the higher, more toxic, levels of CB[7]. Some detrimental effects on cardioactivity were observed on zebrafish exposed to CB[7] concentrations greater than 500 μ M including elevated heart rates, thinning of the atrium, distorted heart shape, decreased stroke volume, and decreased cardiac output, which is consistent with the ex vivo study by Wheate. In terms of locomotive effects, extended exposure to higher concentrations of CB[7] significantly shortened swimming distances of zebrafish, which could be a factor of the observed cardiotoxicity; however, the authors reasoned that this was more likely a neurotoxic effect, conflicting with the Wheate ex vivo study. The authors did not observe any hepatotoxicity on zebrafish embryos, demonstrating a high degree of tolerability of CB[7] by the

liver. This study is promising as detrimental effects were not observed below usual therapeutic concentrations of most drug compounds, suggesting a reasonable level of tolerance of CB[7] *in vivo* and therefore warranting much further study in larger animal models.

12.5. Outlook

A considerable amount of work has been carried out in the area of peptide and protein supramolecular complexation with CB[n], and understanding of aromatic amino acid residues, cavity hydrophobic interactions, hydrogen bonding to portals, and cooperative interactions in the example of CB[8] are progressing from the work of several groups. Protein dimerization is particularly exciting in terms of controlling activity and stability, and many interesting studies into other forms of bioconjugation harnessing such host–guest recognition are likely on the horizon. Particularly remarkable studies are those of insulin and amyloid β and how the interactions of specific Phe residues modulate aggregation pathways. With these reported methodical studies in hand it is not difficult to imagine how many more CB[n]–biomolecule interactions will come to light in the near future with new protocols to control and regulate protein activity. It is also promising that initial studies suggesting application of CB-based materials to human clinical settings will not be hampered by issues of toxicity.

13. SUMMARY AND OUTLOOK

In just over three decades since the isolation and full characterization of the first cucurbit[n]uril homologue, this macrocyclic family has transformed from a laboratory bench curiosity into a compound of industrial significance. The widespread number of fields that CB[n] has found applications in is remarkable. Ranging from applications in (but not limited to) materials design, development of next-generation sensors, sophistication of medical techniques through efficient drug delivery and encapsulation, potential in energy harnessing through its catalytic properties, and green technology, CB[n] has been an exceptional contestant in all these fields. CB[n] has also proven itself as a versatile tool in fundamental research such as in separation science, as a precise molecular ruler for plasmonics, and as a catalytic reagent and nanoreactor. In this review, we intended to focus on themes related to CB[n] that have not been presented in great detail in the literature prior to its writing. For example, we discuss the gas binding properties of CB[n] and the interaction of CB[n] with surfaces and their interesting applications. We also highlighted the recent progress in various fields that have utilized the chemical and physical properties of CB[n] in an innovative manner including polymeric materials and networks as well as biological systems.

The exploration of the complexation capabilities of CB[n] with various guest molecules has led to the discovery of a plethora of species that are of scientific interest. New guests are constantly being reported providing unique insights into the understanding of the molecular recognition properties of CB[n]. The advent of sophisticated characterization techniques has complemented research efforts in elucidating the fundamental processes behind CB[n] host–guest chemistry. In addition, this review on CB[n] notably presents the first comprehensive tabulation of all the binding data that can be readily found in the literature through the first half of 2015. The similarities as well as disparities in the binding constants that result from different techniques and measurement conditions are unmistakable. Therefore, the need to standardize measure-

ment and characterization methods is critical, underpinning the importance of reporting precise conditions in which the measurements are taken.

Driven by the shortcomings exhibited by several CB[n] homologues arising from their extremely low water solubility, various strategies to functionalize CB[n] have been pursued. Additionally, the functionalized host molecules have opened up possibilities to tether them to surfaces and polymeric materials. Although the topic has not been discussed in great detail in this review, the increasing pace of research activity and growing interest in controlled functionalization of CB derivatives is apparent and will likely warrant a dedicated review itself in the next few years.

ASSOCIATED CONTENT

Special Issue Paper

This paper is an additional review for *Chem. Rev.* 2015, 115 (15), “Supramolecular Chemistry”.

AUTHOR INFORMATION

Corresponding Author

*E-mail: oas23@cam.ac.uk. Phone: +44 (0)1223 334370.

Author Contributions

[‡]S.J.B., S.K., and M.J.R. contributed equally to this work

Notes

The authors declare no competing financial interest.

Biographies



Steven Barrow received his B.Sc. degree in Nanotechnology from the Royal Melbourne Institute of Technology (RMIT) in Australia and completed his Ph.D. degree under the supervision of Prof. Paul Mulvaney at the University of Melbourne in 2013. His Ph.D. research involved investigating the optical properties of self-assembled gold nanostructures using dark-field microscopy. In 2014, he began a postdoctoral position with Prof. Oren Scherman in the Melville Laboratory for Polymer Synthesis at the University of Cambridge and was awarded a Marie Curie Fellowship in 2015. His current research concerns utilizing nanoparticle–cucurbit[n]uril systems for the dynamic assembly of nanoparticles as well as monitoring chemical reactions and gas sensing.



Setu Kasera received her B.Sc. degree in Biological Chemistry from Aston University, U.K. She then joined Prof. Oren A. Scherman's group at the University of Cambridge as an M.Phil. candidate and continued as a Ph.D. student. Her research focuses on plasmonic constructs with cucurbit[n]urils for sensing applications using surface-enhanced Raman spectroscopy.



Matthew Rowland graduated from the University of Warwick U.K. in 2011 with his M.Chem. degree in Chemistry with Industrial Training. He then joined the Cambridge University Ph.D. Training Programme in Chemical Biology and Molecular Medicine and began research in the laboratory of Prof. Oren A. Scherman as a Ph.D. student. His research focuses on the development of biocompatible hydrogels which self-assemble on account of utilization of the host–guest chemistry of cucurbit[n]uril. His specific interests lie in healthcare and the delivery of therapeutic agents from soft materials.



Jesús del Barrio studied chemistry at the University of Zaragoza, Spain, and received his doctoral degree in 2010 with a thesis on photoresponsive polymers for optical applications. He then moved to the United Kingdom to work on supramolecular materials at The

University of Cambridge with Professor Oren Scherman. His postdoctoral studies, supported in part by a Marie Curie Intra-European Research Fellowship, were in the area of host–guest interactions and macromolecular self-assembly in aqueous media. In 2014, he took up a position as research scientist at the Schlumberger Gould Research Centre in Cambridge, U.K. His work encompasses both basic and applied research in the soft matter area aimed at developing innovative polymer fluids, viscoelastic systems, and responsive materials.



Oren Scherman graduated from Cornell University in Ithaca, NY, with his B.A. degree in Chemistry in 1999. He then moved to Pasadena, CA, where he completed his Ph.D. degree in 2004 in the area of olefin metathesis and controlled polymerization under the supervision of Professor Robert H. Grubbs at the California Institute of Technology (Caltech). After finishing his Ph.D. degree, he moved to The Netherlands to work on supramolecular polymers with Professors E. W. Meijer and Rint P. Sijbesma at the Eindhoven University of Technology. In 2006, he moved to the University of Cambridge to take up an academic appointment as a University Lecturer and Next Generation Fellow in the Melville Laboratory for Polymer Synthesis in the Department of Chemistry. In 2012, he was promoted to Reader in Supramolecular and Polymer Chemistry, and in March 2013, he was appointed as the Director of the Melville Laboratory; he was promoted to Professor in 2015. During the 2013–2014 academic year, he was on sabbatical at Tsinghua University as the Xuetang Visiting Professor in Chemistry. His research group is interested in dynamic supramolecular self-assembly at interfaces. His current research projects include the application of macrocyclic host–guest chemistry using cucurbit[n]urils in the development of novel supramolecular hydrogels and micro-capsules, drug-delivery systems based on dynamic hydrogels, conservation and restoration of important historical artifacts through the exploitation of supramolecular polymer chemistry and sensing, and catalysis using self-assembled nanophotonic systems.

ACKNOWLEDGMENTS

The authors thank all members of the Scherman group for help compiling the tables and proof-reading the review. S.J.B. thanks the European Commission for a Marie Curie Fellowship (NANOSPHERE, 658360). S.K. thanks The Biochemical Society for the Krebs Memorial Scholarship and the Cambridge Commonwealth Trust for financial support. M.J.R. thanks the University of Cambridge Ph.D. Training Programme in Chemical Biology and Molecular Medicine. J.d.B. is grateful for a Marie Curie Intra-European Fellowship (Project 273807). We also acknowledge support from an ERC Starting Investigator Grant (ASPiRe, 240629) and a Next Generation Fellowship provided by the Walters-Kundert Foundation.

REFERENCES

- (1) Meyer, E. Über die Condensation des Harnstoffs mit Glyoxal und des Glykourils mit Formaldehyd. Heidelberg. Ph.D. Thesis, Heidelberg University, Heidelberg, 1904.
- (2) Behrend, R.; Meyer, E.; Rusche, F. I. Ueber Condensationsprodukte aus Glycoluril und Formaldehyd. Ph.D. Thesis, Heidelberg University, Heidelberg, 1905.
- (3) Freeman, W. A.; Mock, W. L.; Shih, N. Y. Cucurbituril. *J. Am. Chem. Soc.* **1981**, *103*, 7367–7368.
- (4) Kim, J.; Jung, I.-S.; Kim, S.-Y.; Lee, E.; Kang, J.-K.; Sakamoto, S.; Yamaguchi, K.; Kim, K. New Cucurbituril Homologues: Syntheses, Isolation, Characterization, and X-ray Crystal Structures of Cucurbit[n]uril ($n = 5, 7$, and 8). *J. Am. Chem. Soc.* **2000**, *122*, 540–541.
- (5) Day, A.; Arnold, A. P.; Blanch, R. J.; Snushall, B. Controlling Factors in the Synthesis of Cucurbituril and Its Homologues. *J. Org. Chem.* **2001**, *66*, 8094–8100.
- (6) Day, A. I.; Blanch, R. J.; Arnold, A. P.; Lorenzo, S.; Lewis, G. R.; Dance, I. A Cucurbituril-Based Gyroscope: A New Supramolecular Form. *Angew. Chem., Int. Ed.* **2002**, *41*, 275–277.
- (7) Jon, S. Y.; Selvapalam, N.; Oh, D. H.; Kang, J.-K.; Kim, S.-Y.; Jeon, Y. J.; Lee, J. W.; Kim, K. Facile Synthesis of Cucurbit[n]uril Derivatives via Direct Functionalization: Expanding Utilization of Cucurbit[n]uril. *J. Am. Chem. Soc.* **2003**, *125*, 10186–10187.
- (8) Zhao, N.; Lloyd, G. O.; Scherman, O. A. Monofunctionalised Cucurbit[6]uril Synthesis using Imidazolium Host-guest Complexation. *Chem. Commun.* **2012**, *48*, 3070–3072.
- (9) Cao, L.; Isaacs, L. Daisy Chain Assembly Formed from a Cucurbit[6]uril Derivative. *Org. Lett.* **2012**, *14*, 3072–3075.
- (10) Huang, W.-H.; Liu, S.; Zavalij, P. Y.; Isaacs, L. Nor-Seco-Cucurbit[10]uril Exhibits Homotropic Allostery. *J. Am. Chem. Soc.* **2006**, *128*, 14744–14745.
- (11) Isaacs, L.; Park, S.-K.; Liu, S.; Ko, Y. H.; Selvapalam, N.; Kim, Y.; Kim, H.; Zavalij, P. Y.; Kim, G.-H.; Lee, H.-S.; Kim, K. The Inverted Cucurbit[n]uril Family. *J. Am. Chem. Soc.* **2005**, *127*, 18000–18001.
- (12) Cintas, P. Cucurbituril: Supramolecular Perspectives for an Old Ligand. *J. Inclusion Phenom. Mol. Recognit. Chem.* **1994**, *17*, 205–220.
- (13) Gerasko, O. A.; Samsonenko, D. G.; Fedin, V. P. Supramolecular Chemistry of Cucurbiturils. *Russ. Chem. Rev.* **2002**, *71*, 741–760.
- (14) Masson, E.; Ling, X.; Joseph, R.; Kyeremeh-Mensah, L.; Lu, X. Cucurbituril Chemistry: a Tale of Supramolecular Success. *RSC Adv.* **2012**, *2*, 1213–1247.
- (15) Lagona, J.; Mukhopadhyay, P.; Chakrabarti, S.; Isaacs, L. The Cucurbit[n]uril Family. *Angew. Chem., Int. Ed.* **2005**, *44*, 4844–4870.
- (16) Lü, J.; Lin, J. X.; Cao, M. N.; Cao, R. Cucurbituril: A Promising organic Building Block for the Design of Coordination Compounds and Beyond. *Coord. Chem. Rev.* **2013**, *257*, 1334–1356.
- (17) Assaf, K. I.; Nau, W. M. Cucurbiturils: From Synthesis to High-Affinity Binding and Catalysis. *Chem. Soc. Rev.* **2015**, *44*, 394–418.
- (18) Walker, S.; Oun, R.; McInnes, F. J.; Wheate, N. J. The Potential of Cucurbit[n]urils in Drug Delivery. *Isr. J. Chem.* **2011**, *51*, 616–624.
- (19) Elbashir, A. A.; Aboul-Enein, H. Y. Critical Reviews in Analytical Chemistry Supramolecular Analytical Application of Cucurbit[n]urils Using Fluorescence Spectroscopy Supramolecular Analytical Application of Cucurbit[n]urils Using Fluorescence Spectroscopy. *Crit. Rev. Anal. Chem.* **2015**, *45*, 52–61.
- (20) Pemberton, B. C.; Singh, R. K.; Johnson, A. C.; Jockusch, S.; Da Silva, J. P.; Ugrinov, A.; Turro, N. J.; Srivastava, D. K.; Sivaguru, J. Supramolecular Photocatalysis: Insights into Cucurbit[8]uril Catalyzed Photodimerization of 6-methylcoumarin. *Chem. Commun.* **2011**, *47*, 6323–6325.
- (21) Li, H.; Yang, Y.-W. Gold Nanoparticles Functionalized with Supramolecular Macrocycles. *Chin. Chem. Lett.* **2013**, *24*, 545–552.
- (22) Montes-García, V.; Pérez-Juste, J.; Pastoriza-Santos, I.; Liz-Marzán, L. M. Metal Nanoparticles and Supramolecular Macrocycles: a Tale of Synergy. *Chem. - Eur. J.* **2014**, *20*, 10874–10883.
- (23) Gürbüz, S.; Idris, M.; Tuncel, D. Cucurbituril-Based Supramolecular Engineered Nanostructured Materials. *Org. Biomol. Chem.* **2015**, *13*, 330–347.
- (24) Jeon, Y. M.; Kim, J.; Whang, D.; Kim, K. Molecular Container Assembly Capable of Controlling Binding and Release of its Guest Molecules: Reversible Encapsulation of Organic Molecules in Sodium Ion Complexed Cucurbituril. *J. Am. Chem. Soc.* **1996**, *118*, 9790–9791.
- (25) Whang, D.; Heo, J.; Park, J. H.; Kim, K. A Molecular Bowl with Metal Ion as Bottom: Reversible Inclusion of Organic Molecules in Cesium Ion Complexed Cucurbituril. *Angew. Chem., Int. Ed.* **1998**, *37*, 78–80.
- (26) Gerasko, O. A.; Virovets, A. V.; Samsonenko, D. G.; Tripolskaya, A. A.; Fedin, V. P.; Fenske, D. Synthesis and Crystal Structures of Supramolecular Compounds of Sucurbit[n]urils ($n = 6, 8$) with Polynuclear Strontium Aqua Complexes. *Russ. Chem. Bull.* **2003**, *52*, 585–593.
- (27) Danylyuk, O.; Fedin, V. P. Solid-State Supramolecular Assemblies of Tryptophan and Tryptamine with Cucurbit[6]uril. *Cryst. Growth Des.* **2012**, *12*, 550–555.
- (28) Liu, J. X.; Long, L.-S.; Huang, R.-B.; Zheng, L.-S. Molecular Capsules Based on Cucurbit[5]uril Encapsulating Naked Anion Chlorine. *Cryst. Growth Des.* **2006**, *6*, 2611–2614.
- (29) Buschmann, H. J.; Cleve, E.; Jansen, K.; Schollmeyer, E. Determination of Complex Stabilities with Nearly Insoluble Host Molecules: Cucurbit[5]uril, Decamethylcucurbit[5]uril and Cucurbit[6]uril as Ligands for the Complexation of some Multi-charged Cations in Aqueous Solution. *Anal. Chim. Acta* **2001**, *437*, 157–163.
- (30) Gerasko, O. A.; Mainicheva, E. A.; Naumova, M. I.; Neumaier, M.; Kappes, M. M.; Lebedkin, S.; Fenske, D.; Fedin, V. P. Sandwich-Type Tetranuclear Lanthanide Complexes with Cucurbit[6]uril: From Molecular Compounds to Coordination Polymers. *Inorg. Chem.* **2008**, *47*, 8869–8880.
- (31) Thuéry, P. Uranyl Ion Complexes with Cucurbit[5]uril: from Molecular Capsules to Uranyl-Organic Frameworks. *Cryst. Growth Des.* **2009**, *9*, 1208–1215.
- (32) Liu, J. X.; Long, L. S.; Huang, R. B.; Zheng, L. S. Interesting Anion-Inclusion Behavior of Cucurbit[5]uril and Its Lanthanide-Capped Molecular Capsule. *Inorg. Chem.* **2007**, *46*, 10168–10173.
- (33) Samsonenko, D. G.; Lipkowski, J.; Gerasko, O. A.; Virovets, A. V.; Sokolov, M. N.; Fedin, V. P.; Platas, J. G.; Hernandez-Molina, R.; Mederos, A. Cucurbituril as a New Macrocyclic Ligand for Complexation of Lanthanide Cations in Aqueous Solutions. *Eur. J. Inorg. Chem.* **2002**, *2002*, 2380–2388.
- (34) Jansen, K.; Buschmann, H. J.; Wego, A.; Döpp, D.; Mayer, C.; Drexler, H. J.; Holdt, H. J.; Schollmeyer, E. Cucurbit[5]uril, Decamethylcucurbit[5]uril and ucurbit[6]uril. Synthesis, Solubility and Amine Complex Formation. *J. Inclusion Phenom. Mol. Recognit. Chem.* **2001**, *39*, 357–363.
- (35) Márquez, C.; Hudgins, R. R.; Nau, W. M. Mechanism of HostGuest Complexation by Cucurbituril. *J. Am. Chem. Soc.* **2004**, *126*, 5806–5816.
- (36) Ni, X.-L.; Xiao, X.; Cong, H.; Liang, L.-L.; Cheng, K.; Cheng, X.-J.; Ji, N.-N.; Zhu, Q.-J.; Xue, S.-F.; Tao, Z. Cucurbit[n]uril-Based Coordination Chemistry: from Simple Coordination Complexes to Novel Poly-dimensional Coordination Polymers. *Chem. Soc. Rev.* **2013**, *42*, 9480–9508.
- (37) Liu, L.; Zhao, N.; Scherman, O. A. Ionic liquids as Novel Guests for Cucurbit[6]uril in Neutral Water. *Chem. Commun.* **2008**, 1070–1072.
- (38) Zhao, N.; Liu, L.; Biedermann, F.; Scherman, O. A. Binding Studies on CB[6] with a Series of 1-Alkyl-3-methylimidazolium Ionic Liquids in an Aqueous System. *Chem. - Asian J.* **2010**, *5*, 530–537.
- (39) Isaacs, L. Cucurbit[n]urils: from Mechanism to Structure and Function. *Chem. Commun.* **2009**, 619–629.
- (40) Mecozzi, S.; Rebek, J., Jr. The 55% Solution: A Formula for Molecular Recognition in the Liquid State. *Chem. - Eur. J.* **1998**, *4*, 1016–1022.
- (41) Nau, W. M.; Florea, M.; Assaf, K. I. Deep Inside Cucurbiturils: Physical Properties and Volumes of their Inner Cavity Determine the Hydrophobic Driving Force for Host-Guest Complexation. *Isr. J. Chem.* **2011**, *51*, 559–577.

- (42) Biedermann, F.; Scherman, O. A. Cucurbit[8]uril Mediated Donor-Acceptor Ternary Complexes: A Model System for Studying Charge-Transfer Interactions. *J. Phys. Chem. B* **2012**, *116*, 2842–2849.
- (43) Biedermann, F.; Uzunova, V. D.; Scherman, O. A.; Nau, W. M.; De Simone, A. Release of High-Energy Water as an Essential Driving Force for the High-Affinity Binding of Cucurbit[n]urils. *J. Am. Chem. Soc.* **2012**, *134*, 15318–15323.
- (44) Biedermann, F.; Vendruscolo, M.; Scherman, O. A.; De Simone, A.; Nau, W. M. Cucurbit[8]uril and Blue-Box: High-Energy Water Release Overwhelms Electrostatic Interactions. *J. Am. Chem. Soc.* **2013**, *135*, 14879–88.
- (45) Biedermann, F.; Nau, W. M.; Schneider, H.-J. The Hydrophobic Effect Revisited—Studies with Supramolecular Complexes Imply High-Energy Water as a Noncovalent Driving Force. *Angew. Chem., Int. Ed.* **2014**, *53*, 11158–11171.
- (46) Buschmann, H. J.; Cleve, E.; Jansen, K.; Wego, A.; Schollmeyer, E. Complex Formation between Cucurbit[n]urils and Alkali, Alkaline Earth and Ammonium Ions in Aqueous Solution. *J. Inclusion Phenom. Mol. Recognit. Chem.* **2001**, *40*, 117–120.
- (47) Shen, Y.; Xue, S.; Zhao, Y.; Zhu, Q.; Tao, Z. NMR Study on Self-Assembled Cage Complex of Hexamethylenetetramine and Cucurbit[n]urils. *Chin. Sci. Bull.* **2003**, *48*, 2694–2697.
- (48) Buschmann, H. J.; Cleve, E.; Jansen, K.; Wego, A.; Schollmeyer, E. The Determination of Complex Stabilities Between Different Cyclodextrins and Dibenzo-18-Crown-6, Cucurbit(6)uril, Decamethylcucurbit(5)uril, Cucurbit(5)uril, p-tert-butylcalix(4)arene and p-tert-butylcalix(6)arene in Aqueous Solutions using a Spectrophotometer. *Mater. Sci. Eng., C* **2001**, *14*, 35–39.
- (49) Kellersberger, K. A.; Anderson, J. D.; Ward, S. M.; Krakowiak, K. E.; Dearden, D. V. Encapsulation of N₂, O₂, Methanol, or Acetonitrile by Decamethylcucurbit[5]uril(NH₄)₂ Complexes in the Gas Phase: Influence of the Guest on "Lid" Tightness. *J. Am. Chem. Soc.* **2001**, *123*, 11316–11317.
- (50) Mock, W. L.; Shih, N. Y. Host-Guest Binding Capacity of Cucurbituril. *J. Org. Chem.* **1983**, *48*, 3618–3619.
- (51) Kolman, V.; Marek, R.; Strelcova, Z.; Kulhanek, P.; Necas, M.; Svec, J.; Sindelar, V. Electron Density Shift in Imidazolium Derivatives upon Complexation with Cucurbit[6]uril. *Chem. - Eur. J.* **2009**, *15*, 6926–6931.
- (52) Jiao, D.; Scherman, O. A. Isolation of Cucurbit[n]uril Homologues with Imidazolium Salts in a Recyclable Manner. *Green Chem.* **2012**, *14*, 2445–2449.
- (53) Lee, S. J. C.; Lee, J. W.; Lee, H. H.; Seo, J.; Noh, D. H.; Ko, Y. H.; Kim, K.; Kim, H. I. Host-guest Chemistry from Solution to the Gas Phase: An Essential Role of Direct Interaction with Water for High-affinity Binding of Cucurbit[n]urils. *J. Phys. Chem. B* **2013**, *117*, 8855–8864.
- (54) Efremova, O. A.; Mironov, Y. V.; Kuratieva, N. V.; Fedorov, V. E. Novel Supramolecular Compounds Based on Cucurbit[6]uril, 1,8-diaminoctane and Octahedral Thiohydroxo Anions with Cluster Core [Re₆S₈]. *Inorg. Chim. Acta* **2010**, *363*, 4411–4415.
- (55) Rekharsky, M. V.; Yamamura, H.; Kawai, M.; Osaka, I. Sequential Formation of a Ternary Complex among Dihexylammonium, Cucurbit [6] uril and Cyclodextrin with Positive Cooperativity: A Combined Calorimetric, NMR and ESI-MS Study. *Org. Lett.* **2006**, *8*, 815–818.
- (56) Kolman, V.; Khan, M. S. A.; Babinský, M.; Marek, R.; Sindelar, V. Supramolecular Shuttle Based on Inclusion Complex Between Cucurbit[6]uril and Bispyridinium Ethylene. *Org. Lett.* **2011**, *13*, 6148–6151.
- (57) Sun, X.; Li, B.; Cao, J.; Chen, J.; Wang, N.; Wan, D.; Zhang, H.; Zhou, X. Pseudopolyrotaxanes of Cucurbit[6]uril: A Three-Dimensional Network Self-assembled by ClO₄-(H₂O)₂ Water Clusters. *Chin. J. Chem.* **2012**, *30*, 941–946.
- (58) Sun, X.; Li, B.; Xia, C.; Zhou, X.; Zhang, H. "Liquid-like" Type (COO⁻)₂(H₂O)₁₀ Anion Water Clusters in Three-Dimensional Supramolecular Structure of Cucurbit[6]uril. *CrystEngComm* **2012**, *14*, 8525–8529.
- (59) Grigoras, M.; Catargiu, A.-M.; Timpu, D. Modification of Polyanilines Properties Using Macrocyclic Compounds. *Rev. Roum. Chim.* **2012**, *57*, 781–790.
- (60) Yang, H.; Ma, Q.; Tan, Y. Side-Chain Polypseudorotaxanes by Threading Cucurbit[6]uril onto N'-3-vinylbenzylidiaminobutane Dihydrochloride: Synthesis, Characterization, and Properties. *J. Polym. Res.* **2013**, *20*, 2–8.
- (61) Wang, H.; Zhu, Y.; Ren, X.; Wang, M.; Tan, Y. Synthesis and Properties of Block Polypseudorotaxanes by Threading Cucurbit[6]uril. *Iran. Polym. J.* **2012**, *21*, 783–792.
- (62) He, S.; Zhou, C.; Zhang, H.; Zhou, X. Binding Modes of Cucurbit[6]uril and Cucurbit[7]uril with a Series of Bis-pyridinium Compounds. *J. Inclusion Phenom. Macrocyclic Chem.* **2013**, *76*, 333–344.
- (63) Tuncel, D.; Cindir, N.; Koldemir, U. Rotaxane and [5]-pseudorotaxane Based on Cucurbit[6]uril and Anchored to a Mesotetraphenyl Porphyrin. *J. Inclusion Phenom. Mol. Recognit. Chem.* **2006**, *55*, 373–380.
- (64) Pievo, R.; Casati, C.; Franchi, P.; Mezzina, E.; Bennati, M.; Lucarini, M. End-to-End Distance Determination in a Cucurbit[6]uril-Based Rotaxane by PELDOR Spectroscopy. *ChemPhysChem* **2012**, *13*, 2659–2661.
- (65) Tuncel, D.; Ozsar, O.; Tiftik, H. B.; Salih, B. Molecular Switch Based on a Cucurbit[6]uril Containing Bistable [3]rotaxane. *Chem. Commun.* **2007**, 1369–1371.
- (66) Hu, F.; Huang, J.; Cao, M.; Chen, Z.; Yang, Y.-W.; Liu, S. H.; Yin, J. Dithienylethene-based Rotaxanes: Synthesis, Characterization and Properties. *Org. Biomol. Chem.* **2014**, *12*, 7712–7720.
- (67) Im Jun, S.; Wook Lee, J.; Sakamoto, S.; Yamaguchi, K.; Kim, K. Rotaxane-Based Molecular Switch with Fluorescence Signaling. *Tetrahedron Lett.* **2000**, *41*, 471–475.
- (68) Praetorius, A.; Bailey, D. M.; Schwarzlose, T.; Nau, W. M. Design of a Fluorescent Dye for Indicator Displacement from Cucurbiturils: A Macrocycle-Responsive Fluorescent Switch Operating through a pKa Shift. *Org. Lett.* **2008**, *10*, 4089–4092.
- (69) Florea, M.; Nau, W. M. Strong Binding of Hydrocarbons to Cucurbituril Probed by Fluorescent Dye Displacement: A Supramolecular Gas-Sensing Ensemble. *Angew. Chem., Int. Ed.* **2011**, *50*, 9338–9342.
- (70) Carvalho, C. P.; Ferreira, R.; Da Silva, J. P.; Pischel, U. An Aminonaphthalimide-Putrescine Conjugate as Fluorescent Probe for Cucurbituril Host-Guest Complexes. *Supramol. Chem.* **2012**, *25*, 1–10.
- (71) Suello Occello, V. N.; Veglia, A. V. Cucurbit[6]uril Nanocavity as an Enhanced Spectrofluorimetric Method for the Determination of Pyrene. *Anal. Chim. Acta* **2011**, *689*, 97–102.
- (72) Tadini, M. C.; Balbino, M. A.; Eleuterio, I. C.; De Oliveira, L. S.; Dias, L. G.; Jean-François Demets, G.; De Oliveira, M. F. Developing Electrodes Chemically Modified with Cucurbit[6]uril to Detect 3,4-Methylenedioxymethamphetamine (MDMA) by Voltammetry. *Electrochim. Acta* **2014**, *121*, 188–193.
- (73) Danylyuk, O.; Fedin, V. P.; Sashuk, V. Kinetic Trapping of the Host-guest Association Intermediate and its Transformation into a Thermodynamic Inclusion Complex. *Chem. Commun.* **2013**, *49*, 1859–1861.
- (74) Danylyuk, O.; Fedin, V. P.; Sashuk, V. Host-Guest Complexes of Cucurbit[6]uril with Isoprenaline: the Effect of the Metal Ion on the Crystallization Pathway and Supramolecular Architecture. *CrystEngComm* **2013**, *15*, 7414–7418.
- (75) Freeman, B. Y. W. A. Structures of the P-Xylylenediammonium Chloride and Calcium Hydrogensulfate Adducts of the Cavitand Cucurbituril. *Acta Crystallogr., Sect. B: Struct. Sci.* **1984**, *40*, 382–387.
- (76) Huang, W.-H. H.; Zavalij, P. Y.; Isaacs, L. Cucurbit[6]uril P-xylylenediammonium Diiodide Deca-hydrate Inclusion Complex. *Acta Crystallogr., Sect. E: Struct. Rep. Online* **2008**, *64*, o1321–o1322.
- (77) Guo, G.; Tang, Q.; Huang, Y.; Tao, Z.; Xue, S.; Zhu, Q. Influences on Shift of pKa, Solubility and Antifungal Activity of Fuberidazole by Inclusion Complexation with Cucurbit[n]urils. *Youji Huaxue* **2014**, *34*, 2317.

- (78) Zheng, H.; Li, Z.; Zhang, J.; Ma, J.; Zhou, Y.; Jia, Q. Preparation of Cucurbit[6]uril-Modified Polymer Monolithic Column for Micro-extraction of Nitroaromatics. *RSC Adv.* **2015**, *5*, 5850–5857.
- (79) Wang, L.; Wang, X.; Qi, M.; Fu, R. Cucurbit[6]uril in Combination with Guanidinium Ionic Liquid as a New Type of Stationary Phase for Capillary Gas Chromatography. *J. Chromatogr. A* **2014**, *1334*, 112–117.
- (80) El-Sheshtawy, H. S.; Bassil, B. S.; Assaf, K. I.; Kortz, U.; Nau, W. M. Halogen Bonding Inside a Molecular Container. *J. Am. Chem. Soc.* **2012**, *134*, 19935–19941.
- (81) Reddy, K. R. K. K.; Cavallini, T. S.; Demets, G. J. F.; Silva, L. F. Bromine and Iodine-Cucurbit[6]uril Complexes: Preparation and Applications in Synthetic Organic Chemistry. *New J. Chem.* **2014**, *38*, 2262–2264.
- (82) Ren, H.; Huang, Z.; Yang, H.; Xu, H.; Zhang, X. Controlling the Reactivity of the Se-Se Bond by the Supramolecular Chemistry of Cucurbituril. *ChemPhysChem* **2015**, *16*, 523–527.
- (83) Thuéry, P. Supramolecular Assemblies built from Lanthanide Ammoniocarboxylates and Cucurbit[6]uril. *CrystEngComm* **2012**, *14*, 8128–8136.
- (84) Thuéry, P. Uranyl-Lanthanide Heterometallic Assemblies with 1,2-ethanesulfonate and Cucurbit[6]uril Ligands. *CrystEngComm* **2012**, *14*, 3363–3366.
- (85) Thuéry, P. Lanthanide Ion Complexes with 2-, 3-, or 4-Sulfobenzoate and Cucurbit[6]uril. *Cryst. Growth Des.* **2012**, *12*, 1632–1640.
- (86) Blanco, E.; Quintana, C.; Hernández, P. An Electrochemical Study of Cucurbit[6]uril-Cadmium(II) Interactions and the Effect of Electrolyte Cations and Guest Molecules. *Anal. Lett.* **2015**, *48*, 783–795.
- (87) Zhang, T.; Chen, W.-J.; Zhang, Y.-Q.; Tao, Z.; Zhu, Q.-J. Coordination and Supramolecular Assemblies Based on Interaction of Three Different Cucurbit[6]urils with Sr(II) Ion. *Chin. J. Inorg. Chem.* **2014**, *30*, 473–480.
- (88) Ji, N. N. N.; Cheng, X. J. J.; Zhao, Y.; Liang, L. L. L.; Chen, K.; Xiao, X.; Zhang, Y. Q. Q.; Zhu, Q. J. J.; Xue, S. F. F.; Tao, Z. Hexachloroplatinate(IV) Anion Induced Cucurbituril Supramolecular Assembly with Linear Channels. *Eur. J. Inorg. Chem.* **2014**, *2014*, 1435–1438.
- (89) da Silva, F. F.; de Oliveira, C. A. F.; Falcão, E. H. L.; Chojnacki, J.; Neves, J. L.; Alves, S. New Lanthanide-CB[6] Coordination Compounds: Relationships Between the Crystal Structure and Luminescent Properties. *Dalton Trans.* **2014**, *43*, 5435–5442.
- (90) Ren, M.; Pinkowicz, D.; Yoon, M.; Kim, K.; Zheng, L.-M. M.; Breedlove, B. K.; Yamashita, M. Dy(III) Single-ion Magnet Showing Extreme Sensitivity to (De)hydration. *Inorg. Chem.* **2013**, *52*, 8342–8348.
- (91) Chen, K.; Kang, Y. S.; Zhao, Y.; Yang, J. M.; Lu, Y.; Sun, W. Y. Cucurbit[6]uril-Based Supramolecular Assemblies: Possible Application in Radioactive Cesium Cation Capture. *J. Am. Chem. Soc.* **2014**, *136*, 16744–16747.
- (92) Karcher, S.; Kornmüller, A.; Jekel, M. Effects of Alkali and Alkaline-Earth Cations on the Removal of Reactive Dyes with Cucurbituril. *Acta Hydrochim. Hydrobiol.* **1999**, *27*, 38–42.
- (93) Khan, M. S. a.; Heger, D.; Necas, M.; Sindelar, V. Remarkable Salt Effect on Stability of Supramolecular Complex Between Modified Cucurbit[6]uril and Methylviologen in Aqueous Media. *J. Phys. Chem. B* **2009**, *113*, 11054–11057.
- (94) Liu, P.; Shao, X.; Chipot, C.; Cai, W. Complexation Mechanism of Cucurbit[6]uril with Hexamethylene Diammonium Cations in Saline Solution. *Phys. Chem. Chem. Phys.* **2014**, *16*, 24169–24172.
- (95) Lee, J. W.; Samal, S.; Selvapalam, N.; Kim, H.-J.; Kim, K. Cucurbituril Homologues and Derivatives: New Opportunities in Supramolecular Chemistry. *Acc. Chem. Res.* **2003**, *36*, 621–630.
- (96) Chinai, J. M.; Taylor, A. B.; Ryno, L. M.; Hargreaves, N. D.; Morris, C. A.; Hart, P. J.; Urbach, A. R. Molecular Recognition of Insulin by a Synthetic Receptor. *J. Am. Chem. Soc.* **2011**, *133*, 8810–8813.
- (97) Smith, L. C.; Leach, D. G.; Blaylock, B. E.; Ali, O. A.; Urbach, A. R. Sequence-Specific, Nanomolar Peptide Binding via Cucurbit[8]uril-Induced Folding and Inclusion of Neighboring Side Chains. *J. Am. Chem. Soc.* **2015**, *137*, 3663–3669.
- (98) Kasera, S.; Herrmann, L. O.; del Barrio, J.; Baumberg, J. J.; Scherman, O. A. Quantitative Multiplexing with Nano-Self-Assemblies in SERS. *Sci. Rep.* **2014**, *4*, 6785.
- (99) Uzunova, V. D.; Cullinane, C.; Brix, K.; Nau, W. M.; Day, A. I. Toxicity of Cucurbit[7]uril and Cucurbit[8]uril: an Exploratory in Vitro and in Vivo Study. *Org. Biomol. Chem.* **2010**, *8*, 2037–2042.
- (100) Hettiarachchi, G.; Nguyen, D.; Wu, J.; Lucas, D.; Ma, D.; Isaacs, L.; Briken, V. Toxicology and Drug Delivery by Cucurbit[n]uril Type Molecular Containers. *PLoS One* **2010**, *5*, e10514.
- (101) Oun, R.; Floriano, R. S.; Isaacs, L.; Rowan, E. G.; Wheate, N. J. The Ex Vivo Neurotoxic Myotoxic and Cardiotoxic Activity of Cucurbituril-Based Macrocyclic Drug Delivery Vehicles. *Toxicol. Res.* **2014**, *3*, 447–455.
- (102) Chen, H.; Chan, J. Y. W.; Yang, X.; Wyman, I. W.; Bardelang, D.; Macartney, D. H.; Lee, S. M. Y.; Wang, R. Developmental and Organ-Specific Toxicity of Cucurbit[7]uril: in vivo Study on Zebrafish Models. *RSC Adv.* **2015**, *5*, 30067–30074.
- (103) Ryan, S. T. J.; Del Barrio, J.; Ghosh, I.; Biedermann, F.; Lazar, A. I.; Lan, Y.; Coulston, R. J.; Nau, W. M.; Scherman, O. A. Efficient Host-Guest Energy Transfer in Polycationic Cyclophane-Perylene Diimide Complexes in Water. *J. Am. Chem. Soc.* **2014**, *136*, 9053–9060.
- (104) Ahn, Y.; Jang, Y.; Selvapalam, N.; Yun, G.; Kim, K. Supramolecular Velcro for Reversible Underwater Adhesion. *Angew. Chem., Int. Ed.* **2013**, *52*, 3140–3144.
- (105) Chen, H.; Ma, H.; Tan, Y. Synthesis of Linear Cucurbit[7]uril Pendent Copolymers through Radical Polymerization: Polymers with Ultra-high Binding Affinity. *J. Polym. Sci., Part A: Polym. Chem.* **2015**, *53*, 1748.
- (106) Liu, S.; Ruspic, C.; Mukhopadhyay, P.; Chakrabarti, S.; Zavalij, P. Y.; Isaacs, L. The Cucurbit[n]uril Family: Prime Components for Self-Sorting Systems. *J. Am. Chem. Soc.* **2005**, *127*, 15959–15967.
- (107) Kim, S. Y.; Jung, I. S.; Lee, E.; Kim, J.; Sakamoto, S.; Yamaguchi, K.; Kim, K. Macrocycles within Macrocycles: Cyclen, Cyclam, and their Transition Metal Complexes Encapsulated in Cucurbit[8]uril. *Angew. Chem., Int. Ed.* **2001**, *40*, 2119–2121.
- (108) Hart, S. L.; Haines, R. I.; Decken, A.; Wagner, B. D. Isolation of the Trans-I and Trans-II Isomers of Cu-II(cyclam) via Complexation with the Macroyclic Host Cucurbit[8]uril. *Inorg. Chim. Acta* **2009**, *362*, 4145–4151.
- (109) Mitkina, T. V.; Naumov, D. Y.; Gerasko, O. A.; Dolgushin, F. M.; Vicent, C.; Llusrà, R.; Sokolov, M. N.; Fedin, V. P. Inclusion of Nickel(II) and Copper(II) Complexes with Aliphatic Polyamines in Cucurbit[8]uril. *Russ. Chem. Bull.* **2004**, *53*, 2519–2524.
- (110) Kovalenko, E. A.; Mitkina, T. V.; Gerasko, O. A.; Samsonenko, D. G.; Naumov, D. Y.; Fedin, V. P. Cucurbit[8]uril-Based Inclusion Compounds Containing Iron(II), Cobalt(III), and Nickel(II) Complexes with Cyclam and Cyclen as Guest Molecules: Synthesis and Crystal Structures. *Russ. J. Coord. Chem.* **2011**, *37*, 161–167.
- (111) Mitkina, T. V.; Naumov, D. Y.; Gerasko, O. A.; Fedin, V. P. Crystal Structure and Chemical Oxidation of the Palladium(II) Cyclam Complex within the Cavity of Cucurbit[8]uril. *Inorg. Chim. Acta* **2010**, *363*, 4387–4391.
- (112) Wu, X.-j.; Hu, K.; Meng, X. G.; Cheng, G. Z. A cucurbit[8]uril Inclusion Complex with 1,7-Dimethyl-1,4,7,10-Tetraazacyclododecane Tetrachloride. *New J. Chem.* **2010**, *34*, 17–20.
- (113) Jiang, G.; Li, G. Preparation and Biological Activity of Novel Cucurbit[8]uril-Fullerene Complex. *J. Photochem. Photobiol., B* **2006**, *85*, 223–227.
- (114) Ko, Y. H.; Kim, H.; Kim, Y.; Kim, K. U-shaped Conformation of Alkyl Chains Bound to a Synthetic Host. *Angew. Chem., Int. Ed.* **2008**, *47*, 4106–4109.
- (115) Ko, Y. H.; Kim, Y.; Kim, H.; Kim, K. U-Shaped Conformation of Alkyl Chains Bound to a Synthetic Receptor Cucurbit[8]uril. *Chem. - Asian J.* **2011**, *6*, 652–657.

- (116) Xiao, X.; Wang, Q.; Yu, Y. H.; Xiao, Z. Y.; Tao, Z.; Xue, S.-F.; Zhu, Q. J.; Liu, J. X.; Liu, X. H. Contorted Conformations of 1,4-Butylenedipyridinium and 1,10-Decylenedipyridinium Cationic Guests in a Cucurbit[8]uril Host. *Eur. J. Inorg. Chem.* **2011**, *2011*, 2366–2371.
- (117) Baek, K.; Kim, Y.; Kim, H.; Yoon, M.; Hwang, I.; Ko, Y. H.; Kim, K. Unconventional U-Shaped Conformation of a Bolaamphiphile Embedded in a Synthetic Host. *Chem. Commun.* **2010**, *46*, 4091–4093.
- (118) Mileo, E.; Mezzina, E.; Grepioni, F.; Pedulli, G. F.; Lucarini, M. Preparation and Characterisation of a New Inclusion Compound of Cucurbit[8]uril with a Nitroxide Radical. *Chem. - Eur. J.* **2009**, *15*, 7859–7862.
- (119) Bardelang, D.; Banaszak, K.; Karoui, H.; Rockenbauer, A.; Waite, M.; Udachin, K.; Ripmeester, J. A.; Ratcliffe, C. I.; Ouari, O.; Tordo, P. Probing Cucurbituril Assemblies in Water with TEMPO-like Nitroxides: A Trinitroxide Supraradical with Spin-Spin Interactions. *J. Am. Chem. Soc.* **2009**, *131*, 5402–5404.
- (120) Jayaraj, N.; Porel, M.; Ottaviani, M. F.; Maddipatla, M. V. S. N.; Modelli, A.; Da Silva, J. P.; Bhogala, B. R.; Captain, B.; Jockusch, S.; Turro, N. J.; Ramamurthy, V. Self Aggregation of Supramolecules of Nitroxides@Cucurbit[8]uril Revealed by EPR Spectra. *Langmuir* **2009**, *25*, 13820–13832.
- (121) Yi, S.; Captain, B.; Ottaviani, M. F.; Kaifer, A. E. Controlling the Extent of Spin Exchange Coupling in 2,2,6,6-Tetramethylpiperidine-1-oxyl (TEMPO) Biradicals via Molecular Recognition with Cucurbit[n]uril Hosts. *Langmuir* **2011**, *27*, 5624–5632.
- (122) Yi, S.; Captain, B.; Kaifer, A. E. The Importance of Methylation in the Binding of (Ferrocyanlmethyl)tempammonium Guests by Cucurbit[n]uril ($n = 7, 8$) Hosts. *Chem. Commun.* **2011**, *47*, 5500–5502.
- (123) Tootoonchi, M. H.; Yi, S.; Kaifer, A. E. Detection of Isomeric Microscopic Host-Guest Complexes. A Time-Evolving Cucurbit[7]uril Complex. *J. Am. Chem. Soc.* **2013**, *135*, 10804–10809.
- (124) Bardelang, D.; Casano, G.; Poulhes, F.; Karoui, H.; Filippini, J.; Rockenbauer, A.; Rosas, R.; Monnier, V.; Siri, D.; Gaudel-Siri, A.; Ouari, O.; Tordo, P. Spin Exchange Monitoring of the Strong Positive Homotropic Allosteric Binding of a Tetrapolar Radical by a Synthetic Receptor in Water. *J. Am. Chem. Soc.* **2014**, *136*, 17570–17577.
- (125) Porel, M.; Jockusch, S.; Ottaviani, M. F.; Turro, N. J.; Ramamurthy, V. Interaction between Encapsulated Excited Organic Molecules and Free Nitroxides: Communication Across a Molecular Wall. *Langmuir* **2011**, *27*, 10548–10555.
- (126) Rinkevicius, Z.; Frecu, B.; Murugan, N. A.; Vahtras, O.; Kongsted, J.; Agren, H. Encapsulation Influence on EPR Parameters of Spin-Labels: 2,2,6,6-Tetramethyl-4-methoxypiperidine-1-oxyl in Cucurbit[8]uril. *J. Chem. Theory Comput.* **2012**, *8*, 257–263.
- (127) Peresypkina, E. V.; Fedin, V. P.; Maurel, V.; Grand, A.; Rey, P.; Vostrikova, K. E. Inclusion of a Nitronyl Nitroxyl Radical and Its Hydrochloride in Cucurbit[8]uril. *Chem. - Eur. J.* **2010**, *16*, 12481–12487.
- (128) Kim, H.-J.; Heo, J.; Jeon, W. S.; Lee, E.; Kim, J.; Sakamoto, S.; Yamaguchi, K.; Kim, K. Selective Inclusion of a Hetero-Guest Pair in a Molecular Host: Formation of Stable Charge-Transfer Complexes in Cucurbit[8]uril. *Angew. Chem.* **2001**, *113*, 1574–1577.
- (129) Kim, H. J.; Kim, K.; Kim, S. Y.; Oh, J.; Zhao, J. Water- and Organic-Soluble Cucurbituril Derivatives, their Preparation Methods, their Separation Methods and Uses, WO 2003004500 A1, 2003.
- (130) Bush, M. E.; Bouley, N. D.; Urbach, A. R. Charge-Mediated Recognition of N-Terminal Tryptophan in Aqueous Solution by a Synthetic Host. *J. Am. Chem. Soc.* **2005**, *127*, 14511–14517.
- (131) Wang, R.; Yuan, L.; Macartney, D. H. Cucurbit[7]uril Mediates the Stereoselective Hydrochloride in Aqueous Solution. *J. Org. Chem.* **2006**, *71*, 1237–1239.
- (132) Ling, Y.; Wang, W.; Kaifer, A. E. A New Cucurbit[8]uril-Based Fluorescent Receptor for Indole Derivatives. *Chem. Commun.* **2007**, *610*–612.
- (133) Loh, X. J. Supramolecular Host-Guest Polymeric Materials for Biomedical Applications. *Mater. Horiz.* **2014**, *1*, 185–195.
- (134) Gürbuz, S.; Idris, M.; Tuncel, D. Cucurbituril-Based Supramolecular Engineered Nanostructured Materials. *Org. Biomol. Chem.* **2015**, *13*, 330–347.
- (135) Yang, X.; Yu, H.; Wang, L.; Tong, R.; Akram, M.; Chen, Y.; Zhai, X. Self-Healing Polymer Materials Constructed by Macrocycle-Based Host-Guest Interactions. *Soft Matter* **2015**, *11*, 1242–1252.
- (136) Yang, C.; Mori, T.; Origane, Y.; Ko, Y. H.; Selvapalam, N.; Kim, K.; Inoue, Y. Highly Stereoselective Photocyclodimerization of Alpha-Cyclodextrin-Appended Anthracene Mediated by Gamma-Cyclodextrin and Cucurbit[8]uril: A Dramatic Steric Effect Operating Outside the Binding Site. *J. Am. Chem. Soc.* **2008**, *130*, 8574.
- (137) Lei, L.; Luo, L.; Wu, X. L.; Liao, G. H.; Wu, L. Z.; Tung, C. H. Cucurbit[8]uril-Mediated Photodimerization of Alkyl 2-Naphthoate in Aqueous Solution. *Tetrahedron Lett.* **2008**, *49*, 1502–1505.
- (138) Gromov, S. P.; Vedernikov, A. I.; Kuz'Mina, L. G.; Kondratuk, D. V.; Sazonov, S. K.; Strelenko, Y. A.; Alfimov, M. V.; Howard, J. A. K. Photocontrolled Molecular Assembler Based on Cucurbit[8]uril: [2 + 2]-Autophotocycloaddition of Styryl Dyes in the Solid State and in Water. *Eur. J. Org. Chem.* **2010**, *2010*, 2587–2599.
- (139) Kasera, S.; Biedermann, F.; Baumberg, J. J.; Scherman, O. A.; Mahajan, S. Quantitative SERS Using the Sequestration of Small Molecules Inside Precise Plasmonic Nanoconstructs. *Nano Lett.* **2012**, *12*, 5924–5928.
- (140) Roldán, M. L.; Sanchez-Cortes, S.; García-Ramos, J. V.; Domingo, C. Cucurbit[8]uril-Stabilized Charge Transfer Complexes with Diquat Driven by pH: a SERS Study. *Phys. Chem. Chem. Phys.* **2012**, *14*, 4935–4941.
- (141) Taylor, R. W.; Coulston, R. J.; Biedermann, F.; Mahajan, S.; Baumberg, J. J.; Scherman, O. A. In situ SERS Monitoring of Photochemistry within a Nanojunction Reactor. *Nano Lett.* **2013**, *13*, 5985–5990.
- (142) Jeon, W. S.; Kim, H. J.; Lee, C.; Kim, K. Control of the Stoichiometry in Host-Guest Complexation by Redox Chemistry of Guests: Inclusion of Methylviologen in Cucurbit[8]uril. *Chem. Commun.* **2002**, 1828–1829.
- (143) Biedermann, F.; Rauwald, U.; Zayed, J. M.; Scherman, O. A. A Supramolecular Route for Reversible Protein-Polymer Conjugation. *Chem. Sci.* **2011**, *2*, 279–286.
- (144) Uhlenheuer, D. A.; Young, J. F.; Nguyen, H. D.; Scheepstra, M.; Brunsved, L. Cucurbit[8]uril Induced Heterodimerization of Methylviologen and Naphthalene Functionalized Proteins. *Chem. Commun.* **2011**, *47*, 6798–6800.
- (145) Gonzalez-Campo, A.; Brasch, M.; Uhlenheuer, D. A.; Gomez-Casado, A.; Yang, L.; Brunsved, L.; Huskens, J.; Jonkheijm, P. Supramolecularly Oriented Immobilization of Proteins Using Cucurbit[8]uril. *Langmuir* **2012**, *28*, 16364–16371.
- (146) Rauwald, U.; Biedermann, F.; Deroo, S.; Robinson, C. V.; Scherman, O. A. Correlating Solution Binding and ESI-MS Stabilities by Incorporating Solvation Effects in a Confined Cucurbit[8]uril System. *J. Phys. Chem. B* **2010**, *114*, 8606–8615.
- (147) Sindelar, V.; Cejas, M. A.; Raymo, F. M.; Chen, W. Z.; Parker, S. E.; Kaifer, A. E. Supramolecular Assembly of 2,7-Dimethyldiazopyrenium and Cucurbit[8]uril: A New Fluorescent Host for Detection of Catechol and Dopamine. *Chem. - Eur. J.* **2005**, *11*, 7054–7059.
- (148) Biedermann, F.; Rauwald, U.; Czifreszky, M.; Williams, K. A.; Gann, L. D.; Guo, B. Y.; Urbach, A. R.; Bielawski, C. W.; Scherman, O. A. Benzobis(imidazolium)-Cucurbit[8]uril Complexes for Binding and Sensing Aromatic Compounds in Aqueous Solution. *Chem. - Eur. J.* **2010**, *16*, 13716–13722.
- (149) Jiao, D.; Biedermann, F.; Scherman, O. A. Size Selective Supramolecular Cages from Aryl-Bisimidazolium Derivatives and Cucurbit[8]uril. *Org. Lett.* **2011**, *13*, 3044–3047.
- (150) Biedermann, F.; Elmalem, E.; Ghosh, I.; Nau, W. M.; Scherman, O. A. Strongly Fluorescent, Switchable Perylene Bis-diimide) Host-Guest Complexes with Cucurbit[8]uril In Water. *Angew. Chem., Int. Ed.* **2012**, *51*, 7739–7743.
- (151) Biedermann, F.; Hathazi, D.; Nau, W. M. Associative Chemosensing by Fluorescent Macrocycle-Dye Complexes - a

- Versatile Enzyme Assay Platform Beyond Indicator Displacement. *Chem. Commun.* **2015**, *51*, 4977–4980.
- (152) Wang, R.; Bardelang, D.; Waite, M.; Udachin, K. A.; Leek, D. M.; Yu, K.; Ratcliffe, C. I.; Ripmeester, J. A. Inclusion Complexes of Coumarin in Cucurbiturils. *Org. Biomol. Chem.* **2009**, *7*, 2435–2439.
- (153) Wu, X.; Meng, X.; Cheng, G. A novel 1:2 Cucurbit[8]uril Inclusion Complex with N-phenylpiperazine Hydrochloride. *J. Inclusion Phenom. Mol. Recognit. Chem.* **2009**, *64*, 325–329.
- (154) Wang, R.; Yuan, L.; Ihmels, H.; Macartney, D. H. Cucurbit[8]uril/Cucurbit[7]uril Controlled Off/On Fluorescence of the Acridizinium and 9-Aminoacridizinium Cations in Aqueous Solution. *Chem. - Eur. J.* **2007**, *13*, 6468–6473.
- (155) Shaikh, M.; Choudhury, S. D.; Mohanty, J.; Bhasikuttan, A. C.; Pal, H. Contrasting Guest Binding Interaction of Cucurbit[7–8]urils with Neutral Red Dye: Controlled Exchange of Multiple Guests. *Phys. Chem. Chem. Phys.* **2010**, *12*, 7050–7055.
- (156) Jiao, D.; Biedermann, F.; Tian, F.; Scherman, O. A. A Systems Approach to Controlling Supramolecular Architecture and Emergent Solution Properties via Host-Guest Complexation in Water. *J. Am. Chem. Soc.* **2010**, *132*, 15734–15743.
- (157) Miskolczy, Z.; Biczok, L. Sequential Inclusion of Two Berberine Cations in Cucurbit[8]uril Cavity: Kinetic and Thermodynamic Studies. *Phys. Chem. Chem. Phys.* **2014**, *16*, 20147–20156.
- (158) Sayed, M.; Biedermann, F.; Uzunova, V. D.; Assaf, K. I.; Bhasikuttan, A. C.; Pal, H.; Nau, W. M.; Mohanty, J. Triple Emission from p-Dimethylaminobenzonitrile-Cucurbit[8]uril Triggers the Elusive Excimer Emission. *Chem. - Eur. J.* **2015**, *21*, 691–696.
- (159) Senler, S.; Cui, L.; Broomes, A. M.; Smith, E. L.; Wilson, J. N.; Kaifer, A. E. New Guests for the Cucurbit[8]uril Host. Formation of G2H Ternary Complexes. *J. Phys. Org. Chem.* **2012**, *25*, 592–596.
- (160) Zhang, Y.; Zhou, T.-Y.; Zhang, K.-D.; Dai, J.-L.; Zhu, Y.-Y.; Zhao, X. Encapsulation Enhanced Dimerization of a Series of 4-Aryl-N-Methylpyridinium Derivatives in Water: New Building Blocks for Self-Assembly in Aqueous Media. *Chem. - Asian J.* **2014**, *9*, 1530–1534.
- (161) Vincil, G. A.; Urbach, A. R. Effects of the Number and Placement of Positive Charges on ViologenCucurbit[n]uril Interactions. *Supramol. Chem.* **2008**, *20*, 681–687.
- (162) Biedermann, F.; Ross, I.; Scherman, O. A. Host-guest Accelerated Photodimerisation of Anthracene-Labeled Macromolecules in Water. *Polym. Chem.* **2014**, *5*, 5375–5382.
- (163) Carvalho, C. P.; Dominguez, Z.; Da Silva, J. P.; Pischel, U. A Supramolecular Keypad Lock. *Chem. Commun.* **2015**, *51*, 2698–2701.
- (164) Sonzini, S.; Ryan, S. T. J.; Scherman, O. A. Supramolecular Dimerisation of Middle-Chain Phe Pentapeptides via CB[8] Host-Guest Homoternary Complex Formation. *Chem. Commun.* **2013**, *49*, 8779–8781.
- (165) Heitmann, L. M.; Taylor, A. B.; Hart, P. J.; Urbach, A. R. Sequence-Specific Recognition and Cooperative Dimerization of N-Terminal Aromatic Peptides in Aqueous Solution by a Synthetic Host. *J. Am. Chem. Soc.* **2006**, *128*, 12574–12581.
- (166) Ong, W.; Gómez-Kaifer, M.; Kaifer, A. E. Cucurbit[7]uril: A Very Effective Host for Viologens and Their Cation Radicals. *Org. Lett.* **2002**, *4*, 1791–1794.
- (167) Hwang, I.; Ziganshina, A. Y.; Ko, Y. H.; Yun, G.; Kim, K. A New Three-Way Supramolecular Switch based on Redox-controlled Interconversion of Hetero- and Homo-Guest-Pair Inclusion Inside a Host Molecule. *Chem. Commun.* **2009**, 416–418.
- (168) Li, J. R.; Kuppler, R. J.; Zhou, H. C. Selective Gas Adsorption and Separation in Metal-Organic Frameworks. *Chem. Soc. Rev.* **2009**, *38*, 1477–1504.
- (169) Tian, J.; Ma, S.; Thallapally, P. K.; Fowler, D.; McGrail, B. P.; Atwood, J. L. Cucurbit[7]uril: an Amorphous Molecular Material for Highly Selective Carbon Dioxide Uptake. *Chem. Commun.* **2011**, *47*, 7626–7628.
- (170) Kim, H.; Kim, Y.; Yoon, M.; Lim, S.; Park, S. M.; Seo, G.; Kim, K. Highly Selective Carbon Dioxide Sorption in an Organic Molecular Porous Material. *J. Am. Chem. Soc.* **2010**, *132*, 12200–12202.
- (171) Miyahara, Y.; Abe, K.; Inazu, T. "Molecular" Molecular Sieves: Lid-Free Decamethylcucurbit[5]uril Absorbs and Desorbs Gases Selectively. *Angew. Chem., Int. Ed.* **2002**, *41*, 3020–3023.
- (172) Tian, J.; Liu, J.; Liu, J.; Thallapally, P. K. Identification of Solid-State forms of Cucurbit[6]uril for Carbon Dioxide Capture. *CrystEngComm* **2013**, *15*, 1528–1531.
- (173) Haouaj, M. E.; Ho, K. Y.; Luhmer, M.; Kim, K.; Bartik, K. NMR Investigation of the Complexation of Neutral Guests by Cucurbituril. *J. Chem. Soc. Perkin Trans. 2* **2001**, 2104–2107.
- (174) El Haouaj, M.; Luhmer, M.; Ko, Y. H.; Kim, K.; Bartik, K. NMR Study of the Reversible Complexation of Xenon by Cucurbituril. *J. Chem. Soc. Perkin Trans. 2* **2001**, 804–807.
- (175) Fusaro, L.; Locci, E.; Lai, A.; Luhmer, M. NMR Study of the Reversible Trapping of SF₆ by Cucurbit[6]uril in Aqueous Solution. *J. Phys. Chem. B* **2008**, *112*, 15014–15020.
- (176) Assaf, K. I.; Nau, W. M. Cucurbiturils as Fluorophilic Receptors. *Supramol. Chem.* **2014**, *26*, 657–669.
- (177) Kim, B. S.; Ko, Y. H.; Kim, Y.; Lee, H. J.; Selvapalam, N.; Lee, H. C.; Kim, K. Water Soluble Cucurbit[6]uril Derivative as a Potential Xe Carrier for ¹²⁹Xe NMR-Based Biosensors. *Chem. Commun.* **2008**, 2756–2758.
- (178) An, Q.; Li, G.; Tao, C.; Li, Y.; Wu, Y.; Zhang, W. A General and Efficient Method to form Self-Assembled Cucurbit[n]uril Monolayers on Gold Surfaces. *Chem. Commun.* **2008**, 1989–1991.
- (179) Premkumar, T.; Geckeler, K. E. Nanosized CuO Particles via a Supramolecular Strategy. *Small* **2006**, *2*, 616–620.
- (180) Premkumar, T.; Lee, Y.; Geckeler, K. E. Macrocycles as a Tool: a Facile and One-Pot Synthesis of Silver Nanoparticles using Cucurbituril Designed for Cancer Therapeutics. *Chem. - Eur. J.* **2010**, *16*, 11563–11566.
- (181) Premkumar, T.; Geckeler, K. E. Cucurbit[7]uril as a Tool in the Green Synthesis of Gold Nanoparticles. *Chem. - Asian J.* **2010**, *5*, 2468–2476.
- (182) Lee, T. C.; Scherman, O. A. Formation of Dynamic Aggregates in Water by Cucurbit[5]uril Capped with Gold Nanoparticles. *Chem. Commun.* **2010**, *46*, 2438–2440.
- (183) Taylor, R. W.; Lee, T. C.; Scherman, O. A.; Esteban, R.; Aizpurua, J.; Huang, F. M.; Baumberg, J. J.; Mahajan, S. Precise Subnanometer Plasmonic Junctions for SERS within Gold Nanoparticle Assemblies Using Cucurbit[n]uril "Glue". *ACS Nano* **2011**, *5*, 3878–3887.
- (184) Lee, T. C.; Scherman, O. A. A Facile Synthesis of Dynamic Supramolecular Aggregates of Cucurbit[n]uril (n = 5–8) Capped with Gold Nanoparticles in Aqueous Media. *Chem. - Eur. J.* **2012**, *18*, 1628–1633.
- (185) Lanterna, A.; Pino, E. Enhanced Catalytic Electrochemical Reduction of Dissolved Oxygen with Ultraclean Cucurbituril[7]-Capped Gold Nanoparticles. *Nanoscale* **2014**, *6*, 9550–9553.
- (186) Lu, X.; Masson, E. Formation and Stabilization of Silver Nanoparticles with Cucurbit[n]urils (n = 5–8) and Cucurbituril-Based Pseudorotaxanes in Aqueous Medium. *Langmuir* **2011**, *27*, 3051–3058.
- (187) Romero, I.; Aizpurua, J.; Bryant, G. W.; Abajo, F. J. G. D. Plasmons in Nearly Touching Metallic Nanoparticles: Singular Response in the Limit of Touching Dimers. *Opt. Express* **2006**, *14*, 9988–9999.
- (188) Prodan, E.; Radloff, C.; Halas, N. J.; Nordlander, P. A Hybridization Model for the Plasmon Response of Complex Nanostructures. *Science* **2003**, *302*, 419–422.
- (189) Esteban, R.; Borisov, A. G.; Nordlander, P.; Aizpurua, J. Bridging Quantum and Classical Plasmonics with a Quantum-Corrected Model. *Nat. Commun.* **2012**, *3*, 825.
- (190) Scholl, J. A.; García-Etxarri, A.; Koh, A. L.; Dionne, J. A. Observation of Quantum Tunneling between Two Plasmonic Nanoparticles. *Nano Lett.* **2013**, *13*, 564–569.
- (191) Savage, K. J.; Hawkeye, M. M.; Esteban, R.; Borisov, A. G.; Aizpurua, J.; Baumberg, J. J. Revealing the Quantum Regime in Tunnelling Plasmonics. *Nature* **2012**, *491*, 574–577.

- (192) Zhu, W.; Crozier, K. B. Quantum Mechanical Limit to Plasmonic Enhancement as Observed by Surface-Enhanced Raman Scattering. *Nat. Commun.* **2014**, *5*, 5228.
- (193) Esteban, R.; Zugarramurdi, A.; Zhang, P.; Nordlander, P.; Garcia-Vidal, F. J.; Borisov, A. G.; Aizpurua, J. A Classical Treatment of Optical Tunneling in Plasmonic Gaps: Extending the Quantum Corrected Model to Practical Situations. *Faraday Discuss.* **2015**, *178*, 151–183.
- (194) Esteban, R.; Taylor, R. W.; Baumberg, J. J.; Aizpurua, J. How Chain Plasmons Govern the Optical Response in Strongly Interacting Self-Assembled Metallic Clusters of Nanoparticles. *Langmuir* **2012**, *28*, 8881–8890.
- (195) Herrmann, L. O.; Valev, V. K.; Aizpurua, J.; Baumberg, J. J. Self-sifting of Chain Plasmons: the Complex Optics of Au Nanoparticle Clusters. *Opt. Express* **2013**, *21*, 32377–32385.
- (196) de Nijs, B.; Bowman, R. W.; Herrmann, L. O.; Benz, F.; Barrow, S. J.; Mertens, J.; Sigle, D. O.; Chikkaraddy, R.; Eiden, A.; Ferrari, A.; Scherman, O. A.; Baumberg, J. J. Unfolding the Contents of Sub-nm Plasmonic Gaps using Normalising Plasmon Resonance Spectroscopy. *Faraday Discuss.* **2015**, *178*, 185–193.
- (197) Herrmann, L. O.; Valev, V. K.; Tserkezis, C.; Barnard, J. S.; Kasera, S.; Scherman, O. A.; Aizpurua, J.; Baumberg, J. J. Threading Plasmonic Nanoparticle Strings with Light. *Nat. Commun.* **2014**, *5*, 4568.
- (198) Hüskens, N.; Taylor, R. W.; Zigah, D.; Taveau, J. C.; Lambert, O.; Scherman, O. A.; Baumberg, J. J.; Kuhn, A. Electrokinetic Assembly of One-Dimensional Nanoparticle Chains with Cucurbit[7]uril Controlled Subnanometer Junctions. *Nano Lett.* **2013**, *13*, 6016–6022.
- (199) Jones, S. T.; Taylor, R. W.; Esteban, R.; Abo-Hamed, E. K.; Bomans, P. H. H.; Sommerdijk, N. a. J. M.; Aizpurua, J.; Baumberg, J. J.; Scherman, O. A. Gold Nanorods with Sub-nanometer Separation using Cucurbit[n]uril for SERS Applications. *Small* **2014**, *10*, 4298–4303.
- (200) Tao, C.-A.; An, Q.; Zhu, W.; Yang, H.; Li, W.; Lin, C.; Xu, D.; Li, G. Cucurbit[n]urils as a SERS Hot-Spot Nanocontainer through Bridging Gold Nanoparticles. *Chem. Commun.* **2011**, *47*, 9867–9869.
- (201) Le Ru, E.; Etchegoin, P. *Principles of Surface-Enhanced Raman Spectroscopy: and Related Plasmonic Effects*, 1st ed.; Elsevier Science: Great Britain, 2008.
- (202) Bell, S. E. J.; Sirimuthu, N. M. S. Quantitative Surface-Enhanced Raman Spectroscopy. *Chem. Soc. Rev.* **2008**, *37*, 1012–1024.
- (203) Alvarez-Puebla, R. A.; Liz-Marzán, L. M. Traps and Cages for Universal SERS Detection. *Chem. Soc. Rev.* **2012**, *41*, 43–51.
- (204) Guerrini, L.; Graham, D. Molecularly-Mediated Assemblies of Plasmonic Nanoparticles for Surface-Enhanced Raman Spectroscopy Applications. *Chem. Soc. Rev.* **2012**, *41*, 7085–7107.
- (205) Corma, A.; Garcia, H.; Montes-Navajas, P. A Pseudopolyrotaxane Consisting in PPV Threaded in Multiple Cucurbiturils. *Tetrahedron Lett.* **2007**, *48*, 4613–4617.
- (206) Mahajan, S.; Lee, T.-C.; Biedermann, F.; Hugall, J. T.; Baumberg, J. J.; Scherman, O. A. Raman and SERS Spectroscopy of Cucurbit[n]urils. *Phys. Chem. Chem. Phys.* **2010**, *12*, 10429–10433.
- (207) Mohanty, J.; Nau, W. M. Ultrastable Rhodamine with Cucurbituril. *Angew. Chem., Int. Ed.* **2005**, *44*, 3750–3754.
- (208) El-Baghouthi, M. I.; Assaf, K. I.; Rawashdeh, A. M. M. Molecular Dynamics of Methyl Viologen-Cucurbit[n]uril. *J. Chem. Theory Comput.* **2010**, *6*, 984–992.
- (209) Chen, Y.; Klimczak, A.; Galoppini, E.; Lockard, J. V. Structural Interrogation of a Cucurbit[7]uril-Ferrocene Host-Guest Complex in the Solid State: a Raman Spectroscopy Study. *RSC Adv.* **2013**, *3*, 1354–1358.
- (210) Young, J. F.; Nguyen, H. D.; Yang, L.; Huskens, J.; Jonkheijm, P.; Brunsved, L. Strong and Reversible Monovalent Supramolecular Protein Immobilization. *ChemBioChem* **2010**, *11*, 180–183.
- (211) Wasserberg, D.; Uhlenheuer, D. a.; Neirynck, P.; Cabanas-Danés, J.; Schenkel, J. H.; Ravoo, B. J.; An, Q.; Huskens, J.; Milroy, L. G.; Brunsved, L.; Jonkheijm, P. Immobilization of Ferrocene-Modified SNAP-Fusion Proteins. *Int. J. Mol. Sci.* **2013**, *14*, 4066–4080.
- (212) Neirynck, P.; Brinkmann, J.; An, Q.; van der Schaft, D. W. J.; Milroy, L.-G.; Jonkheijm, P.; Brunsved, L. Supramolecular Control of Cell Adhesion via Ferrocene-Cucurbit[7]uril Host-Guest Binding on Bold Surfaces. *Chem. Commun.* **2013**, *49*, 3679–3681.
- (213) Freitag, M.; Galoppini, E. Cucurbituril Complexes of Viologens Bound to TiO₂ Films. *Langmuir* **2010**, *26*, 8262–8269.
- (214) Kim, K. K.; Jeon, W. S.; Kang, J.-K.; Lee, J. W.; Jon, S. Y.; Kim, T. A Pseudorotaxane on Gold: Formation of Self-Assembled Monolayers, Reversible Dethreading and Rethreading of the Ring, and Ion-Gating Behavior. *Angew. Chem.* **2003**, *115*, 2395–2398.
- (215) Ma, X.; Xue, Y.; Dai, L.; Urbas, A.; Li, Q. Hydrophilic Cucurbit[7]uril-Pseudorotaxane-Anchored-Monolayer-Protected Gold Nanorods. *Eur. J. Inorg. Chem.* **2013**, *2013*, 2682–2686.
- (216) Halterman, R. L.; Moore, J. L.; Yip, W. T. Cucurbit[7]uril Disrupts Aggregate Formation Between Rhodamine B Dyes Covalently Attached to Glass Substrates. *J. Fluoresc.* **2011**, *21*, 1467–1478.
- (217) Tang, Y.; Yang, S.; Zhao, Y.; You, M.; Zhang, F.; He, P. The Host - Guest Interaction Between Cucurbit[7]uril and Ferrocenemocarboxylic Acid for Electrochemically Catalytic Determination of Glucose. *Electroanalysis* **2015**, *27*, 1387–1393.
- (218) Yang, H.; An, Q.; Zhu, W.; Li, W.; Jiang, Y.; Cui, J.; Zhang, X.; Li, G. A New Strategy for Effective Construction of Protein Stacks by using Cucurbit[8]uril as a Glue Molecule. *Chem. Commun.* **2012**, *48*, 10633.
- (219) Yeh, Y.-C.; Rana, S.; Mout, R.; Yan, B.; Alfonso, F. S.; Rotello, V. M. Supramolecular Tailoring of Protein-nanoparticle Interactions using Cucurbituril Mediators. *Chem. Commun.* **2014**, *50*, 5565–5568.
- (220) Tian, F.; Cheng, N.; Nouvel, N.; Geng, J.; Scherman, O. A. Site-Selective Immobilization of Colloids on Au Substrates via a NoncovalentSupramolecular "Handcuff". *Langmuir* **2010**, *26*, 5323–5328.
- (221) Tian, F.; Jiao, D.; Biedermann, F.; Scherman, O. a. Orthogonal Switching of a Single Supramolecular Complex. *Nat. Commun.* **2012**, *3*, 1207.
- (222) Hu, C.; Lan, Y.; Tian, F.; West, K. R.; Scherman, O. A. Facile Method for Preparing Surface-Mounted Cucurbit[8]uril-Based Rotaxanes. *Langmuir* **2014**, *30*, 10926–10932.
- (223) Jones, S. T.; Zayed, J. M.; Scherman, O. A. Supramolecular Alignment of Gold Nanorods via Cucurbit[8]uril Ternary Complex Formation. *Nanoscale* **2013**, *5*, 5299–5302.
- (224) Fraire, J. C.; Suelo Occello, V.; Allende, L. G.; Veglia, A. V.; Coronado, E. A. Towards the Design of Highly Stable Small Colloidal SERS Substrates with Supramolecular Host-Guest Interactions for Ultrasensitive Detection. *J. Phys. Chem. C* **2015**, *119*, 8876–8888.
- (225) Wei, L.; Wang, X.; Li, C.; Li, X.; Yin, Y.; Li, G. Colorimetric Assay for Protein Detection Based on Nano-Pumpkin Induced Aggregation of Peptide-Decorated Gold Nanoparticles. *Biosens. Bioelectron.* **2015**, *71*, 348–352.
- (226) Lan, Y.; Wu, Y.; Karas, A.; Scherman, O. A. Photoresponsive Hybrid Raspberry-Like Colloids Based on Cucurbit[8]uril Host-Guest Interactions. *Angew. Chem., Int. Ed.* **2014**, *53*, 2166–2169.
- (227) Alberti, S.; Soler-Illia, G. J. A. A.; Azzaroni, O. Gated Supramolecular Chemistry in Hybrid Mesoporous Silica Nanoarchitectures: Controlled Delivery and Molecular Transport in Response to Chemical, Physical and Biological Stimuli. *Chem. Commun.* **2015**, *51*, 6050–6075.
- (228) Yang, Y. W.; Sun, Y. L.; Song, N. Switchable Host-Guest Systems on Surfaces. *Acc. Chem. Res.* **2014**, *47*, 1950–1960.
- (229) Ambrogio, M. W.; Thomas, C. R.; Zhao, Y.-L. L.; Zink, J. I.; Stoddart, J. F. Mechanized silica Nanoparticles: A New Frontier in Theranostic Nanomedicine. *Acc. Chem. Res.* **2011**, *44*, 903–913.
- (230) Klichko, Y.; Khashab, N. M.; Yang, Y. W.; Angelos, S.; Stoddart, J. F.; Zink, J. I. Improving Pore Exposure in Mesoporous Silica Films for Mechanized Control of the Pores. *Microporous Mesoporous Mater.* **2010**, *132*, 435–441.
- (231) Angelos, S.; Yang, Y.-W. W.; Patel, K.; Stoddart, J. F.; Zink, J. I. pH-Responsive Supramolecular Nanovalves Based on Cucurbit[6]uril Pseudorotaxanes. *Angew. Chem., Int. Ed.* **2008**, *47*, 2222–2226.

- (232) Angelos, S.; Khashab, N. M.; Yang, Y.-W. W.; Trabolsi, A.; Khatib, H. A.; Stoddart, J. F.; Zink, J. I. pH Clock-Operated Mechanized Nanoparticles. *J. Am. Chem. Soc.* **2009**, *131*, 12912–12914.
- (233) Angelos, S.; Yang, Y. W.; Khashab, N. M.; Stoddart, J. F.; Zink, J. I. Dual-Controlled Nanoparticles Exhibiting AND Logic. *J. Am. Chem. Soc.* **2009**, *131*, 11344–11346.
- (234) Thomas, C. R.; Ferris, D. P.; Lee, J. H. H.; Choi, E.; Cho, M. H.; Kim, E. S.; Stoddart, J. F.; Shin, J. S. S.; Cheon, J.; Zink, J. I. Noninvasive Remote-Controlled Release of Drug Molecules in Vitro using Magnetic Actuation of Mechanized Nanoparticles. *J. Am. Chem. Soc.* **2010**, *132*, 10623–10625.
- (235) Liu, J.; Du, X. pH- and Competitor-Driven Nanovalves of Cucurbit[7]uril Pseudorotaxanes Based on Mesoporous Silica Supports for Controlled Release. *J. Mater. Chem.* **2010**, *20*, 3642–3649.
- (236) Liu, J.; Du, X.; Zhang, X. Enzyme-inspired Controlled Release of Cucurbit[7]uril Nanovalves by using Magnetic Mesoporous Silica. *Chem. - Eur. J.* **2011**, *17*, 810–815.
- (237) Ambrogio, M. W.; Pecorelli, T. A.; Patel, K.; Khashab, N. M.; Trabolsi, A.; Khatib, H. A.; Botros, Y. Y.; Zink, J. I.; Stoddart, J. F. Snap-Top Nanocarriers. *Org. Lett.* **2010**, *12*, 3304–3307.
- (238) Sun, Y.-L. L.; Yang, B. J. J.; Zhang, S. X. A. A.; Yang, Y. W. W. Cucurbit[7]uril Pseudorotaxane-Based Photoresponsive Supramolecular Nanovalve. *Chem. - Eur. J.* **2012**, *18*, 9212–9216.
- (239) Hwang, I.; Baek, K.; Jung, M.; Kim, Y.; Park, K. M.; Lee, D.-W.; Selvapalam, N.; Kim, K. Noncovalent Immobilization of Proteins on a Solid Surface by Cucurbit[7]uril-Ferrocenemethylammonium Pair, a Potential Replacement of Biotin-Avidin Pair. *J. Am. Chem. Soc.* **2007**, *129*, 4170–4171.
- (240) Cui, S.-C.; Tachikawa, T.; Fujitsuka, M.; Majima, T. Photoinduced Electron Transfer in a Quantum Dot-Cucurbituril Supramolecular Complex. *J. Phys. Chem. C* **2011**, *115*, 1824–1830.
- (241) Kimoon, K.; Young-Ho, K.; Kyeng-Min, P.; Narayanan, S.; Erumaiappat, R. N. Stationary Phase and Column Using Cucurbituril Bonded Silica Gel, and Separation Method of Taxol Using the Column. Patent 20,080,290,028, 2008.
- (242) Liu, S. M. M.; Xu, L.; Wu, C. T. T.; Feng, Y. Q. Q. Preparation and Characterization of Perhydroxyl-Cucurbit[6]uril Bonded Silica Stationary Phase for Hydrophilic-Interaction Chromatography. *Talanta* **2004**, *64*, 929–934.
- (243) Li, L. S.; Wang, S. W.; Chen, X. Q.; Liu, C.; Xu, L.-L. Studies on Chromatographic Properties of Perhydroxycucurbit[6]uril as a New Type of Gas Chromatographic Column Packing Material. *Chin. J. Chem.* **2008**, *26*, 307–314.
- (244) Nagarajan, E. R.; Oh, D. H.; Selvapalam, N.; Ko, Y. H.; Park, K. M.; Kim, K. Cucurbituril Anchored Silica Gel. *Tetrahedron Lett.* **2006**, *47*, 2073–2075.
- (245) Miyake, J.; Chujo, Y. Molecular Recognizable Cucurbituril/Silica Hybrids. *Chem. Lett.* **2008**, *37*, 312–313.
- (246) Zhang, P.; Qin, S.; Qi, M.; Fu, R. Cucurbit[n]urils as a New Class of Stationary Phases for Gas Chromatographic Separations. *J. Chromatogr. A* **2014**, *1334*, 139–148.
- (247) Ma, L.; Liu, S.-M.; Yao, L.; Xu, L. Preparation and Chromatographic Performance Evaluation of Cucurbit[7]uril Immobilized Silica. *J. Chromatogr. A* **2015**, *1376*, 64–73.
- (248) Zhu, X.; Fan, X.; Ju, G.; Cheng, M.; An, Q.; Nie, J.; Shi, F. A Facile Method to Immobilize Cucurbituril on Surfaces through Photocrosslinking with Azido Groups. *Chem. Commun.* **2013**, *49*, 8093–8095.
- (249) del Pozo, M.; Hernandez, P.; Hernandez, L.; Quintana, C. The Use of Cucurbit[8]uril Host-Guest Interactions in the Development of an Electrochemical Sensor: Characterization and Application to Tryptophan Determination. *J. Mater. Chem.* **2011**, *21*, 13657–13663.
- (250) Kim, J.; Kim, Y.; Baek, K.; Ko, Y. H.; Kim, D.; Kim, K. Direct Force Measurement Between Cucurbit[6]uril and Spermine using Atomic Force Microscopy. *Tetrahedron* **2008**, *64*, 8389–8393.
- (251) Gomez-Casado, A.; Jonkheijm, P.; Huskens, J. Recognition Properties of Cucurbit[7]uril Self-Assembled Monolayers Studied with Force Spectroscopy. *Langmuir* **2011**, *27*, 11508–11513.
- (252) Blanco, E.; Quintana, C.; Hernández, L.; Hernández, P. Atomic Force Microscopy Study of new Sensing Platforms: Cucurbit[n]uril (n = 6, 7) on Gold. *Electroanalysis* **2013**, *25*, 263–268.
- (253) Liu, Y.; Yang, H.; Wang, Z.; Zhang, X. Cucurbit[8]uril-Based Supramolecular Polymers. *Chem. - Asian J.* **2013**, *8*, 1626–1632.
- (254) Dong, S.; Zheng, B.; Wang, F.; Huang, F. Supramolecular Polymers Constructed from Macrocycle-Based Host-Guest Molecular Recognition Motifs. *Acc. Chem. Res.* **2014**, *47*, 1982–1994.
- (255) Hu, J.; Liu, S. Engineering Responsive Polymer Building Blocks with Host-Guest Molecular Recognition for Functional Applications. *Acc. Chem. Res.* **2014**, *47*, 2084–2095.
- (256) Li, H.; Wu, L. Metallo/clusto Hybridized Supramolecular Polymers. *Soft Matter* **2014**, *10*, 9038–9053.
- (257) Yan, X.; Wang, F.; Zheng, B.; Huang, F. Stimuli-Responsive Supramolecular Polymeric Materials. *Chem. Soc. Rev.* **2012**, *41*, 6042–6065.
- (258) Guo, D. S.; Liu, Y. Calixarene-Based Supramolecular Polymerization in Solution. *Chem. Soc. Rev.* **2012**, *41*, 5907–5921.
- (259) Sijbesma, R. P.; Beijer, F. H.; Brunsved, L.; Folmer, B. J. B.; Hirschberg, J.; Lange, R. F. M.; Lowe, J. K. L.; Meijer, E. W. Reversible Polymers Formed from Self-Complementary Monomers using Quadruple Hydrogen Bonding. *Science* **1997**, *278*, 1601–1604.
- (260) Lehn, J. M. Supramolecular Polymer Chemistry- Scope and Perspectives. *Polym. Int.* **2002**, *51*, 825–839.
- (261) Yang, S. K.; Ambade, A. V.; Weck, M. Main-chain Supramolecular Block Copolymers. *Chem. Soc. Rev.* **2011**, *40*, 129–137.
- (262) Brunsved, L.; Folmer, B. J. B.; Meijer, E. W.; Sijbesma, R. P. Supramolecular Polymers. *Chem. Rev.* **2001**, *101*, 4071–4097.
- (263) Wittmer, J. P.; van der Schoot, P.; Milchev, A.; Barrat, J. L. Dynamical Monte Carlo Study of Equilibrium Polymers. II. The Role of Rings. *J. Chem. Phys.* **2000**, *113*, 6992–7005.
- (264) Vermonden, T.; van der Gucht, J.; de Waard, P.; Marcelis, A. T. M.; Besseling, N. A. M.; Sudholter, E. J. R.; Fleer, G. J.; Stuart, M. A. C. Water-Soluble Reversible Coordination Polymers: Chains and Rings. *Macromolecules* **2003**, *36*, 7035–7044.
- (265) Kricheldorf, H. R. The Role of Ring-Ring Equilibria in Thermodynamically Controlled Polycondensations. *Macromol. Symp.* **2003**, *199*, 15–22.
- (266) Fox, J. D.; Rowan, S. J. Supramolecular Polymerizations and Main-Chain Supramolecular Polymers. *Macromolecules* **2009**, *42*, 6823–6835.
- (267) Liu, S. M.; Zavalij, P. Y.; Isaacs, L. Cucurbit[10]uril. *J. Am. Chem. Soc.* **2005**, *127*, 16798–16799.
- (268) Nally, R.; Isaacs, L. Toward Supramolecular Polymers Incorporating Double Cavity Cucurbituril Hosts. *Tetrahedron* **2009**, *65*, 7249–7258.
- (269) Lee, J. W.; Kim, K.; Choi, S.; Ko, Y. H.; Sakamoto, S.; Yamaguchi, K.; Kim, K. Unprecedented Host-Induced Intramolecular Charge-transfer Complex Formation. *Chem. Commun.* **2002**, 2692–2693.
- (270) Ko, Y. H.; Kim, K.; Kim, E.; Kim, K. Exclusive Formation of 1:1 and 2:2 Complexes Between Cucurbit[8]uril and Electron Donor-Acceptor Molecules Induced by Host-Stabilized Charge-Transfer Interactions. *Supramol. Chem.* **2007**, *19*, 287–293.
- (271) Kim, K.; Kim, D.; Lee, J. W.; Ko, Y. H.; Kim, K. Growth of Poly(Pseudorotaxane) on Gold Using Host-Stabilized Charge-Transfer Interaction. *Chem. Commun.* **2004**, 848–849.
- (272) Ko, Y. H.; Kim, K.; Kang, J. K.; Chun, H.; Lee, J. W.; Sakamoto, S.; Yamaguchi, K.; Fettinger, J. C.; Kim, K. Designed Self-Assembly of Molecular Necklaces using Host-Stabilized Charge-Transfer Interactions. *J. Am. Chem. Soc.* **2004**, *126*, 1932–1933.
- (273) Liu, Y.; Yu, Y.; Gao, J.; Wang, Z.; Zhang, X. Water-Soluble Supramolecular Polymerization Driven by Multiple Host-Stabilized Charge-Transfer Interactions. *Angew. Chem., Int. Ed.* **2010**, *49*, 6576–6579.

- (274) Wang, L. X.; Bloomfilde, V. A. Small-Angle X-Ray Scattering of Semidilute Rodlike DNA Solutions—Polyelectrolyte Behavior. *Macromolecules* **1991**, *24*, 5791–5795.
- (275) Muroga, Y.; Sakuragi, I.; Noda, I.; Nagawasa, M. Effect of Beta-Substitution on Chain Flexibility. *Macromolecules* **1984**, *17*, 1844–1847.
- (276) del Barrio, J.; Horton, P. N.; Lairez, D.; Lloyd, G. O.; Toprakcioglu, C.; Scherman, O. A. Photocontrol over Cucurbit[8]uril Complexes: Stoichiometry and Supramolecular Polymers. *J. Am. Chem. Soc.* **2013**, *135*, 11760–11763.
- (277) Liu, Y.; Liu, K.; Wang, Z.; Zhang, X. Host-Enhanced pi-pi Interaction for Water-Soluble Supramolecular Polymerization. *Chem. - Eur. J.* **2011**, *17*, 9930–9935.
- (278) Liu, Y.; Fang, R.; Tan, X.; Wang, Z.; Zhang, X. Supramolecular Polymerization at Low Monomer Concentrations: Enhancing Intermolecular Interactions and Suppressing Cyclization by Rational Molecular Design. *Chem. - Eur. J.* **2012**, *18*, 15650–15654.
- (279) Tan, X.; Yang, L.; Liu, Y.; Huang, Z.; Yang, H.; Wang, Z.; Zhang, X. Water-Soluble Supramolecular Polymers Fabricated through Specific Interactions Between Cucurbit[8]uril and a Tripeptide of Phe-Gly-Gly. *Polym. Chem.* **2013**, *4*, 5378–5381.
- (280) Yang, H.; Liu, Y.; Liu, K.; Yang, L.; Wang, Z.; Zhang, X. Rational Adjustment of Multicolor Emissions by Cucurbiturils-Based Host-Guest Chemistry and Photochemistry. *Langmuir* **2013**, *29*, 12909–12914.
- (281) Ramaekers, M.; Wijnands, S. P. W.; van Dongen, J. L. J.; Brunsved, L.; Dankers, P. Y. W. Cucurbit[8]uril Templatized Supramolecular Ring Structure Formation and Protein Assembly Modulation. *Chem. Commun.* **2015**, *51*, 3147–3150.
- (282) Nguyen, H. D.; Dang, D. T.; van Dongen, J. L. J.; Brunsved, L. Protein Dimerization Induced by Supramolecular Interactions with Cucurbit[8]uril. *Angew. Chem., Int. Ed.* **2010**, *49*, 895–898.
- (283) Fang, R.; Liu, Y.; Wang, Z.; Zhang, X. Water-Soluble Supramolecular Hyperbranched Polymers Based on host-Enhanced pi-pi Interaction. *Polym. Chem.* **2013**, *4*, 900–903.
- (284) Yang, H.; Ma, Z.; Wang, Z.; Zhang, X. Fabricating Covalently Attached Hyperbranched Polymers by Combining Photochemistry with Supramolecular Polymerization. *Polym. Chem.* **2014**, *5*, 1471–1476.
- (285) Liu, Y.; Huang, Z.; Liu, K.; Kelgtermans, H.; Dehaen, W.; Wang, Z.; Zhang, X. Porphyrin-Containing Hyperbranched Supramolecular Polymers: Enhancing O-1(2)-Generation Efficiency by Supramolecular Polymerization. *Polym. Chem.* **2014**, *5*, 53–56.
- (286) Zhang, L.; Zhou, T.-Y.; Tian, J.; Wang, H.; Zhang, D.-W.; Zhao, X.; Liu, Y.; Li, Z.-T. A Two-dimensional Single-Layer Supramolecular Organic Framework that is Driven by Viologen Radical Cation Dimerization and Further Promoted by Cucurbit[8]uril. *Polym. Chem.* **2014**, *5*, 4715–4721.
- (287) Zhang, K. D.; Tian, J.; Hanifi, D.; Zhang, Y.; Sue, A. C. H.; Zhou, T. Y.; Zhang, L.; Zhao, X.; Liu, Y.; Li, Z. T. Toward a Single-Layer Two-Dimensional Honeycomb Supramolecular Organic Framework in Water. *J. Am. Chem. Soc.* **2013**, *135*, 17913–17918.
- (288) Moon, K.; Grindstaff, J.; Sobransingh, D.; Kaifer, A. E. Cucurbit[8]uril-mediated Redox-Controlled Self-Assembly of Viologen-containing Dendrimers. *Angew. Chem., Int. Ed.* **2004**, *43*, 5496–5499.
- (289) Ziganshina, A. Y.; Ko, Y. H.; Jeon, W. S.; Kim, K. Stable [pi]-Dimer of a Tetraphiafulvalene Cation Radical Encapsulated in the Cavity of Cucurbit[8]uril. *Chem. Commun.* **2004**, 806–807.
- (290) Spanggaard, H.; Prehn, J.; Nielsen, M. B.; Levillain, E.; Allain, M.; Becher, J. Multiple-bridged Bis-tetrathiafulvalenes: New Synthetic Protocols and Spectroelectrochemical Investigations. *J. Am. Chem. Soc.* **2000**, *122*, 9486–9494.
- (291) Coskun, A.; Spruell, J. M.; Barin, G.; Fahrenbach, A. C.; Forgan, R. S.; Colvin, M. T.; Carmieli, R.; Benitez, D.; Tkatchouk, E.; Friedman, D. C.; Sarjeant, A. A.; Wasielewski, M. R.; Goddard, W. A., III; Stoddart, J. F. Mechanically Stabilized Tetraphiafulvalene Radical Dimers. *J. Am. Chem. Soc.* **2011**, *133*, 4538–4547.
- (292) Frasconi, M.; Kikuchi, T.; Cao, D.; Wu, Y.; Liu, W. G.; Dyer, S. M.; Barin, G.; Sarjeant, A. A.; Stern, C. L.; Carmieli, R.; Wang, C.; Wasielewski, M. R.; Goddard, W. A., III; Stoddart, J. F. Mechanical Bonds and Topological Effects in Radical Dimer Stabilization. *J. Am. Chem. Soc.* **2014**, *136*, 11011–11026.
- (293) Tian, J.; Ding, Y.-D.; Zhou, T. Y.; Zhang, K. D.; Zhao, X.; Wang, H.; Zhang, D. W.; Liu, Y.; Li, Z. T. Self-Assembly of Three-Dimensional Supramolecular Polymers through Cooperative Tetraphiafulvalene Radical Cation Dimerization. *Chem. - Eur. J.* **2014**, *20*, 575–584.
- (294) Chen, L.; Zhang, S. C.; Wang, H.; Zhou, Y. M.; Li, Z. T.; Zhang, D. W. Three-Dimensional Supramolecular Polymers Driven by Rigid Tetrahedral Building Blocks Through Tetraphiafulvalene Radical Cation Dimerization. *Tetrahedron* **2014**, *70*, 4778–4783.
- (295) Li, S. L.; Xiao, T.; Lin, C.; Wang, L. Advanced Supramolecular Polymers Constructed by Orthogonal Self-assembly. *Chem. Soc. Rev.* **2012**, *41*, 5950–5968.
- (296) Wei, P.; Yan, X.; Huang, F. Supramolecular Polymers Constructed by Orthogonal Self-Assembly Based on Host-Guest and Metal-Ligand Interactions. *Chem. Soc. Rev.* **2015**, *44*, 815–832.
- (297) Kim, K. Mechanically Interlocked Molecules Incorporating Cucurbituril and their Supramolecular Assemblies. *Chem. Soc. Rev.* **2002**, *31*, 96–107.
- (298) Robins, M. J.; Wnuk, S. F.; Hernández-Thirring, A. E.; Samano, M. C. Nucleic Acid Related Compounds. 91. Biomimetic Reactions Are in Harmony with Loss of 2'-Substituents as Free Radicals (Not Anions) during Mechanism-Based Inactivation of Ribonuclease Reductases. Differential Interactions of Azide, Halogen, and Alkylthio. *J. Am. Chem. Soc.* **1996**, *118*, 11341–11348.
- (299) Whang, D.; Kim, K. Polycatenated Two-Dimensional Polyrotaxane Net. *J. Am. Chem. Soc.* **1997**, *119*, 451–452.
- (300) Park, K. M.; Lee, E.; Roh, S. G.; Kim, J.; Kim, K. A Double-Chained Polyrotaxane: Cucurbituril ‘Beads’ Threaded onto a Double-chained One-Dimensional Coordination Polymer. *Bull. Korean Chem. Soc.* **2004**, *25*, 1711–1713.
- (301) Liu, Y.; Huang, Z.; Tan, X.; Wang, Z.; Zhang, X. Cucurbit[8]uril-Based Supramolecular Polymers: Promoting Supramolecular Polymerization by Metal-Coordination. *Chem. Commun.* **2013**, *49*, 5766–5768.
- (302) Joseph, R.; Nkrumah, A.; Clark, R. J.; Masson, E. Stabilization of Cucurbituril/Guest Assemblies via Long-Range Coulombic and CH-O Interactions. *J. Am. Chem. Soc.* **2014**, *136*, 6602–6607.
- (303) Patrick, C. R.; Prosser, G. S. A Molecular Complex of Benzene and Hexafluorobenzene. *Nature* **1960**, *187*, 1021.
- (304) Coates, G. W.; Dunn, A. R.; Henling, L. M.; Dougherty, D. A.; Grubbs, R. H. Phenyl-Perfluorophenyl Stacking Interactions: A New Strategy for Supermolecule Construction. *Angew. Chem., Int. Ed. Engl.* **1997**, *36*, 248–251.
- (305) Yang, H.; Bai, Y.; Yu, B.; Wang, Z.; Zhang, X. Supramolecular Polymers Bearing Disulfide Bonds. *Polym. Chem.* **2014**, *5*, 6439–6443.
- (306) Song, Q.; Li, F.; Tan, X.; Yang, L.; Wang, Z.; Zhang, X. Supramolecular Polymerization of Supramonomers: a way for Fabricating Supramolecular Polymers. *Polym. Chem.* **2014**, *5*, 5895–5899.
- (307) Tan, X.; Yang, L.; Huang, Z.; Yu, Y.; Wang, Z.; Zhang, X. Amphiphilic Diselenide-Containing Supramolecular Polymers. *Polym. Chem.* **2015**, *6*, 681–685.
- (308) Hou, C.; Li, J.; Zhao, L.; Zhang, W.; Luo, Q.; Dong, Z.; Xu, J.; Liu, J. Construction of Protein Nanowires through Cucurbit[8]uril-based Highly Specific Host-Guest Interactions: An Approach to the Assembly of Functional Proteins. *Angew. Chem., Int. Ed.* **2013**, *52*, 5590–5593.
- (309) Huang, Z.; Yang, L.; Liu, Y.; Wang, Z.; Scherman, O. A.; Zhang, X. Supramolecular Polymerization Promoted and Controlled through Self-Sorting. *Angew. Chem., Int. Ed.* **2014**, *53*, 5351–5355.
- (310) Rauwald, U.; Scherman, O. A. Supramolecular Block Copolymers with Cucurbit[8]uril in Water. *Angew. Chem., Int. Ed.* **2008**, *47*, 3950–3953.

- (311) Chen, C. J.; Li, D. D.; Wang, H. B.; Zhao, J.; Ji, J. Fabrication of Dual-Responsive Micelles Based on the Supramolecular Interaction of Cucurbit[8]uril. *Polym. Chem.* **2013**, *4*, 242–245.
- (312) Ji, Z.; Liu, J.; Chen, G.; Jiang, M. A Polymeric Chain Extension Driven by HSCT Interaction. *Polym. Chem.* **2014**, *5*, 2709–2714.
- (313) Geng, J.; Jiao, D.; Rauwald, U.; Scherman, O. A. An Aqueous Supramolecular Side-Chain Polymer Designed for Molecular Loading. *Aust. J. Chem.* **2010**, *63*, 627–630.
- (314) Geng, J.; Biedermann, F.; Zayed, J. M.; Tian, F.; Scherman, O. A. Supramolecular Glycopolymers in Water: A Reversible Route Toward Multivalent Carbohydrate-Lectin Conjugates Using Cucurbit[8]uril. *Macromolecules* **2011**, *44*, 4276–4281.
- (315) Loh, X. J.; del Barrio, J.; Toh, P. P. C.; Lee, T.-C.; Jiao, D.; Rauwald, U.; Appel, E. A.; Scherman, O. A. Triply Triggered Doxorubicin Release From Supramolecular Nanocontainers. *Biomacromolecules* **2012**, *13*, 84–91.
- (316) Zhao, J.; Chen, C.; Li, D.; Liu, X.; Wang, H.; Jin, Q.; Ji, J. Biocompatible and Biodegradable Supramolecular Assemblies formed with Cucurbit[8]uril as a Smart Platform for Reduction-Triggered Release of Doxorubicin. *Polym. Chem.* **2014**, *5*, 1843–1847.
- (317) Jiao, D.; Geng, J.; Loh, X. J.; Das, D.; Lee, T. C.; Scherman, O. A. Supramolecular Peptide Amphiphile Vesicles through Host-Guest Complexation. *Angew. Chem., Int. Ed.* **2012**, *51*, 9633–9637.
- (318) Loh, X. J.; del Barrio, J.; Lee, T. C.; Scherman, O. A. Supramolecular Polymeric Peptide Amphiphile Vesicles for the Encapsulation of Basic Fibroblast Growth Factor. *Chem. Commun.* **2014**, *50*, 3033–3035.
- (319) Mondal, J. H.; Ahmed, S.; Das, D. Physicochemical Analysis of Mixed Micelles of a Viologen Surfactant: Extended to Water-in-Oil (w/o) Microemulsion and Cucurbit[8]uril-Assisted Vesicle Formation. *Langmuir* **2014**, *30*, 8290–8299.
- (320) Mondal, J. H.; Ghosh, T.; Ahmed, S.; Das, D. Dual Self-Sorting by Cucurbit[8]uril To Transform a Mixed Micelle to Vesicle. *Langmuir* **2014**, *30*, 11528–11534.
- (321) Appel, E. A.; Biedermann, F.; Rauwald, U.; Jones, S. T.; Zayed, J. M.; Scherman, O. A. Supramolecular Cross-Linked Networks via Host-Guest Complexation with Cucurbit[8]uril. *J. Am. Chem. Soc.* **2010**, *132*, 14251–14260.
- (322) Appel, E. A.; Loh, X. J.; Jones, S. T.; Biedermann, F.; Dreiss, C. A.; Scherman, O. A. Ultrahigh-Water-Content Supramolecular Hydrogels Exhibiting Multistimuli Responsiveness. *J. Am. Chem. Soc.* **2012**, *134*, 11767–73.
- (323) Appel, E. A.; Loh, X. J.; Jones, S. T.; Dreiss, C. A.; Scherman, O. A. Sustained Release of Proteins from High Water Content Supramolecular Polymer Hydrogels. *Biomaterials* **2012**, *33*, 4646–4652.
- (324) Walsh, Z.; Janeček, E.-R.; Hodgkinson, J. T.; Sedlmair, J.; Koutsoubas, A.; Spring, D. R.; Welch, M.; Hirschmugl, C. J.; Toprakcioglu, C.; Nitschke, J. R.; Jones, M.; Scherman, O. A. Multifunctional Supramolecular Polymer Networks as Next-generation Consolidants for Archaeological wood Conservation. *Proc. Natl. Acad. Sci. U. S. A.* **2014**, *111*, 17743–17748.
- (325) Rowland, M. J.; Appel, E. A.; Coulston, R. J.; Scherman, O. A. Dynamically Crosslinked Materials via Recognition of Amino Acids by Cucurbit[8]uril. *J. Mater. Chem. B* **2013**, *1*, 2904–2910.
- (326) Appel, E. A.; Dyson, J.; del Barrio, J.; Walsh, Z.; Scherman, O. A. Formation of Single-Chain Polymer Nanoparticles in Water through Host-Guest Interactions. *Angew. Chem., Int. Ed.* **2012**, *51*, 4185–4189.
- (327) Lin, Y.; Li, L.; Li, G. A New Supramolecular Gel via Host-Guest Complexation with Cucurbit[8]uril and N-(4-diethylaminobenzyl)chitosan. *Carbohydr. Polym.* **2013**, *92*, 429–434.
- (328) Appel, E. A.; Forster, R. A.; Koutsoubas, A.; Toprakcioglu, C.; Scherman, O. A. Activation Energies Control the Macroscopic Properties of Physically Cross-Linked Materials. *Angew. Chem., Int. Ed.* **2014**, *53*, 10038–10043.
- (329) Appel, E. A.; Forster, R. A.; Rowland, M. J.; Scherman, O. A. The Control of Cargo Release from Physically Crosslinked Hydrogels by Crosslink Dynamics. *Biomaterials* **2014**, *35*, 9897–9903.
- (330) McKee, J. R.; Appel, E. A.; Seitsonen, J.; Kontturi, E.; Scherman, O. A.; Ikkala, O. Healable, Stable and Stiff Hydrogels: Combining Conflicting Properties Using Dynamic and Selective Three-Component Recognition with Reinforcing Cellulose Nanorods. *Adv. Funct. Mater.* **2014**, *24*, 2706–2713.
- (331) Janeček, E.-R.; McKee, J. R.; Tan, C. S. Y.; Nykänen, A.; Kettunen, M.; Laine, J.; Ikkala, O.; Scherman, O. A. Hybrid Supramolecular and Colloidal Hydrogels that Bridge Multiple Length Scales. *Angew. Chem., Int. Ed.* **2015**, *54*, 5383–5388.
- (332) Li, C.; Rowland, M. J.; Shao, Y.; Cao, T.; Chen, C.; Jia, H.; Zhou, X.; Yang, Z.; Scherman, O. A.; Liu, D. Responsive Double Network Hydrogels of Interpenetrating DNA and CB[8] Host-Guest Supramolecular Systems. *Adv. Mater.* **2015**, *27*, 3298–3304.
- (333) Park, K. M.; Yang, J. A.; Jung, H.; Yeom, J.; Park, J. S.; Park, K. H.; Hoffman, A. S.; Hahn, S. K.; Kim, K. In Situ Supramolecular Assembly and Modular Modification of Hyaluronic Acid Hydrogels for 3D Cellular Engineering. *ACS Nano* **2012**, *6*, 2960–2968.
- (334) Jung, H.; Park, J. S.; Yeom, J.; Selvapalam, N.; Park, K. M.; Oh, K.; Yang, J. A.; Park, K. H.; Hahn, S. K.; Kim, K. 3D Tissue Engineered Supramolecular Hydrogels for Controlled Chondrogenesis of Human Mesenchymal Stem Cells. *Biomacromolecules* **2014**, *15*, 707–714.
- (335) Coulston, R. J.; Jones, S. T.; Lee, T.-C.; Appel, E. A.; Scherman, O. A. Supramolecular Gold Nanoparticle-Polymer Composites formed in Water. *Chem. Commun.* **2011**, *47*, 164–166.
- (336) Zhang, J.; Coulston, R. J.; Jones, S. T.; Geng, J.; Scherman, O. A.; Abell, C. One-Step Fabrication of Supramolecular Microcapsules from Microfluidic Droplets. *Science* **2012**, *335*, 690–694.
- (337) Stephenson, G.; Parker, R. M.; Lan, Y.; Yu, Z.; Scherman, O. A.; Abell, C. Supramolecular Colloidosomes: Fabrication, Characterisation and Triggered Release of Cargo. *Chem. Commun.* **2014**, *50*, 7048–7051.
- (338) Zheng, Y.; Yu, Z.; Parker, R. M.; Wu, Y.; Abell, C.; Scherman, O. A. Interfacial Assembly of Dendritic Microcapsules with Host-guest Chemistry. *Nat. Commun.* **2014**, *5*, 5772.
- (339) Mock, W. L.; Irra, T. a.; Wepsic, J. P.; Adhya, M. Catalysis by Cucurbituril. The Significance of Bound-Substrate Destabilization for Induced Triazole Formation. *J. Org. Chem.* **1989**, *54*, 5302–5308.
- (340) Klöck, C.; Dsouza, R. N.; Nau, W. M. Cucurbituril-Mediated Supramolecular. *Org. Lett.* **2009**, *11*, 2595–2598.
- (341) Hang, C.; Fang-fang, Z.; Jian-xin, Z.; Xi, Z.; Zhu, T.; Sai-feng, X.; Qian-jiang, Z. Rapid Transformation of Benzylic Alcohols to Aldehyde in the Presence of Cucurbit[8]uril. *Catal. Commun.* **2009**, *11*, 167–170.
- (342) Lu, X.; Masson, E. Silver-Promoted Desilylation Catalyzed by Ortho- and Allosteric Cucurbiturils. *Org. Lett.* **2010**, *12*, 2310–2313.
- (343) Jon, S. Y.; Ko, Y. H.; Park, S. H.; Kim, H. J.; Kim, K. A Facile, Stereoselective [2 + 2] Photoreaction Mediated by Cucurbit[8]uril. *Chem. Commun.* **2001**, 1938–1939.
- (344) Berbeci, L. S.; Wang, W.; Kaifer, A. E. Drastically Decreased Reactivity of Thiols and Disulfides Complexed by Cucurbit[6]uril. *Org. Lett.* **2008**, *10*, 3721–3724.
- (345) Tuncel, D.; Steinke, J. H. G. Catalytically Self-Threading Polyrotaxanes. *Chem. Commun.* **1999**, 1509–1510.
- (346) Tuncel, D.; Steinke, J. H. G. Mainchain Pseudopolyrotaxanes via Post-THREADING with Cucurbituril. *Chem. Commun.* **2001**, 253–254.
- (347) Tuncel, D.; Steinke, J. H. G. The Synthesis of [2], [3] and [4] Rotaxanes and Semirotaxanes. *Chem. Commun.* **2002**, 496–497.
- (348) Tuncel, D.; Katterle, M. PH-Triggered Dethreading-Rethreading and Switching of Cucurbit[6]uril on Bistable [3]pseudorotaxanes and [3]rotaxanes. *Chem. - Eur. J.* **2008**, *14*, 4110–4116.
- (349) Tuncel, D.; Ünal, O.; Artar, M. Supramolecular Assemblies Constructed by Cucurbituril-Catalyzed Click Reaction. *Isr. J. Chem.* **2011**, *51*, 525–532.
- (350) Basilio, N.; García-Río, L.; Moreira, J. A.; Pességo, M. Supramolecular Catalysis by Cucurbit[7]uril and Cyclodextrins: Similarity and Differences. *J. Org. Chem.* **2010**, *75*, 848–855.
- (351) Wang, Y. H.; Cong, H.; Zhao, F. F.; Xue, S. F.; Tao, Z.; Zhu, Q. J.; Wei, G. Selective Catalysis for the Oxidation of Alcohols to

- Aldehydes in the Presence of Cucurbit[8]uril. *Catal. Commun.* **2011**, *12*, 1127–1130.
- (352) Pattabiraman, M.; Natarajan, A.; Kaliappan, R.; Mague, J. T.; Ramamurthy, V. Template Directed Photodimerization of Trans-1,2-bis(n-pyridyl)ethylenes and Stilbazoles in Water. *Chem. Commun.* **2005**, 4542–4544.
- (353) Maddipatla, M. V. S. N.; Kaanumalle, L. S.; Natarajan, A.; Pattabiraman, M.; Ramamurthy, V. Preorientation of Olefins toward a Single Photodimer: Cucurbituril-Mediated Photodimerization of Protonated Azastilbenes in Water. *Langmuir* **2007**, *23*, 7545–7554.
- (354) Pemberton, B. C.; Barooah, N.; Srivatsava, D. K.; Sivaguru, J. Supramolecular Photocatalysis by Confinement-Photodimerization of Coumarins within Cucurbit[8]urils. *Chem. Commun.* **2010**, *46*, 225–227.
- (355) Pattabiraman, M.; Kaanumalle, L. S.; Natarajan, A.; Ramamurthy, V. Regioselective Photodimerization of Cinnamic Acids in Water: Temptation with Cucurbiturils. *Langmuir* **2006**, *22*, 7605–7609.
- (356) Chen, B.; Cheng, S. F.; Liao, G. H.; Li, X.-W.; Zhang, L. P.; Tung, C. H.; Wu, L. Z. Efficient and Selective Photodimerization of 2-Naphthalenecarbonitrile Mediated by Cucurbit[8]uril in an Aqueous Solution. *Photochem. Photobiol. Sci.* **2011**, *10*, 1441–1444.
- (357) Smitka, J.; Lemos, A.; Porel, M.; Jockusch, S.; Belderrain, T. R.; Tesařová, E.; Da Silva, J. P. Phototransformation of Benzimidazole and Thiabendazole inside Cucurbit[8]uril. *Photochem. Photobiol. Sci.* **2014**, *13*, 310–5.
- (358) De Lima, S. M.; Gómez, J. A.; Barros, V. P.; Vertuan, G. D. S.; Assis, M. D. D.; Graeff, C. F. D. O.; Demets, G. J. F. A New Oxovanadium(IV)-Cucurbit[6]uril Complex: Properties and Potential for Confined Heterogeneous Catalytic Oxidation Reactions. *Polyhedron* **2010**, *29*, 3008–3013.
- (359) Koner, A. L.; Márquez, C.; Dickman, M. H.; Nau, W. M. Transition-Metal-Promoted Chemoselective Photoreactions at the Cucurbituril Rim. *Angew. Chem., Int. Ed.* **2011**, *50*, 545–548.
- (360) Masson, E.; Shaker, Y. M.; Masson, J. P.; Kordesch, M. E.; Yuwono, C. "Supramolecular Circuitry": Three Chemiluminescent, Cucurbit[7]uril-Controlled On/Off Switches. *Org. Lett.* **2011**, *13*, 3872–3875.
- (361) Miskolczy, Z.; Megyesi, M.; Tárkányi, G.; Mizsei, R.; Biczók, L. Inclusion Complex Formation of Sanguinarine Alkaloid with Cucurbit[7]uril: Inhibition of Nucleophilic Attack and Photooxidation. *Org. Biomol. Chem.* **2011**, *9*, 1061–1070.
- (362) Cong, H.; Li, C.-R.; Xue, S.-F.; Tao, Z.; Zhu, Q.-J.; Wei, G. Cucurbituril-Resisted Acylation of the Anti-Tuberculosis Drug Isoniazid via a Supramolecular Strategy. *Org. Biomol. Chem.* **2011**, *9*, 1041–1046.
- (363) Ghosh, S.; Isaacs, L. Biological Catalysis Regulated by Cucurbit[7]uril Molecular Containers. *J. Am. Chem. Soc.* **2010**, *132*, 4445–4454.
- (364) Buschmann, H. J.; Mutihac, L.; Mutihac, R. C.; Schollmeyer, E. Complexation Behavior of Cucurbit[6]uril with Short Polypeptides. *Thermochim. Acta* **2005**, *430*, 79–82.
- (365) Reczek, J. J.; Kennedy, A. A.; Halbert, B. T.; Urbach, A. R. Multivalent Recognition of Peptides by Modular Self-Assembled Receptors. *J. Am. Chem. Soc.* **2009**, *131*, 2408–2415.
- (366) Logsdon, L. A.; Schardon, C. L.; Ramalingam, V.; Kwee, S. K.; Urbach, A. R. Nanomolar Binding of Peptides Containing Non-canonical Amino Acids by a Synthetic Receptor. *J. Am. Chem. Soc.* **2011**, *133*, 17087–17092.
- (367) Logsdon, L. A.; Urbach, A. R. Sequence-Specific Inhibition of a Nonspecific Protease. *J. Am. Chem. Soc.* **2013**, *135*, 11414–11416.
- (368) Ghale, G.; Ramalingam, V.; Urbach, A. R.; Nau, W. M. Determining Protease Substrate Selectivity and Inhibition by Label-Free Supramolecular Tandem Enzyme Assays. *J. Am. Chem. Soc.* **2011**, *133*, 7528–7535.
- (369) Dang, D. T.; Bosmans, R. P. G.; Moitzi, C.; Voets, I. K.; Brunsved, L. Solution Structure of a Cucurbit[8]uril Induced Compact Supramolecular Protein Dimer. *Org. Biomol. Chem.* **2014**, *12*, 9341–9344.
- (370) Dang, D. T.; Schill, J.; Brunsved, L. Cucurbit[8]uril-Mediated Protein Homotetramerization. *Chem. Sci.* **2012**, *3*, 2679–2684.
- (371) Dang, D. T.; Nguyen, H. D.; Merkx, M.; Brunsved, L. Supramolecular Control of Enzyme Activity through Cucurbit[8]uril-Mediated Dimerization. *Angew. Chem.* **2013**, *125*, 2987–2991.
- (372) Lee, H. H.; Choi, T. S.; Lee, S. J. C.; Lee, J. W.; Park, J.; Ko, Y. H.; Kim, W. J.; Kim, K.; Kim, H. I. Supramolecular Inhibition of Amyloid Fibrillation by Cucurbit[7]uril. *Angew. Chem.* **2014**, *126*, 7591–7595.
- (373) Heo, S. W.; Choi, T. S.; Park, K. M.; Ko, Y. H.; Kim, S. B.; Kim, K.; Kim, H. I. Host-Guest Chemistry in the Gas Phase: Selected Fragmentations of CB[6]-Peptide Complexes at Lysine Residues and Its Utility to Probe the Structures of Small Proteins. *Anal. Chem.* **2011**, *83*, 7916–7923.
- (374) Lee, J. W.; Heo, S. W.; Lee, S. J. C.; Ko, J. Y.; Kim, H. I. H.; Kim, H. I. H. Probing Conformational Changes of Ubiquitin by Host-Guest Chemistry using Electrospray Ionization Mass Spectrometry. *J. Am. Soc. Mass Spectrom.* **2013**, *24*, 21–29.
- (375) Parente Carvalho, C.; Norouzy, A.; Ribeiro, V.; Nau, W. M.; Pischel, U. Cucurbiturils as Supramolecular Inhibitors of DNA Restriction by Type II Endonucleases. *Org. Biomol. Chem.* **2015**, *13*, 2866–2869.
- (376) Rekharsky, M. V.; Mori, T.; Yang, C.; Ko, Y. H.; Selvapalam, N.; Kim, H.; Sobrangsingh, D.; Kaifer, A. E.; Liu, S.; Isaacs, L.; Chen, W.; Moghaddam, S.; Gilson, M. K.; Kim, K.; Inoue, Y. A Synthetic Host-Guest System Achieves Avidin-Biotin Affinity by Overcoming Enthalpy-Entropy Compensation. *Proc. Natl. Acad. Sci. U. S. A.* **2007**, *104*, 20737–20742.
- (377) Mock, W. L.; Shih, N. Y. Structure and Selectivity in Host-Guest Complexes of Cucurbituril. *J. Org. Chem.* **1986**, *51*, 4440–4446.
- (378) Zhang, H.; Ferrell, T. A.; Asplund, M. C.; Dearden, D. V. Molecular Beads on a Charged Molecular String: Alpha, Omega-Alkyldiammonium Complexes of Cucurbit[6]uril in the Gas Phase. *Int. J. Mass Spectrom.* **2007**, *265*, 187–196.
- (379) Rekharsky, M. V.; Yamamura, H.; Mori, T.; Sato, A.; Shiro, M.; Lindeman, S. V.; Rathore, R.; Shiba, K.; Ko, Y. H.; Selvapalam, N.; Kim, K.; Inoue, Y. Supramolecular Complexation of N-alkyl- and N,N'-Dialkylpiperazines with Cucurbit[6]uril in Aqueous Solution and in the Solid State. *Chem. - Eur. J.* **2009**, *15*, 1957–1965.
- (380) Occello, V. N. S.; Rossi, R. H. D.; Veglia, A. V.; Suello Occello, V. N.; de Rossi, R. H.; Veglia, A. V. Complexation (Cucurbit[6]uril-Pyrene): Thermodynamic and Spectroscopic Properties. *J. Lumin.* **2015**, *158*, 435–440.
- (381) Choi, T. S.; Ko, J. Y.; Heo, S. W.; Ko, Y. H.; Kim, K.; Kim, H. I. Unusual Complex Formation and Chemical Reaction of Haloacetate Anion on the Exterior Surface of Sucurbit[6]uril in the Gas Phase. *J. Am. Soc. Mass Spectrom.* **2012**, *23*, 1786–1793.
- (382) Ong, W.; Kaifer, A. E. Unusual Electrochemical Properties of the Inclusion Complexes of Ferrocenium and Cobaltocenium with Cucurbit[7]uril. *Organometallics* **2003**, *22*, 4181–4183.
- (383) Jeon, W. S.; Moon, K.; Park, S. H.; Chun, H.; Ko, Y. H.; Lee, J. Y.; Lee, E. S.; Samal, S.; Selvapalam, N.; Rekharsky, M. V.; Sindelar, V.; Sobrangsingh, D.; Inoue, Y.; Kaifer, A. E.; Kim, K. Complexation of Ferrocene Derivatives by the Cucurbit[7]uril Host: A Comparative Study of the Cucurbituril and Cyclodextrin Host Families. *J. Am. Chem. Soc.* **2005**, *127*, 12984–12989.
- (384) Moghaddam, S.; Yang, C.; Rekharsky, M.; Ko, Y. H.; Kim, K.; Inoue, Y.; Gilson, M. K. New Ultrahigh Affinity Host-Guest Complexes of Cucurbit[7]uril with Bicyclo[2.2.2]octane and Adamantane Guests: Thermodynamic Analysis and Evaluation of M2 Affinity Calculations. *J. Am. Chem. Soc.* **2011**, *133*, 3570–3581.
- (385) Cao, L.; Šekutor, M.; Zavalij, P. Y.; Mlinarić-Majerski, K.; Glaser, R.; Isaacs, L. Cucurbit[7]uril Guest Pair with an Attomolar Dissociation Constant. *Angew. Chem., Int. Ed.* **2014**, *53*, 988–993.
- (386) Wang, R.; Yuan, L.; Macartney, D. H. Stabilization of the (E)-1-Ferrocenyl-2-(1-methyl-4-pyridinium)ethylene Cation by Inclusion in Cucurbit[7]uril. *Organometallics* **2006**, *25*, 1820–1823.

- (387) Ma, D.; Zavalij, P. Y.; Isaacs, L. Acyclic Cucurbit[n]uril Congeners Are High Affinity Hosts. *J. Org. Chem.* **2010**, *75*, 4786–4795.
- (388) Ong, W.; Kaifer, A. E. Salt Effects on the Apparent Stability of the Cucurbit[7]uril-Methyl Viologen Inclusion Complex. *J. Org. Chem.* **2004**, *69*, 1383–1385.
- (389) Ling, Y.; Mague, J. T.; Kaifer, A. E. Inclusion Complexation of Diquat and Paraquat by the Hosts Cucurbit[7]uril and Cucurbit[8]uril. *Chem. - Eur. J.* **2007**, *13*, 7908–7914.
- (390) Sindelar, V.; Cejas, M. A.; Raymo, F. M.; Kaifer, A. E. Tight Inclusion Complexation of 2,7-Dimethyldiazapyrenium in Cucurbit[7]uril. *New J. Chem.* **2005**, *29*, 280–282.
- (391) Wintgens, V.; Biczók, L.; Miskolczy, Z. Thermodynamics of Inclusion Complex Formation Between 1-alkyl-3-methylimidazolium Ionic Liquids and Cucurbit[7]uril. *Supramol. Chem.* **2010**, *22*, 612–618.
- (392) Miskolczy, Z.; Biczók, L.; Megyesi, M.; Jablonkai, I. Inclusion Complex Formation of Ionic Liquids and Other Cationic Organic Compounds with Cucurbit[7]uril Studied by 4',6-Diamidino-2-phenylindole Fluorescent Probe. *J. Phys. Chem. B* **2009**, *113*, 1645–1651.
- (393) Megyesi, M.; Biczók, L.; Jablonkai, I. Highly Sensitive Fluorescence Response to Inclusion Complex Formation of Berberine Alkaloid with Cucurbit[7]uril. *J. Phys. Chem. C* **2008**, *112*, 3410–3416.
- (394) Shaikh, M.; Mohanty, J.; Bhasikuttan, A. C.; Uzunova, V. D.; Nau, W. M.; Pal, H. Salt-Induced Guest Relocation from a Macro cyclic Cavity into a Biomolecular Pocket: Interplay between Cucurbit[7]uril and Albumin. *Chem. Commun.* **2008**, 3681–3683.
- (395) Liu, Y.; Li, C.-J.; Guo, D.-S.; Pan, Z.-H.; Li, Z. A Comparative Study of Complexation of β -Cyclodextrin, Calix[4]arenesulfonate and Cucurbit[7]uril with Dye Guests: Fluorescence Behavior and Binding Ability. *Supramol. Chem.* **2007**, *19*, 517–523.
- (396) Choudhury, S. D.; Mohanty, J.; Pal, H.; Bhasikuttan, A. C. Cooperative Metal Ion Binding to a Cucurbit[7]uril-Thioflavin T Complex: Demonstration of a Stimulus-Responsive Fluorescent Supramolecular Capsule. *J. Am. Chem. Soc.* **2010**, *132*, 1395–1401.
- (397) Mohanty, J.; Bhasikuttan, A. C.; Choudhury, S. D.; Pal, H. Noncovalent Interaction of 5,10,15,20-Tetrakis(4-N-methylpyridyl)-porphyrin with Cucurbit[7]uril: A Supramolecular Architecture. *J. Phys. Chem. B* **2008**, *112*, 10782–10785.
- (398) St-Jacques, A. D.; Wyman, I. W.; Macartney, D. H. Encapsulation of Charge-Diffuse Peralkylated Onium Cations in the Cavity of Cucurbit[7]uril. *Chem. Commun.* **2008**, 4936–4938.
- (399) Freitag, M.; Gundlach, L.; Piotrowiak, P.; Galoppini, E. Fluorescence Enhancement of Di-p-tolyl Viologen by Complexation in Cucurbit[7]uril. *J. Am. Chem. Soc.* **2012**, *134*, 3358–3366.
- (400) Sindelar, V.; Parker, S. E.; Kaifer, A. E. Inclusion of Anthraquinone Derivatives by the Cucurbit[7]uril Host. *New J. Chem.* **2007**, *31*, 725–728.
- (401) Chakraborty, B.; Basu, S. Deciphering the Host-Guest chemistry of Acridine Yellow and Cucurbit[7]uril: An Integrated Spectroscopic and Calorimetric Study. *Chem. Phys. Lett.* **2011**, *507*, 74–79.
- (402) Zhou, Y.; Yu, H.; Zhang, L.; Sun, J.; Wu, L.; Lu, Q.; Wang, L. Host Properties of Cucurbit [7] uril: Fluorescence Enhancement of Acridine Orange. *J. Inclusion Phenom. Mol. Recognit. Chem.* **2008**, *61*, 259–264.
- (403) Montes-Navajas, P.; Corma, A.; Garcia, H. Complexation and Fluorescence of Tricyclic Basic Dyes Encapsulated in Cucurbiturils. *ChemPhysChem* **2008**, *9*, 713–720.
- (404) Wang, R.; Wyman, I. W.; Wang, S.; Macartney, D. H. Encapsulation of a Beta-carboline in Cucurbit[7]uril. *J. Inclusion Phenom. Mol. Recognit. Chem.* **2009**, *64*, 233–237.
- (405) Cao, L.; Isaacs, L. Absolute and Relative Binding Affinity of Cucurbit[7]uril Towards a Series of Cationic Guests. *Supramol. Chem.* **2014**, *26*, 251–258.
- (406) Miskolczy, Z.; Harangozo, J. G.; Biczok, L.; Wintgens, V.; Lorthioir, C.; Amiel, C. Effect of Torsional Isomerization and Inclusion Complex Formation with Cucurbit[7]uril on the Fluorescence of 6-methoxy-1-methylquinolinium. *Photochem. Photobiol. Sci.* **2014**, *13*, 499–508.
- (407) Lee, J. W.; Lee, H. H. L.; Ko, Y. H.; Kim, K.; Kim, H. I. Deciphering the Specific High-Affinity Binding of Cucurbit[7]uril to Amino Acids in Water. *J. Phys. Chem. B* **2015**, *119*, 4628–4636.
- (408) Hang, C.; Ling, T. L.; Yi-Hua, Y.; Fan, Y.; Ying, D.; Sai-Feng, X.; Zhu, T. Molecular Recognition of Aminoacid by Cucurbiturils. *Acta Chimica Sinica* **2006**, *64*, 989–996.
- (409) Bailey, D. M.; Hennig, A.; Uzunova, V. D.; Nau, W. M. Supramolecular Tandem Enzyme Assays for Multiparameter Sensor Arrays and Enantiomeric Excess Determination of Amino Acids. *Chem. - Eur. J.* **2008**, *14*, 6069–6077.
- (410) Wyman, I. W.; Macartney, D. H. Host-guest Complexations of Local Anaesthetics by Cucurbit[7]uril in Aqueous Solution. *Org. Biomol. Chem.* **2010**, *8*, 247–252.
- (411) Wyman, I. W.; Macartney, D. H. Cucurbit[7]uril Host-Guest Complexes of Cholines and Phosphonium Cholines in Aqueous Solution. *Org. Biomol. Chem.* **2010**, *8*, 253–260.
- (412) Wang, R.; Macartney, D. H. Cucurbit[7]uril Stabilization of a Diarylmethane Carbocation in Aqueous Solution. *Tetrahedron Lett.* **2008**, *49*, 311–314.
- (413) Hettiarachchi, D. S. N.; Macartney, D. H. Cucurbit[7]uril Host-Guest Complexes with Cationic Bis(4,5-dihydro-1H-imidazol-2-yl) Guests in Aqueous Solution. *Can. J. Chem.* **2006**, *84*, 905–914.
- (414) Choi, S.; Park, S. H.; Ziganshina, A. Y.; Ko, Y. H.; Lee, J. W.; Kim, K. A Stable Cis-Stilbene Derivative Encapsulated in Cucurbit[7]uril. *Chem. Commun.* **2003**, 2176–2177.
- (415) Kuz'mina, L. G.; Vedernikov, A. I.; Lobova, N. A.; Howard, J. A. K.; Strelenko, Y. A.; Fedin, V. P.; Alfimov, M. V.; Gromov, S. P. Photoinduced and Dark Complexation of Unsaturated Viologen Analogues Containing Two Ammonium Tails with Cucurbit[8]uril. *New J. Chem.* **2006**, *30*, 458–466.
- (416) Biedermann, F.; Nau, W. M. Noncovalent Chirality Sensing Ensembles for the Detection and Reaction Monitoring of Amino Acids, Peptides, Proteins, and Aromatic Drugs. *Angew. Chem., Int. Ed.* **2014**, *53*, 5694–5699.